SAPIENZA
UNIVERSITÀ DI ROMA

Sapienza University of Rome

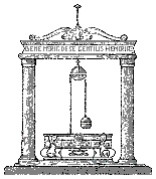

Doctorate of Philosophy in Electronic Engineering
XXX Cycle

Nanomedicine Applications mediated by Electromagnetic fields

Candidate
Elena della Valle
ID Number 1204705

Thesis Advisor
Prof. Francesca Apollonio

Thesis Co-Advisor
Prof. Marco Balucani
Prof. Micaela Liberti
Prof. Emanuele Piuzzi

A.Y. 2017/2018

SAPIENZA
UNIVERSITÀ DI ROMA

Sapienza University of Rome

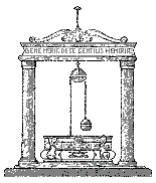

Doctorate of Philosophy in Electronic Engineering
XXX Cycle

Nanomedicine Applications mediated by Electromagnetic fields

Candidate

Elena della Valle

ID Number 1204705

Thesis Committee

Prof. Francesca Apollonio (Thesis Advisor)
Prof. Marco Balucani
Prof. Micaela Liberti
Prof. Emanuele Piuzzi (Thesis Co-Advisor)

Reviewers

Prof. P. Thomas Vernier
Prof. Delia Arnaud-Cormos

A.Y. 2017/2018

Nanomedicine Applications mediated by Electromagnetic fields
Ph.D. Thesis - Sapienza University of Rome

Thesis submitted in partial fulfillment of the requirements for the degree of Doctor of Philosophy in Electronic Engineering.
Thesis defended on the 22^{nd} of February 2018.

This thesis has been typeset by LaTeX.
Version: February 20, 2018.

Author's address:
Elena della Valle
Sapienza - University of Rome
Via Eudossiana 25, 00184 Rome, Italy
e-mail: elena.dellavalle@uniroma1.it
web-site:

"To Jacopo, with whom
I will walk 500 miles and
I will walk 500 more just to be the girl
who walks a thousand miles
to spend her life with him"
—

Contents

List of Figures

List of Tables

Abstract

Recently, the introduction of nanotechnologies into medical applications has become more frequent due to the growing of several diseases originating from alteration of biological processes at molecular and nanoscale level (e.g. mutated genes, cell malfunction due to viruses or bacteria).
The nanomedicine combines the innovation of the nanotechnology materials (shape and size of nm scale) to health care, providing new promising techniques for the diagnosis, the prevention, the tissue regeneration and therapeutic fields.
Disorders like cancer, Alzheimer's, Parkinson's disease, cardiovascular problems or inflammatory diseases are serious challenges to be dealt with. For this reason researches are focusing their attention to the nanomaterials unique properties [Murty et al., 2013, Xia et al., 2009]. The progress in nanomedicine ranges from nanoparticles for molecular diagnostics, imaging and therapy to integrated medical nanosystems [Nune et al., 2009, Shi, 2009] to act at the cellular level inside the body. For a recent review on challenges, opportunities, and clinical applications in nanomedicine an interesting review is the one of Wicki et al. [Wicki et al., 2015]. Despite the concerns raised by the authors in their review, the expert opinion on clinical opportunities finds a generalized consensus on stimuli-responsive systems for targeting the compound (drug, gene, biomolecule) at the site of interest and on the use of lipid based nanosystems for the biocompatible platform to be used in clinical trials.
In this scenario is placed the main activity of this Ph.D. thesis whose aim is to provide a multiscale and multidisciplinary approach to demonstrate the capability to activate lipid-based nanosystems by means of electromagnetic fields (EMFs). Specifically, the attention will be focused, on a first part, on the liposome-based systems mediated by EMF to provide a proof-of-concept of EMF stimuli-response systems for applications of drug delivery. This aspect will be approached both form a theoretic, technological and experimental point of view. Moreover, because proteins are considered a fundamental pattern as bio-sensors for signaling cell processes, a molecular dynamics simulation approach will be provided to study the interaction mechanisms between EMFs and proteins structures for potential protein activation.

Chapter 1

Introduction and purpose of the research

During the last years the global trend to improve the efficacy of medical treatments to prevent the patient safety by the use of nanotechnologies, became of fundamental importance for the overall scientific community.
It is since 2005 that the European Technology Platform for Nanomedicine (ETPN) [KM Weltring et al., 2016] defined, through vision papers, the scope of Nanomedicine in Europe and by create international networks with the aim to integrate innovation aspects for the further development of Nanomedicine both in the academia and industry panorama. The Strategic Research and Innovation Agenda (SRIA) of the ETPN offers the opportunity to assess the state of the art and to provide the larger nanomedicine community focused on the clinical needs in selected diseases, highlighting the potential of the current and future nanomedical products to provide new and efficient solutions for health care. In particular the road-map highlights future applications in nanomedicine up to 2030 and as reported in Fig. 1.1 research is mainly focused in developing new promising approaches and prototypes for nanomedicine applications in the areas of therapeutics, diagnostics and regenerative medicine. It explores different area from the nanoparticles for therapeutic and imaging systems to the 3D printing cells for the new regenerative medicine.

In the following a schematic diagram is proposed with the purpose of the classification of the different research areas present in Nanomedicine: the nanodiagnostic, the nanotherapeutic and the nanotheranostic as reported in Fig. 1.2.

Area	Nanotechnologies applied to medicine to address medical needs
Therapeutics	- **Nanotechnologies to cross biological barriers,** using nanoformulations, nanoemulsions or nanodevices - **"Smart" nanocarriers:** Encapsulation of actives into nanodelivery devices / Highly targeted and fast acting drug delivery systems and nano devices for localised drug delivery and release in critical regions / enhanced bioavailability (nanoemulsions) and increased target specificity / - **Biocompatible nanoparticles:** Lipid/micellar or polymeric nanoparticles to reduce toxicity (biocompatibility) and improve efficacy - **Activable nanoparticles providing physical therapeutic effects** (crystalline inorganic nanoparticles) - **Monitoring of therapeutic efficacy** - **Theranostic nanoparticles and nanodevices carrying a drug and acting as diagnostic tool**: diagnosis and monitoring / active and passive targeting (cancer)
Diagnostics / Imaging	- **Nano-enabled biomarkers, vectors and contrast agents with high-sensitivity and specificity:** functionalised nanoparticles for diagnostics and therapy / Molecular monitoring of markers / Multifunctional contrast agents - **Nanotechnologies to cross biological barriers (BBB)**, using nanoformulations, nanoemulsions or nanodevices - **High throughput systems** for multiplexed detection of biomarkers of diseases, for optimization of therapy and sensing interfaces - **Nanostructured surfaces for biosensors** tailored to work within the body, on the body, or out of body - **Non-invasive and painless monitoring** (diabetes and endocrine disorders)
Regenerative Medicine	- **"Smart" nanostructured and functionalised surfaces**: functionalisation of 2D-3D materials - **Scaffolds and nanoparticles for new and advanced therapeutic treatments** - **3D printing of cells and biomaterials for implants and/or reconstruction** - **Intelligent biomaterials/bioactive materials:** site specific delivery of active molecules / nanoparticles with spatial and temporal control over the release of biochemical molecules and/or in vivo activation of stem cells / mimic the morphological, mechanical and biochemical environment of tissues / Biomimetic, biocompatible, biocompetent biomaterials - **Nanofunctionalisation for increased biocompatibility of implants:** polymer coated medical implants to improve biocompatibility

Figure 1.1: Current applications of Nanotechnologies in Medicine.

Nanodiagnostic

The first principal area is related to Nanodiagnostic. In particular, non-invasive imaging can be used to provide feedback on the tissues circulation properties, the target site accumulation and the off-target localization of therapeutic drugs, also to report on the efficiency of drug release at the target site, and to monitor therapeutic efficacy. Among the different applications nanoparticles can be used in patients for the MR monitoring of the perfusion of tumor blood vessels and coronary arteries [Fink et al., 2003, Wagner et al., 2002, Chiribiri et al., 2008], the imaging of labelled stem cells [Politi et al., 2007] and the visualization of primary and/or metastatic liver lesions [Reimer and Balzer, 2003]. For the cancer imaging, is increasing the use of paramagnetic iron oxide nanopartiles (SPIONs) injected into patient to detect the cancer cells or to detect possible lymph-node metastases [Harisinghani et al., 2003, Perrault et al., 2009]. Moreover, nanoparticles are also used for the in-vitro diagnostic assays as for protein markers [Posthuma-Trumpie et al., 2009], or for genetic mutations [Lefferts et al., 2009] thanks to a particular gold coating depending on the genetic sequence. Several

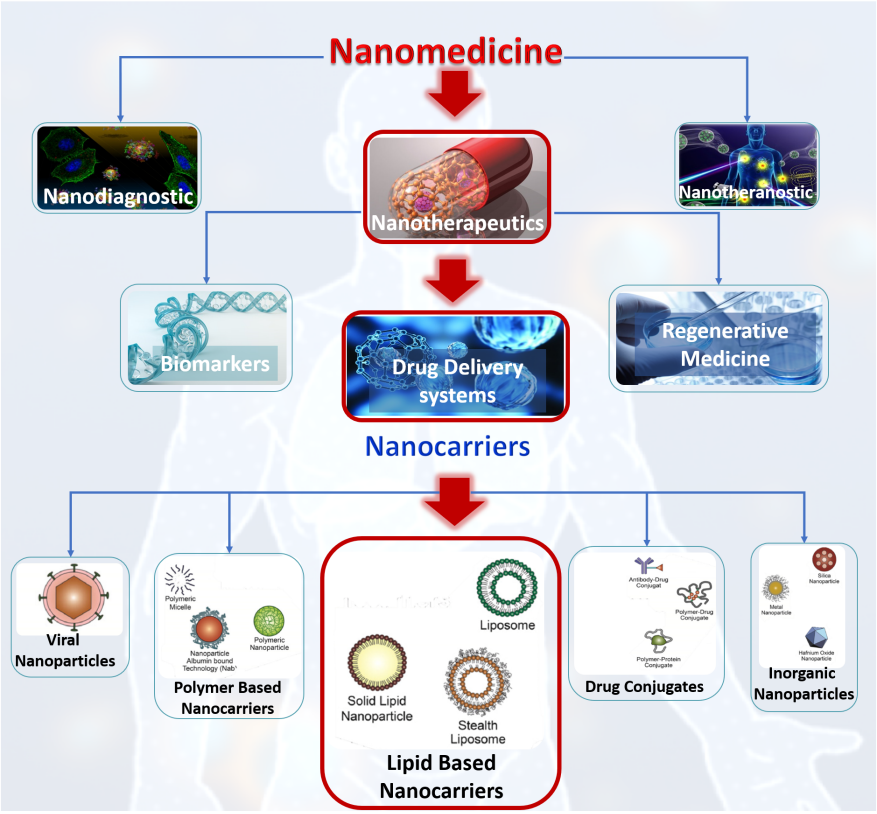

Figure 1.2: Scheme of the basics principles of Nanomedicine applications, focusing the attention on the therapeutic area and on liposomal drug delivery system.

additional studies in these and other pathological settings are currently ongoing as the labeled nanoparticles with contrast agents which is highly useful for better understanding the properties and the potential of the formulations developed in order to treat different diseases [Duncan and Gaspar, 2011]. Moreover, in recent years the use of nanodiagnostics for visualizing tumors and receptor structures over expressed by tumor blood vessels, it has growth by giving idea of the tumor distributions [Takahashi et al., 2015, Azmi et al., 2014, Jackson et al., 2017].

Nanotheranostic

By the combination of drugs and imaging agents, one has the so-called nanotheranostic which couples the disease diagnosis and the therapy. Theranostic strategies start from a selection of a set of preselected patient, based on initial studies using a given diagnostic radionuclide-labeled antibody, and then followed by a radio-immunotherapy

with the same antibody coupled to a therapeutic radionuclide [Imhof et al., 2011]. In this way it is possible to monitor the treatment efficacy providing the diagnosis and the treatment with the same nanoformulation. It is important to take into account that theranostic does not means to have a simultaneously imaging and treatment of the disease, but firstly it is important to find a prediction of potential therapeutic responses, in this way the drug is personalized and based on the diagnosis study the monitor of the treatment occurs. Nevertheless, the advantage of theranostic is that can be used to have a non-invasive monitoring of the target site, visualize bio-distribution, assess therapeutic efficacy and also a possible tumor-targeted drug delivery as showed from the use of polymers or liposomes both in patients and animals [Lammers et al., 2008b, Mura et al., 2013].

Nanotherapeutic

As therapeutic agents the aim of nanomaterials is, in order to overcome biologic barriers, to enhance the efficacy of medical treatments. Nanotherapeutics are able to improve the action of a therapeutic agents, by increasing their accumulation at pathological sites and their therapeutic efficacy, reducing also the incidence and possible side effects [Lammers et al., 2008a, Davis et al., 2008, Ganju et al., 2017]. The nanotherapy can assess in different ways as shown in fig. 1.2. One branch is the regenerative nanomedicine. It is since 1960s and 1970s that the first generation of materials was developed for the use inside the human body. Biomaterials involve tailoring of resolvable polymers at the molecular level to elicit specific cellular responses. These materials show great promise as scaffolds or matrices in tissue regeneration which means the use of a combination of cells, engineering and materials methods to improve or replace biological tissues. Tissue engineering involves the use of a scaffold for the formation of new viable tissue for a medical purpose [Nasseri et al., 2001, Neves et al., 2017]. Also biomarkers can be used as therapeutics agent like esosomes for dermatology illnesses [McBride et al., 2017].

Drug Delivery systems

Nanomedicine mainly acts improving the efficiency of drugs to pathological sites with a local release on the diseased tissues. This process takes the name of targeted drug delivery (see Fig. 1.2). The incorporation of external or internal stimulus as a remote control to trigger the release of therapeutic payloads has received much attention in this recent years [Rahoui et al., 2017]. Drug delivery refers to approaches for drugs transporting in a specific site to have a localized action of the pharmaceutics, reducing side effects for the healthy tissues. As showed in Fig. 1.2 the drug delivery can be achieved trough the use of different nanocarriers or nanoparticles. A large number of nanomaterials have

been designed and evaluated over the years, relying e.g. on lipid based nanocarriers (liposomes, solid lipid nanoparticles), polymer based liposomes (e.g. polymers, micelles), drug conjugates (polymer-protein conjugate, antibody conjugate), viral nanomarticles and inorganic nanoparticles (e.g. metal or silica nanoparticles) (see Fig. 1.2). Nanoparticles have the peculiarity that can be engineered in shape and size from 1 to hundred nanometers depending on the biological need. Basically they can be used as bio-sensors for the detection of a particular disease or as a drug delivery nanocarrier for treatment purpose. Nanocarriers have unique properties such as nanoscale size, high surface-to-volume ratio, and favorable physico-chemical characteristics. They have the potential to modulate both the pharmacokinetic and pharmacodynamic profiles of drugs, thereby enhancing their therapeutic index. Loading of drugs into nanocarriers can increase in vivo stability, extend a compound's blood circulation time, and allow for controlled drug release. Thus, nanomedicine compounds can alter the biodistribution of drugs by allowing them to accumulate preferably at the tumor site. The advantage consists due to the smaller size (around 10 nm) to be taken more easily from the tumor cells and ejected from the body after a long time, permitting to be distinguished on MRI for a longer period [Enochs et al., 1999]. For the nanoparticles use there are two main aspects that need to be considered, one is the possible toxicity of nanoparticles and their bio-compatibility and the other one is the invasiveness of the technique used as external agent for the illness treatment (i.e thermal, magnetic or electric). Moreover, nanocarriers have also the advantage to protect the drug from degradation and, reduce the renal clearance, allow the control of the release kinetics of the anticancer drugs and improve the solubility of those insoluble [Danhier et al., 2010, Xu et al., 2016, Song et al., 2017].

Among all nanoparticles that can be used, liposomes represent one of the most used nanocarriers [Vahed et al., 2017] and hold a great promise in the drug delivery panorama as will be explained in details in chapter 2. Liposomes are self-assembled colloidal vesicles with a characteristic lipid bi-layered membrane composed of amphilic phospholipids, that not only allow the encapsulation of numerous hydrophilic anticancer drugs and siRNAs in its aqueous core, but also can host hydrophobic cytotoxic agents in its hydrophobic membrane. On liposomal drug delivery systems is focused the main part of this Ph.D. thesis (see Fig. 1.3) by focusing the attention on a remote liposomal drug delivery system by the activation of external electric or magnetic fields.

As shown in fig. 1.3 and as will be discussed later (see Ch. 2), there are mainly three

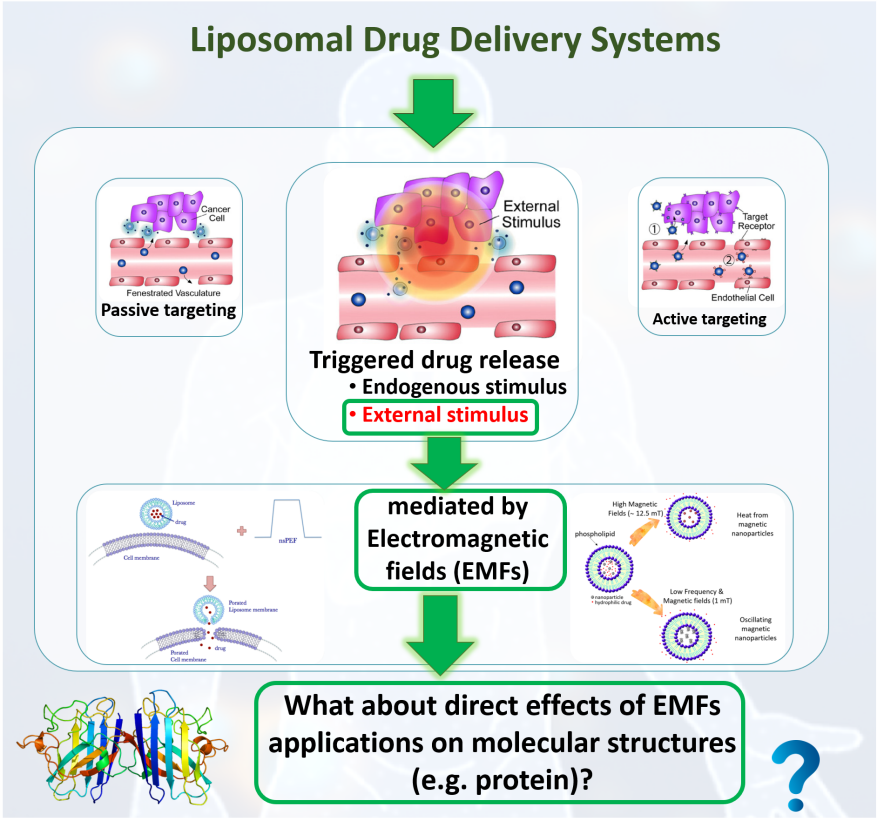

Figure 1.3: Scheme of this Ph.D. thesis, focusing the attention on liposomal drug delivery systems mediated by electromagnetic fields (EMF) and a possible direct action of the EMF on protein activation.

kind of targeted drug delivery systems (see Fig. 1.3):

- passive targeting drug release which means non functionalized nanoparticles that release the drugs a prior;
- active targeting release by using functionalized particles depending on the target tissue treated;
- triggered release which means a physiological or a remote controlled system that triggers the drug release in a specific site.

Specifically, remote controlled drug delivery systems can be activated from physically or external stimulus [Rahoui et al., 2017], in detail there are endogenous (pH variation,

redox responsive liposomes) or exogenous stimulus (thermal stimulus, magneto-thermal activation, acoustic or ultrasound) as will be discussed in the next chapter (see Ch. 2). Among the different external stimuli that can be used, an innovative scenario is opening on the use of "non-thermal" low intensity magnetic fields and also on ultra short and intense electric pulses (see Sec 2.2) as external trigger, on which I focused the main part of my Ph.D. thesis.

Magnetic fields applications

Recently with the wide spread of the technological progress the use of magnetic field as external stimulus for inflammatory and neuronal disease therapies and drug delivery systems for nanomedicine has considerably increased [Ross, 2013, Rodzinski et al., 2016]. Highly interesting applications of magnetic fields have been developed concerning the non-invasive stimulation of the central nervous system, such as the Transcranial Magnetic Stimulation (TMS) technique [Di Lazzaro et al., 2013] or the low-intensity pulsed magnetic field stimulation [Varani et al., 2008, 2017] for inflammatory illness as will be discussed in the section 2.4. Besides, the use of magnetic nanoparticles as contrast agent combined with the MRI is more often used [Idiyatullin et al., 2017, Jog et al., 2016], an innovative upcoming technique is the magnetoliposome drug delivery system, which combines the action of magnetic nanoparticles loaded into liposomes (vesicles of nm dimension) core with the application of an external low intensity magnetic field [Nappini et al., 2010, Spera et al., 2014, Cheng et al., 2014, Spera et al., 2015] without generating secondary effects. The advantage of the use of a low intensity magnetic field is its non-invasive action and no thermal secondary effects are caused to the treated tissues as will be discussed in the chapter 2. This innovative technique could give more comfort to the patient during the treatment, since with low intensity magnetic field no thermal effects could be perceptible and it will be localized on the diseased tissue.

Electric fields applications

Moreover, in the scientific community an increasing interest towards the possibility to use ultra short pulsed electric fields in different medical applications has been developed (as the cancer therapy [Miklavčič et al., 2012, Cadossi et al., 2014], gene electrotransfer [Mir et al., 1999, Calvet et al., 2014] and food processing [Saulis, 2010]). The biological effects at cellular and sub-cellular levels of ultra short electric pulses (usPEFs), with duration between few microseconds (μsPEFs) and nanoseconds (nsPEFs) and amplitudes from kV/m up to few MV/m, are at the basis of various promising and powerful applications of electromagnetic (EM) fields to medical treatments, as underlined in recent papers and reviews [Vernier et al., 2006, Craviso et al., 2009, Joshi and Schoen-

bach, 2010, Neal, 2012, Zorec et al., 2013, Breton and Mir, 2012, Weaver et al., 2012, Silve et al., 2014]. This technique takes the name of electroporation. It is based on the use of short nanosecond electric pulses (nsPEF), which due to their wider frequency content (first lobe up to one GHz, see section 2.3), are able to pass the cell membrane and penetrate into the cell core [Schoenbach et al., 2007, Nuccitelli et al., 2006, Ibey et al., 2011, Nuccitelli et al., 2013, Tolstykh et al., 2013]. The internal membranes electroporation triggers secondary bio-responses as genes modulation expression, action potential activation and apoptotic marker expression, Ca^{2+} release [Joshi and Schoenbach, 2010, Schoenbach et al., 2001, Pakhomova et al., 2014] based on the application of a short electric pulse (10 nanosecond). The mechanism of coupling of nsPEFs and cells is still under study. The E pulses cause primarily a kind of cell membrane rearrangement evidenced by transient (reversible) or permanent (irreversible) permeability changes, as firstly evidenced by Neumann and coworkers in the early 1972 [Neumann and Rosenheck, 1972] identifying such membrane defects as aqueous pores [Tieleman, 2004, Tarek, 2005, Casciola et al., 2014]. Since cell membranes can be thought to be very similar to the membrane of liposome in terms of lipid composition, an upcoming interest is arising in the development of new drug delivery systems mediated by the coupling of nsPEFs and liposomes for a controlled drug release.

In this context different network cooperation have been active during the present research project. In particular I had the opportunity during my first year of Ph.D. to participate to two different calls of two associations that gave me the opportunity to work for three months at the Oncology Institute Gustave Roussy in Paris. One of the association, is the COST EMF-MED that provides a cooperative framework to support the research on beneficial biological effects of non-ionizing EMFs and their use in biomedical applications. This Action focuses on beneficial effects, aiming for breakthrough results, new discoveries and innovative biomedical technologies. Another action more focused on the electroporation phenomena is the COST-European Cooperation in Science and Technology which is focused on building connection between the different scientific communities throughout Europe and worldwide and provide networking opportunities for early career researchers.

Direct EMF effects

Finally, one of the main question often discussed in the scientific community (see Fig. 1.3) but not yet fully elucidated is about the effects generated by a direct electromagnetic fields application on molecular structures (e.g. proteins) and what is the basic mechanism of this interaction. Recently experimental techniques have been used

to investigate the effects of electromagnetic fields on biological structures [Azan et al., 2017b,a, Carr et al., 2017, Marklund et al., 2017]. Among these, Azan et al. [Azan et al., 2017a], investigated about different regions of interest around the nucleus of the cells and the dose-effect relationship related to different electric pulse parameters using the confocal Raman microspectroscopy.
On this question is focused the last part of my Ph.D. thesis (see Part V) where by the means of molecular dynamics simulations the effects of the application of an electric and a magnetic fields have been investigated on the superoxide dismutase and the adenosine A_{2A} receptor respectively. Indeed the aspect to take into account is that biological effect can be also achieved by acting on proteins (e.g. receptors, enzymes, etc.), which can respond to the exposure of an external electric or magnetic stimuli and they can enhance or reduce the cells activity or biological functions [Varani et al., 2002, 2008, Capelli et al., 2017, Beebe, 2015] as will be detailed explained in the chapter 3.

Purpose of the research: thesis outline

The purpose of the presented Ph.D. research project wants to be a multidisciplinary and multiscale approach for the investigation of both low level magnetic fields and nanosecond electric pulses interactions with biological structures. This research has been carried out both from a theoretical, technological and experimental point of view focusing the attention on liposomal drug delivery systems mediated by electromagnetic fields and on the understanding of the interactions between electromagnetic fields and proteins (see Fig. 1.3).
Following a briefly overview of this Ph.D. thesis is given.
In the part I, an overview will be given concerning the liposomal drug delivery system research area (see Sec. 2.2). Drug delivery systems will be explored by giving a general knowledge and then focusing the attention on the actual liposomal drug delivery systems mediated by the application of electric and magnetic fields (section 2.2).
Not only liposomes but also proteins are often used as biosensors to mediate cellular functions. Proteins as potential biosensor will be discussed in the chapter 3, both under the action of magnetic or electric fields, starting from experiments with proteins in cell culture.
In the part II an entire chapter will be dedicated to the modeling tools used for performing this project as molecular dynamics simulations (section 4.2) and microdosimetry models (section 4.3). After that, the thesis will be divided into three part:

- Liposomal drug delivery systems activated by low intensity magnetic fields
- Nanosecond pulsed electric fields for liposomal drug delivery systems
- Direct EMF effects investigation on proteins structure using MD simulations

In the part III experimental work will be presented about magnetoliposomes (MLs) exposure to a low magnetic field intensity for testing the feasibility of MLs drug delivery systems (see chapter 5). The last chapter of this part will be dedicated to the project and a design of a new exposure magnetic setup able to produce magnetic field with intensity of mT in a frequency range up to 20 kHz (see chapter 6).
Concerning the nsPEFs applications (Part IV), two different studies have been carried out for a proof of concept of possible liposomal drug delivery systems mediated by 10 nsPEF by the use of microdosimetry models considering both the theoretical (see chapter 7) and technological and experimental aspects (chapter 8).
In the Part V we firstly performed a modeling work regarding magnetic molecular dynamics simulations on the adenosine receptor A_{2A} to explore the interactions between a low intensity magnetic field and a protein structure (see chapter 9). In the last chapter we investigated the ability of 100 ns electric pulses to possibly interact with the enzyme superoxide dismutase by the means of molecular dynamics simulations (see chapter 10).

Part I

Electromagnetic fields on nanomedicine applications

As mentioned in the introduction, the use of electromagnetic fields for therapeutic purposes is becoming highly interesting due to the possibility to optimize medical treatments taking attention to the patient safety.
Recently, one of the new nanotechnology used for the treatment of inflammations and diseases is the new liposomal drug delivery approach. This kind of application, as will be reported, is a kind of active targeting drug release system, where the delivery of the drug comes after the application of an endogenous or exogenous stimulus. Due to the peculiarity of the electric pulses, in this part firstly a general knowledge will be given concerning liposomal drug delivery systems. The liposomes as nanocarriers will be described and the kind of liposomal drug delivery systems will be presented moving form the more traditional use of endogenous stimuli to the more innovative one related to exogenous stimuli. The applicability of nanosecond pulsed electric fields as external trigger to activate a potential liposome drug delivery system will be discussed. Besides, another promising external trigger for this kind of application, can be the use of low intensity magnetic field, due to their use in the clinical treatment of inflammations and due to their good penetration in the human tissues. On this aspect is also focused, this part, by proposing the use of magnetoliposomes as nanocarriers for a controlled drug release activated by low intensity magnetic fields.
Moreover, since electromagnetic fields are currently adopted for the treatment of different inflammations diseases as neurodegenerative diseases, in this case trans-membrane and internal cell proteins could play a fundamental role. For this reason the last chapter of this part is dedicated to an overview on the present use of proteins as biosensors and their potential to be used as sensor in cells, responding to an external electric or magnetic fields.

Chapter 2

Drug delivery systems: from endogenous to external stimuli activation

2.1 Introduction

In recent years, we are witnessing a growing applications of new nanotechnology techniques in traditional medicine, improving the efficiency and precision in the treatment of a broad category of disease. Among all the possible application of nanomedicine the one related to the delivery of a certain drug or molecule in situ at the target site is becoming more and more attractive. In this context stimuli-response release of a drug from an ad hoc designed nanocarrier, at a specific time and location is one of the most aimed results of the drug delivery research. The goal is to design, engineer and introduce into the body molecular nano-scale carriers (1-1000 nm, nano-carriers) capable to carry the drug and release it in the place where it must act. In this way to avoid any damage to the surrounding healthy tissue, thus acting locally only on the site where the disease it has been developed.
Generally, the drug release is obtained by changing environmental conditions as pH, temperature, an higher redox potential [Koo et al., 2008, Li et al., 2011], ultrasound, etc. [Ganta et al., 2008, Karanth and Murthy, 2007]. Among the different trigger methods, recently an integrated control release has been approached combining the temperature and magnetic fields as triggering agent using magnetoliposomes (MLs),

which are vesicles containing super-paramagnetic iron oxide nanoparticles [Pradhan et al., 2010, Preiss and Bothun, 2011] that release the content next to the magnetic field application.
In this chapter an overview both of the electroporation phenomena associated to the drug delivery mediated by nsPEF and the use of magnetic fields as trigger agent for drug delivery purpose will be given. The aim is to define the scientific area in which will take place the part of this Ph.D. thesis concerning the drug delivery systems mediated by electric or magnetic fields.

2.2 Liposomal Drug delivery systems

Drug delivery systems

Smart drug delivery systems are multi-targeted, stimuli sensitive, delivery carriers that can release drugs to the infected cells in the body avoiding the need for frequent and massive drug doses, reducing systemic secondary effects [Mirza and Siddiqui, 2014, Yatoo et al., 2014, Allen and Cullis, 2013]. The aim of smart drug delivery technologies is to deliver drugs at the right time and with a controlled dose enhancing the efficiency of the therapy. Basically, there are three different way to achieve the drug delivery (Fig. 2.1):

- passive targeting
- active targeting
- triggered targeting

Passive targeting

Passive targeting (Fig. 2.1a) is based on the release of the drugs by the recognition of the diseased tissue based on the morphological differences between the healthy and the ailing tissues. In case of tumor cells, pathophysiological characteristics of cancers and their environment have been exploited for passive targeting. In particular, the permeability and retention (EPR) effect promotes accumulation of nanomedicine drugs in the tumor based on the presence of leaky intratumoral blood vessels. For example, Kaposi sarcoma is a tumor type with fenestrated vasculature [Lammers et al., 2012] and by convection and diffusion processes, passive directing of nanomedicine therapeutics into tumors can occur without any specific ligand attached to the surface of the nanocarrier. However, the passive targeting is not sufficient to control the side effects of cytotoxic drugs and fully exploit the benefits of targeted delivery, because of the heterogeneity of

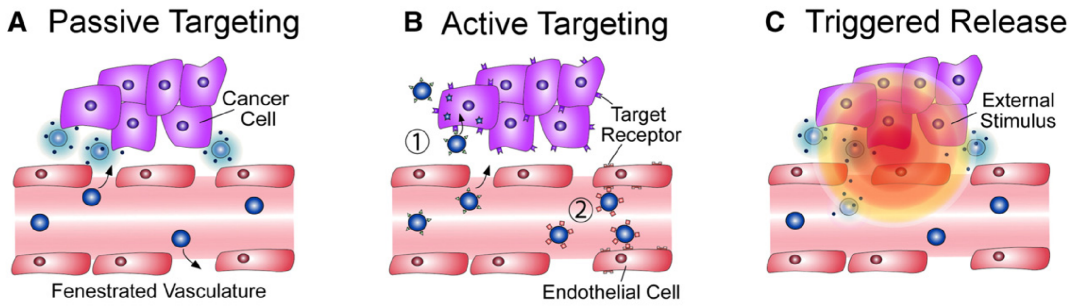

Figure 2.1: Illustration of the targeted strategies: passive targeting, active targeting and triggered targeting.

the diseased tissues [Prabhakar et al., 2013] and the increased interstitial fluid pressure of tumor cells [Jain and Stylianopoulos, 2010].

Active targeting

Active targeting (Fig. 2.1b) requires the conjugation of specific receptor ligand that can promote the site specific targeting. A wide range of ligands can be used including small molecules such as folic acid and carbohydrates, or macromolecules such as peptides, proteins or antibodies. The ligand must allow binding to the target diseased cells while minimizing binding to healthy cells. Moreover, a prolonged circulation of the drug is vital to avoid unwanted interactions with serum proteins or the immune system [Detampel et al., 2014]. However, actively targeted nanoparticles delivery can enhance drug retention in the tumor due to increased cellular binding, minimize non-specific uptake, and also circumvent mechanisms of resistance from biological barriers [van der Meel et al., 2013].

Triggered targeting

The last method to achieve a drug release is to use an endogenous or exogenous stimulus to trigger the release of the drug in a specific target site. Stimuli-responsive systems, on which we will focus the attention, act in response to physical, chemical, or biological triggers that promote release of drugs by modifying the structure or conformation of the nanocarrier. The advantage of using stimuli-responsive systems is that the drug is released through a trigger thus minimizing the exposure of the surrounding healthy tissues to the pharmaceutic. In all of these scenarios, the drug is previously loaded into a nanocarrier and then released. At this purpose one of the classical carriers used in medicine for drug encapsulation and delivery [Xiang and Anderson, 2006, Seigneuric et al., 2010, Stuart et al., 2010] are the liposomes.

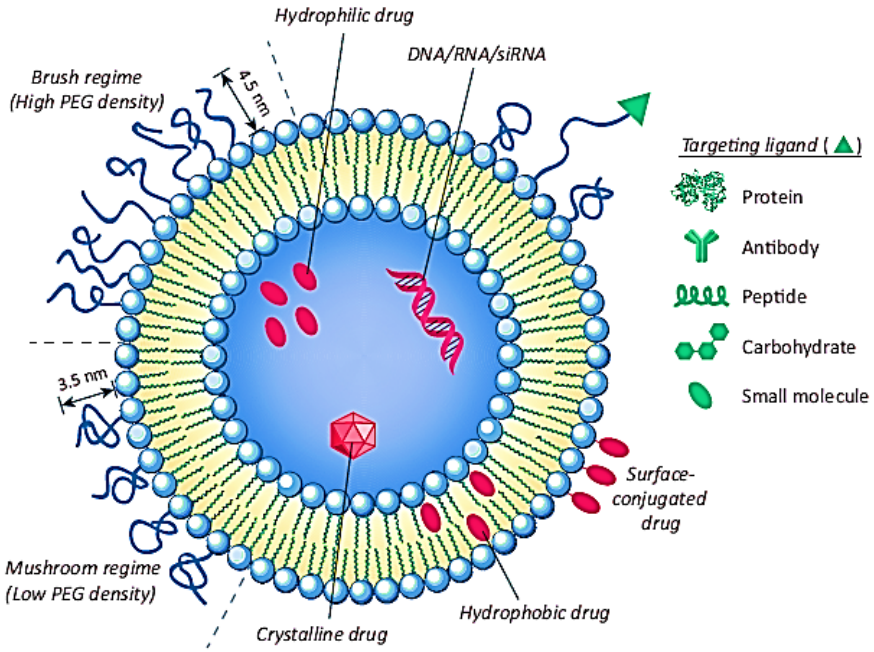

Figure 2.2: Liposomal drug delivery design. Liposomes can be surface functionalized to endow stealth through PEGylation and to promote receptor-mediated endocytosis by using targeting ligands such as antibodies, peptides, proteins, carbohydrates, and various other small molecules.

Liposomes are one of the most studied nanocarriers [Lee and Kataoka, 2011]. They consist of a biocompatible phospholipid bilayer and they can protect amphiphilic, hydrophilic, and/or hydrophobic drugs (see Fig. 2.2) against a variety of threats that lead to immediated vesicles degradation [Kulkarni et al., 2011].

Liposomes nanocarriers

Liposomes consist of an aqueous core surrounded by a lipid bilayer, much like a membrane, separating the inner aqueous core from the bulk outside. Depending on the preparation methods [Petralito et al., 2012, Hope et al., 1985, Çağdaş et al., 2014], liposomes can be distinguished in multilamellar or unilamellar liposomes (see Fig. 2.3). Unimellar vesicles are of special interest to researchers due to their well-characterized membrane properties and facile preparation in a laboratory. Multimellar vesicles show a greater range of physical properties and general behavior when compared to unilamellar vesicles, and are more used with industrial applications like drug delivery.

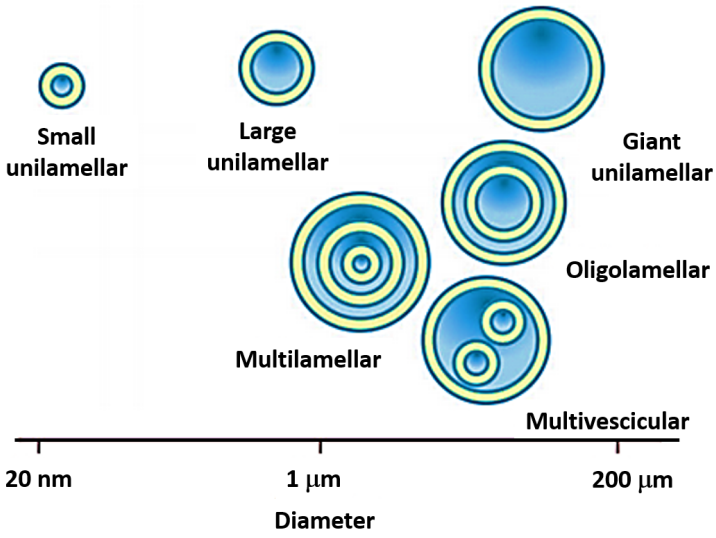

Figure 2.3: Liposoms classification depending on the size and the lipid unilamellar or multilamellar bilayer.

The use of liposomes for drug delivery started shortly after their invention by Bangham and coworkers in 1965 [Bangham et al., 1965, Lindner and Hossann, 2010]. The first liposome-based drugs (Myocet and Doxil) were approved by USA Food and Drug Administration (FDA) for cancer treatment in 1995 [Pinheiro et al., 2011]. Since then, a wide range of therapeutics small molecules have been incorporated in liposomes to improve their efficacy.

The main advantage of using liposomes is their biocompatibility and biodegradability since they are made with naturally occurring lipids [Oh and Park, 2009, Alhajlan et al., 2013]. Moreover, some of the first demonstrations of the improved in vivo activity of liposome-entrapped drugs in animal models, used the anti-cancer drug cytosine arabinoside to demonstrate significant increases in the survival times of mice bearing L1210 leukemia [KOBAYASHI et al., 1975]. The stability of liposomes in the circulation with retention of their contents has long been recognized as a desirable liposome characteristic for successful drug delivery to diseased tissues. Besides, it has been also recognized that being able to trigger the release of liposomal contents once they reached the target site, would lead to improvements in therapeutic outcomes. Indeed, new strategies in

liposomal research have gained interest, and some clinical trials based on the combination of different chemotherapeutic agents and stimuli-responsive release approaches have been started [Dicko et al., 2010, Malekigorji et al., 2014].
Due to this, liposomes can be used as triggered nanocarriers through internal (e.g. pH variation, enzyme action) or external (e.g. temperature,electric or magnetic field) stimuli. Consequently, the release of loaded drugs can be controlled and concentrated at the target site [Zhu and Torchilin, 2013]. A briefly knowledge of different kind of endogenous or exogenous triggers will be given in the following sections.

2.2.1 Endogenous stimuli-responsive liposomes

Endogenous stimuli arise from the different environment between normal and diseased areas, such as higher redox potential [Koo et al., 2008, Li et al., 2011], reduced intra/inter-cellular pH, ionic strength, and increased levels of certain enzymes as the lysosomal enzyme cathepsine B, overexpressed in several malignant tumours [Lee et al., 2011].
Among these, liposomes responding to a potential difference can be utilized for the construction of stimuli-sensitive liposomes [Ganta et al., 2008, Saito et al., 2003]. Their structure is maintained under normal condition by the disulfide bonds until its entering in the intracellular area, where the disulfide bonds is perturbed, destabilizing the liposomes and releasing the encapsulated cargo [Deshpande et al., 2013].
Moreover, a micro-environment that can serve as a trigger for drug release is the hypoxic area of tumors exhibiting low oxygen pressure and poor nutrient levels. The low oxygen level can be used for triggered release from redox-responsive nanocarriers [Fleige et al., 2012].
Another kind of destabilization is a possible intracellular pH variation (see Fig. 2.4). The pH of intracellular organelles (e.g., liposomes,endosomes or lysosomes) differs from that of the cytoplasm or blood. This condition can be used to enhance intracellular release of drugs. This is the case of pH-responsive liposomes that are used to trigger the release of the drug and therefore increase the therapeutic efficacy (Fig. 2.4). pH-responsive liposomes are stable in physiological condition (pH = 7.4) but they are destabilized in acid environment which are common in some pathological tissues such as tumors [Gao et al., 2012]. In this way the liposomes under a repulsion pressure, due to the pH variation, can release the cargo in the tumor cells next to the increase of the

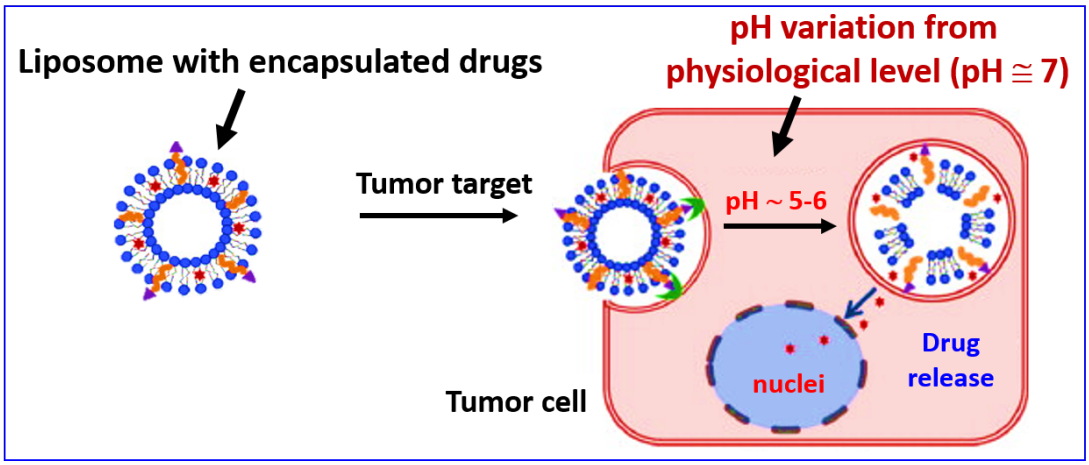

Figure 2.4: Liposomal drug delivery system mediated by a pH variation of the cell with respect to a physiological level.

membrane fluidity (Fig. 2.4).

2.2.2 Exogenous stimuli-responsive liposomes

Exogenous stimuli relate to stimuli that are applied externally such as heat [Tagami et al., 2011, Al-Ahmady et al., 2012], the ultrasounds [Schroeder et al., 2009, Kheirolomoom et al., 2010], magnetic [Plassat et al., 2011] or also an electric field [Lu et al., 2014, Liu et al., 2008].

When the exogenous stimuli is applied to the nanocarrier the drug is released in a certain amount and in a short period of time [Kikuchi and Okano, 2002]. The advantage of the exogenous stimulation is that stimuli are generated by machines protocols can be easily standardized to achieve regulated release [Mura et al., 2013].

Thermoresponsive drug delivery

Thermoresponsive drug delivery is among the most investigated stimuli-responsive strategies widely explored in oncology. The response from the nanocarriers to the temperature variation is expressed in terms of a non linear sharp change of the nanocarrier material. Thermosensitive liposomes (TSLs) are one of the most advanced thermoresponsive nanosystems, as shown by their use in several clinical trials. They respond to the temperature variation with a phase transition of the constituent lipids and the associated conformational variations in the lipid bilayers. The response from the nanocarriers triggers the release of the drug following a variation in the surrounding

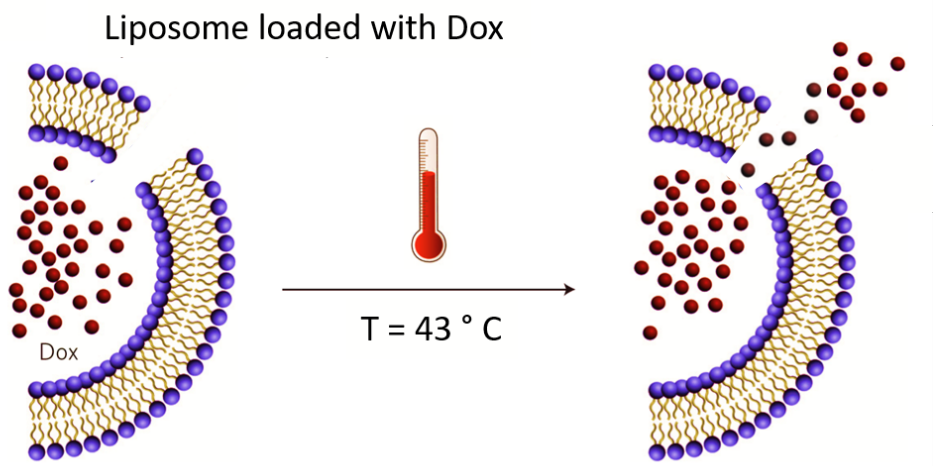

Figure 2.5: Activation of the liposomal drug delivery system mediated by the temperature increase.

temperature (Fig. 2.5). Ideally, thermosensitive liposomes retain their load at body temperature ($\sim$ 37 °C), and rapidly deliver the drug within a locally heated tumor ($\sim$ 40−42 °C) to counteract rapid blood-passage time and washout from the tumor [Tagami et al., 2011, Al-Ahmady et al., 2012]. Neverthless, the drug release can also occur on a brief temperature decrease (also called cold shock or cryotherapy) and in this case, a thermally reversible swelling or de-swelling of the nanocarrier leads to a free diffusion of the encapsulated drugs as a consequence of increased porosity [Lee et al., 2008]. The main concern about the temperature is a possible heating that could cause damages to the surrounding healthy tissues.

Magnetic and Ultrasound stimulus

Magnetic field and ultrasound have been the major strategies investigated due to their ability to penetrate into deeper tissue enhancing their potential in translating from bench to bedside [Schroeder et al., 2009, Kheirolomoom et al., 2010, Plassat et al., 2011]. Ultrasound has been used to trigger the release of drugs (mainly contrast agents) from responsive systems for cancer diagnosis [Rapoport et al., 2011]. Ultrasound waves can trigger the release of the drug from a variety of nanocarriers through the thermal and/or mechanical effects generated by cavitation phenomena or radiation forces [Schroeder et al., 2009, Kheirolomoom et al., 2010]. In fig. 2.6 an illustration of

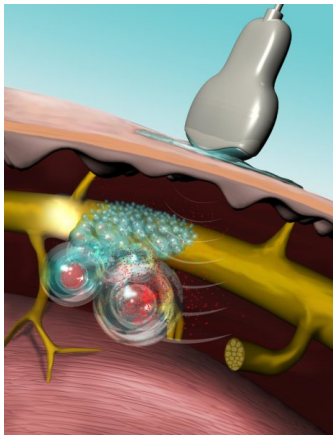

Figure 2.6: Activation of the liposomal drug delivery system mediated by ultrasound triggers.

the ultrasound drug release is presented, where the bubbles are formed through acoustic droplet vaporization and are subjected to cavitation leading to the drug release to the tumor tissue.

Electric field stimulus

Although, another external stimulus that has been investigated is the application of an external electric pulse to activate the drug release previously loaded into a nanocarrier which can be conducting polypyrrole nanoparticles [Ge et al., 2011] or liposomes [Denzi et al., 2017].
In the next sections (2.3 and 2.4) details will be given about the potential application of nanosecond pulsed electric fields or of low intensity magnetic field to induce a controlled release of the cargo loaded into liposomes.
This aspect has been explored in my Ph.D. both theoretically and experimentally in the chapter 5 and 7.

2.3 nsPEF for liposomal drug delivery systems

Low electric fields (typically about 1 V) can be used to achieve pulsed or sustained drug release through a variety of actuation mechanisms [Liu et al., 2008, Im et al., 2010]. One of these mechanism can be an oxidizing voltage activated by the splitting of a vesicle membrane into smaller organelles like micelles releasing the cargo and then reassemble on the application of a reductive voltage [Kim et al., 2011].

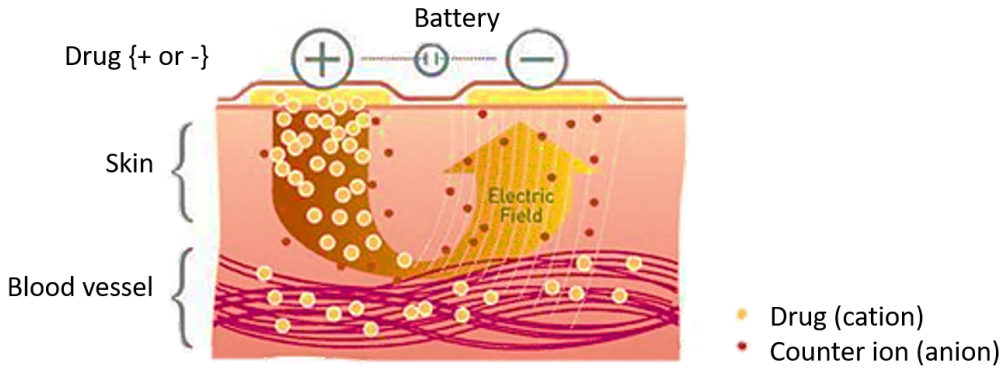

Figure 2.7: Active iontophoresis drug delivery.

Iontophoresis, which uses an electric field to enhance the transdermal delivery of charged compounds, is a particularly versatile approach [Ita, 2016, Malinovskaja-Gomez et al., 2017]. In fig. 2.7 an example is reported of active iontophoresis, where basically the charge applied to the skin changes the flow of ions through the skin, reducing it's resistance and enhancing the amount of and type of medication that can travel below the skin's surface to produce a therapeutic dosing effect. It has been recently applied to various types of nanoscaled systems, including liposomes containing insulin [Chen et al., 2009].

nsPEF applications

Lately the scientific research on electropulsation techniques, which causes the formation of pores in cell membranes increasing its permeability to molecules that otherwise cannot cross them, has significantly improved the practice of medicine by the use of electric pulses of shorter duration (nanosecond) and higher intensity (in the order of MV/m) (nanosecond pulsed electric elds, nsPEF) which allows to directly interact with internal cell organelles (e.g. nucleus, endoplasmic reticulum, mitochondria, etc.) [Denzi et al., 2013, Beebe et al., 2003b, Scarlett et al., 2009, Breton and Mir, 2012, Weaver et al., 2012] and also with the plasma membrane [Napotnik et al., 2012, Chopinet and Rols, 2015].

Since 2003, nsPEF effects related to the plasma membrane have been reported [Vernier et al., 2003a]. Among these, the application of a single 30 ns pulse with intensity of

25 kV/cm has been shown to permit the translocation of phosphatidylserine (PS) from the inner leaflet of the lipid bilayer to the outer leaflet, involving a membrane effect and causing cell apoptosis [Vernier et al., 2004]. Recently Napotnik et al. [Napotnik et al., 2016], reviewed different papers regarding in-vitro applications on eukaryotic cells exposed to nsPEF, highlighting how the plasma membrane is more affected with longer pulses than with short pulses, leading to the best uptake of dye molecules after applying single pulses. Several works have also shown a release of calcium independently of intra-cytoplasmic membrane calcium channels, which was directly linked to the destabilization of organelle envelopes by pulses shorter than 100 ns [Vernier et al., 2003b].

One aspect to take into account is the cell viability next the application of nsPEF. Because of their very short duration, nsPEF do not transfer a large energy to the sample and thus the observed effects are probably non-thermal. Anyhow, the destabilization of the cell membrane could cause, depending on the duration and pulse intensity, the cell death. The first work [Beebe et al., 2003a] focusing on cell survival has shown that for very high intensities of 300 kV/cm and duration of 300 ns, apoptotic phenomena were observed on up to 90 % of cell population in less than 10 min following the application of the pulses. Despite of this, it has been demonstrated that reducing the pulse duration to 10 ns or less with intensity in the order of kV/cm could help to destabilize cell membranes (internal and external) without causing cell death [Chopinet and Rols, 2015]. At this regard, Napotnik et al. [Napotnik et al., 2012] investigated about the effects of 4 ns electric pulses duration with intensity of 10 MV/m at 1 kHz of repetition rate and a loss of the mitochondrial membrane potential and a plasma membrane permeabilization has been highlighted, possibly due to the permeabilization of the inner mitochondrial membrane by the nsPEF application.

nsPEF for liposome drug delivery systems

Due to the present research activity on the use of electroporation on cells for different medical applications and due to the similarity of the cell and liposome membrane composition, recently the attention is going on the use of liposomes. In detail the ability of nsPEF to interact with small internal structures has been the starting point for investigations of nsPEF applicability for drug delivery using liposomes of small dimensions with respect to the cells [Tekle et al., 2005, Allen and Cullis, 2013]. The use of nsPEF for potential drug delivery applications can be a promising technique (Fig. 2.8) because it might allow the controlled release of drugs encapsulated in a nanocarrier (e.g. liposomes) by the application of an appropriate electrical stimulus that allows a controlled

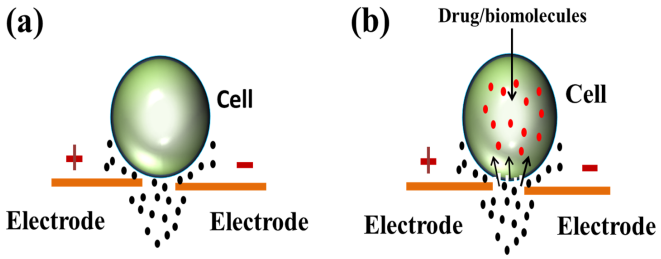

Figure 2.8: Drug delivery inside a single cell **(a)** mediated by permeabilization of the cell membrane next to the application of an electric field in a very small region of the cell membrane area **(b)**.

release and uptake of drugs from liposome to the cell, thanks to the accumulation of charges on both sides of the plasma membrane and consequently the formation of an induced transmembrane voltage (TMP) which causes the pore formation and the drug uptake.

Indeed, electroporation it has been applied to nucleic acid delivery against cancer, either by using PEG-coated silica nanoparticles with opposite polarities to enhance gene transfection [Kim and Lee, 2011] or by using liposomes loaded with exogenous oligonucleotides [Wang et al., 2010] in order to obtain the drug release.

As will be detailed explained in the chapter 7, the main concern about the use of the nsPEF for drug delivery applications is the difference between the liposome dimension (nanometer range) and the cell (micrometer range). Firstly, vesicles larger than 500 nm of diameter could be recognized as a pathogen agents by the immune system, while at the same time liposomes of smaller size would require an higher electric field intensity to the one needed to porate the cell membrane while compromising cell viability. Moreover, it is also important to underline how not only the dimension but also the liposomes composition is important when an immunologic response is generated [Perrie et al., 2001, Watson et al., 2012]. The classical electroporation serves of rectangular pulses of micro or millisecond duration with amplitudes in the range of kV/cm. These pulses have a frequency content in the range of kHz which will be able to destabilize the cell membrane but not the one of nanometer liposomes. Taking a look to the Fig. 2.9 it can be noticed how by the application of a 10nsPEF the TMP accross the cell and liposome membrane becomes comparable leading to a possible simultaneously electroporation of both membranes. This aspect will be fully explained in the chapter 7 where a proof of concept of the liposomal drug delivery system mediated by nsPEF is

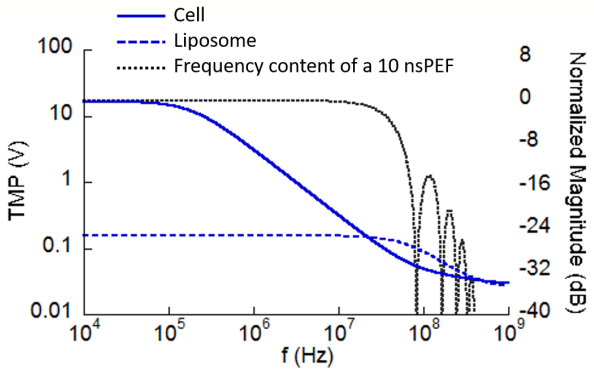

Figure 2.9: Proof of concept of liposomal drug delivery systems mediated by nsPEF.

given thanks to dosimetric models.

Moreover the engineering of a 10 nsPEF exposure setup (chapter 8) will be presented and preliminary experiments of electroporation on liposomes population will be discussed.

2.4 Low intensity magnetic fields for a controlled drug release

The applications previously discussed on the use of nsPEF for medical treatments, have the disadvantage of being limited to the penetration of the electric field thinking about the treatment of a deep tumor or inflammations, due to the difficulty to reach deep tissues. This would result in using invasive instrumentation like needles. In this case the magnetic field has the major advantage of to easily penetrate in the human tissue without loosing any transmission power.

Due to this, recently with the technological progress the use of magnetic field to treat inflammatory and neuronal diseases, therapies and drug delivery systems for nanomedicine has considerably increased [Ross, 2013, Rodzinski et al., 2016]. The progresses in nanomedicine ranges from nanoparticles for molecular diagnostics, imaging and therapy to integrated medical nanosystems [Nune et al., 2009, Shi, 2009] to act at the cellular level inside the body.

The advantage of using a magnetic field relies on the different nature that the magnetic response can take, which can be a magnetic guidance under a permanent magnetic field, a temperature increase when an alternating magnetic field is applied, or both of them. Furthermore, in medicine there is the possibility of performing magnetic resonance imaging, and hence to associate diagnostics and therapy within a single system, the so-called theranostic approach [Yang et al., 2011].

In recent years, a great number of investigations have been reported on exploiting possible role of magnetic nanoparticles (MNPs) in enhancing magnetoliposomes delivery of the drug. In most cases hybrid liposomes composed of thermo sensitive phospholipids and magneto-heating mediators, such as iron oxide MNPs, were shown to have enhanced release of a model drug when exposed to an external alternating current magnetic field (AMF) and negligible release without exposure to an AMF [Pradhan et al., 2010, Preiss and Bothun, 2011]. The enhanced release was essentially attributed to the to the magnetocaloric effect resulting in the liposome phase transition [Plassat et al., 2011].

The heat generation efficiency of MNPs heavily depends on the particle size and frequency of external AMF, in particular, when exposed to appropriate magnetic fields of proper strength (1-10 kA/m) and frequency (10-100 kHz), MNPs embedded into liposomes are able to convert magnetic field into heat, either from hysteresis losses or from Neel or Brownian relaxation processes [Guardia et al., 2012]. The magnetically induced heat is transferred to the entire magneto-carrier causing temperature increases from 25 °C to tolerable hyperthermia (41-46 °C) with structural changes in the lipid bilayer (that is designed to shift from a gel to liquid phase at a characteristic transition temperature, Tm) which may act as a smart trigger for the drug release [Yatvin et al., 1978, Pradhan et al., 2010, Preiss and Bothun, 2011].

Despite the heat generation is the main pattern of AMF energy consumption, a magnetic field can also induce vibration or rotation of iron oxide particles, hence the oscillating MNPs can mechanically damage membrane of nanoscale actuators (e.g. liposomes). In particular, researchers [Nappini et al., 2010, Spera et al., 2014] proposed an alternative mechanical explanation based on MNPs oscillation induced by external AMF: MNPs motions in AMF could improve the bilayer permeability and it could contribute to the magnetocaloric effect, allowing for cargo release. This hypothesis arises from the finding that AMF-induced oscillation of MNPs was proved to be able to mechanically damage cancer cells in vitro [Cheng et al., 2014]. The magneto-mechanical effect

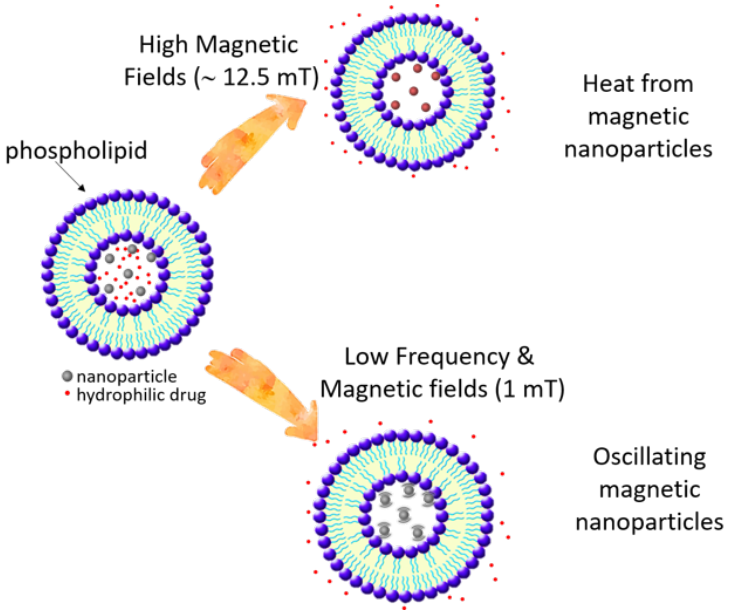

Figure 2.10: Magnetoliposomes drug delivery process

produced by the oscillation of the MNPs was extensively addressed to find efficacy for trigger a mechanical disturbance to the cells and therefore inducing cell death in a non-chemotoxic way, but it could find application also for the control of drug release. In order to support this purpose, researchers have deliberately selected field frequencies and strength that are several orders of magnitude lower than those needed for the magnetic thermal approach [Nappini et al., 2010, Spera et al., 2014]. It will allow to reduce the heating contribution of the MNPs in the AMF to negligible levels with the objective to evaluate the peculiarities and advantages of a non- non-heating action of MNPs in AMF in the drug delivery control. Magnetic guidance is typically obtained by focusing an extracorporeal magnetic field on the biological target during the injection of a magnetically responsive nanocarrier. This concept has demonstrated great potential in experimental cancer therapy because of improved drug accumulation inside solid-tumor models. Nanosystems for such a therapeutic approach can be magnetoliposomes (Fe_3O_4 or maghemite (Fe_2O_3) nanocrystals encapsulated in liposomes) [Plassat et al., 2011].

An example of this technique can be, as reported in [Hoare et al., 2011], a composite membranes containing thermoresponsive nanogels and magnetic nanoparticles that

enable on-off drug delivery on de-swelling or swelling of the polymer.
Not only for the drug delivery, an AMF can also remotely regulate protein production, as insulin, by using a modified temperature-sensitive channel (TRPV1) decorated with iron oxide nanoparticles [Stanley et al., 2012]. Moreover, some studies suggested that magnetic fields of low intensities (A/m) are a good trigger to control the releasing of the drugs [Nappini et al., 2010, Spera et al., 2014] but without heat generation. Via the application of an external magnetic field, the idea is to induce a mechanical stress on the liposome membrane, due to MNPs oscillations, in order to obtain the drug release (Fig. 2.10). In Spera et al. [Spera et al., 2014] an experimental study is reported concerning the exposure of HSPC liposomes loaded with magnetic nanoparticles to an AMF of 60 A/m of intensity. A 20 % of the fluorescent dye release is detected up to 9 hours of exposure due to the magnetic field application.
In the chapter 5 of this Ph.D. thesis, experiments on magnetoliposomes will be presented both applying an AMF or pulsed electromagnetic fields (PEMFs) considering different intensities (up to 100 μT).
Besides, starting from an existing exposure system consisting of two coaxial magnetic coils of square shape that can release magnetic fields of low intensity (≤ 100 μT), and based on the experimental results, we numerically performed a new magnetic exposure setup consisting of two squared Helmholtz coils, by analyzing all parameters involved to reach a magnetic field with intensity in the order of mT in a frequency range between 1-20 kHz (see chapter 6).

Chapter 3

Electromagnetic fields and protein interaction

3.1 Introduction

One of the major challenges in medicine, is the accurate measurement of cells signals in order to possibly prevent the upcoming of inflammations or serious illnesses as cancers or cardiac disorders. For this reasons, researchers started to perform methods to measure protein biomarkers, cells, and pathogen agents in biological samples. A number of new diagnostic platforms have recently been developed to measure biomolecules and cells with high sensitivity that could enable early disease detection or provide valuable insights into biology at the molecular level [Cheng et al., 2006, Wulfkuhle et al., 2003]. Fluorescent-protein biosensors have become an important tool as reagents to extract data from living cells which express parameters concerning some upcoming molecular processes related to illnesses or stresses (Fig. 2.10). Recent applications of fluorescent-protein biosensors to biological problems have provided a foundation for their use in biotechnology [Senutovitch et al., 2015]. This kind of biosensors evolved by combining sensitive fluorescent dyes with proteins in order to monitor specific physiological events such as production of metabolites, changes in various ion concentrations, and the dynamic interaction of proteins. Fluorescence-based reagents have been used extensively to elucidate and quantify fundamental biological processes within and between cells both in vitro [Giuliano et al., 1995, Zhang et al., 2002] and in vivo [Provenzano et al., 2009, Niesner and Hauser, 2011].

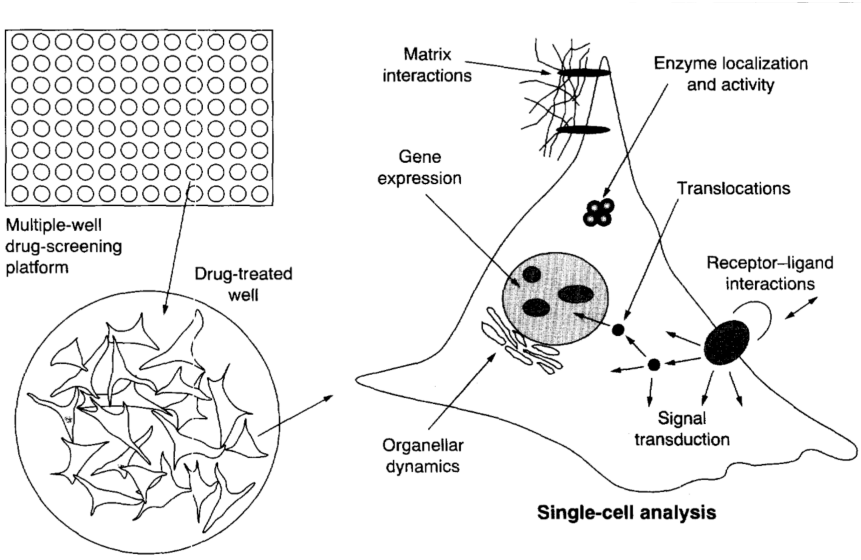

Figure 3.1: Fluorescent-protein biosensors and high-content screens in drug discovery. A multiple-well drug screening platform containing living cells is treated with a combination of drug types and concentrations. In figure referring to a the single-cell level different examples of the processes that can be measured with fluorescent-protein biosensors are reported.

In order to detect protein signaling a fluorescent marked is linked to the protein sending fluorescent signals in correspondence of the occurring of a biological effect.
Some recently described fluorescent protein biosensors designed to report chemical events occurring at or near the plasma membrane [Gonzalez and Tsien, 1995]. Besides fluorescent-protein biosensors have become powerful tools when applied to the processes involved in cytoplasmic signal transduction as for example the identification of the cAMP involved in converting transient signals into long term gene expression within the nervous systems [Hempel et al., 1996].
Proteins have the role to mediate the chemical reactions within cells. When converted to sensors proteins have the potential to report not only the dynamic distribution of specific reactions but also data concerning reaction kinetics and protein interactions. One way to define the activity of proteins is through the environmental changes that occur either internally or on their surface, including binding to other proteins [Giuliano et al., 1995].
Not only as detector but also as mediator of chemical reactions, proteins respond to

external stimuli by enhancing or decrease their activity and their interaction with living cells [Wetzel et al., 2001, Capelli et al., 2017]. In the next paragraph a briefly overview will be given about the exposure of proteins to electromagnetic fields and their role in biological effects.

3.2 Protein activation from Electric or Magnetic fields

The enhancing of enzymes activity under specific physiological conditions or under external stimuli, represent the proteins response and their eligibility to be used as drug target or as illnesses sensors.
Recently, researchers investigate the effects of EM fields on intra-cellular and transmembrane proteins exposed to nanosecond pulsed electric fields (nsPEFs) [Beebe, 2015] or low frequency low energy pulsed electromagnetic fields (PEMFs) [Varani et al., 2002, 2008, Capelli et al., 2017].

PEMFs action for medical treatments

Recently, it has been highlighted that different physiologic systems seem to be influenced by PEMFs exposure. Many studies have aimed to identify the biophysical stimulation induced by PEMFs as potential alternative to the pharmacological treatments in several inflammatory related diseases [Cadossi, 2011, Di Lazzaro et al., 2013]. It has been reported that PEMF exposure could act on modulating cartilage and bone metabolism, stimulating chondrocyte and/or osteoblast cells proliferation [Chalidis et al., 2011] reporting a positive effect in the treatment of fracture healing [Lin and Lin, 2011]. The action of PEMFs has been also investigated in various pathological conditions such as in cancer cells where the electromagnetic fields with intensity around 3 mT were able to reduce tumor growth and proliferation for breast cancer cells up to 60 minutes of stimulation at low frequency of 20 Hz, growing its effects after three days of daily treatment [Crocetti et al., 2013]. Nevertheless PEMF therapy significantly reduced postoperative pain and narcotic use in the immediate postoperative period by a mechanism that involves endogenous IL-1β in the wound bed [Rohde et al., 2010].
Not only on cancer cells or in bone healing but also in neurological diseases the use of PEMFs is widely spread to map the brain human activity and could affect almost all cerebral functions such as motor control, sensory perception, cognitive activities [Di Lazzaro et al., 2013]. The molecular pathways underlying the previous medical treatments are all related to the involvement of a transmembrane protein of the adenosine receptors (ARs) family.

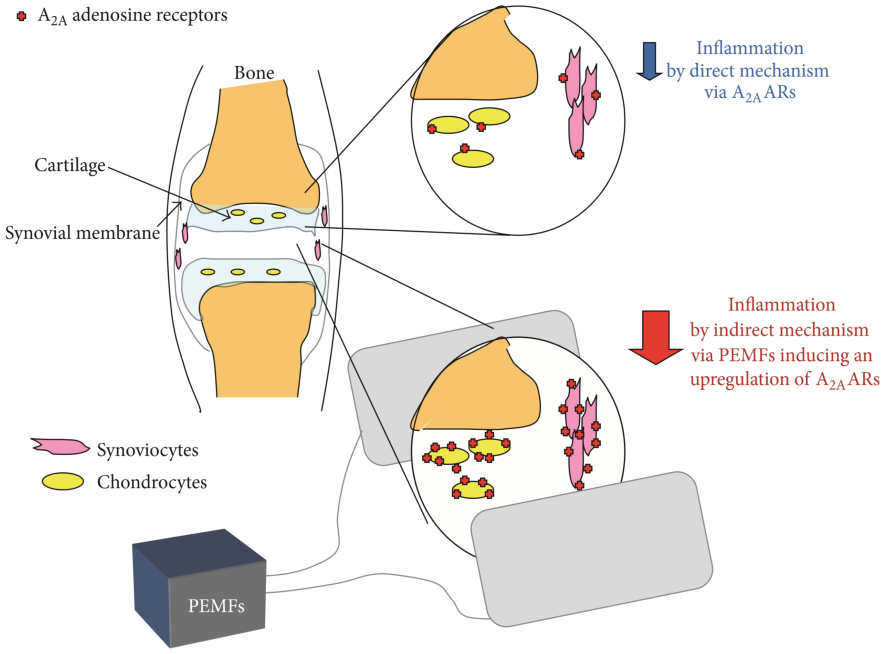

Figure 3.2: Representation of the adenosine A_{2A} proliferation under PEMFs action by enhancing the anti-inflammatory effect.

Proteins under the PEMFs action

Increasing evidence suggests that the beneficial effects of PEMFs on neurological system are mediated by the modulation of adenosine receptors (ARs), specifically increasing the expression of A_{2A} subtypes [Varani et al., 2017]. The adenosine receptor A_{2A} is an important G-coupled protein regulator of neurotransmission signals released from cells next to a metabolic stress. From a study of Varani et al. [Varani et al., 2002, 2008] it has been experimentally proven how the application of low intensity magnetic field in the range of 0.5 - 3.5 mT is able not only to enhance the ant-inflammatory effects of the adenosine receptor A_{2A} on neutrophilis cells but also to increase its enzymatic activity and a reduction of the superoxide anion has been reveled probably due to the density increase of the adenosine receptor on cells surface when exposed to the magnetic field action (Fig. 3.2).

nsPEFs applied on proteins

Not only magnetic field but also electric field pulses (PEF) may affect protein response and its activity. It has been experimentally proven how pulsed electric fields of 3.6 MV/m with duration higher than 150 μs are able to induce secondary struc-

tures changes and inactivation of protein structures as lysozyme [Zhao et al., 2007] and pepsin [Yang et al., 2004]. However, studies of the effect of PEF on protein structure are limited in number [Van Loey et al., 2001], although PEF treatments of soybean protein isolates [Li et al., 2007] purified horseradish peroxidase and pectin esterase [Zhang et al., 2006] have shown interesting effects on protein denaturation, aggregation and structure depending on the protein examined.

As mentioned in the previous chapter, effects related to conventional electroporation with long pulse duration (μs - ms range) and and low electric fields (up to 1 MV/m) are mostly focused on the lipid bilayer of the plasma membranes. Nevertheless, electroporation pulses with short duration (ns) and high intensity (MV/m) may have some effects on intracellular membranes and could be able to directly interact with internal cell organelles (as nucleus, endoplasmic reticulum, mitochondria,etc.) [Esser et al., 2010]. This was initially hypothesized and demonstrated by breaching vesicular membranes in human eosinophils [Schoenbach et al., 2001]. Distinct effects of nsPEFs have also been observed to rapidly and transiently release Ca^{2+} from the intracellular cavity [Vernier et al., 2003b, Semenov et al., 2013].

The correlation of nsPEFs and intracellular structures is related to their frequency content. Indeed a 1 ns pulse has a spectral frequency content of 1 GHz and thus it appears that high frequency components, residing in the rapid rise and fall times of ns pulses, maximize electric field interactions with intracellular structures [Schoenbach et al., 2001, Beebe et al., 2012]. In the study of Beebe [Beebe, 2015], it has been evaluated how nsPEF can act not only on the membrane permeabilization but also on proteins. They analysed the dissipation of the mitochondria membrane under nsPEF actions directly related to the Ca^{2+} presence. Since, the Ca^{2+} dependent events require proteins, to determine if nsPEFs could have direct effects on proteins, they showed the inactivation of the C-subunit of PKA, a prototype for all protein kinases, which have highly conserved catalytic mechanisms. This inhibition was correlated to the inhibition of the mitochondria membrane and thus indication of the nsPEFs effects on protein. Moreover, by Pakhomov et al. [Pakhomov et al., 2014] the effects on CHO cells that express actine protein have been presented, highlighting cells swelling and actin disruption when an electric field of 600 ns pulses and 1.92 MV/m of intensity and a frequency of 2 Hz are applied as shown in Fig. 3.3. Also an experimental study has been conducted on different type of superoxide dismutase enzymes, the SOD1 [Shi et al., 2015], to evaluate the behavior under electric field of physiological strength (10^4 V/m), a

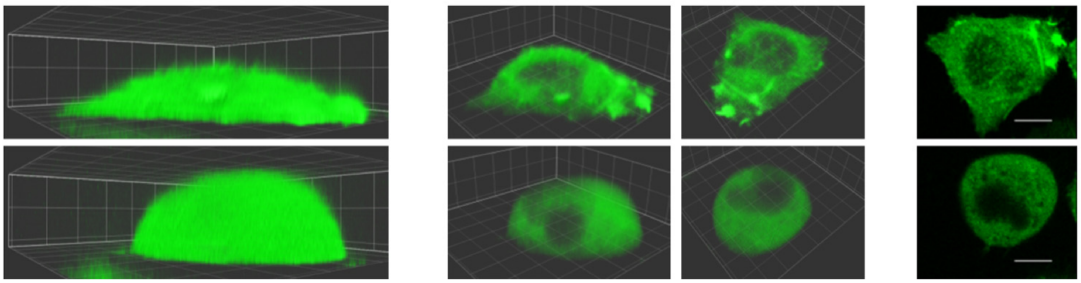

Figure 3.3: CHO cells exposed to 4 pulses at 19.2 kV/cm (600 ns,2 Hz).The side views (left column) are intended to demonstrate cell reshaping by nsPEF. Two different 3D views (center columns) and one X-Y slice (right) were selected to provide the best observation of the structured actin.

monomerization and partial unfolding was reached only for the A4V-SOD1 protein.
Not only through experimental setup but also using molecular dynamics simulations, the protein interaction with electric fields have been explored. Through the simulation of a "virtual" experiment, MD simulations give the possibility to observe the electric field action on microscopic structures in an accurate and rigorous way. In different simulation studies with MD, high intensity pulses were shown to disrupt secondary structures of proteins as myoglobin, the soybean hydrophobic protein and the insulin β-chain [Marracino et al., 2013b,a, Singh et al., 2013, Budi et al., 2005]. The loss of secondary structures suggest changes in the protein activity and it means that the protein differs from its physiological condition. The changes predictable using molecular dynamics simulations could give information in order to explain the protein response and the interaction mechanism when a protein, or in general a biological sample, undergoes to an external forces. Indeed, Wang et al. [Wang et al., 2014] investigated the effects of strong electric field applied on the insulin enzyme by the means of MD simulations. They explored electric field with strength from 1.5 to 6x10^8 V/m, highlighting a disruption of secondary structure and a loss of hydrogen bond for electric field higher than 2.5x10^8 V/m.
Molecular dynamics (MD) simulations have been used during my research project both concerning the application of nsPEFs on the superoxide enzyme and studying the action of a magnetic field on the adenosine A_{2A} receptor as will be discussed in the 10 and the 9 chapter respectively. In the next chapter a brief overview will be given regarding MD simulations in order to understand one of the adopted modeling approach.

Part II

Modeling approach: from molecular dynamics simulations to microdosimetric models

In this part, the methodology used in the present Ph.D. research project will be reported.
Usually to perform a modeling analysis, different methods can be adopted depending on the levels of the biological complexity going from the microscopic one of atoms and molecules, up to the macroscopic one of the whole organism, going through subcellular structures, cells, tissues, organs and systems. The interaction of the EMFs with nanosystems can occur at any of these biological levels, and to model all the possible interactions different and specific tools are needed.
In the following chapter, a multiscale approach will be presented from the molecular dynamics simulations level (nm scale) to the microdosimetric models for the cellular level analysis (up to mm scale).
Theoretical methods and computational approaches applied to predict the behavior of biological compound at the atomic level are all part of the molecular modeling category. In this case, Molecular Dynamics(MD) simulations provide atomic details of the structures and motions of a classical biological structures allowing the computing of its structural, dynamic and thermodynamic properties. By applying the Newton's equation of motion, from given initial conditions the evolution of the system in time can be predicted. In this context, in the following chapter the integration algorithms and the different force fields usually used in MD simulations will be reported to understand the modeling used for the study of the electromagnetic fields action on protein structures, presented in the Part V.
Furthermore, when dealing, with nanosystems as liposomes interacting with biological cells the mesoscale and finite element method have to be adopted. Thanks to these methods is possible to perform a dosimetric analysis to assess the amount of the EMF induced in a target structure in different exposure conditions. On these aspects is focused the section 4.3 in the following chapter, to explain the method used in the Part III and Part IV for the modeling study of the electromagnetic fields effects on cell and liposomes under the EMFs action.

Chapter 4

Modeling Methods

4.1 Introduction

In order to understand and possibly predict the interaction mechanisms between electromagnetic fields and nanosystems interacting with the human body, modeling tools can be adopted. By Apollonio et al. [Apollonio et al., 2013], a schematic representation of possible multiscale methodologies, for modeling the interactions between electromagnetic fields and a biological system, has been proposed (see Fig. 4.1). On the scheme reported in Fig. 4.1, based on the biological effects (right side) different methods (left side) can be used to predict possible effects and functions evidenced by experimental investigations (e.g., in-vitro, in-vivo, and on humans) when cells are exposed to exogenous EM fields. Different levels of biological structures can be modeled, such as molecules, cells, tissues, organs, and organisms as represented in details at the right branch of the Fig. 4.1 with the inclusion of the dimension. Regarding the modeling methods (left side) the inputs for the smallest models depends on the quantities induced in the upper level, while for the biophysical one the functionality of a level is related to those of all the lower levels.

Now, depending on the nanosystem that we want to study and depending on its interactions with cells dimension, in this chapter two different methodologies will be presented: molecular dynamics simulations and microdosimetry models.
To analyze at molecular level (dimension up 10^{-8} m) possible interactions, molecular dynamics (MD) simulations provide atomic details of the molecular structures and hence allow for computing dynamic and thermodynamic properties. The first section

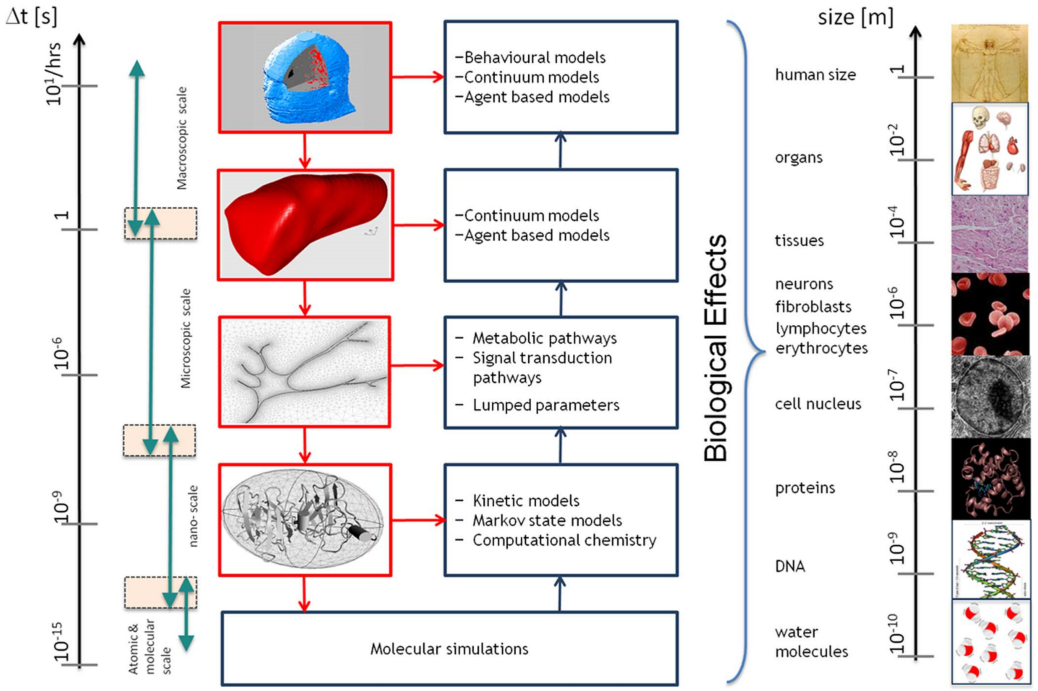

Figure 4.1: Scheme of a multiscale methodology for modeling the interaction between an exogenous EM field and a biological system.

of this chapter will be dedicated to a general overview of the molecular dynamics algorithm to understand its functions and potentiality to predict the behavior of biological molecules.

Moreover, when cells complex want to be explored MD simulations because of the limit in the computational costs depending on the structure size (ns time and up to nm) cannot be used, but microdosimetry models (range dimensions from 100 nm to μm) can be adopted to achieve information of dose dependent effects generated by the application of an exogenous electric or a magnetic field. The microdosimetry models permit the quantification and the assessment of fundamental parameters involved in biological processes in order to understand the basic mechanism of the phenomenon (as electroporation or magnetic field action) and becomes a predictive tool that could be use to set the experimental parameters.

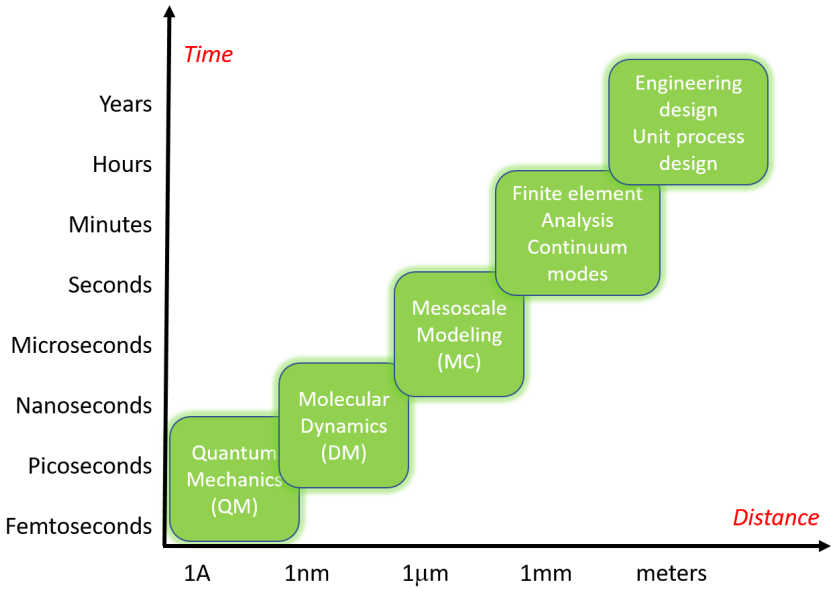

Figure 4.2: Molecular structure investigation techniques from the femtosecond to the continuous range.

4.2 Molecular dynamics simulations

The molecular structures can be investigated with different techniques, measured essentially according to the degree of accuracy and size of microscopic systems treated. The choice of the appropriate technique depends on the particular application, and then by the ability to produce reliable results. There are several methods based on the analysis time and the size of the molecule (Fig. 4.2). The use of quantum mechanical (QM) methods allows the explicit treatment of electronic distribution of microscopic systems, essential in the rigorous description of processes such as enzymatic reactions and mechanisms of binding / unbinding. The quantum methods represent a fundamental tool for a rigorous study of the electronic transitions of the underlying biochemical phenomena, such as the process of binding / unbinding or enzymatic reactions. The main disadvantage is that it does not allow the study of complex systems such as the investigation of biochemical reactions; analysis QM is only applied to the reaction center isolated, without considering the whole protein and the environment in which it is immersed, which is crucial in the re-activity of chemical processes [D'Alessandro et al., 2004, Amadei et al., 2007].

Instead, the molecular dynamics is used to model and study the physical phenomena from a realistic point of view and provide a dynamic framework at the microscopic level, laying the foundation for the theoretical treatment or for the interpretation of experiments. It models the motion of the group of particles (e.g. atoms) present in the simulation box by solving the classical Newton's equations of motion. Firstly, as input conditions the energy potential is expressed in function of the velocities and positions of all atoms present in the system. Then the force on any atoms is computed (Eq. 4.1) by calculating the force between non-bonded atom pairs (Eq. 4.2).

$$F = -\nabla V(r) \tag{4.1}$$

$$F_i = \sum_{i \neq j} F_{ij} \tag{4.2}$$

Subsequently, the update of the configuration is done by solving the Newton's equation of motion (Eq. 4.3) with a finite difference algorithm:

$$\vec{r}_i(t + \Delta t) = \vec{r}_i(t) + \vec{v}_i(t)\Delta t + \frac{1}{2}\vec{a}_i(t)\Delta t^2 \tag{4.3}$$

Finally, the output are written as velocities, positions, pressure and temperature of the system. It's the most widely used method to do simulation in condensed matter physic. The MD performs a calculation and the deterministic trajectory is uniquely determined by the form of the potential energy function that describes the interactions between the atoms in the system. The simulations always require the definition of a model (force field) for the interactions between the various components of the system. Each simulation requires a set of initial coordinates and optionally the initial velocity of the particles involved. Before the start of a simulation, the system must be defined and must be loaded with an empirical force field. Empirical force fields, indeed, are collective of several energy terms to describe the interactions between atoms (bonded like energy of bonds, valence and dihedral angles, etc.; non bonded as electrostatic and van der Waals terms), implemented to reproduce the structural properties of biomolecules and parameterized accordingly. All information associated with the force field are static in the sense that remain unchanged during the generation of the MD trajectories and include: type of atom, mass and charge, potential function, the parameters of binding

and non-binding, constraints.
The Protein Data Bank (PDB) provides the initial coordinates and the 3D structure of the molecular system that needs to be simulated; it is an archive of three-dimensional structures of biomolecules obtained from experimental techniques. The pdb files for a given molecule provides the atomic coordinates, information on the structure of primary and secondary data on the experimental techniques applied and references. In many cases, the 3D structure is not available or not suitable for the problem being treated. In this case, molecular modeling techniques are applied to provide the topology (e.g. connectivity chemistry) as input to run an MD simulation to explore the conformational changes of a complex molecule and map the biochemical phenomena at the molecular and atomistic level. The initial speeds are generally randomly assigned by the Maxwellian distribution, relative to the desired temperature ($\sim$ 300 K). The main actions are common to all protocols, such as the preparation of data, for an MD run, by assigning the initial coordinates and the initial speeds. Then the heating of the system goes up to the desired temperature, associated with a short dynamic equilibrium achieving balance for the simulation is stable and free from unwanted fluctuations. This step takes from tens to hundreds of ps. Finally production of the trajectory and its analysis is done.
This method suffers from some limitations, such as only allows classical description of the motion of the particles thereby not allowing the study of phenomena such as quantum processes of electron transfer or training / breaking of bonds. Another limitation is related to the electrons that are in the ground state, preventing an analysis of the electronic motions to finally allow a maximum observable time scale of the order of hundreds of ns. Molecules in MD simulation by default also lack polarizability. Although the effects of polarizability can be introduced by various methods such as adding virtual sites (Drudeparticles) or effective pair potential,the treatment of polarizability is often ignored in order to reduce computing cost. Nevertheless several physical phenomena can be described with a good approximation neglecting the electron wave functions.
Despite its limitations, MD opens the way to a better understanding of the relationship between molecular structure and biological function of the essential components in the vital processes such as proteins and peptides.
In the next section an overview of the force field, boundary conditions and temperature/pressure ensemble will be given to understand parameters we used to perform our simulations.

4.2.1 Integration Algorithms

One of the most used integrator in molecular dynamics simulations is the Velocity Verlet algorithm [Verlet, 1967].

$$r(t + \Delta t) = r(t) + \Delta t \mathbf{v} + \frac{\Delta t^2}{2m}\mathbf{F}(t) \tag{4.4}$$

$$v(t + \Delta t) = v(t) + \frac{\Delta}{2m}\left[\mathbf{F}(t) + \mathbf{F}(t + \Delta t)\right] \tag{4.5}$$

The equation 9.2 and 9.3 represent the update of positions and velocities choosing a Δt small enough, leading to an overall better approximation of the whole integration process. As lower limit one can consider highest frequency proper of the system, namely the vibrations of bonds involving hydrogen atoms in solvated biological macromolecules. The bond stretching frequency of an O-H bond is typically about 10^{14} Hz, so the average period would be of the order of 10 fs [Schlick et al., 1997]. This limits the time-step tobe taken in MD simulations to about 0.5 fs. For our simulations concerning the magnetic field applications on the adenosine A_{2A} receptor we employed the velocity verlet algorithm as will be explained in the chapter 9.
Moreover, to increase the time step to a typical value of 2 fs usually algorithms (SHAKE [Ryckaert et al., 1977], RATTLE [Andersen, 1983], LINCS [Hess et al., 1997], SETTLE [Miyamoto and Kollman, 1992]) are employed to constrain all covalent bonds,i.e. the distance between mass points is maintained constant. In general, the algorithm is constructed by following procedures:

- choosing novel unconstrained coordinates (internal coordinates)
- introducing explicit constraint forces
- minimizing constraint forces implicitly by the technique of Lagrange multipliers or projection methods.

These approximations are acceptable as these bond vibrations can be considered uncoupled from all other vibrations in the system so that the dynamics of the system is not altered.
For the simulations concerning the enzyme superoxide dismutase (SOD1) exposed at nsPEF (see Ch. 10), we used the leapfrog integration algorithm with an integration time-step of 2 fs. With the leapfrog algorithm positions and velocities leap over each

other. The velocities are updated at half time steps and leap ahead the positions. The positions (Eq. 4.6) and velocities (Eq. 4.7) can be obtained from:

$$r(t + \Delta t) = r(t) + \Delta t \mathbf{v_i} \left(t + \frac{\Delta t}{2} \right) \tag{4.6}$$

$$v \left(t + \frac{\Delta t}{2} \right) = \mathbf{v_i} \left(t - \frac{\Delta t}{2} \right) + \frac{\Delta t}{m_\mathrm{i}} \mathbf{F_i}(t) \tag{4.7}$$

4.2.2 Force fields and boundary conditions

As mentioned in 4.2 in order to compute forces MD simulations require a potential energy function, which describes the interactions among all the atoms in the system. Once the potential energy of the system is known, given the coordinates of a starting structure and a set of velocities, the force acting on each atom can be calculated. A force field is characterized by a specific functional, implemented to reproduce the structural properties of biomolecules and parameterized accordingly. The force field it is composed by a set of equations, the so-called potential functions, which are used to generate the potential energies and their derivatives (e.g. the forces) correlated with a set of parameters empirically tuned to reproduce the properties of biomolecules. A general potential energy function,commonly used in the most know force fields,is:

Force fields

$$U_\mathrm{total} = U_\mathrm{bond} + U_\mathrm{angles} + U_\mathrm{dihedrals} + U_\mathrm{nb} \tag{4.8}$$

These four contributions account for bonded and non-bonded interactions. The first three terms of Eq. 4.8 define the bonded interactions corresponding to two (stretching), three (bending), and four (torsion) body interactions, respectively.

$$U_\mathrm{bond} = k_b \frac{1}{2} \, (l - l_0)^2 \tag{4.9}$$

$$U_\mathrm{angles} = k_\theta \frac{1}{2} (\theta\text{-}\theta_0)^2 \tag{4.10}$$

$$U_\mathrm{dihedral} = \sum_n v_n \frac{1}{2} (1 + (-1)^{\mathrm{n}+1} \cos(n\phi - \psi_\mathrm{n})) \tag{4.11}$$

These interactions are represented by harmonic potentials for the bond lengths b (Eq. 4.9), for the bond angle θ (Eq. 4.10) with k_b and k_θ their harmonic force constants, for the dihedral angle ψ (Eq. 4.11) with n, ψ_n and v_n the torsion, multiplicity, phase angle and barrier height respectively. The final term of the Eq. 4.11 is meaningful of the interaction between non-bonded atom pairs. This term is split into 1-body, 2-body, 3-body, ...subterms. Interactions between particles separated by more than three covalent bonds are usually represented by two components: by Coulomb's law for the electrostatic interactions (Eq. 4.12) and by a Lennard-Jones potential for the Vander Waals interactions(Eq. 4.13). The Coulomb potential is described by:

$$U_{qq} = \sum_{i<j} \sum_{j} \frac{q_i q_j}{4\pi\epsilon_{ij} r_{ij}} \tag{4.12}$$

where the q_i is i^{th} atomic charge, r_{ij} is the distance between the i^{th} an j^{th} point charges, and ϵ is the permittivity of the medium between this two. The Lennard-Jones potential(Eq. 4.13) can be written as:

$$U_{vdW} = \sum_{i<j} \sum_{j} 4\pi\epsilon_{ij} \left[\left(\frac{\sigma_{ij}}{r_{ij}} \right)^{12} - \left(\frac{\sigma_{ij}}{r_{ij}} \right)^{6} \right] \tag{4.13}$$

where σ_{ij} and ϵ_{ij} are the collision diameter(the finite distance at which the inter-particle potential is zero) and the well depth respectively. The Lennard-Jones potentials describe the van der Waals (vdW) interactions, that differ from covalent and ionic bonding because they are caused by correlations in the fluctuating polarization of nearby particles.

In addition to the force fields, other parameters are included as values for atomic mass,Van der Waals radius, partial charge for individual atoms, equilibrium values of bond lengths, bond angles, dihedral angles for pairs. Popular force fields for MD simulations of biomolecular systems are AMBER [Cornell et al., 1996], CHARMM [MacKerell Jr et al., 1998],GROMOS [Oostenbrink et al., 2004] and OPLS-AA [Jorgensen et al., 1996]. In this work, we considered GROMOS45 force field [Oostenbrink et al., 2004] to model the SOD enzyme and the adenosine A_{2A} receptor (see Ch. 10 and 9, respectively).

Gromacs In order to compute MD simulations we used the software GROMACS [Hess et al., 2008] v. 4.6 and 5.1.

GROMACS is a versatile package designed for biochemical molecules like proteins, lipids and nucleic acids including a lot of complicated bonded interactions. It is the aim of GROMACS to provide a versatile and efficient MD program with source code, it is designed especially for the simulation of biological molecules in aqueous and membrane environments, and able to run on single processors as well as on parallel computer systems using MPI or threads. It is very fast due to algorithmic and processor specific optimization, typically running 3-10 times faster than many simulation programs. It is operated via the command line using file for input and output and provides calculation progress, a trajectory viewer, and an extensive library for trajectory analysis.

Boundary conditions

Anyway, due to computational limits, a typical simulated system contains hundreds of thousand of atoms, and hence is quite small compared to macroscopic matter. This means that, if the molecules are arranged in a cubic box, are latively great part of them will lie on the surface and will experience quite different forces from molecules in the bulk. Usually, periodic boundary conditions (PBCs) 4.3 are adopted to reduce the surface effects. PBCs are a set of boundary conditions which are often chosen for approximating a large (infinite) system by using a small part called a unit cell. In Fig. 4.3 the shaded box represents the system we are simulating, while the surrounding boxes are the exact copies of each particle in the simulation box. Even the velocities (indicated by the arrows) are the same. This arrangement is imagined to fill the whole of space. A result of this is that whenever an atom leaves the simulation cell, it is replaced by another with exactly the same velocity, entering from the opposite cell face. So the number of atoms in the cell is conserved.

Thermodynamics ensembles

Moreover, when a simulations is settled one of the most important parameter is the type of thermodynamic ensemble that can be chosen, with particular statistical characteristics and in statistical mechanics. Three important thermodynamic ensembles can be considered:

- NVE ensemble, a statistical ensemble where the total energy E of the system, its volume V and the number N of particles in the system are each fixed to particular values. The system must remain totally isolated (unable to exchange energy or particles with its environment) in order to stay in statistical equilibrium.

- NVT ensemble, a statistical ensemble where the energy is not known exactly but the number of particles N, its volume V , and the temperature T are maintained constant. The canonical ensemble is appropriate for describing a closed system

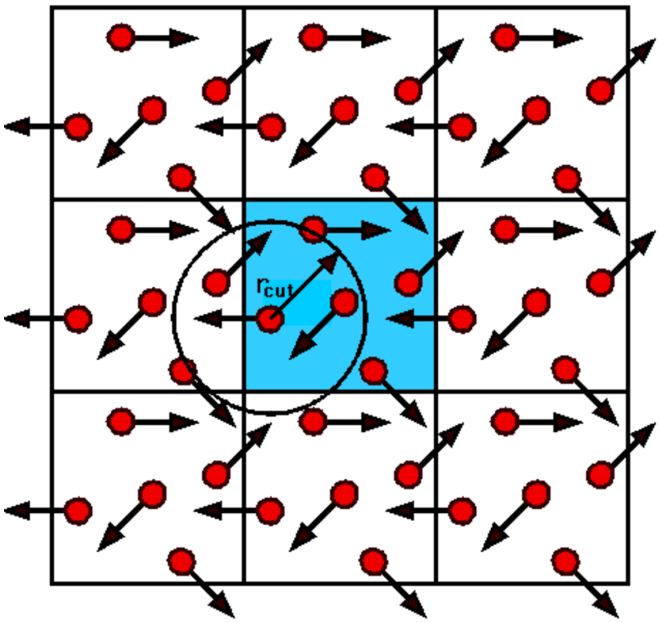

Figure 4.3: Schematic of PBCs. The simulation cell (central) is replicated throughout the space, forming an infinite lattice with images of atoms. In such scheme each atom interacts with all the other atoms of its cell and also with their images, thus this interaction is limited to the closest image of other atoms as shown by the blue dashed box.

which is in, or has been in, weak thermal contact with a heat bath.

- μVT ensemble, a statistical ensemble where neither the energy nor particle number are fixed. In this case the chemical potential mu, the volume V and the temperature T are specified.

- NPT ensemble, were the number of atoms N, pressure P and temperature T are constrained.

In this Ph.D. project an NVT ensemble has been used both for the electric (chapter 10) and magnetic fields (chapter 9) simulations.

4.3 Microdosimetry numerical models

As mentioned in the introduction to this chapter, when the final target that needs to be simulated has dimensions major than 100 nm, the MD simulations require high computational costs that are not affordable if you are not working on parallel computer

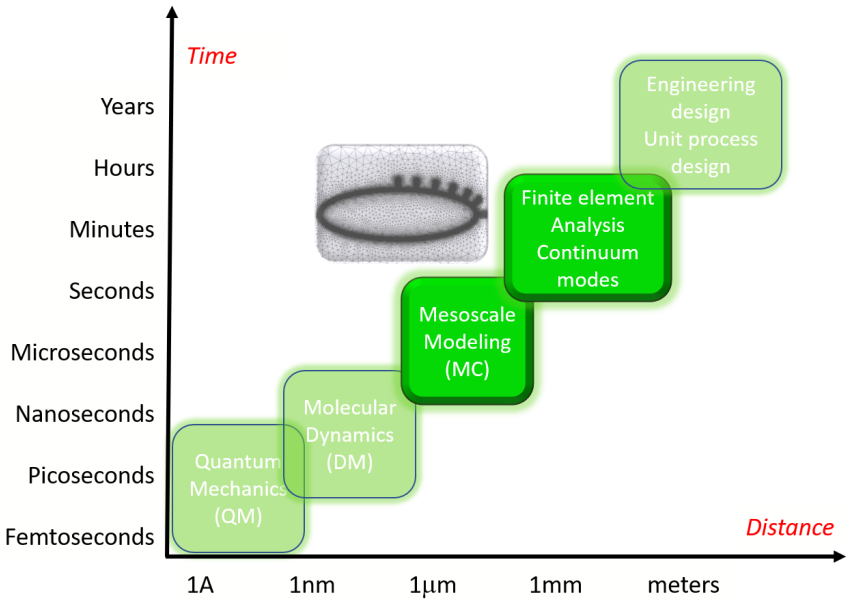

Figure 4.4: Molecular structure investigation techniques from the femtosecond to the continuous range.

clusters.

In this case to simulate the behavior of a biological system or for the design of electrical or magnetic exposure systems, mesoscale model and finite element models, including microdosimetry, can be adopted (see Fig. 4.4).

In recent times, the study of the amount of EMF that is absorbed by humans and the related effects has acquired more importance. In particular, the term dosimetry summarized all the techniques aimed to the assessment of the amount of the EMF induced in a biological structure in different exposure conditions; this assessment can be used both for prevention as well as for the study of the possible effects of electromagnetic fields and for the design of new applicators. Microdosimetry employs geometric and electric models of single cells and small cell or liposomes clusters under the action of an external force which can be electric, thermal or magnetic using circuital, analytically, or numerical approaches. Microdosimetry models permit to compute a dose dependent analysis to predict cells behavior before proceeding to the experiments setup.

Concerning the electroporation phenomena, as mentioned in the section 2.3 the actual mechanisms underlying the membrane electroporation caused by ultra-short electric pulses (nsPEF) is not yet fully understood and it has been shown that membrane rear-

rangement or even ruptures, fundamentally depend on the level of the electric potential induced across the cell membranes [Krassowska and Filev, 2007], referred to as transmembrane potential (TMP). Microdosimetric models are of fundamental importance when the interaction between an exogenous E field and biological matter is to be investigated [Apollonio et al., 2013, Gowrishankar et al., 2013]. Furthermore, the local E field applied to cells can be used to relate the observed effects of in vitro experiments to the macroscopic E "dose" delivered to the biological sample. In vitro research can be used as an initial test of the therapeutic efficacy of novel medical treatments. Microdosimetry is of major importance to hypothesize and quantitatively study plausible interaction mechanisms at the molecular level that take place in the cell membrane and the intracellular environment [Tarek, 2005, Hu et al., 2005, Marracino et al., 2013b]. Moreover, microdosimetry can predict the microscopic E-field threshold for an effect to occur and so can be useful as technological support in the design of pulse applicators and the choice of appropriate pulse generators for experiments. Moreover not only electric but also a magnetic field can be simulated using appropriate software to perform both the dose dependent analysis and to validate the project of an exposure setup as will be explained in the chapter 6.
The electromagnetic solution (EM) usually, when dealing with microdosimetric models, can be obtained either in time or in the frequency domain, turning back into time through the inverse Fourier transform, depending on the specific formulations for the boundary EM conditions at the cell interfaces. Indeed, as highlighted in [Kotnik et al., 2010], for a spherical cell, using the steady-state Schwan equation [Pauly and Schwan, 1959] as an approximation, is valid only for pulses longer than hundreds of μs, whereas a first order approximation [Pauly and Schwan, 1959] is possible for pulses longer than 1 μs. Moreover, when dealing with shorter E fields, or when the extracellular medium has a conductivity well below the range of physiologic values [Kotnik et al., 2010], a complete formulation of the boundary conditions, accounting for both conductivity and permittivity of cell compartments, needs to be considered [Kotnik et al., 2010].

Analytic models

Usually a microdosimetric model can be approached with an analytic, circuital or a numerical model. The analytic solutions are often used for single cell model or for simplest geometry. Analytic approaches were first developed in microdosimetric studies for electroporation and are still largely used since they provide simple solutions and allow the complete spatio-temporal characterization of the E field within different cell

compartments [Merla et al., 2011, Hu and Joshi, 2009, Hu et al., 2005, Schoenbach et al., 2004]. The main drawback is that only simple cell geometries can be considered without or with concentric organelles. The analytic solution is often used to validate numerical approaches for simplified geometries.

Circuit models

On the other hand, cell circuit models are very useful for rapid microdosimetric analyses since they are able to deal easily with different kinds of external E pulses. Circuit analyses on a wide frequency band (from a few Hz up to GHz) have also been performed allowing the definition of transfer functions of the cell response [Yao et al., 2009, Merla et al., 2012, Denzi et al., 2013, Ellappan and Sundararajan, 2005]. Moreover, such circuits provide the possibility of developing a relationship with more sophisticated physical and biophysical cell descriptions. The main assumption made by the different authors [Yao et al., 2009, Merla et al., 2012, Schoenbach et al., 2007, Croce et al., 2010, Ellappan and Sundararajan, 2005] is that the cell model, encompassing an extracellular medium, a membrane and an internal cytoplasm, shows a passive resistive-capacitance (RC) behavior for each compartment. The values of the RC elements of each cell compartment were calculated on the basis of their static dielectric properties and conductivities, as well as from their geometric characteristics (e.g. cell radius and membrane thickness). A five-layered cell configuration, including the nucleoplasm and the nuclear membrane, has been considered [Joshi and Schoenbach, 2000, Denzi et al., 2013, Yao et al., 2009].

Numerical models

Numerical solutions imply the discretization of the simulation domain into meshed grids of different shapes. The great advantage of such an approach is the possibility to calculate the electric or magnetic field distribution in cells of any geometry, as well as for small cell aggregates [Kotnik et al., 2010, Joshi et al., 2008, Pucihar et al., 2006, 2009]. In particular numerical approaches can be used to study non-concentric and complex shaped intracellular organelles. Besides, numerical approaches are necessary when dealing with realistically shaped cells, including cell organelles, and clusters of cells. Thus they are suitable for answering recent research trends of moving towards the tissue level and the sub-cellular level.

4.3.1 Microdosimetry numerical models

As described above, the need to solve complex problems, has suggested the development of a series of numerical methods for the evaluation of the induced Electromagnetic fields. The numerical methods can be divided in methods based on differential type techniques and methods based on integral ones. For the first case, it involves solving Maxwell's equations in the differential form, and the algorithms make a spatial discretization of the equations in the space region that has to be analyzed (and possibly also a time discretization if one operates in the time domain); the integral approach, instead, is useful when the starting point are the integral equations for the description of the electromagnetic quantities. For low-frequency situations, where the dimension of the biological body are small compared to the wavelength (i.e. $<$ 30 to 40 MHz for the human body), a quasi-static approximation can be introduced and this fact implies that some methods are based on simplified Maxwell's equations. Following, the main numerical methods used by the principal simulative software, are described:

- the method of moments (MoM) [Harrington and Harrington, 1996] has become more popular since the 1980s. The MoM it can be defined as "source method" since requires to discretize only the structure in question, not the free space surrounding the geometry. Boundary conditions do not have to be set and in terms of memory requirements, these are proportional to the size of the geometry in question and the required solution frequency. However, MOM methods are significantly computationally less efficient than volume-discretization methods (finite element method, finite difference method, finite volume method). Boundary element discretization typically give rise to matrices that require a storage and computational that will tend to grow according to the square of the problem size. Moreover, this method usually involve fields in linear homogeneous media. However, the MoM cannot handle electromagnetically penetrable materials, especially if the material is in-homogeneous, and requires the surfaces to be closed;

- the finite difference time domain (FDTD) method [Yee, 1966] is a time-domain method; the solutions can cover a wide frequency range with a single simulation run, it is partial differential equations based, that solves Maxwell's curl equations by directly modeling propagation of waves into a volume (cubical or parallelepiped with different dimensions) containing the biological body. The components of

electric E and magnetic H field are calculated in a specific manner on the surfaces of the single cell alternately with half-time steps. It is a very easy method to be implemented and the computation time limited, but it could be expensive in terms of memory occupation because of all the space discretized;

- the finite element method (FEM) [Jin, 2015] solve the Maxwell's differential equations in the frequency domain. By solving partial differential equations, a first challenge is to create an equation which approximates the equation to be studied and it needs to be numerically stable, in a way to not destroy the meaning of the resulting output. The finite element method is a good choice for solving partial differential equations over complex domains or when the desired precision varies over the entire domain. It divides the simulation space into mesh grids of small volumes of tetrahedral elements, making this method very suitable in modeling inhomogeneities and complex geometries. For each tetrahedral volume the field is approximated using linear extrapolation, starting from a sparse system equations matrix; the solution is given by the inversion of this matrix. The FEM can couple the EM solution with other physics, like, for example, mechanical and thermal problems;

- the boundary element method (BEM) [Banerjee and Butterfield, 1981] requires calculating only boundary values, rather than the total simulation space and it works by constructing a "mesh" over the modeled surface. For this reason it is significantly more efficient in terms of computational costs. Moreover, the meshes can easily be generated and design changes do not require a complete remeshing. The BEM is especially advantageous in the case of problems with infinite or semi-infinite domains, e.g. so-called exterior domain problems, because only the finite surface of the infinite domain has to be discretized and the solution at any arbitrary point of the domain can be found after determining the unknown boundary data;

- the impedance method (IM) [Armitage et al., 1983] is based on the quasi-static approximation [Armitage et al., 1983], where the region of interest is described by a 3D network of impedances, representing each space grids in which the domain is divided. So, the whole space is represented by a linear circuit applied to compute the currents in the impedances; this representation bring to a system

of Kirchhoff's law equations, that can be solved using iterative process starting from an initial guess.

In order to perform numerical models different software can be adopted. In this Ph.D. thesis the software COMSOL Multiphysics v.5.0 has been used for the numerical part concerning drug delivery systems mediated by nanosecond pulsed electric fields (see Part IV). COMSOL Multiphysics is a commercial software that permits to solve complex electromagnetic models, based on the finite element method (FEM) described above. COMSOL Multiphysics, like all FEM software, makes a spatial discretization of the system that has to be analyzed in many elements with geometry and shape known. The fundamental steps to setup a generic microdosimetry simulations are:

1. construct the geometry defying as first the dimension of the simulation box and then the dimension of cells or of the electrical component that is to be simulated;
2. define the materials associated to each geometries;
3. define the mesh grid for the discretization with which we want to visualize the results;
4. define the source which means the current source or the potential and the ground;
5. impose continuity condition at the internal boundaries;
6. define the integration step to save the results;
7. visualization of results in 2D or 3D graphs.

The software consists of several modules, capable of solving different physical problems: chemical transport, heat transfer, etc.; for the present thesis the module of the electromagnetism was chosen.
As will be discussed in the chapters 7 and 8, the Comsol Multiphysics Software has been used to simulate a cell and a liposomes populations exposed to 12 nsPEFs.

Overall Conclusions

To conclude as whole in this chapter, the multiscale approach adopted in this Ph.D. thesis have been presented. We are faraway to build a kind of bridging domain between the molecular dynamics simulations and the mesoscale level analysis. Anyhow Kohler at

al. [Kohler et al., 2015] tried to link the two different methods; indeed they presented an atomistic-to-continuum methodology, which computes and subsequently displays 3-D spatio temporal profiles of the electric potential, field, and field gradients immediately preceding and following the electroporation phenomena. The authors obtained a more detailed model for the pore formation process through interactions between external electric field gradients and the cellular membrane. With this paper the authors proposed a methodology that provides a new analyses to these studies by decomposing continuum parameters such as the electric field into discretized quantities.

Part III

Drug delivery systems activated by low intensity magnetic fields

The use of low-intensity magnetic fields in therapeutic applications has increased widely during these last years. Many researchers focused their attention on the use of magnetic field for therapeutic purposes, as cancer treatment, inflammation, and neuronal diseases, even including the most recent approaches based on nanotechnology and nanomedicine. Among the new nanotechnologies, the liposomal drug delivery system is a novel technique that allows having a controlled release of a drugs encapsulated in a nanocarrier (i.e. liposomes) by the application of an external (electric, magnetic, thermal) stimulus. Moreover, the ability of pulsed electromagnetic fields (PEMFs) for the treatment of inflammations status is well know and more often researchers are focusing their attention on the capability of such pulses to generate a cell response despite the low magnetic field intensity. In this part, firstly experiments and then the design of a magnetic exposure setup will be presented for magneto-liposomes drug delivery applications.

In detail in Chapter 5 an experimental activity will be presented concerning liposomes vesicles preparation loaded with superparamagnetic nanoparticles and exposed to a low intensity pulsed magnetic fields (PEMFs), to prove the feasibility of a magnetoliposomal (MLs) drug delivery system mediated by PEMFs. The starting point of this work has been to firstly reproduce experimental data presented in [Spera et al., 2015] testing the feasibility of MLs poration exposed to an alternate magnetic field (AMF). Here experiments using an AMFs exposure are presented to verify the triggered MLs release with our sample preparation, before proceeding with the PEMFs stimulation.

Pulsed magnetic fields are not only employed as trigger agent on magnetoliposomes systems, but for other interesting biomedical applications involving stimulation of the nervous system as the Transcranial Magnetic Stimulation (TMS) used to map possible neuronal damages due to strokes or to treat neuronal disorders. Usually, both for drug delivery systems or the TMS stimulation laboratory experiments are needed to properly define in-vitro and in-vivo outcomes, therefore the need of a multipurpose exposure system for low intensity magnetic fields is demanding. In Chapter 6 of this part a closed-form analysis and a numeric modeling approach are reported for the design of a versatile magnetic exposure system suitable for different in-vitro applications (i.e. magnetoliposomes drug delivery and studies for the understanding of magnetic stimulation action at single cell level) that could able to generate intensities of the order of mT in a frequency range up to 20 kHz.

Chapter 5

Drug delivery systems mediated by low intensity magnetic fields

5.1 Introduction

In recent years, a great number of investigations have been reported on exploiting possible role of magnetic nanoparticles (MNPs) in enhancing magnetoliposomes delivery of the drug as explained in the Section 2.4. In fact as previously mentioned (see Sec. 2.4) hybrid liposomes composed of thermo sensitive phospholipids and magnetic nanoparticles (MNPs), such as iron oxide MNPs, were shown to have enhanced release of a model drug when exposed to an external alternating current magnetic field (AMF) due to the magnetocaloric effect and a negligible release without exposure to an AMF ([Pradhan et al., 2010, Preiss and Bothun, 2011]). The release due to the thermal increase depend on the magnetic field intensity (1-10 kA/m) and frequency (10-100 kHz), at which MNPs embedded into liposomes, are able to convert magnetic field into heat, either from hysteresis losses or from Neel or Brownian relaxation processes [Guardia et al., 2012]. As explained in the section 2.4, researchers [Nappini et al., 2010, Spera et al., 2014], by selecting field frequencies and strength that are several orders of magnitude lower than those needed for the magnetic thermal approach [Nappini et al., 2010, Spera et al., 2014], have investigated the possibility to induce a possible release coming from the MNPs oscillation without a thermal increase. This hypothesis arises from the finding that AMF-induced oscillation of MNPs was proved to be able to mechanically damage cancer cells in vitro [Cheng et al., 2014].

Indeed, aimed to investigate only the mechanical actuation of MNPs by non-heating alternating magnetic field , Spera et al. [Spera et al., 2015] used a low amplitude ($\backsim$ 70 μ, 20 kHz) alternating magnetic field (AMF) as a remote trigger for magnetoliposomes release. Under such conditions, no heating effect occurred and therefore, the employed field was called "non-heating", and hence only non-thermal effects was taken into account. The authors combined hydrophilic Fe_3O_4 nanoparticles (MNPs) with the hydrogenated soybean phosphatidylcholine (HSPC) and cholesterol to design a suitable carrier model. The obtained vesicles are referred as non-temperature sensitive magnetovesicles (Tm > 50 °C) since their membrane can exist only in the ordered state within the experimental temperature interval and neither spontaneous leakage nor thermal responsiveness can occur up to 50 °C. It was demonstrated that these high-Tm MLs, including in their aqueous core 5-(6)carboxyfluorescein (CF) used as hydrophilic model drug, were able to release almost 20 % of dye fluorescent after three hours of AMF exposure with intensity of 60 A/m. Such low amplitude non thermal AMF gives some more supplementary advantages to the classic magneto-thermal approach (see Sec. 2.4). Mechanical actuation of magnetic nanoparticles, by non-heating alternating magnetic field, provides an opportunity to overcome the drawback of heating-AMF actuation an to create conditions to consider MNPs and low amplitude AMF prospective as powerful therapeutic tools.

By the way, non-thermal magnetic fields are already employed in therapy because of their ability to down-regulate specific cytokines in an inflamed environment [Varani et al., 2017, Setti et al., 2017]. In particular, biophysical stimulation with pulsed electromagnetic fields (PEMFs) has been demonstrated to exert an anti-inflammatory effect resulted in early pain control and enhanced functional recovery in the knee diseases as mentioned in the section 9.1. Recently, the I-ONE medical device from IGEA (Carpi, Italy), able to generate a peak magnetic field of 1.5 mT at a frequency of 75 Hz, was tested in order to reduce knee osteoarthritis lesion progression with long term positive benefits for patients [Veronesi et al., 2014, Gobbi et al., 2014]. It is well known that when loaded with a suitable therapeutic agent, an anti-inflammatory in this case, a single-dose intra-articular administration within a synovial joint of liposomes, can be used to treat the inflammatory process [Ramos et al., 2007, Soriano-Romaní et al., 2017, Stokes et al., 2016].

In this context, the combination of magneto-carriers and PEMFs is an exciting direction of research, where synergistic properties of both modalities could be effectively

utilized for inflammatory reduction and remotely-activated drug delivery. A novel concept of combined action in multiple localized treatments could be proposed joining the functionalities of the magneto-mechanical actuation and the healing properties of a non-thermal magnetic field: both could work in close synergy together with drug-loaded nanocarriers that are able to control drug release by application of a remote magnetic field in order to maximize the efficiency of an anti-inflammatory therapy in future medical applications.

For this purpose, in this chapter, the aim is to point out evidence of the mechanical actuation of high-Tm MLs by a pulsed electromagnetic fields (PEMFs).

Firstly experiments of MLs exposed to an non thermal alternate (AMF) magnetic field generated by two Helmholtz coils, have been performed to replicate the data from Spera et al. [Spera et al., 2015] and to asses the already verified triggered release from the MLs. Magnetoliposomes were prepared by means of incorporating commercially available carboxymethyl-dextran coated magnetite nanoparticles within the aqueous core of the HSPC vesicles. 5(6)-carboxyfluorescein (CF), was co-incorporated in the core of magneto-vesicles and used as hydrophilic model drug to test the release of the investigated nanosystems. Samples were exposed firstly to the AMF with B field intensity of 70 μT in continuum modality for different time intervals and the drug release was compared to the one obtained without the magnetic field application (sham exposure). Subsequently, the drug release profile from high-Tm MLs and the I-One device has been tested for its potentiality to mechanically modify the structure of the HSPC/cholesterol high-Tm liposomes, thereby providing spatial and temporal control over drug release. In this case the intensity increased to 100 μT and the release trends related to sequential PEMFs switching ON and OFF, were also evaluated.

The experiments have been carried out in collaboration with the research group of Prof. Petralito, expert in liposomes preparation, from the faculty of Chemistry and Technology of Drugs of "Sapienza", University of Rome. Regarding the experiments carried out with PEMFs, the I-ONE medical device from Igea group (Carpi, Italy) has been used, in collaboration with Dr. Ruggero Cadossi.

5.2 Materials and Methods

5.2.1 Materials for liposomes preparation

Hydrogenated soybean phosphatidylcholine (HSPC) Phospholipon 90H from Lipoid GmbH (Germany)was kindly gifted by AVG Srl (Italy). Cholesterol, 4-(2-hydroxyethyl) piperazine-1-ethanesulfonic acid (HEPES), 5(6)-carboxyfluorescein (CF), Triton X-100 (TX-100), Sephadex G-50 and hydrochloric acid (HCl) were purchased from Sigma Aldrich (Italy). Chloroform was obtained fromMerck (Italy).
Bidistilled water, thiocyanatoiron, 1,2-dichloroethane and ethanol were supplied by CarloErba Reagents (Italy). Aqueous dispersion ofcarboxymethyl-dextran coated magnetite (Fe_3O_4) 50 nm nanoparticles fluidMAG-CMX were obtained from Chemicell GmbH (Germany).
Calorimetric investigations with Differential scanning calorimetry (DSC131 (Setaram, France)) was performed on HSPC/Chol/MNPs and HSPC/Chol without MNPs mixtures in the same molar ratio used for vesicles preparation. Samples (5 mg) were weighted in sealable aluminum pans, 20 μl of distilled water was added, and then the pans were hermetically sealed. At least three heating/cooling cycles in a temperature range from 20 to 70 °C under nitrogen flow (20 ml/min) were performed on all the samples before thermograms were recorded at a rate of 5 °C/min. An empty aluminum pan was used as reference.

Liposome preparation

Magnetoliposomes, MNPs-embedded liposomes, were prepared by the thin lipid film hydration method (Fig. 5.1), followed by sequential extrusion. HSPC and cholesterol (5:1 molar ratio) were dissolved in the minimum volume of chloroform and the organic solution was poured into a round bottom flask. The organic solvent was evaporated under reduced pressure at 60 °C until a thin lipid film was formed on the bottom of the flask. The dry lipid film was then hydrated at 60 °C in a 10ml of 10 mM HEPES buffer solution (pH = 7.4) containing Fe_3O_4 nanoparticles and 20 mM 5(6)-carboxyfluorescein sodium salt. Final lipid concentration was 10 mM and magnetite to phospholipid ratio was 200 g Fe_3O_4/mol HSPC. Control liposomes, without MNPs, have been prepared by adding CF to the buffer used during the hydration step. The

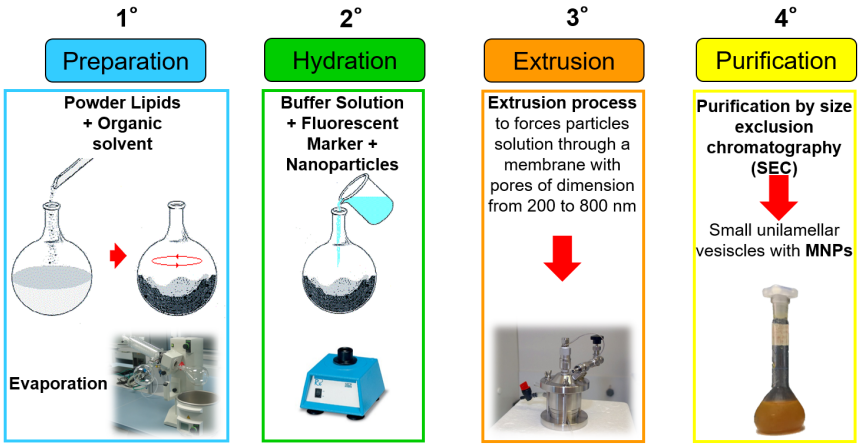

Figure 5.1: Thin lipid film hydration method for the magnetoliposomes (MLs) preparation.

suspensions were vigorous stirred until complete dispersion of the film. Multilamellar polydisperse vesicles were downsized by repeated extrusion (Lipex extruder, Canada) at 60 °C through Cyclopore polycarbonate membrane filters (Whatman). Two steps of ten extrusions through membranes of 0.8 μm; 0.4 μm and 0.2 μm pore sizes allowed the preparation of unilamellar vesicles with a narrow size distribution (peak around 200 nm) as is possible to appreciate from fig. 5.2. The unencapsulated fluorescent tracer CF and the non-entrapped ferrofluid nanoparticles were removed by size exclusion chromatography (SEC, see Fig 5.1) with a Sephadex G-50 column. The eluent was 10 mM HEPES buffer solution (pH = 7.4). All liposome formulations were stored in dark at 4 °C and used within 1 week.

Physicochemical characterization of liposomes

The Size, size distribution and ζ-potential of both control liposomes (CLs) and MLs were measured with a Zetasizer Nano ZS90 (Malvern Instruments Ltd., UK). Hydrodynamic diameter and polydispersity index (PdI) were evaluated by dynamic light scattering (DLS) experiments, whereas ζ-potential was measured by electrophoretic light scattering (ELS) experiments. The DLS and ELS techniques used a photon correlator spectrometer equipped with a 4 mW He/Ne laser source operating at 633 nm. The

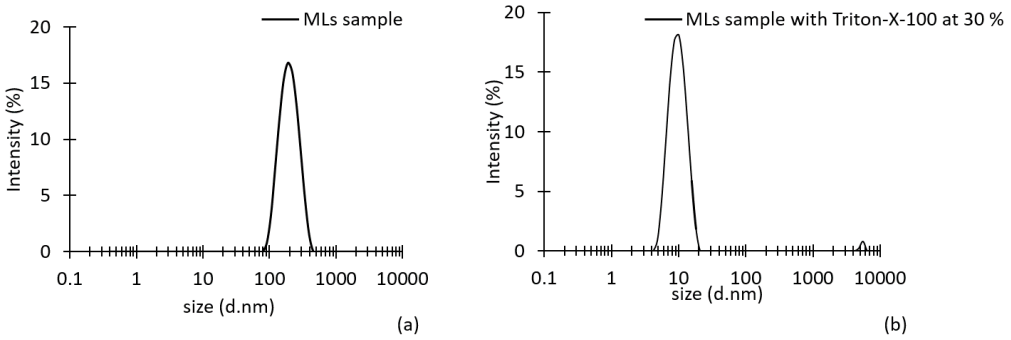

Figure 5.2: Dynamic light scattering (DLS) of the magnetoliposomes solution. It is possible to appreciate a well uniform 200 nm liposomes population. The measure was repeated three times.

particle size diameter was determined by Stokes-Einstein relationship. All experiments were performed at a scattering angle of 90 °C after diluting 10 times the samples with HEPES buffer solution pH=7.4 and were thermostatically controlled at 25 °C. In figure 5.2a the DLS for the MLs sample is reported. Moreover in figure 5.2b the DLS for the MLs sample when the Triton-X-100 is added to disrupt the vesicles and have the 100 % of CF released as will be explained in the next section; it is possible to notice how only one peak is present at 10 nm, meaning the no entire liposomes are present in the solution.

Measurements of the CF released from liposomes

The fluorescence intensity of CF (excitation 492 nm, emission 512 nm) was monitored by means of the spectrofluorometer LS 50B (Perkin Elmer, USA). The purified liposome suspension was diluted with HEPES buffer pH 7.4 (10 ml) and the fluorescence was measured before and after treatment with 50 μl of Triton X-100 to induce vesicles lysis. For all the fluorescence measurements the overture of the slit was settled 2.5/4 for the excitation and emission wavelength respectively. The CF calibration curve was obtained working with and without Triton X-100 at lithic concentration in order to evaluate the influence of the non-ionic surfactant on the fluorescence-based measurement. In the figure 5.3 the calibration curve of the CF is shown. With the calibration curve of the CF, the aim is to find the highest concentration of CF that can be incorporated

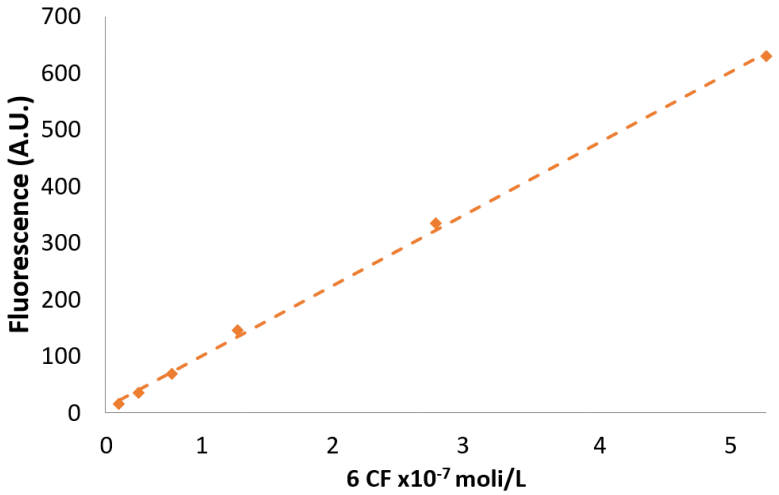

Figure 5.3: Fluorescence measurements for the CF solution from low to high CF concentration.

into liposomes in order to avoid quenching or de-quenching phenomena to be able to read a fluorescent measure at the spectrofluorometer, which has a limit of 900 A.U. Here, in order to have a margin for the fluorescence evaluation, the limit for the highest CF concentration has been considered 700 A.U. In this way the concentration value of $5x10^{-7}$ moli/L is the maximum CF concentration that can be incorporated into liposomes. In order to reduce the influence of excitation light irradiation, all data were obtained at the same timing as soon as the excitation and emission conditions were set up. The released CF percentage was calculated as:

$$CF_{\text{releasae}}\,(\%) = \frac{(F_t - F_0)}{(F_{\max} - F_0)} \times 100 \tag{5.1}$$

where F_t is the fluorescence of individual liposomal samples, F_0 is the background fluorescence of the purified liposomal solution and $F_{\max}$ is the final intensity when vesicles are completely destroyed by adding TX−100 solution at 30 %. In figure 5.4 an example is reported for the fluorescence measurements at different lipid concentrations. At chosen Mls sample concentration (based on the CF calibration curve) the fluorescent is read and the percentage of the CF release is calculated by considering the fluorescence

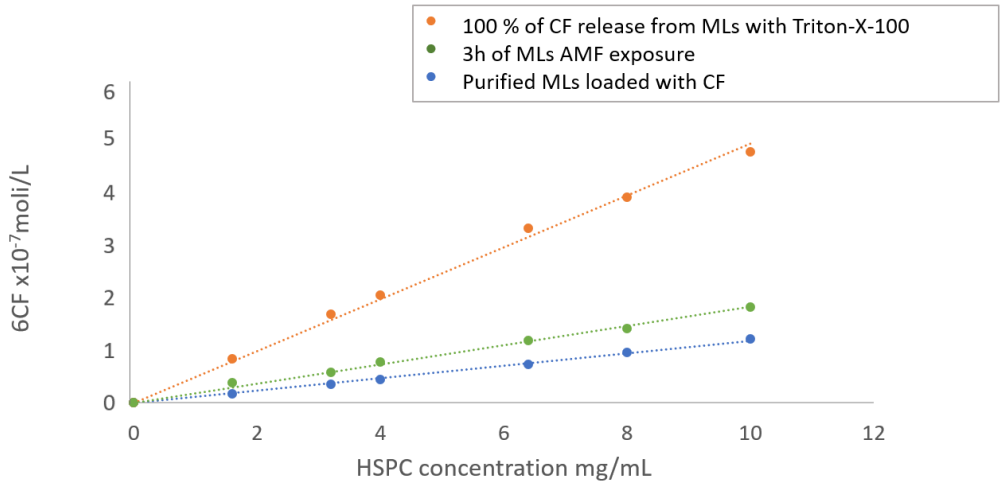

Figure 5.4: fluorescent release of the purified liposomal solution (blue line), exposed MLs sample to three hours of AMF exposure (green line), the final CF intensity when vesicles are completely destroyed by adding TX−100 solution (orange line).

value before the AMF exposure and when the Triton-X-100 is added to have the 100 % of CF loaded into vesicles.

Moreover in order to ensure that no CF release occurred next to a thermal increase, the HSPC liposomes have been heated in a thermal bath at a temperature up to 60 °C. In Fig. 2.5 it can be appreciated how the liposomes start to release at the lipid transition temperature of 48°C, ensuring no CF release in the thermal bath of 37°C, at which the magnetoliposomes are immersed during the magnetic exposure.

Negative staining transmission electron microscopy

The morphology of the vesicles was examined using transmission electron microscopy (TEM). A drop of a water-diluted suspension of the Mls (0.05 mg/ml) was placed on a copper grid, which allowed the adsorption of the vesicles. The excess of water was removed letting the grid drying on a filter paper. Then, a drop of an aqueous solution of uranyl acetate (1% w/v) was added and left in contact with the sample for 5 min. After this time, the excess of the uranyl acetate solution was removed with a filter

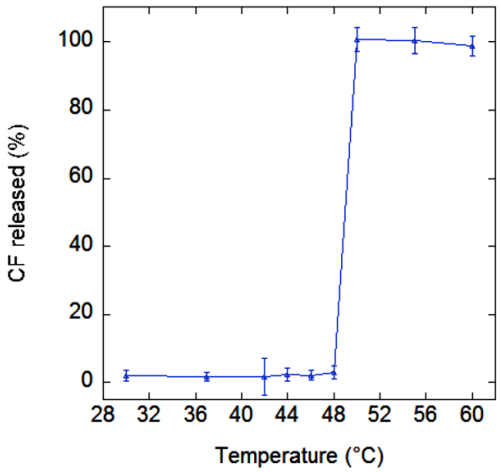

Figure 5.5: Thin lipid film hydration method for the magnetoliposomes (MLs) preparation.

paper and the samples were dried at room temperature before the vesicles were imaged with a TEM (Zeiss EM 10, Germany) operating at an acceleration voltage of 60 kV.

Assay of phospholipids

Phospholipid concentration was determined using the phosphorus colorimetric assay. Briefly, aliquots (0.4 ml) of phospholipids in 50 % v/v ethanol were added to a mixture of 1 ml of thiocyanatoiron reagent and 0.6 ml of 0.17 N HCl. The solution was incubated for 5 min at 37 °C and then the thiocyanatoironphospholipid complex formed was extracted with 3 ml of 1,2- dichloroethane by vigorous shaking for 2 min in a vortex-type mixer. The mixture was centrifuged for 2 min and the absorbance of the lower layer was measured at 470 nm against a blank without substrate, using a double beam Lambda 25 (Perkin Elmer, USA) UV-Vis spectrophotometer. The measurements were repeated both before and after SEC purification of extruded samples.

Assay of magnetite

Magnetite content in magnetoliposomes was determined through the method described by Belikov et al. An opportune amount of magnetite solution was added with 0.08 ml of Triton X-100 20 % to disrupt the phospholipid vesicles. The volume was adjusted

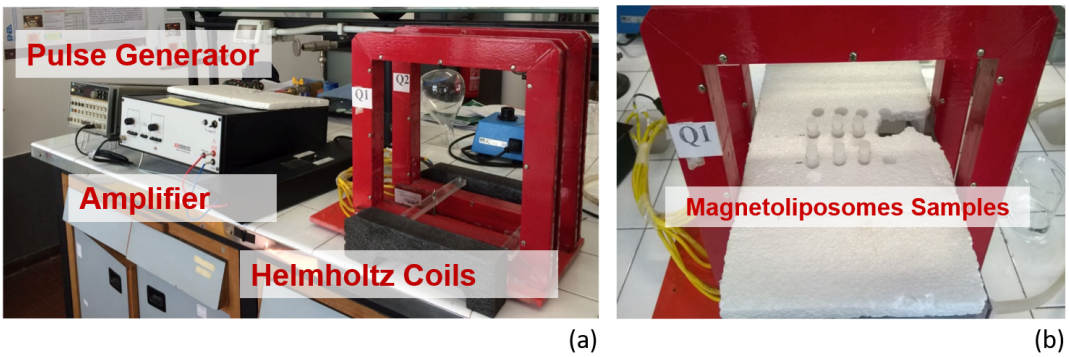

Figure 5.6: AMF exposure setup **(a)** consisting of a pulse generator, an amplifier and two squared Helmholtz coils, generating a magnetic field of 70 μT; **(b)** exposure of the magnetoliposomes solutions immersed in a thermal bath at 37 °C and exposed to AMF.

to 5 ml with 8.5 % HCl and the absorbance was read at 320 nm in a Lambda 25 spectrophotometer (Perkin Elmer, USA). The calibration curve was performed with standards solutions of magnetite. The measurements were repeated both before and after SEC purification of extruded MLs. All the data collected were used to calculate magnetite/phospholipid ratio as μmol of magnetite by mmol of lipid.

5.2.2 AMF exposure setup

For the AMF exposure setup, we used a Hewlett Packard HP−3314A pulse generator applying a voltage of 1.67 V at frequency of 20 kHz. Next the generator, a Krohn−Hite 7500 amplifier was connected to feed two Helmholtz magnetic coils (see Fig. 5.6a), generating a magnetic field intensity of 70 μT. The dimension of the Coil is a length of 20 cm, thickness of 5 cm and placed at distance of 10 cm.

The magnetoliposomes samples were placed at the center, between the two coils (see Fig. 5.6b) in a thermal bath at 37 °C to ensure a stable temperature during the experiments, well below the transition temperature of the HSPC vesicles ($\backsim$ 50 °C). Both Mls and liposomes with no nanoparticles (sham) were exposed to the AMF, in order to possibly quantify the spontaneous leakage of the vesicles. The exposure time was of three hours in continuum and then period of ON (3 hr) and OFF (21 hr) for the same sample was done for a total of 12 hours of exposure. The fluorescent release was measured for both samples next the AMF exposure as explained in the section 5.2.1.

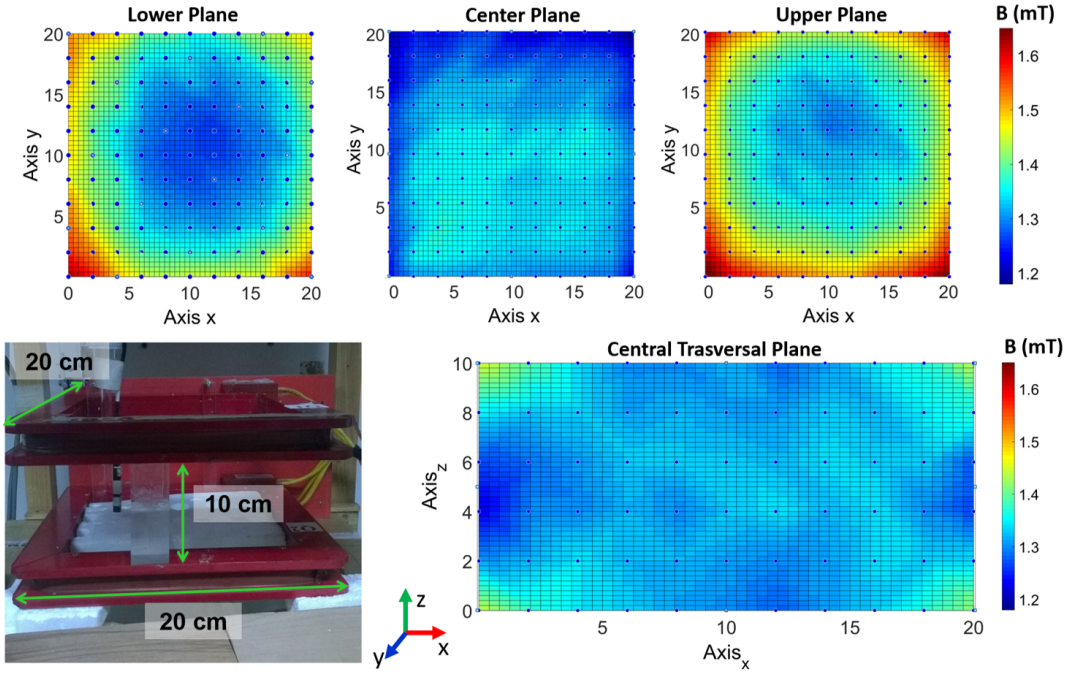

Figure 5.7: Magnetic fields maps of four different planes. Lower plane, center plane and upper plane. Then a trasversal center plane in the z direction.

Characterization of the AMF exposure setup

Because the Helmholtz coils, were not characterized in terms of homogeneity of the B field, before proceeding with the experiments we measured the magnetic field inside the coils as follow. We performed measurements with a triaxial magnetic probe (Metrolab THM1176-MF three axis hall magnetometer, 1.65 x 0.5 x 0.23 cm^3), at the ENEA Center "Casaccia". Four different planes were mapped and the results are reported in Fig. 5.7. It is possible to appreciate an homogeneity of 60 % in the center volume of 15 x 15 x 6 cm^3.

5.2.3 PEMF exposure setup

For the PEMF exposure, the medical device IGEA called I-ONE, a product that is already CE certified, has been used. The coil generated a pulse of magnetic field with intensity of 1.5 mT with a repetition frequency of 75 Hz.

In fig. 5.8 it is visible the system I-ONE and the following elements are shown:

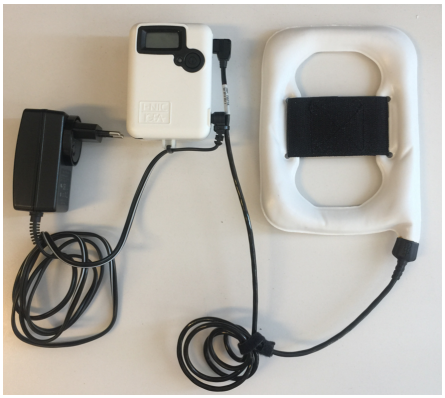

Figure 5.8: I-One coil exposure setup with the generator, the power supply and the solenoid.

1. generator;
2. power supply;
3. solenoid.

I-ONE is constituted by a generator of low frequency pulsed electromagnetic field which generates a current pulse signal and delivers this signal to an external coil (the solenoid), generating a pulsed electromagnetic field with specific characteristics. The pulsed signal has the following temporal characteristics:

- duration of the active phase of the signal: 1.3 ± 0.1 ms;
- repetition frequency: 75 Hz (which is equivalent to a repetition time period between two successive pulses of 13.3 ms);
- amplitude of the peak value: 1.05 A.

In table 5.1 the geometric and electric characteristics of the I-ONE coil are reported.

The magnetoliposomes samples were placed at a distance of 13 cm obtaining a magnetic field of 100 μT (Fig. 5.9a) on the exposed samples. The samples were placed also in this case in a thermal bath (Fig. 5.9a) and during the exposure an aluminum foil was used to cover the bath, in order to avoid any release due to the light. The choice of the distance at which place the samples, has been done following a dosimetry analysis of the I−One Coil and a sample of exposed solution as will be explained in

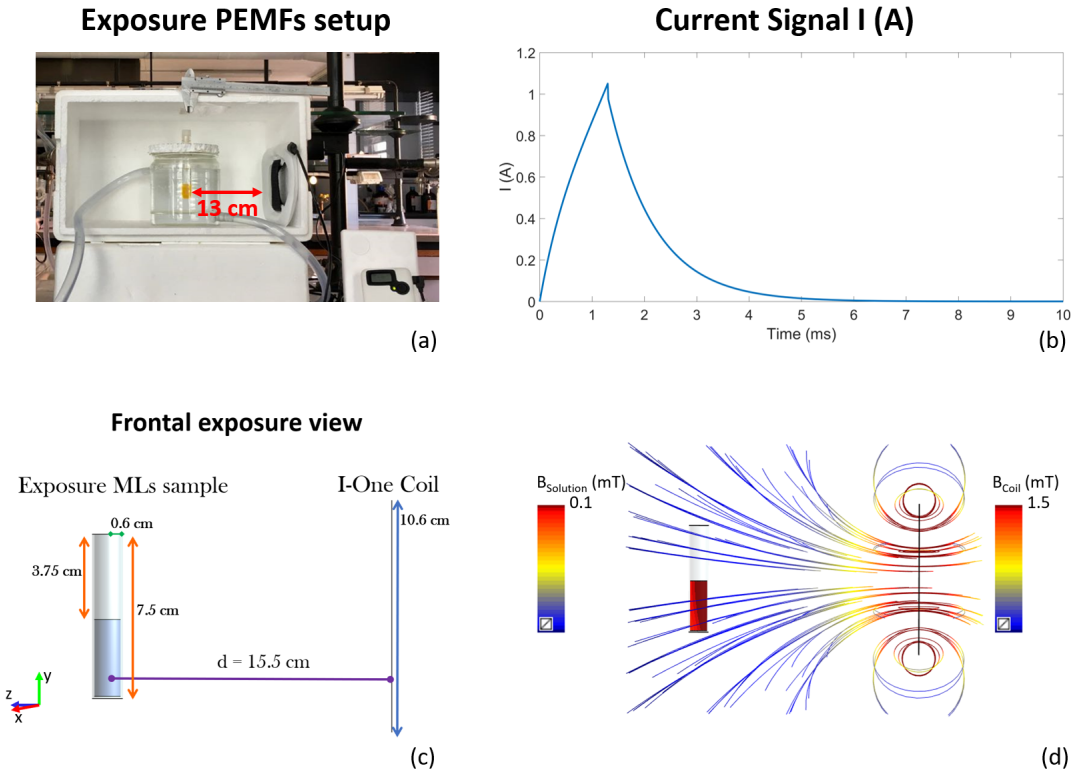

Figure 5.9: **(a)** Exposure setup of the MLv sample and the I-One coil; the MLs samples are placed in a thermal bath at 37 °C, at a distance of 13 cm from the I-ONE medical device **(b)** current signal feeding the coil; **(c)** coil geometry used to perform dosimetric simulations in the frontal exposure view; **(d)** magnetic field streamline of the coils and the magnetic field surface inside the exposed sample.

the following section. One sample was used for the experiment, repeated four times to perform statistical analysis.

Numerical Modeling of the I−One for the choice of the B field intensity

To evaluate the intensity to which expose the sample, numerical simulations have been performed with the Software Sim4Life 2.1 in the frequency domain for Magneto Quasi-static simulations. In particular having fixed an intensity comparable to the one of the experiments in CW (100 μT), the distance between the exposure samples and the coil has been derived. The Sim4Life v2.2 (ZMT, Zurich MedTech AG) platform combine

computable human phantoms with the most powerful physics solvers and tissue models, for directly analyzing biological real-world phenomena and complex technical devices in a validated biological and anatomical environment. The Sim4Life platform also offers many physics solvers and advanced tissue models, for analyzing biological phenomena and complex technical devices. The Sim4Life is an interactive environment for modeling and simulating scientific and engineering problems. Here the Magneto Quasi-static solver has been used. The simulations were performed at frequency of 250 Hz (the first lobe of the spectral of the signal). The model geometry is reported in Fig. 5.9c. The cuvette has been simulated as a cylinder with 7.5 cm of height and a radius of 0.6 cm, filled for a half with a conductivity solution (0.049 S/m), which represents the magnetoliposome solution conductivity (see Fig. 5.9c) experimentally measured. Such solution has been measured thanks to the dynamic light scattering (DLS) instrument. The conductivity value has been obtained as mean value on 28 measurements with a standard deviation of 0.005.
A fine grid mesh (0.6 nm of resolution) has been adopted for the mesh of the coils and a more accurate resolution has been chosen for the cuvette discretization (0.4 mm of resolution). The feeding current was of 240 A, considering one simulated current wire ($N_{wires} = 240$). The distance between the sample and the coil is, starting from the single simulated wire, of 15.5 cm, chosen based on a linear fitting (13 cm) considering a magnetic field of the coil of 1.5 mT plus taking into account the thickness of the I-One device (white color in Fig. 5.9a) and the thickness of the cuvette and thermal bath recipient.

Magnetic, electric and current density distributions

Number of Coils	240
Copper section	0.355 mm
Mean coil	49.3 cm
Resistance (nominal)	21.2 ohm
Inductance (nominal)	18.5 mH
Length	16 cm
Width	12 cm

Table 5.1: Solenoid characteristics

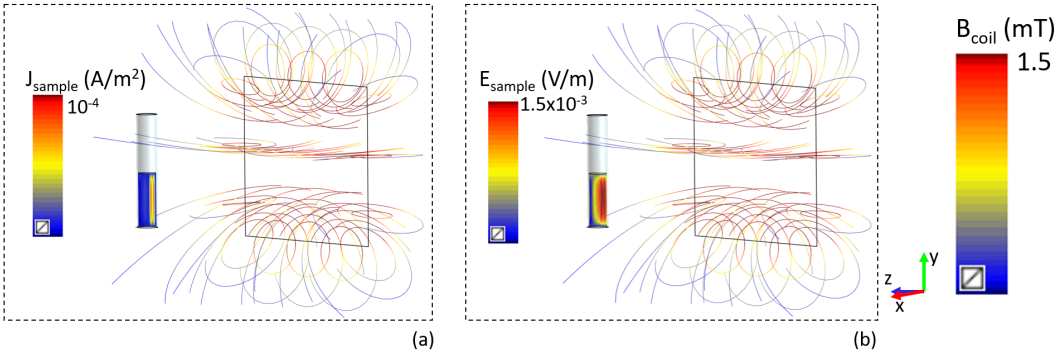

Figure 5.10: **(a)** current density and the electric field **(b)** distribution inside the exposure sample is reported.

In figure 5.9d and 5.10 the magnetic, electric field and current density are reported for the exposure sample when a 1.5 mT of magnetic field is applied.

In figure 5.9d the magnetic field streamline and the B field distribution inside the exposure sample is reported, showing a B field of 100 μT when 1.5 mT is applied. The magnetic field appear to be homogeneous in the exposed sample. As expected, also the electric field and current density are reported 5.10a and b, showing low intensities, the range of mV/m and less than mA/m^2, that determine no significant heating during the exposure to the PEMFs.

Moreover, the dosimetry of the I-One medical device has been done experimentally from a previous Ph.D. student, Dr. Francesca Camera (Ph.D. in Electronic Engineering Cycle XXVIII at Sapienza University of Rome).

5.3 Results

Physicochemical characterization of liposomes

With the regard to the liposomes characterization, no differences was observed in vesicles size among control liposomes (CLs) and MLs as shown in table 5.2.

Both nanocarriers arranged in a monomodal distribution with a PdI values < 0.200. The ζ-potential value of CLs in the buffer medium is negative, moreover the more electronegative character of the MLs system suggests the presence of some negatively charged MNPs absorbed onto the external leaflet of the phospholipid bilayer. Hydration step of the dry lipid film during liposome preparation was not influenced by the

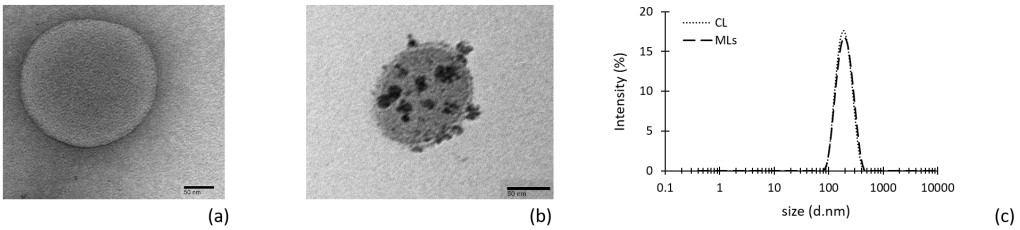

Figure 5.11: TEM images of soybean HSPC liposomes conventional **(a)** or iron oxide nanoparticle-liposome hybrids MLs **(b)**(scale bar: 200 nm).

presence of MNPs in the hydrating medium. Finally, the drug-loading efficiency is not limited by the co-loaded MNPs inside vesicles (Table 5.2). This finding is of paramount importance for the possibility to use of the investigated MLs as smart drug carrier. After SEC purification, the lipid and the magnetite content were determined. In Figure 5.11a and b the TEM images of conventional (CLs) and MLs structures are showed, respectively. CLs and MLs exhibited similar size and structure, which indicates that MNPs interaction did not affect MLs formation at the lipid/MNPs ratio employed. The average diameter of all the structures observed was 200 nm, consistent with membrane extrusion (Fig. 5.11c). TEM images (Fig. 5.11) suggest that interaction between MNps and HSPC lipids leads to hybrid colloidal structures magnetoliposomes, the iron oxide nanoparticle can either decorate the liposomal surface or be internalized inside the vesicles as either individual nanoparticles or MNP aggregates. Sometimes, nanoparticles are concentrated on one side of the vesicles. Unencapsulated nanoparticles were not observed outside the liposome vesicles throughout the TEM grid, as consistent with the efficacy in the SEC purification step.

AMF exposure

Next to the characterization of the MLs, with the aim to replicate and assess the CF release from HSPC MLs exposed to AMFs [Spera et al., 2015], firstly we performed experiments of MLs under an AMF of 70 μT of intensity at a frequency of 20 kHz. The experiments were carried out considering one sample of MLs and one of conventional

Sample	z-average (nm)	Pdl	ζ-potential (mV)	5 (6)CF E.E. (μl/mg)
CL	220.9 $\pm$ 22.4	0.046 $\pm$ 0.028	-10.28 $\pm$ 1.43	2.29 $\pm$ 0.26
MLs	240.9 $\pm$ 26.6	0.131 $\pm$ 0.031	-15.42 $\pm$ 1.51	1.84 $\pm$ 0.13

Table 5.2: Physicochemical characterization of conventional liposomes (Cl) and magnetoliposomes (MLs).

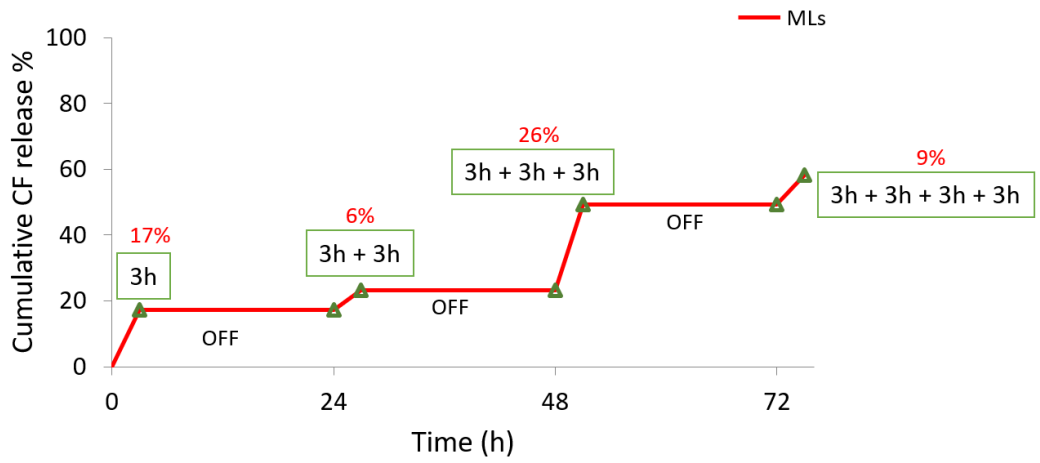

Figure 5.12: Results of the CF release from MLs (magnetoliposomes) in time domain with a total of 12 hours of AMF exposure with OFF time of 21 hours for each 3 hours of exposure.

liposomes (CLs), with no nanoparticles, placed at the center between two Helmholtz coils, in a thermal bath at 37 °C. The results in terms of percentage of fluorescent release are reported in fig. 5.12. After three hours of exposure a fluorescent release of 17 % of CF was appreciated, by confirming the data from [Spera et al., 2015]. After that, the samples were stored at 4 °C for 21 hours and then exposed again for additional 3 hours with a 6 % of release. Next the AMF was turned off for more 21 hours and then turned it on for more 3 hours and an additional release of 26 % was reached. At the end after 3h + 3h + 3h + 3h the last 9 % of Cf was released form the MLs samples. A total of 58 % has been obtained, by confirming the triggered release from the alternate magnetic field, as proven by [Spera et al., 2015]. For the conventional liposomes (CLs) in figure 5.13 the total percentage of CF release was about 11 % after 12 hours, meaning that the spontaneous CLs release is negligible with the respect to the 58 % obtained with the AMF application. Probably the 11 % of CF release is due to the thermal shock between the liposomes storage temperature (4°C) and the thermal bath (at 37°C) during the magnetic field exposure.

Moreover, with the respect to the data published in [Spera et al., 2015], here a triggered release is achieved with the AMF application, but not in the same amount for each ON period of 3 hours. These behavior could be addressed to the possible aggregation of nanoparticles after the first 3 hours of AMF exposure or for the losing of

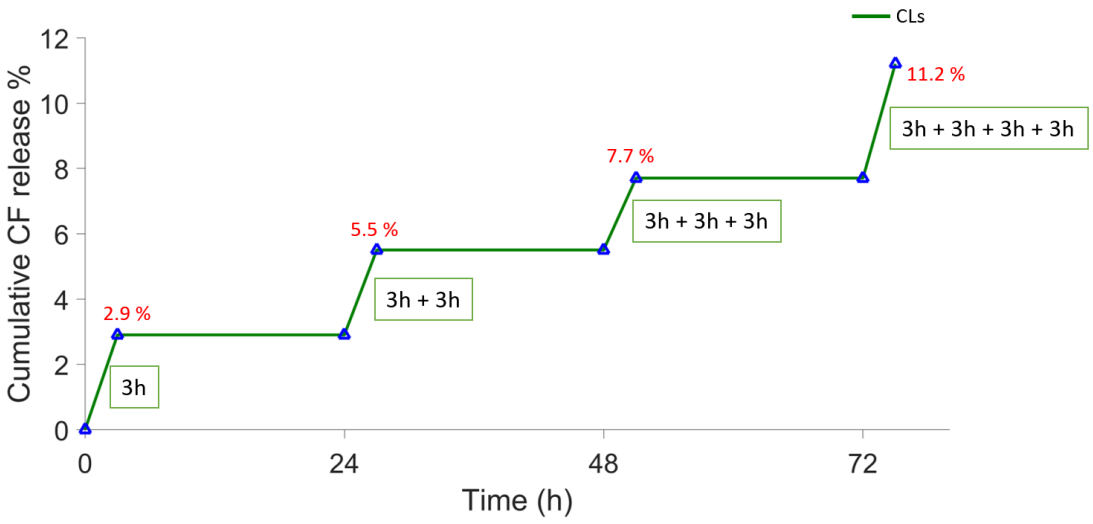

Figure 5.13: Results of the CF release of CLs (conventional liposomes) after 12 hours of switching ON (3h) and OFF (21h) the AMF exposure.

the magnetic nanoparticles from some liposomes structures. This last hypothesis has been supported by the TEM (transmission electron microscopy) images taken after the 12 hours of AMF exposures (see Fig. 5.14). As explained 5.2.1 the TEM is a technique that allow visualize molecular structures of nm dimensions and to possible predict the presence, in our specific case, of nanoparticle on the vesicles surface. From the figure 5.14 the TEM images of MLs after 12 hours of AMF exposure is reported and a particular shape of the liposomes is highlighted (see Fig. 5.14b). The membrane of some liposomes changed its shape by losing the nanoparticles (see Fig. 5.14b). Moreover, few nanoparticles can be appreciate. This could explain how after 12 hours no release occurred. Unfortunately no images were taken before the AMF exposure.

PEMFs exposure

Once confirmed the results of the release after 12 hours of ON - OFF exposure to AMF, the MLs samples have been exposed to a pulsed electromagnetic fields (PEMFs) of 100 μT of intensity, by using the I-One medical device as described in 5.2.3. We placed one samples of MLs for four different exposures in order to perform a statistical analysis (see Fig. 5.9). We did a set of exposures from 15 minutes up to 3 hours

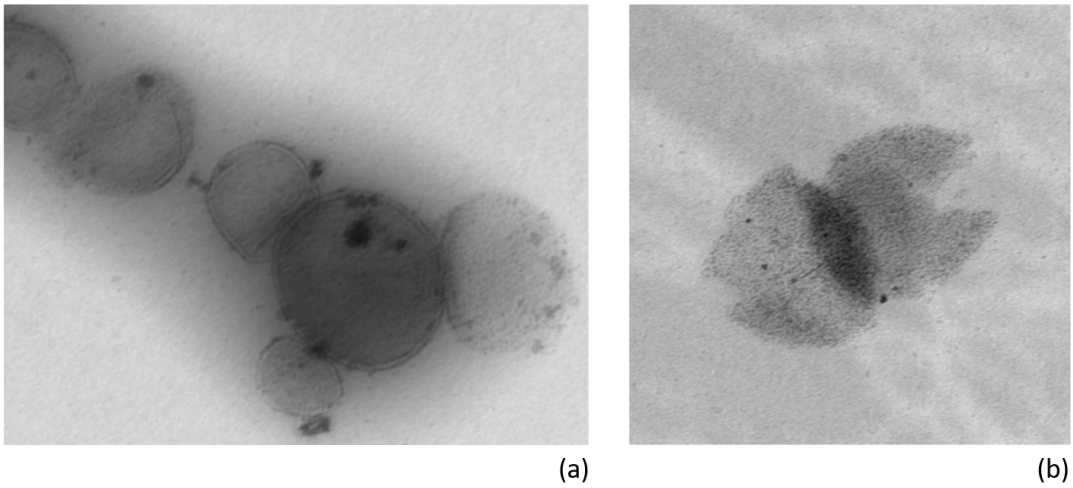

Figure 5.14: **(a)-(b)**TEM images of the MLs after 12 hours of ON-OFF AMF exposure (3h + 3h + 3h + 3h).

in continuum modality. As is possible to appreciate in fig 5.15, after 15 minutes of magnetic field application more than 5 % of the CF is released (see Fig. 5.15). After the three hours of exposure the CF released reached the value of 17 % (see Fig. 5.15) with a standard deviation not higher than 0.8. These data suggest the possibility with the PEMFs signal to obtain a liposomal drug delivery systems without disrupting the vesicles membranes. Besides, the temperature (with a Luxtron 3100 fiber optic temperature probe) was monitored inside the MLs sample during the exposure and no thermal increase was denoted.

Moreover, MLs samples were monitored in a thermal bath of 37 ° (shame samples) for a time up 9 hours in order to detect the release coming from the MLS leakage when no B field is applied. No significant CF release was denoted, a release of 3 % after three hours and of 4.7% after 9 hours was obtained.

In order to evaluate the capability of PEMFs to trigger the CF release with ON and OFF periods as done in [Spera et al., 2015]), we exposed the same MLs samples to additional 3 hours of B field application (after 21 hours of OFF state, storage at 4 °C) and an extra release of 7 % was obtained (Fig. 5.16). After additional 3 hours (3h + 3h +3h, for a total of 9 hours) no release was appreciated. The CF release saturated after 3h + 3h + 3h hours of exposure, showing almost 2 % of CF release. With the respect

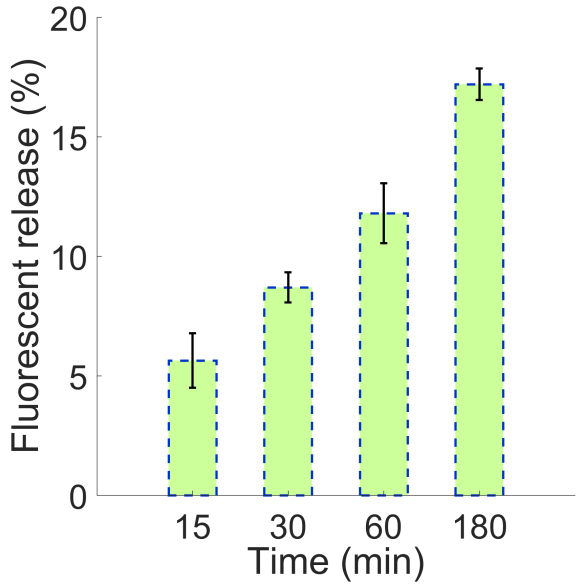

Figure 5.15: Results of the CF release from MLs (magnetoliposomes) next to the PEMFs exposure of 100 μT.

to the MLs exposed to the AMF, here with PEMFs it seems that the release was not repeatable after the same time of exposure (3h + 3h + 3h) suggesting a possible loss of magnetic nanoparticles due to the different signal applications.
In order to valued this hypothesis, after each PEMFs exposures, TEM (Transmission Electron Microscopy) images were taken as explained in section 5.2.1. It is good to keep in mind that with the TEM technique it is not possible to determine if the magnetic nanoparticles are inside or outside the vesicles, because it is a 2D surface representation. The TEM images were taken right after each exposure (Fig. 5.17). In figure 5.17 the images of the different exposures time are showed, at the 0 time (before PEMFs exposure, Fig. 5.17a), after 3h (Fig. 5.17b), at 3h + 3h (Fig. 5.17c) and 3h + 3h + 3h hours(Fig. 5.17d). Before the exposures to PEMFs, the MLs structures is perfectly integer with the magnetic nanoparticles on the surface or/and presumably internalized into vesicles (see Fig. 5.17a); after three hours the MNPs are widespread distributed into solution but still present also on the liposomes surface and also into the membrane (Fig. 5.17b). When an additional three hour of exposure is done (5.17c), the most part of the MNPs seem to be escaped from the liposomes vesicles, indeed

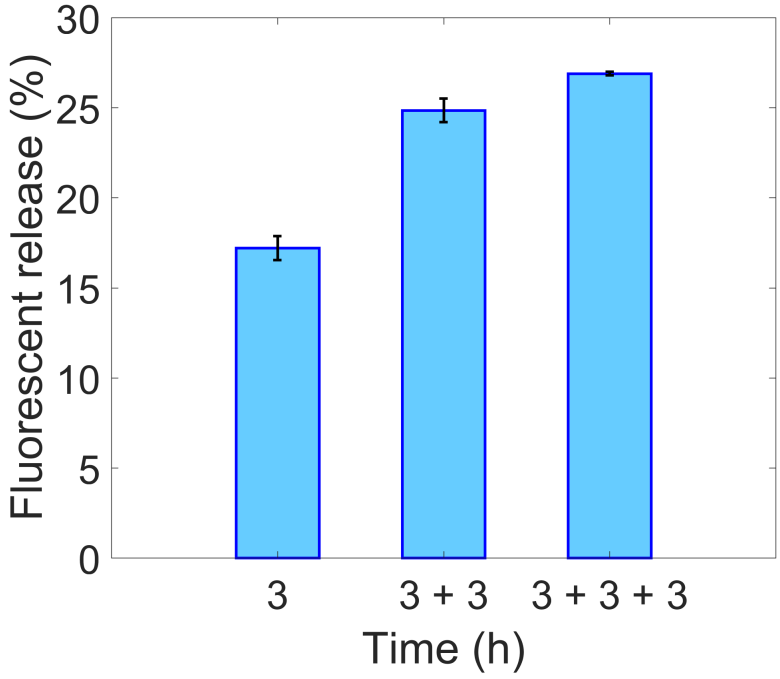

Figure 5.16: Results of the CF release from MLs (magnetoliposomes) next to the PEMFs exposure of 3h +3h and 3h + 3h + 3h (with OFF periods of 21 hours).

is possible to highlight how the MNPs visible are out of the vesicles on the liposomes membrane (see Fig. 5.17c, green circle). This "MLs escape"could explained the 7 % of release obtained with the respect to the 17 % of the first 3 hours. Furthermore, after 3h + 3h +3h of exposure (see Fig. 5.17d) no MNPs are present, justifying the 2 % of CF release.

By the analysis from the TEM images, is possible to conclude that by the PEMFs stimulation, the MLs loss their nanoparticles almost after six hours of exposure, differently from the AMF system were the release was repeatable for a time up 12 hours [Spera et al., 2015]. This behaviors could be addressed to the different kind of signal; in the case of AMF is a sinusoidal signal with a 50 μs duration of one period of the signal, that could stimulate the MLs at one side and then in the opposite side giving the same release after the same time of stimulation. While, a single pulse of the PEMF has a duration of 13.3 ms and could stimulate for a longer time and in the same direction

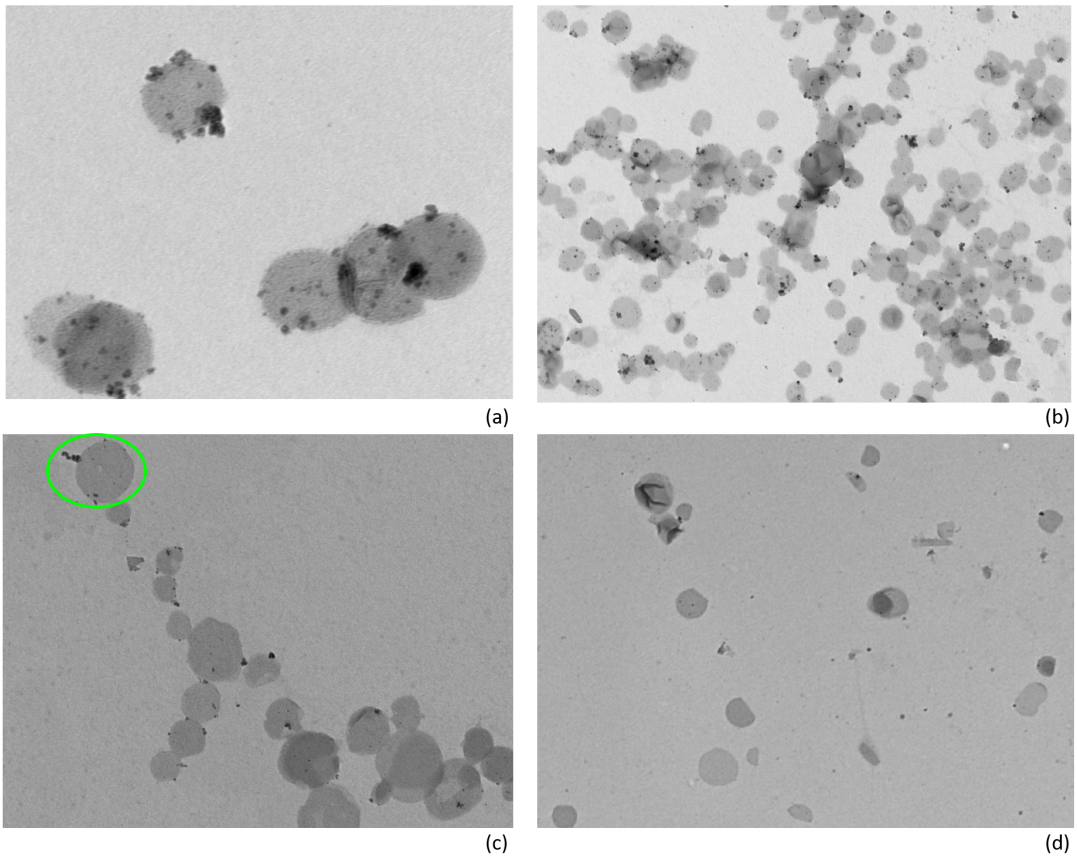

Figure 5.17: TEM (Transmission Electron Microscopy) images of Mls before the PEMFs exposure **(a)**, after 3h, 3h + 3h and 3h + 3h + 3h of B field application **(b, c and d)**.

the MLs, by leading to the loss of the magnetic nanoparticles from the liposomes core.

5.4 Conclusions

In summary, in this chapter a proof-of-concept of the magnetoliposomes release under a PEMFs exposure has been given. High-Tm magnetoliposomes (MLs) using the HSPC lipid were prepared and iron oxide nanoparticle MNPs, were encapsulated into the liposomes aqueous core. To probe the membrane permeation and release behavior of high-Tm MLs, CF as a model of hydrophilic drug, was loaded into the MLs core, with satisfactory values of CF-loading efficiency (see Tab. 5.2).

The Mls and the conventional liposomes (Cls) were exposed to an alternate magnetic field (AMF) of 70 μT. From our experiments a triggered release was reached with a 58% of CF release after 12 hours by switching ON and OFF the alternate magnetic field (ON period of 3h and OFF of 21h) until almost complete depleting of the carrier as already demonstrated in Spera et al. [Spera et al., 2015].
Once, assessed the MLs release next to the AMF application, the goal has been to test a liposomal drug delivery mediated by PEMFs using the I-One medical device, able to generate a magnetic field of 1.5 mT of absolute value. Thanks to numerical simulation the distance at which place the sample, was chosen in order to have a magnetic field of 100 μT of root-mean square value. The samples were immersed in a thermal bath at 37 °C. The CF release was around the 5 % after 5 minutes of exposure and the 17 % was reached after the first 3 hours of B field application, as happened with the AMF application. Conversely, switching ON (3h) and OFF (21h) the magnetic field, only the 7 % of CF was released (3h + 3h) and an additional 2 % was reached by adding 3 more exposure hours (3h + 3h + 3h). By the TEM images analysis, it has been possible to asses how after the 3h + 3h of exposure (switching ON and OFF the B field), the magnetic nanoparticles escaped from the liposomes core, possibly due to the different signal duration and shape with the respect to the alternate magnetic field as explained in the result section (see Sec. 5.3). Anyhow, it is important to highlight how also with PEMFs usually used for the treatment of inflammation status, it seems possible to have a controlled release from MLs structures, that could be used as future anti-inflammatory cargo release system from magnetoliposomes to diseased tissues.
Generally, both with the AMF and with PEMFs we have demonstrated the possibility in two different way to have a controlled CF release from liposomes vesicles due to the mechanical stimulation and not to the thermal exposure. In fact, these experiments demonstrated that the cargo release from the high-Tm MLs was due to reversible and controllable permeability change of the bilayer, rather than the destructure of the high-Tm MLs, that maintain their structures over the whole experiment duration as demonstrated by the TEM images and from the dynamic light scattering measurements. The hypothesis done is a release mechanism due to a mechanical stress on the liposome membrane due to nanoparticles oscillations in its proximity.

Chapter 6

Versatile exposure system for laboratory experiments finalized to therapeutic applications in the IF range

6.1 Introduction

As already mentioned in the previous chapter (see 5.1), more often researchers are focusing the attention on the ability of low intensity magnetic fields for the treatment of different inflammation status, cancer or neuronal disorders. With the wide spread of the technological progress the use of magnetic field as external stimulus for inflammatory and neuronal disease therapies and drug delivery systems for nanomedicine has considerably increased [Rodzinski et al., 2016, Ross, 2013]. The progresses in nanomedicine, as described in the part I ranges from nanoparticles for molecular diagnostics, imaging and therapy to integrated medical nanosystems [Nune et al., 2009, Shi, 2009] to act at the cellular level inside the body.

At this purpose, stimuli-response release of a drug from an ad hoc designed nanocarrier (e.g. liposomes), at a specific time and location is one of the most aimed results of the drug delivery research (see Ch. 5). Besides the typical triggers used for the liposomes drug delivery systems (pH, temperature, ultrasound, etc.) some studies and the experiments presented in the previous chapter (Ch. 5) suggested that even magnetic fields

of low intensities are a good trigger to control the release of the drugs has reported in the previous chapter (Ch. 5) and in [Nappini et al., 2010, Spera et al., 2015]. The aim, with this kind of applications, is to achieve the therapeutic efficacy without a thermal effect, which could affect the patient for prolonged time of the treatment, and to this regard in-vitro and in-vivo laboratory experiments are required to tune the intensity and the frequency of the applied field.

On the other side, highly interesting applications of magnetic fields concern non-invasive stimulation of the central nervous system, such as the Transcranial Magnetic Stimulation (TMS) technique [Corthout et al., 2001] or the low-intensity pulsed magnetic field stimulation (PEMFs) [Di Lazzaro et al., 2013]. Although TMS efficacy has been clinically proved [Corthout et al., 2001] to map possible neuronal damages from strokes, neuronal diseases or amyotrophic lateral sclerosis [Pashut et al., 2014], the action of magnetic fields on neuronal structures is still poorly known, so that in-vitro and ex-vivo studies are necessary to explore such effects at molecular and cell level [Di Lazzaro et al., 2013, Pashut et al., 2014].

In this context, to obtain a precise dose-response relationship, specific exposure systems are necessary, mainly based on single or multiple coils [Di Lazzaro et al., 2013, Pashut et al., 2014], that guarantee a uniform and well-known magnetic field within the exposed sample, in terms of peak value, waveform and polarization. The aim of the work presented in this chapter is to design a versatile magnetic exposure system, suitable for different in vitro experiments, at the basis of the therapeutic applications of MLs drug delivery and magnetic stimulation techniques. For the drug delivery application, the aim is a system able to porate MLs by a mechanical stress without a thermal increase at the typical experimental frequency of 20 kHz [Spera et al., 2015]. Concerning the in vitro application the aim is the exposure of brain slices, adherent to the surface of an exposure chamber, to a low-intensity magnetic field at the frequency of 3 kHz [Paffi et al., 2015], to stimulate and map the cells avoiding any thermal increase.

The exposure system able to fulfill the requirements of both applications, consists of two new squared Helmholtz coils, designed to produce a magnetic field with intensity in the order of mT in a frequency range between 1 and 20 kHz, by analyzing all geometrical and electrical parameters involved. After the analytic identification of the geometrical parameters, numerical simulations have been performed for both applications to calculate the dose on the exposed sample in terms of magnetic induction (B), electric field (E), and current density (J). Moreover, also a circuital analysis is reported

to adapt the present magnetic exposure system (see Sec. 5.2.2) to the new coils both for a sinusoidal or a pulse signal application. This procedure will ensure a multi-purpose system suitable to validate laboratory experiments at the basis of the most adopted therapeutic applications using magnetic fields in the IF frequency range.

6.2 Material and Methods: design of the exposure system

Analytical model

The design of the new magnetic field exposure system started from the specific requirements of the versatile exposure system as:

- intensity of the B field in the order of up to some mT;
- frequency range [1-20 kHz];
- exposure region able to host either a disposable plexiglas cuvette or a suitable chamber for brain slices;
- overall impedance adequate to be fed by a commercial low cost chain of generator and amplifier.

We performed a first analytic study through the standard set of equations of Helmholtz coils [Wang et al., 2002], dimensioning the geometry and composition of the setup (Fig. 6.1), in order to reach magnetic field intensities in the order of mT and in a wide frequency range (from 1 to 20 kHz).

Numerical model

To validate the chosen geometrical and electric parameters, we performed numerical simulations using the Software Sim4Life 2.1 in the frequency domain for Magneto Quasi-static simulations. Sim4Life is a simulation platform, combining computable human phantoms with the most powerful physics solvers and advanced tissue models, for analyzing biological phenomena and complex technical devices. The Sim4Life is an interactive environment for modeling and simulating scientific and engineering problems. Taking into account fabrication requirements indicating a practical easiness in realizing square coils vs circular ones, we simulated the two coils as squared current

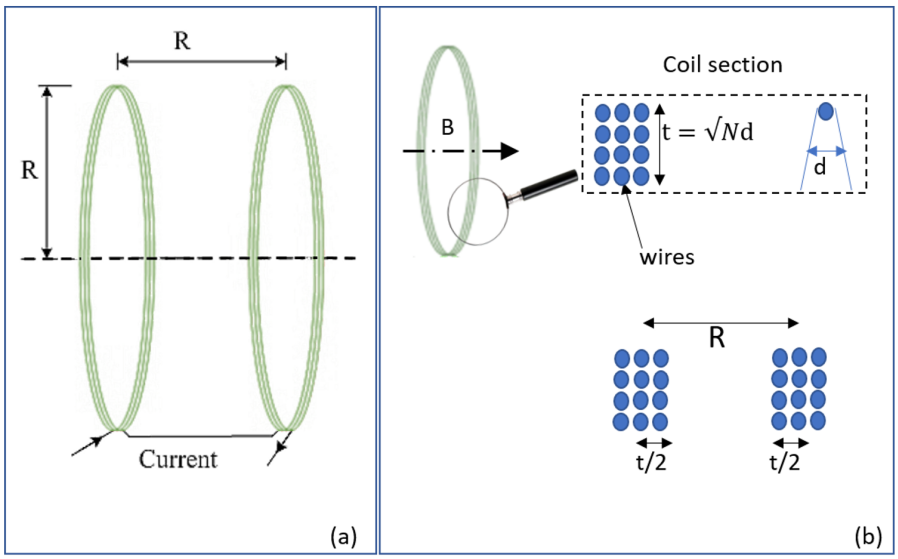

Figure 6.1: **(a)** Geometry of the Helmholtz coil, R is the radius and distance between the two coil, I the current; **(b)** zoom of the coil section with the wires number N, the coil thickness t and the wire diameter d.

wire of 15 cm, placed at 7.5 of distance (see Fig. 6.2a) powered with a current of 120 A (the project required current of 0.6 A multiplied per the number of 200 wires). For both applications, the magnetic field has been applied in the perpendicular direction with the respect to the current flow.

MLs exposure system

Concerning the simulations for the MLs exposure system, we performed two simulations considering a cuvette placed at the center between the two squared coils and considering the upper and lower bounds of the frequency interval of interest: 1 and 20 kHz (Fig. 6.2b), also according to previous experiments carried out with a different magnetic exposure system (see Sec. 5.2.2, [Spera et al., 2015]). The cuvette has been simulated as a cylinder with 7.5 cm of height and a radius of 0.7 cm, filled for a half with a conductivity solution (0.049 S/m), which represents the magnetoliposome solution conductivity, experimentally measured. Such solution has been measured thanks to the dynamic light scattering (DLS) instrument. The conductivity value has been obtained as mean value on 28 measurements with a standard deviation of 0.005. A fine grid mesh (0.6 nm of resolution) has been adopted for the coils and a more accurate resolution has been chosen for the cuvette discretization (0.2 mm of resolution).

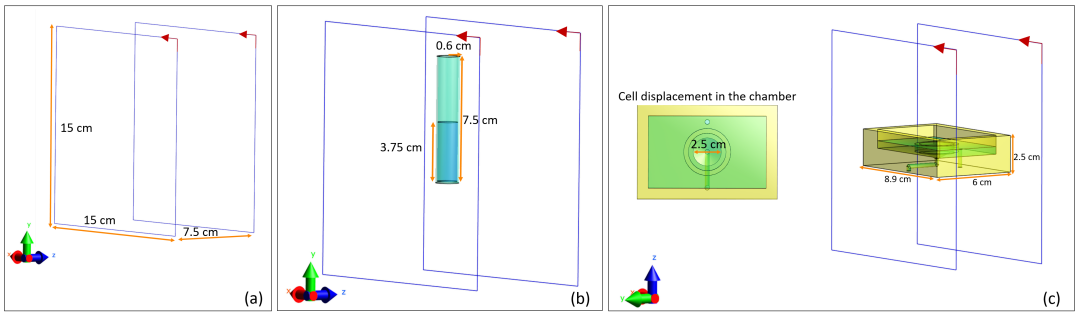

Figure 6.2: **(a)** Coils geometrical model with coil side of 15 cm placed at 7.5 of distance. In red the current flow; **(b)** drug delivery exposure system consisting of a cuvette placed at the center between the two coils with dimension of 7.5 of height, 0.6 of radius and per 3.5 cm filled with the solution;**(c)** in-vitro exposure system with the chamber placed between the Helmholtz coils, to the left of the image the section for the chamber is reported with a diameter of 2.5 cm, filled with the artificial cerebrospinal fluid solution.

in-vitro neuronal cells B exposures

Regarding the numerical simulations of the magnetic exposure system for the neuronal cells in-vitro experiments, we simulated a chamber placed at the center between the two coils (Fig. 6.2c) containing a circular section (2.5 cm of diameter) in which are supposed to be placed the cell slices. We carried out the simulations at frequency of 3 kHz, typically used for this kind of applications [Di Lazzaro et al., 2013]. The dimensions of the chamber are 8.9 x 6 x 2.5 cm^3. The chamber is made of plexiglass with the solution simulated as artificial cerebrospinal fluid, typically used in these kind of experiments, with 1.7 S/m of conductivity and a permittivity value of 66830.8. The artificial cerebrospinal fluid is present both in the cone representing the slice holder and in the rest of the plexiglass chamber. A fine grid mesh has been used for the coils and the chamber while a resolution of 0.5 nm has been adopted for the artificial cerebrospinal fluid solution.

Circuital Model

In order to match the load impedance of the projected coils to the existing exposure system (see Sec. 5.2.2), specifically to the Krohn−Hite 7500 amplifier, a circuital study has been performed by using the LTSpice software. LTSpice is a high performance spice simulator, which provides a variety of custom design simulation tools and device models to allow a quickly and easily circuits evaluation using high performance

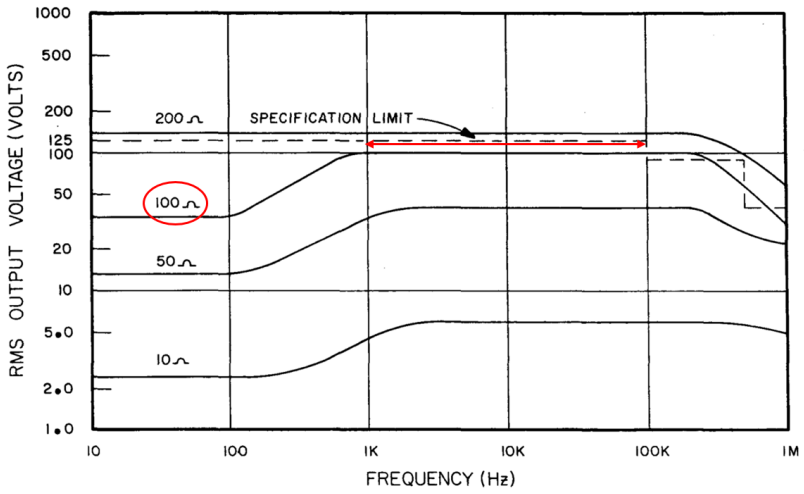

Figure 6.3: Datasheet of the Krohn−Hite 7500 amplifier.

switching regulators, amplifiers, data converters, filters. By the data-sheet of the amplifier, the working voltage and current of the amplifier are 100 V and 0.6 A and a load impedance of $Z_L = 100\ \Omega$ (see Fig. 6.3) is required in order to achieve the maximum current transmission between the amplifier and the coils system at frequencies up to 100 kHz.

6.3 Results

Analytical design

By the analytic model using the formula reported in [Wang et al., 2002], the geometrical and electric parameters as coil geometry and shape, coil thickness, number of wires have been calculated as reported in Table 6.1. The dimension of the Helmholtz coil system satisfies the requisite of suitable volume available for the sample holder leaving an overall volume accessible of 12 x 12 x 7.4 cm^3.

Numerical model

Once identified the geometrical and electric parameters, a numerical study has been performed. As a first step, the magnetic field distribution between the two Helmholtz coils has been evaluated, when an electric current of 120 A is applied at a frequency of 20 kHz. The data are shown in Fig. 6.4 in terms of a 2D map of the magnetic field intensity in the xz and yz plane (see Fig. 6.4a and b). The field reaches an intensity of

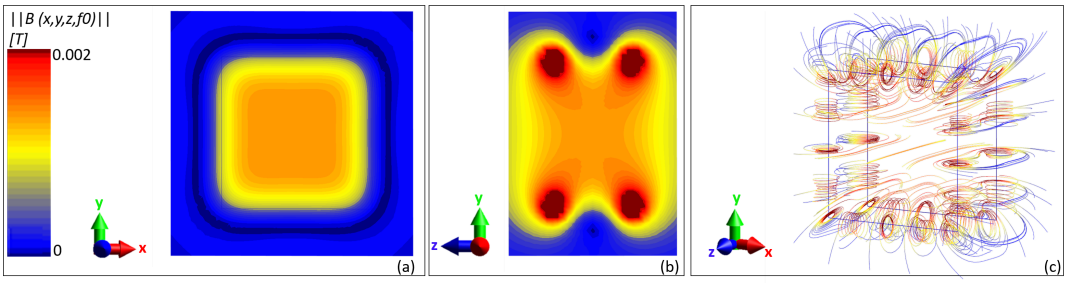

Figure 6.4: Magnetic field distribution. **(a)** 2D map of the magnetic field intensity in the xz and yz plane **(b)**, a magnetic field up to 2 mT is achieved with a good uniformity. **(c)** Streamline of the magnetic field is presented with flow lines going in the field direction.

2 mT near the coils and of 1.4 mT in the volume where the samples are supposed to be exposed. The magnetic field streamlines are reported in Fig. 6.4c showing the direction of the magnetic field between the two Helmholtz coils. The magnetic field intensity of 1.4 mT validates the project guidelines identified with the analytic study.
This result is also confirmed from the study of the magnetic field uniformity in the volume between the coils (see Table 6.2). In Table 6.2 it is possible to notice a homogeneity of the magnetic field of 95 % in the exposure volume of 9.12 x 9.12 x 7.5 cm^3.
Successively the aim has been to evaluate the electric and current distribution when the exposure sample was exposed to the magnetic field for a dose-dependent analysis. Our sample holders are the cuvette (Fig. 6.2b) and the chamber (Fig. 6.2c) respectively for MLs drug delivery and the TMS in−vitro applications. As for the magnetic field distribution, the result is the same reported for the coils system without the presence of the sample (data not shown). To evaluate the electric field inside the cuvette sample,

The exposure system for Drug Delivery applications

Diameter **2R**	15 cm
Thickness **t**	0.89 cm
Current **I**	0.6 A
Number of wires **N**	200
Distance **R**	7.5 cm
Resistance **R**	1.76 ohm
Inductance **I**	23.5 mH

Table 6.1: Geometrical and electric parameters of the Helmholtz coil.

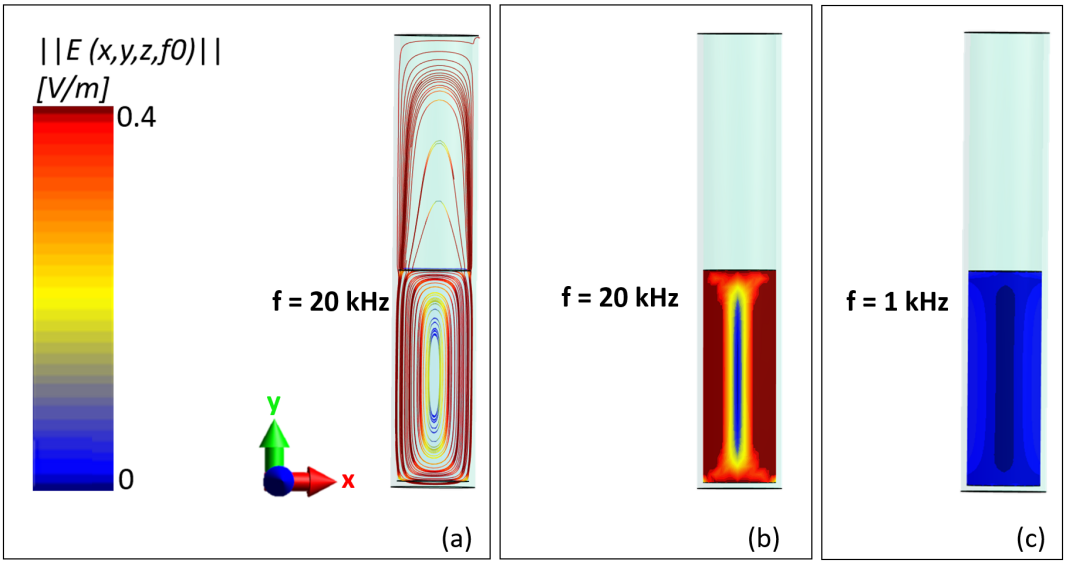

Figure 6.5: Magnetic field distribution. **(a)** Electric field streamlines are reported in the xy plane, suggesting a high electric field at the cuvette side and lower electric field inside the cuvette as showed in the 2D map of E **(b)** at the frequency of 20 kHz. **(c)** 2D map of the electric field at the frequency of 1 kHz resulting in a good homogeneity of the electric field inside the solution.

the streamline and a 2D map of the electric field distribution is reported (Fig. 6.5a and b respectively) for the experimental frequency of 20 kHz compared with the one of 1 kHz (Fig. 6.5a). It is possible to notice how inside the cuvette the electric field distribution is not highly homogeneous, highest to the side of the cuvette and lower to the center (Fig. 6.5a and b), in particular for the frequency of 20 kHz. Nevertheless, the electric field never reaches the value of 1 V/m, which means that no appreciable thermal increase can be generated from these electric field distributions, despite their in-homogeneity. As expected, decreasing the frequency to 1 kHz a higher homogeneity

Magnetic field homogeneity			
	95 %	**90** %	**80** %
Δx cm	9.12	10.36	11.86
Δy cm	9.12	10.36	11.86
Δz cm	7.49	8.98	11.60
Useful Volume cm^3	622.97	963.52	1631.65

Table 6.2: Magnetic field homogeneity

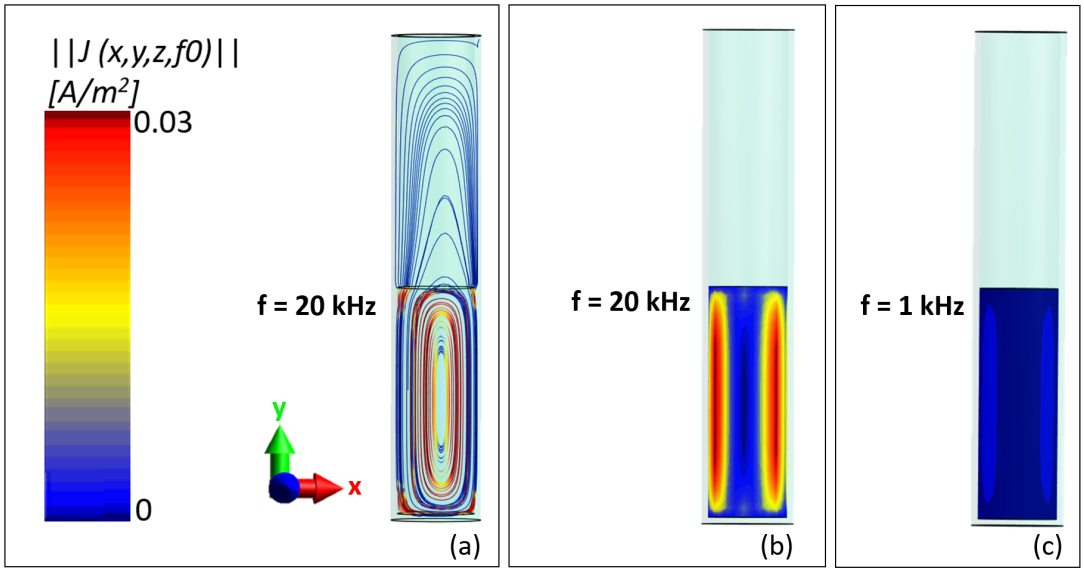

Figure 6.6: Magnetic field distribution. **(a)** Current density streamline inside the cuvette and the 2D current density map **(b)** for the frequency of 20 kHz in the xy plane. **(c)** 2D map of the current density inside the cuvette at the frequency of 1 kHz.

is reached for the electric field (Fig. 6.5c), with even lower intensities in the order of some mV/m.

A similar result is observable looking at the 2D maps of the current distribution inside the cuvette at 20 and 1 kHz (Fig. 6.6a, b and c). In fact, also current density distributions are more homogeneous at the lower frequency of 1 kHz, with values always below 0.03 A/m^2, ensuring a negligible thermal increase to the sample for the magnetic field exposure.

Moreover, in order to study the electric field variation inside the cuvette sample depending on the samples number and their position between the coils, we performed simulations at 20 kHz with 8 cuvette (Fig. 6.7a), by using always a conductivity of 0.049 S/m.

No variations were detected for the E field distribution with the respect to the one cuvette case, and a mean electric field of 0.413 V/m was reached inside of all the cuvette (Fig. 6.7) with a standard deviation of 0.075 V/m.

In-vitro magnetic stimulation exposure system

The second part of this work is related to an exposure system for in-vitro experiments on real cells and in particular on neuronal cell slices stimulation. To reach this objec-

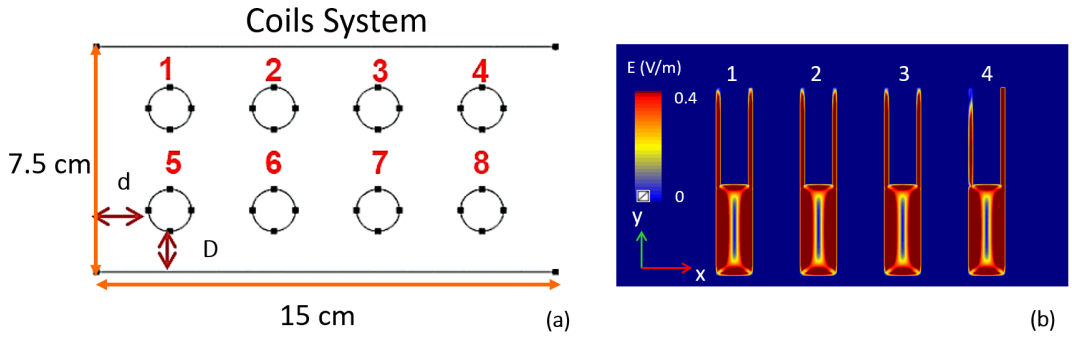

Figure 6.7: **(a)**Geometric distributions of the 8 cuvette between the coils, d = 1.7 cm and D = 1.35 cm; **(b)** E field distribution inside 4 cuvette, the result is the same also for the 4 on the other side.

tive we simulated a plexiglass chamber, i.e. the slice holder, placed between the two Helmholtz coils (Fig. 6.2c), at the frequency of 3 kHz [Di Lazzaro et al., 2013]. The aim has been to evaluate the electric and density current distribution inside the chamber to possibly detect secondary effects due to the magnetic field application. The magnetic field distribution for this setup is the same (data not shown) presented for the MLs system, ensuring a good exposure of the slices in a wide frequency range (up to 20 kHz). The results for the electric field distribution are reported in terms of streamlines (Fig. 6.8a) and 2D maps in three different planes, xz, yz and xy respectively (Fig. 6.8b, c, d). The electric field results to be higher to the plastic region of the chamber and lower in the liquid solution (blue color) as expected due to the higher permittivity value of the artificial cerebrospinal fluid solution. Moreover, looking at the 2D map in the xy plane (Fig. 6.8d) it is possible to appreciate a homogeneous electric field in the volume in which are expected to be exposed the slices (blue circle) with an intensity in the order of mV/m. This result guarantees a negligible effect of the induced electric field and a good isolation of the solution to the thermal effect.

Regarding the current density inside the exposure system, the results are shown in Fig. 6.9. The streamlines of the current density are reported confirming the current flowing in the region where the solution is present (red lines). This behavior is confirmed also from the 2D maps presented in Fig. 6.9b, c, d in three different planes (xz, xy and yz respectively). A good homogeneity of the current is achieved in the region where the slices are supposed to be exposed (red circle). Anyhow, the current increment (up to 2 mA/m^2) can be considered slight to do not provoke a significant

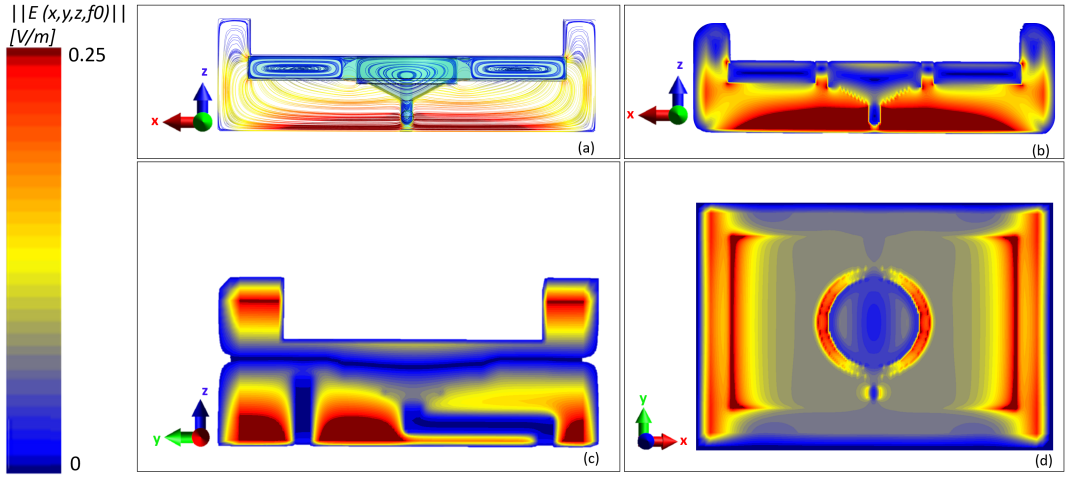

Figure 6.8: **(a)** The electric field streamlines are reported in the xz plane. The electric field results to be lower where the liquid is present and higher to the plastic region of the chamber (red and yellow lines); **(b,c,d)** 2D map electric field distribution in the xz, yz and xy plane, showing an homogeneous distribution of the field where the slices are supposed to be placed (d, blue circle).

thermal increase.

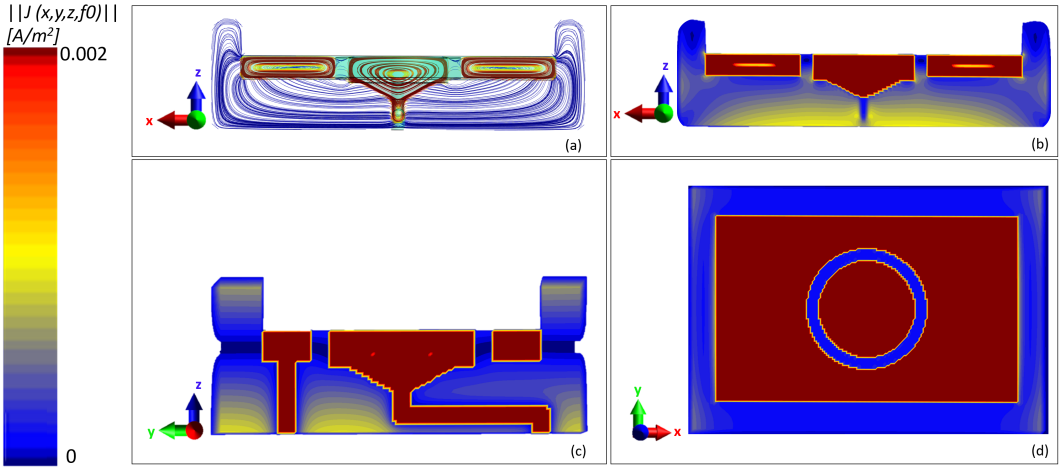

Figure 6.9: **(a)** The streamlines of the current density J are reported, in blue the current density in the plastic region of the chamber and in red the one inside the solution;**(b,c,d)** 2D maps of the current distributions in three different planes along the chamber, xz, xy and yz respectively.

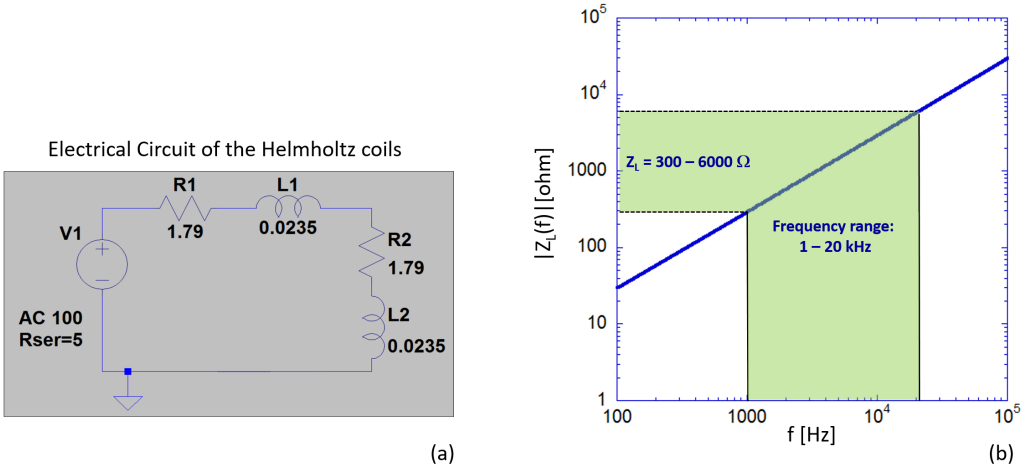

Figure 6.10: **(a)** Circuital model of the Helmholtz coils represented as two RL branches in series; **(b)** impedance values of the coils electric circuit at frequencies between 100 Hz and 100 kHz.

Circuital study

Once numerically evaluated the magnetic and electric distributions inside the twofold target (cuvette for MLs exposure and cell slices for in-vitro exposure) the matching problem is faced. As already mentioned in the material and methods section 6.2, in order to adapt the projected exposure system to the existing amplifier, we needed to match the load impedance for the coils at a value of 100 Ω as required by the amplifier data-sheet (see Sec. 6.2 Circuital Model). To reach this objective, a circuital analysis has been performed by using the LTSpice software. The two coils have been simulated as two RL (resistance and inductance) in series (Fig. 6.10a). The circuit was feed with an alternate signal (sinusoidal wave) with intensity of 100 V and an internal resistance of 5 Ω. The inductance and resistance values, simulating the two coils, are the one shown in Table 6.1 from the analytic study. In Fig. 6.10b the load impedance value are reported depending on the frequency. The impedance has been calculated using the formula:

$$|Z_L| = \sqrt{4R^2 + \left(2\Omega \mathrm{L} - \frac{1}{\Omega \mathrm{C}}\right)^2} \tag{6.1}$$

where R, L and C represent the resistance, inductance and the capacity respectively and ω the cutoff frequency. As can be noticed in Fig. 6.10b in our frequency of interest (1−20 kHz) the value of the load impedance Z_L is higher than 100 Ω, not satisfying

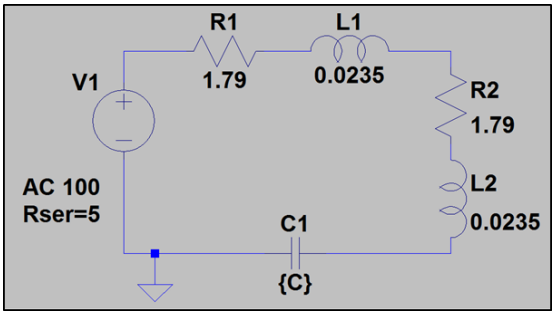

Figure 6.11: Electric circuit showing the two coils (R1L1 and R2L2) with the insertion of the capacity to obtain a load impedance ZL of 100 Ω.

the impedance required from the amplifier. Due to the need of a load impedance Z_L of 100 Ω, we inserted a capacity in series to the RL circuit as showed in Fig. 6.11.

In table 6.3 we reported all the capacity values, that provide the requested impedance of 100 Ω at frequency of 1, 5, 10 and 20 kHz. The capacity values range from 1.32 to 400 nF.

To conclude the circuital study, in order to match the exposure system, not only when a sinusoidal signal is applied, the circuit has been adapted when a single pulse of 100 V and an active phase of 1.3 ms is applied (see Fig. 6.12a). Firstly, we verified if also with a pulsed signal as input, the circuit resulted already adapted with the insertion of the capacity as done for the alternate signal. The study has been performed considering the capacity value of 400 nF, founded for the 1 kHz frequency to match the 100 Ω of load impedance to the previous alternate signal. As is possible to notice in Fig. 6.12, when a 100 V pulse is applied (Fig. 6.12a) to the RLC circuit, the current does not give the expected signal amplitude ($\backsim$ 1.5 A) and shape (see the input voltage shape), in fact a correlation coefficient of 0.17 is founded between the real and the expected output signal. With the aim to adapt the circuit, a resistance of 50 Ω has been placed in series

	f (kHz)	**C1 (nF)**
	1	400
Z_L = 100 Ω	5	20.2
	10	5.21
	20	1.32

Table 6.3: Capacity values at frequencies of interest, that match the 100 Ω of load impedance.

to the RLC circuit, instead of the capacity, as showed in Fig. 6.13. In Fig. 6.13a the electric circuit is presented with the insertion of the 50 Ω of resistance that is able to produce an output signal with a correlation coefficient of 94 (Fig. 6.13b), which means that the circuit is adapted to the input signal.

From this circuital study, it is possible to conclude that in order to adapt the designed exposure system both to an alternate (sinusoidal) and a pulsed signal, a capacity or a resistor, respectively, needs to be placed in series to the coils.

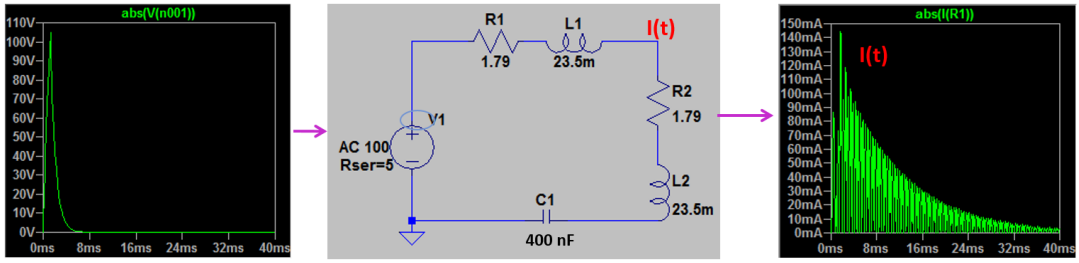

[Paffi et al., 2016] (a) (b) (c)

Figure 6.12: **(a)** 100 V input pulse of 1.3 ms of active phase; **(b)** Electric circuit showing the two coils (R1L1 and R2L2) with the insertion of the capacity of 400 nF (frequency of 1 kHz) to obtain a load impedance ZL of 100 Ω; **(c)** current output signal that arrives to the coils

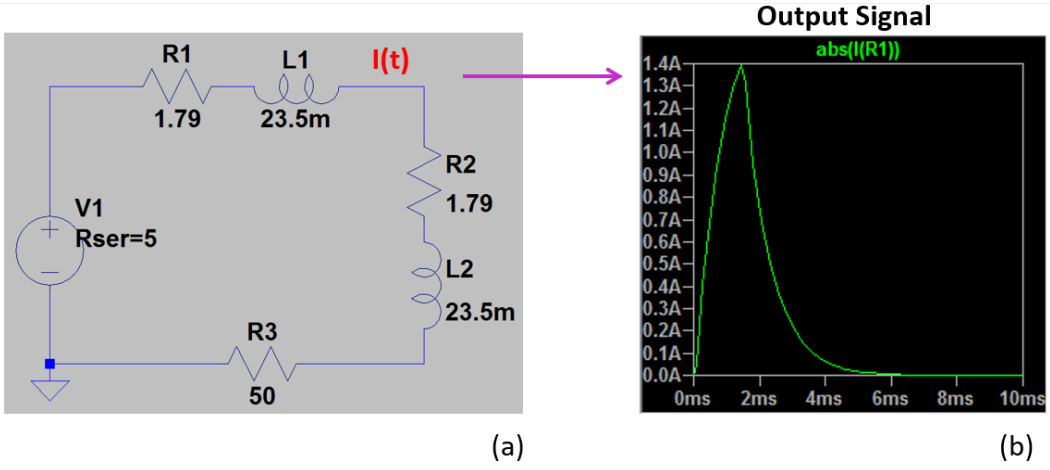

(a) (b)

Figure 6.13: **(a)** Electric circuit showing the two coils (R1L1 and R2L2) with the insertion of the resistance of 50 Ω **(b)** output signal.

6.4 Conclusions

In the last years, there has been an increasing attention in new medical treatments which involve the application of magnetic field in a broad category of diseases (i.e. neuronal disorders, inflammations, gene and cancer therapies, etc.) [Di Lazzaro et al., 2013]. In this chapter, the design of a versatile magnetic exposure system has been presented. The designed system is a multipurpose exposure setup able to be used for experimental applications as MLs poration for drug delivery and in-vitro magnetic neuronal cells stimulation. The aim has been a dose-dependent analysis for both applications to verify the generation of a magnetic field intensity in the order of mT with no secondary effect on the exposed sample, as a thermal increase due to high endogenous electric field or current density.

The system is based on a couple of squared Helmholtz coils able to provide an intensity of 1-2 mT at frequencies up to 20 kHz. Firstly an analytic study has been done to identify the geometric and electrical parameters to fulfill the project requirements. A dimension of 15 cm and a current of 0.6 A with 200 wires have been identified.

Next to this analytic study, numerical simulations were performed using the software Sim4Life to validate the geometric and electrical parameters and to analyze the magnetic field intensity. A magnetic field intensity of 1.4 mT has been obtained in the volume between the coils where is supposed to be placed an exposure sample. A homogeneity of 95 % has been calculate in a volume of 9.1 x 9.1 x 7.5 cm^3 of exposure. Next to this evaluation, two different simulations have been carried out, one considering a cuvette filled with a conductivity solution of 0.049 S/m (experimentally measured) for MLs drug delivery purpose and another one with a chamber placed at the center of the coils filled with artificial cerebrospinal fluid solution for in-vitro applications.

Regarding the simulations of the MLs drug delivery system, at the frequency of 20 kHz, we reported the 2D map of the E and J inside the solution obtaining an electric field below 1 V/m and a current density in the order of mA/m^2. With this results it can be excluded any possible thermal effect acting on the solution during the magnetic field exposure. This outcome has been confirmed also at the frequency of 1 kHz where a more uniform and low E and J values have been reached inside the cuvette.

Concerning the exposure system for in-vitro experiments, we simulated a plexiglass chamber containing an artificial cerebrospinal fluid solution, the typical buffer used for brain slices in-vitro exposure, placed at the center between the two coils. The simula-

tion has been made at the typical TMS frequency [Di Lazzaro et al., 2013] of 3 kHz. Both for the induced E and J the results have been a good homogeneity in the volume of the slice exposure with low values for both observable in the mV/m and mA/m^2 range respectively.

Next to the numerical study, a circuital study has been carried out to match the 100 Ω of load impedance of the amplifier already present in the laboratory experimental setup. In order to have the maximum current feeding the coils system, a capacity is needed to be placed in series to our coils when an sinusoidal signal is applied. The capacity values have been calculated ranging from 1 to 400 nF for frequencies from 1 up to 20 kHz. Moreover, in order to match our system when a pulsed signal is applied of 1.3 ms of active phase, a resistance of 50 Ω is needed in series to the coils instead of the capacitor to have the maximum transferred current.

The results obtained suggest that the designed exposure setup could give the possibility to have negligible thermal increase in two of the principal therapeutic applications of low intensity magnetic fields in the IF frequency range, with the possibility to reach intensity in the order of mT without compromising the sample due to secondary effects.

Part IV

Nanosecond pulsed electric fields for liposomal drug delivery systems

As already mentioned in the section Sec.2 smart drug delivery systems represent an interesting tool to significantly improve the efficiency and the precision in the treatment of a broad category of diseases.
Because with this Ph.D. thesis the aim is to investigate the application of EM fields for medical purposes, in this context, a drug delivery mediated by nanosecond pulsed electric fields is reported since it seems a promising technique, allowing for a controlled release and uptake of drugs by the synergy between the electropulsation and nanocarriers (e.g. liposomes) with encapsulated drugs. The main concern about the use of electroporation for drug delivery applications is the difference in dimension between the liposome (nm range) and the cell (μm range). The choice of liposome dimension is not trivial. Liposomes larger than 500 nm of diameter could be recognized as pathogen agents by the immune system, while liposomes of smaller size would require external electric field of high amplitudes for the membrane electroporation that could compromise the cell viability.
The aim in the Chapter 7 has been to theoretically study the possibility of a simultaneous cell and liposomes electroporation. The analytic study of a 12 nsPEF will be performed by the analysis of its spectral frequency content. Then, the liposomes membrane poration will be explored for liposomes of 100, 200 and 400 nm of diameter. As latter, numerical simulations of a cell plus 200 nm liposomes are reported to study the possibility to electroporate the cell and a significant percentage of liposomes with comparable values of external electric field, when a 12 nsPEF is used.
Next in the Chapter 8 the design and characterization of a 10 nsPEF exposure system is presented for liposomes exposure and preliminary experimental data are reported. The design and the characterization of the applicator have been carried out choosing an electroporation cuvette with 1 mm gap between the electrodes. The structure efficiency has been evaluated at different experimental conditions by changing the solution conductivity. Moreover, with the aim to analyze the influence of device performances on the liposomes electroporation, microdosimetric simulations have been performed considering liposomes of 200 and 400 nm of dimension with different inner and outer conductivity in order to identify the voltage needed for their poration. Then, to perform a more realistic microdosimetric model, a non uniformly liposomes population has been simulated by using the chosen conductivity values. Finally, preliminary experiments have been carried out on a 250 nm liposomes population applying an electric field of 9 MV/m.

Chapter 7

Exploring the Applicability of Nano-Poration for Remote Control Liposomal Smart Drug Delivery Systems

7.1 Introduction

The application of pulsed electric fields on a cell structure causes the permeability of its membrane due to the rise of the transmembrane potential with respect to a resting condition [Kotnik et al., 2010, Joshi and Schoenbach, 2010].
This phenomenon, known as electropulsation, has allowed the development of several interesting applications, as mentioned in the Section 2.3 such as the anticancer electrochemotherapy [Miklavčič et al., 2012, Cadossi et al., 2014], electrofusion [Teissie and Rols, 1986, Rems et al., 2013], gene electrotransfer [Mir et al., 1999, Calvet et al., 2014], beverages sterilization and food processing [Saulis, 2010].
As already anticipated in the Section 2.3, with the advancement of technology, the use of electric pulses of shorter duration (nanosecond) and higher intensity (in the order of MV/m) (nanosecond pulsed electric fields, nsPEF) allows to directly interact with internal cell organelles (e.g. nucleus, endoplasmic reticulum, mitochondria, etc.) [Beebe et al., 2003b, Scarlett et al., 2009, Breton and Mir, 2012, Denzi et al., 2013]. This aspect expanded the horizon of the scientic experiments [Breton and Mir, 2012] and

the development of microdosimetric models [Kotnik and Miklavčič, 2006, Merla et al., 2011] helping clarify the not yet completely understood effects of the nsPEF on internal organelles. The use of nsPEF for potential drug delivery applications can be a promising technique because it might allow the controlled release of drugs encapsulated in a nanocarrier (i.e. liposomes) by the application of an appropriate electrical stimulus. The goal is to design, engineer and introduce into the body molecular carriers of nanoscale dimension (hundreds of nm) that would release drugs close to the target cells directly at the place where the drugs must act using controlled application of an external electric field and avoiding any damage to healthy cells and to the surrounding tissues. Thus, the drugs would act locally, and additionally their release could be sustained over a period of time in a controlled manner.

Liposomes are one of the classical carriers (see Section 2.2) used in medicine for drugs encapsulation and delivery [Xiang and Anderson, 2006, Seigneuric et al., 2010, Stuart et al., 2010]. They are widely used in medicine applications thanks to their non− toxic, biocompatible and biodegradable characteristics [Mitsopoulos and Suntres, 2011], and they act as physical barriers to protect the internal drug from degenerative enzymes. As mentioned in the Section 2.2, liposomes can be activated both from endogenous and exogenous stimuli as pH variation, thermal increase, magnetic or electric stimuli. Recently, some studies began to evaluate the effects of pulsed electric fields on liposomes of giant dimension (micrometer scale) because they are representative of a good cell model [Breton and Mir, 2012, Portet et al., 2012, Breton et al., 2015]. However, their large size does not allow this kind of liposomes to be used for drug delivery applications because they could be recognized as a pathogen agent by the immune system [Miyata et al., 2011] and also the liposomes composition is important whenever or not an immunologic response is generated [Perrie et al., 2001, Watson et al., 2012].

Recently, Retelj et al. [Retelj et al., 2013] studied, by means of a numerical model, a biological cell containing a nucleus and small internalized artificial lipid vesicles (liposomes) of different nanometer sizes (from 50 to 500 nm) located in different sites in the cytoplasm. The authors of the paper predicted the selective electroporation of the liposome and cell membrane as a function of the inner liposome conductivity and/or the cytoplasm conductivity through the application of electric pulses of different duration (4, 10, 20 and 50 ns). In addition, it was also shown that the position of the liposomes inside the cell does not play a significant role in the electroporation process. For the study, the liposomes were placed inside the cell with the aim of an intracellular

drug release. Conversely with the work presented in this chapter, the idea of using liposomes placed outside the cell is carried out as it seems a situation easier to achieve. The novelty in the usage of nsPEFs relies in the possibility to cause both the cells and the liposomes membranes electroporation; in such a way, the liposome poration could permit the drugs release in the extracellular medium, close to the cells, and an easy uptake of the drugs by the electroporated cells can be achieved (concept similar to the electrochemotherapy one, with the benefit of the increased drug concentration in the tumor due to its vectorization in liposomes, used as nanocarriers). The size of the liposomes is a critical parameter that needs a compromise between the amplitude of the field and the immune system response. The first one has to be intense enough to allow for the electroporation process, while it is important to avoid the immune system reaction to liposomes of large dimensions (i.e. with diameter 500 nm) [Miyata et al., 2011]. Until now, the main concern in the use of liposomes combined with electroporation is that the biological cells are of much larger dimensions than the liposomes, and, according to the usual Schwan′s equation at steady-state [Postow and Polk, 1996, Kotnik and Miklavcic, 2000], they are permeabilized by field values much smaller than the ones needed to permeabilize a liposome [since, under these conditions, there is a direct proportionality between the transmembrane potential (TMP) and the radius], as usually is required in electrofusion applications [Ramos et al., 2002, Demange et al., 2011]. As a consequence of this, the intensity of the electric pulse able to reversibly permeabilize the liposome would cause, at the same time, too drastic effects on the biological cell (e.g. irreversible electroporation, cell death, etc.). Here, the idea is to combine cell and liposomes for drug delivery mediated by electroporation relies on the high frequency content of the nsPEF signals that cause the steady-state Schwan′s equation to lose its validity [Pakhomov et al., 2010]. In such case, it is necessary to consider a second-order model as in [Postow and Polk, 1996, Kotnik and Miklavcic, 2000, Merla et al., 2012] in which the dimension effect is not as critical and the permittivity and conductivity values become more important [Silve et al., 2015].

The aim of this chapter is to present the proof-of-concept of the nsPEF inducing a TMP variation (e.g. 1 V) able to achieve electropermeabilization in the liposome membrane with electric field amplitudes similar to the ones needed to simultaneously permeabilize a biological cell membrane. This demonstration would open the way to a feasible use of nanopulses for smart drug delivery applications where the electric pulse acts as a remote controller of the drug release by the carrier and as facilitator of the drug loading

by the cell. To explore this possibility, this work is focused on a theoretical analysis through a microdosimetric study of liposome vesicles with dimensions up to 400 nm both alone and in more complex systems such as a 200 nm liposomes distribution surrounding a cell, in order to study the influence of liposomes between each other and with respect to the cell electroporation.

7.2 Materials and Methods

Microdosimetric Models: Liposome Alone and a Complex System of a Cell plus liposomes

To demonstrate the possibility to use nsPEF on liposomes with dimension in the range of hundreds of nanometers, 2D numerical simulations were carried out using the software Comsol Multiphysics v. 5.0. The 2D models consist of a rectangular box with dimensions of 70 x 100 μm representing the extracellular medium in which first a liposome alone and then a complex of a cell plus liposomes in different positions were placed (Fig. 7.1). The field amplitude was set to 1 MV/m and the pulse duration, considered as width at half height, is of 12 ns (rise and fall time of 2 ns and t_{ON} = 10 ns). The simulation was settled considering the right and the left sides of the box as electrodes, while the upper and the lower sides as electrically insulated. The right electrode was set to the ground, and the 12 nsPEF excited the left one.

Liposome Model

Considering that in the experiments the dimensions of the liposomes, the ionic concentration of the buffer solution and of the vesicle core can be controlled and varied, the numerical simulations were carried out with a different set of liposome dimensions and of external and inner conductivity values. Firstly, a single liposome with diameters (d_{lip}) of 100, 200, and 400 nm (Fig. 7.1a) was placed in the centre of the box, between the two electrodes. The membrane thickness (dm) was set to 5 nm, and the external and the inner liposome conductivities (σ_{ext} and σ_{int}) were set from 0.05 to 1.5 S/m. All the other parameter values are displayed in Table 7.1.

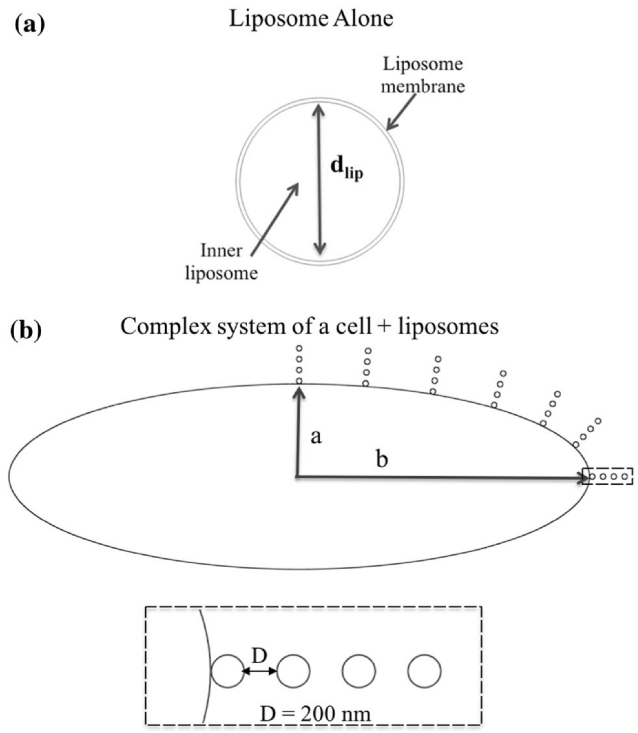

Figure 7.1: **(a)** The model of the liposome alone considering different liposome diameters: d_{lip} = 100, 200 and 400 nm. **(b)** The cell plus the 200 nm liposomes distribution model; the liposomes are placed at a distance D of 200 nm between each other and up to 1.2 μm from the cell surface; cell dimensions are a = 3.5 μm and b = 11 μm.

System of the Cell Plus a 200 nm Liposomes Distribution

After the evaluation of the nsPEF effects on liposomes of different dimensions, as will be discussed in the next section, a system of an ellipsoidal cell (i.e. myocyte), plus a 28 liposome distribution of 200 nm size (Fig. 7.1b) surrounding the cell, was implemented, in order to analyze the effects of the simultaneous presence of them. Since the ellipsoidal shape could well represent a number of human cells (i.e. myotubes, retina photoreceptor cells, etc.) [Hu and Joshi, 2009, Radu et al., 2005], we decided to model the cell with an ellipsoid with minor and major semiaxes of 3.5 and 11 μm (a and b, respectively, Fig. 7.1b). The membrane thickness (μm) of the cell was set to 5 nm. At the pole side, four 200 nm spherical liposomes were placed from tangent position up to 1.2 μm of distance with respect to the cell. The same set was replicated considering different

angles starting from the pole to the equator. The simulations were carried out with the external conductivity fixed at $\sigma_{\text{ext}} = 1.5$ S/m (the same for the inner conductivity of the liposomes σ_{int}). The high conductivity medium can induce a more efficient cell reversible permeabilization [Silve et al., 2015] and hence could permit the auspicated simultaneous cell and liposome membrane poration with the same E field intensity. The cytoplasm conductivity was set to 0.3 S/m as in [Denzi et al., 2015]. The permittivity values for the cell are also reported in Table 7.1.

7.3 Results and Discussion

The Concept

Cell and liposome dimension

The combination of a liposome of small dimensions and a cell of large ones (ratio $R_{\text{cell}}/R_{\text{lip}} \approx 100$) leads to the analysis of how the dimensions of the liposome and the cell can influence the electroporation effects on this type of structures. The results for the TMP in the frequency domain, due to the applied nsPEF (Fig. 7.2a), are reported in Fig. 7.2b for the ellipsoid cell and a liposome with 200 nm size, described in the Section 7.2. The figure 7.2 shows how the geometrical and electrical parameters could influence the TMP response in terms of physical mechanisms that occur in the cell or liposome. In static conditions and at low frequency values, the well−known Schwan′s equation, for spherical structures, reports a linear relationship between the TMP and the dimension of the structures [Postow and Polk, 1996]:

$$TMP = f_{\text{s}}\text{ER}\cos(\phi) \tag{7.1}$$

Dielectric properties	ϵ_{r}	σ (S/m)
External medium	67[a]	1.5[c]
Cell and Liposome Membrane	11.7[a]	1.1x10^{-7}[a]
Cytoplasm	67[a]	0.3[a]
Inner Liposome	67[a]	1.5[c]

Table 7.1: Electric parameters for cell and liposomes; [a] [Merla et al., 2012];[a] [Denzi et al., 2015]; [c] [Silve et al., 2015]

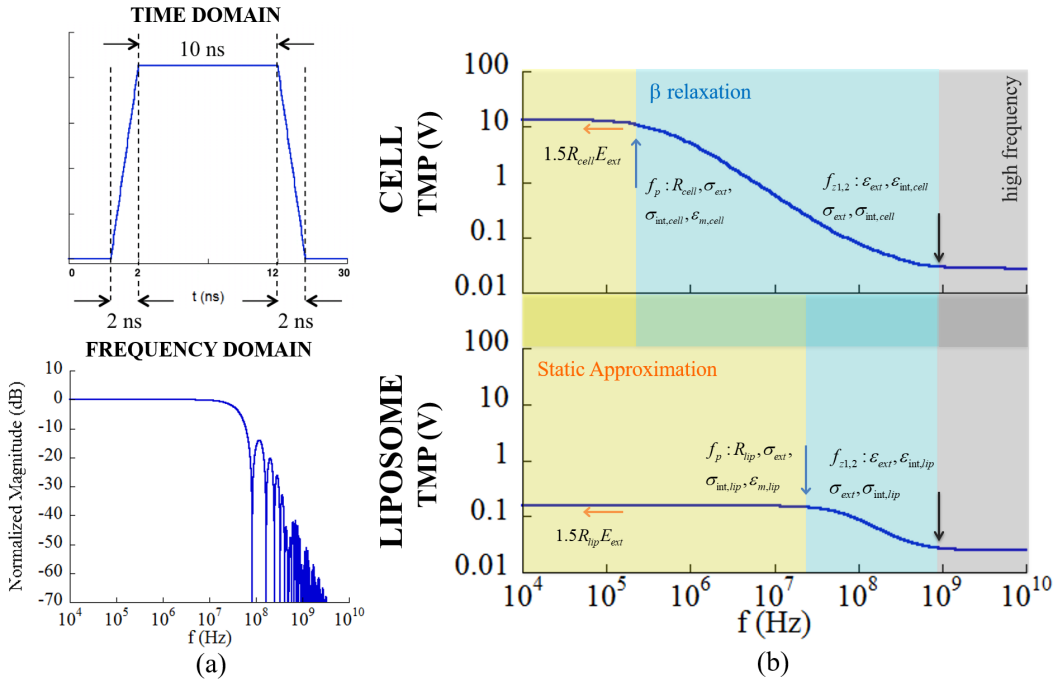

Figure 7.2: **(a)** Applied electric field and its spectrum, **(b)** TMP in frequency for cell and liposome structure.

where f_s is a function that depends on cell and external medium characteristics [Kotnik et al., 1997], its value for a spherical shape in physiological conditions is about 3/2, E is the applied external electric field, R is the radius of the considered structure and ϕ is the angle with respect to the electric field direction. The direct proportionality of the TMP and the radius in Schwan's equation at low frequency determines that the ratio between the fields necessary to electroporate the cell and the liposome is equal to $R_{\text{cell}}/R_{\text{lip}}$, and this is confirmed from Fig. 7.2b. Moreover, the differences in terms of liposome and cell radii determine a different validity limit of the static approximation in the frequency range; in particular, for the cell its validity is for a frequency value up to hundreds of kHz and for the liposomes it is up to tens of MHz. This means that a different physical phenomenon occurs in the liposome and cell in the frequency range [100 kHz $\backsim$ 10 MHz] in which the static approximation is not valid for the cell but still valid for the liposome. For frequencies above the limits of the static approximation, the previous formula 7.3 is not valid, and the TMP starts to decrease

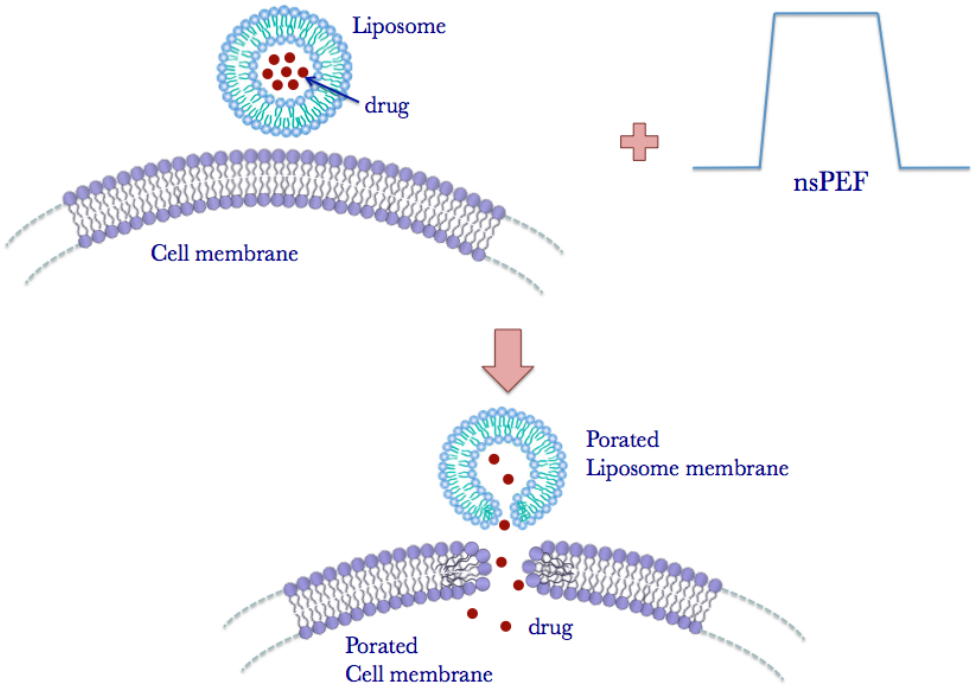

Figure 7.3: Concept of liposomal drug delivery system mediated by nano-electroporation.

with the frequency [Postow and Polk, 1996, Kotnik and Miklavcic, 2000, Kotnik et al., 1998]:

$$TMP(\omega) = f_s(\omega)\mathrm{ERcos}(\phi) \tag{7.2}$$

where

$$f_s(\omega) = \frac{3\sigma^*_{ext}\left[3d_m R^2\sigma^*_{int} + (3d^2_m R - d^3_m)(\sigma^*_m - \sigma^*_{int})\right]}{2R^3(\sigma^*_m + 2\sigma^*_{ext})(\sigma^*_m + \frac{1}{2}\sigma^*_{int}) - 2(R - d_m)^3(\sigma^*_{ext} - \sigma^*_m)(\sigma^*_{int} - \sigma^*_m)} \tag{7.3}$$

and $\sigma^*_i = \sigma^*_i + j\ \omega\ \epsilon_i$, with *ext* referring to the extracellular medium, *int* for the internal of the structure and *m* for the membrane. In this case, the TMP(ω) is a second-order system with two poles and two zeros as it can be seen by the decay followed by the plateau in Fig. 7.2b.

E_{th} for the liposomes poration

100 nm Liposome

σ_{ext} = extra-cell conductivity
σ_{int} = inner liposome conductivity

σ_{ext} \ σ_{int}	**0.05**	**0.55**	**1.05**	**1.55**
0.05	25.7 MV/m	18.1 MV/m	17.6 MV/m	17.5 MV/m
0.55	18.0 MV/m	10.3 MV/m	9.8 MV/m	9.7 MV/m
1.05	17.6 MV/m	9.8 MV/m	9.4 MV/m	9.3 MV/m
1.55	17.4 MV/m	9.7 M V/m	9.3 MV/m	9.2 MV/m

200 nm Liposome

σ_{ext} = extra-cell conductivity
σ_{int} = inner liposome conductivity

σ_{ext} \ σ_{int}	**0.05**	**0.55**	**1.05**	**1.55**
0.05	22.1 MV/m	14.3 M V/m	13.8 MV/m	13.6 MV/m
0.55	14.3 MV/m	6.6 MV/m	6.0 MV/m	5.8 MV/m
1.05	13.8 MV/m	6 MV/m	5.4 MV/m	5.2 MV/m
1.55	13.6 MV/m	5.8 MV/m	5.2 MV/m	5 MV/m

400 nm Liposome

σ_{ext} = extra-cell conductivity
σ_{int} = inner liposome conductivity

σ_{ext} \ σ_{int}	**0.05**	**0.55**	**1.05**	**1.55**
0.05	20.1 MV/m	12.6 MV/m	12 MV/m	11.8 MV/m
0.55	12.3 MV/m	4.8 MV/m	4.1 MV/m	3.9 MV/m
1.05	12 MV/m	4.1 MV/m	3.5 MV/m	3.2 MV/m
1.55	11.8 MV/m	3.9 MV/m	3.2 MV/m	2.9 MV/m

Figure 7.4: E_{th} is the electric field intensity necessary for the membrane liposome poration of different dimension.

The dependence of these poles and zeros by the cell or liposome parameters is reported in Fig. 7.2b and is analysed in detail in [Merla et al., 2012]. The first pole that determines the beginning of the β relaxation range depends mainly on the dimension of the structures, the membrane characteristics and the internal and external conductivities. The second pole and the two zeros depend mainly on all the electrical characteristics (conductivity and permittivity) of the internal and external media. As widely explained in [Merla et al., 2012] and [Denzi et al., 2013], in the highest frequency range (grey background in Fig. 7.2b), mostly in the GHz region, the main effect is due to the dispersion of the compartments. In this work, this effect is disregarded since the pulse duration is of 12 ns [Merla et al., 2012]. Considering the frequency content of a 12 ns pulsed electric field (first lobe at around 100 MHz, Fig. 7.2a), it is possible to notice that both the cell and the liposome are above the β relaxation. In this region, the two curves are very close together and the ratio between the two TMP values is very close to 1. This means that for a pulse with high frequency content, as a 12 nsPEF, the electric field necessary to permeabilize a liposome (nanometer size) and a cell (micrometer size) could be very similar leading to a possible simultaneous permeabilization without compromising the cell vitality, so that reversible electropermeabilization could occur on both membranes facilitating the drugs release from the liposomes to cell (Fig. 7.3).

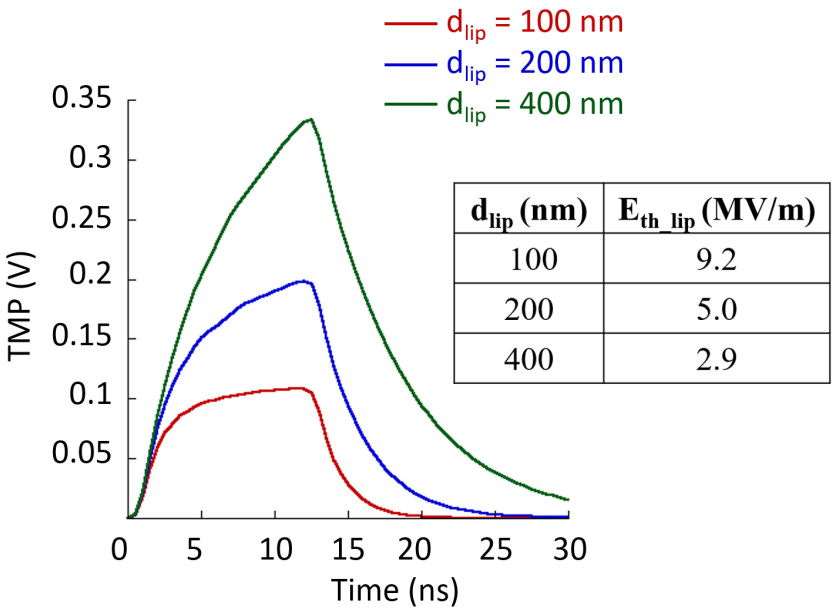

d_{lip} (nm)	E_{th_lip} (MV/m)
100	9.2
200	5.0
400	2.9

Figure 7.5: Liposome transmembrane potential variation (calculated at the pole of the liposome) increases with liposome diameter (d_{lip}= 100, 200, 400 nm); E_{th_lip} is the electric eld intensity necessary for the membrane poration.

Analysis of the Liposome Parameters

Choice of the Liposome Dimension

In order to analyze the influence of the liposome dimension, three numerical simulations considering liposomes with diameters of 100, 200, and 400 nm have been carried out considering different conductivity values as explained in the material and methods section. In Fig. 7.4 the results in terms of electric field needed for the liposome poration are reported, considering that a TMP of $\sim$ 1 V is needed for the poration [Smith et al., 2006]. A high inner conductivity value is chosen, for the simulation with the cell, which facilitates (see E_{th} values in Fig. 7.4, yellow highlight) the electroporation of liposome as already reported also in [Tekle et al., 2005]. As expected, by comparing with equal high internal and external liposome conductivity ($\sigma_{ext} = \sigma_{int} = 1.55$ S/m), the TMP (calculated for an external electric field of 1 MV/m) increases with the liposome dimension (Fig. 7.5). The higher is the liposome dimension and the lower

are the E field intensities necessary for the membrane electroporation. The 200 nm liposome seems to be the best compromise between the E field intensity necessary for the membrane poration and the response of the immune system that could recognize too large liposomes as a pathogen agents [Miyata et al., 2011].

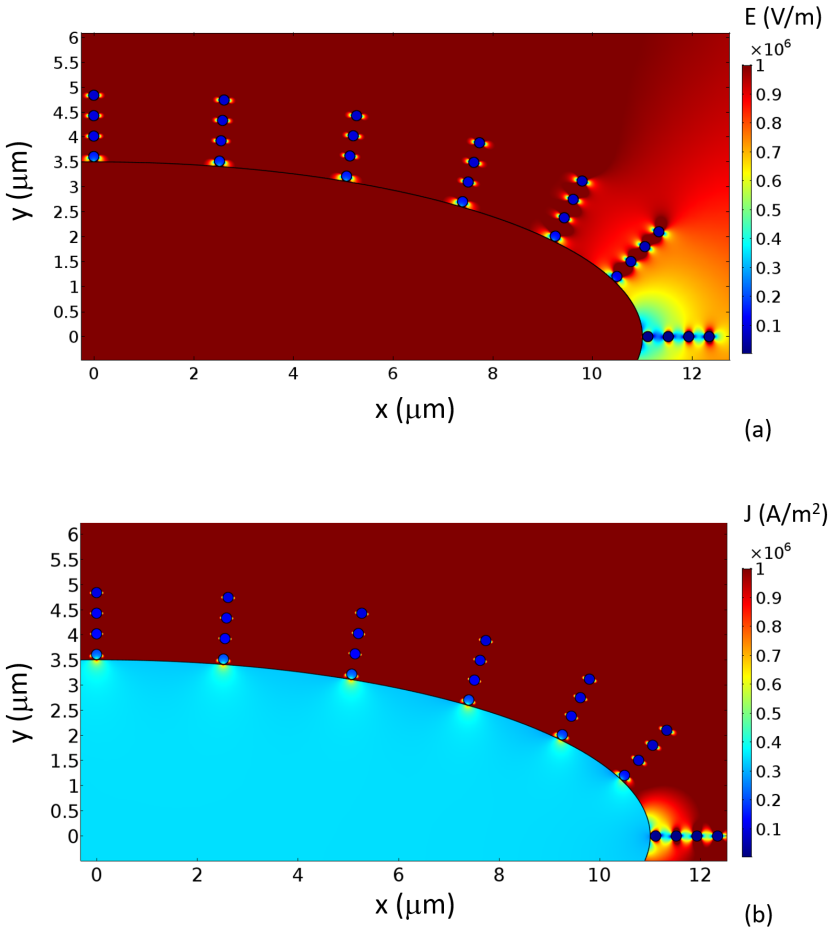

Figure 7.6: 2D map of electric field **(a)** and of the current density **(b)** around the cell and liposomes excited with an external pulsed electric field of 1 MV/m at time t = 12 ns

Analysis of Results of the Complex of the Cell and the 200 nm Liposomes Distribution

Electric field 2D map

Based on the previous chosen parameters for the liposome (200 nm of diameter), a

complex system of a cell plus a 28 liposomes distribution was modeled as described in Fig. 7.1b. In Fig. 7.6 , a 2D map of the electric field and current density distribution around the cell and liposomes is presented at t = 12 ns (time of the maximum TMP variation across the membrane). It is possible to notice how the external E field (see Fig. 7.6a) and also the current density (see Fig. 7.6b) intensity is lower to the equator and higher to the pole of the cell as well as of the liposomes. The electric field intensity distribution is symmetric on the other sides of the cell. This behavior could suggest a more facilitated poration for the liposomes at the cell pole.

TMP on liposomes and cell

In Fig. 7.7, the result in terms of TMP in the time domain is reported for the cell and liposomes placed in different angles with respect to the cell (from pole to equator). The TMP trend shows that the voltage value across liposomes membrane is similar to the one of the cell when they are placed closer to the cell pole (Fig. 7.7a, b). Moreover, at the equator, the difference between the cell and liposomes is more significant but still remaining with a ratio less than 3 (Fig. 7.7c). Besides, the closer is the liposome to the cell (i.e. tangent), the higher is the TMP across its membrane, showing a strong interaction between the liposome and the cell. This result confirms the concept that, due to the high frequency content of the 12 ns pulse (up to 108 Hz with the highest frequency contribution occurring during the transients and lowest frequency during the plateau of the pulse), the dimension is not playing a fundamental role: giving a ratio, between the external E field intensities necessary for the cell and liposome permeabilization, in the range of 1/2.5, very far from the ratio of ∼100 predicted in the low frequency range.

Percentage of porated liposomes

In order to study the percentage of porated liposomes with respect to the cell, the electric field necessary for the membrane poration (E_{th} poration) has been analyzed (see Fig. 7.8).

The result, reported in Fig. 7.8, shows almost the 50 % of porated liposomes when the cell membrane starts to be permeabilized (green arrow). When the cell membrane reaches the 10 % of electroporated area, the 80 % of liposomes have been porated (red arrow). This result suggests that in particular electrical conditions (12 nsPEF), it will be possible to electroporate almost all liposomes when the cell is at the 10 % of electroporation, considering this cell exposure level to nsPEFS acceptable in order to prevent the cell viability, possibly avoiding cell permanent damages [Ibey et al., 2011].

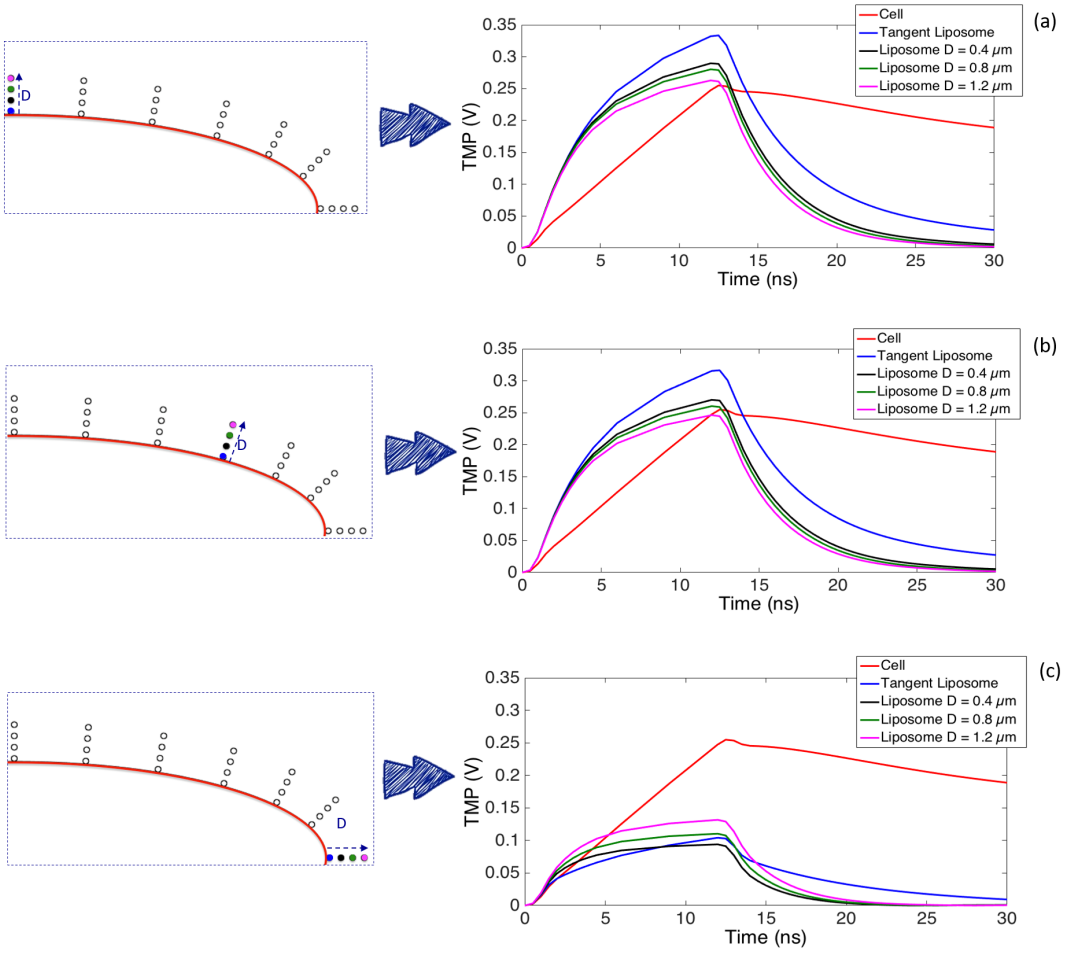

Figure 7.7: TMP variation of the complex of the cell plus the 200 nm liposomes distribution (placed tangent and at distance up to at 1.2 μm from the cell) in a medium highly conductive ($\sigma_{\text{ext}} = \sigma_{\text{int}} =$ 1.5 S/m) and at different angles, from pole **(a)** to the equator **(c)** of the cell.

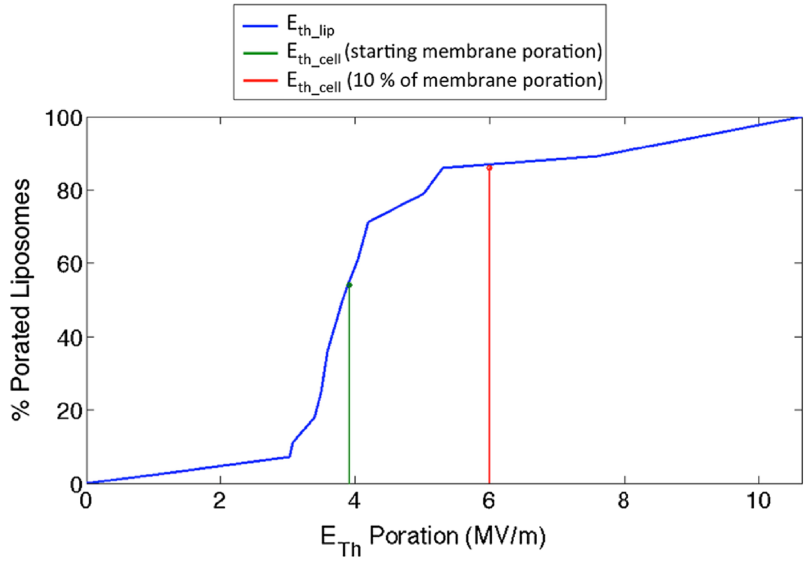

Figure 7.8: E_{th} poration is the E field necessary for the permeabilization of the liposomes (E_{th_lip}) and cell (E_{th_cell}). The blue line represents the E field necessary to porate liposomes, and the green and red lines represent the cell poration at beginning and at the 10 % of membrane poration, respectively.

7.4 Conclusions

In this chapter, the feasibility of the use of nsPEFs for drug delivery applications based on liposomes as nanocarriers is investigated numerically, analyzing the influence of both the geometrical and the electric parameters on the cell and liposomes electroporation. The concept is based on the broad spectra content of a 12 ns electric pulse for which the Schwan′s equation of the TMP becomes a second−order model [Postow and Polk, 1996, Kotnik and Miklavcic, 2000, Merla et al., 2012] in which the dimension effect is not as crucial as at the low frequency range. This has been elaborated with the analysis of the influence on the TMP in time domain due to the geometrical and electric parameters, which can be controlled in an experimental setup. As for the influence of liposome dimension on its membrane electroporation, the best choice is a liposome with a diameter of 200 nm as it results in a good compromise between the E field intensity required for the membrane poration and the absence of recognition by the immune system. Based on these results, with the same geometric (d_{lip} = 200 nm) and electrical parameters ($\sigma_{ext} = \sigma_{int}$ = 1.5 S/m), we carried out an analysis of a complex system

with one cell and a 28 liposomes distribution. The aim has been to study the influence of liposomes between each other and with respect to the cell in electroporation. Giving an excitation with a 12 nsPEF, it has been demonstrated that it is possible to permeabilize the liposomes and the cell with comparable E field intensity in particular when the liposomes are placed near to the cell pole. This result is confirming that the difference of the dimensions is not so crucial when using nsPEF.

Moreover, studying the percentage of permeabilized liposomes compared to the cell membrane, it has been proved that when the 80 % of liposomes is porated, the cell membrane is porated for the 10 % of its area; in this way, the cell viability is not compromised, and the liposomes and cell poration can occur with the same E field intensity. With this numerical study, the possibility to use nsPEF for drug delivery mediated by liposomes, has been proven. The models permit to identify the electric pulse characteristics, the external solution and the liposome parameters (d_{lip} = 200 nm and $\sigma_{ext} = \sigma_{int}$ = 1.5 S/m) to obtain the electroporation of the cell and liposomes population applying a comparable electric field intensity, with the possibility to simultaneously porate both of them without compromising the cell viability, opening the way for a possible drug delivery system controlled by the electropulsation.

In the next chapter the design of a liposomes exposure systems to nsPEFs and preliminary experiments will be reported concerning a liposomes solution exposed to 10 nsPEF.

Chapter 8

Technological and experimental aspects for testing electroporation on liposomes

8.1 Introduction

In the previous chapter (see Chapter 7) a technique has been proposed combining the application of nanosecond pulsed electric fields(nsPEFs) with liposomes as nanocarriers in drug delivery applications. The possibility of simultaneously porating cell membrane and liposomes with nanometer dimension has been numerically demonstrated in the case of the delivery of a single electric pulse of 10 ns duration and few MV/m of amplitude. This could open the way to a liposomal drug delivery system mediated by nanoelectroporation, facilitating drugs release from the liposomes to the cell.

The application to cells of one or several nsPEF of 10 ns duration is very common in nanoporation [De Menorval et al., 2016, Pakhomov et al., 2004]. Different types of applicators and devices can be used without compromising the shape of the applied pulse [Denzi et al., 2015, Merla et al., 2010]. Moreover, with the advances in micro and nano fabrication techniques, some micro-devices are proposed for nanosecond exposure, integrated also with a microfluidic system [Denzi et al., 2015, Dalmay et al., 2011a,b, Arnaud-Cormos et al., 2011].

A typical applicator is a standard electroporation cuvette consisting of two plate parallel electrodes with a gap of 4, 2, or 1 mm [Silve et al., 2016, 2012, Kohler et al., 2012,

Merla et al., 2010]. In particular, the 1 mm gap cuvette permits generating higher values of the electric field in the solution,but in such cases the matching with the 50Ω of the pulse generator can be critical [Silve et al., 2012, Kenaan et al., 2011]. However, the choice of a 10 ns pulse, due to its frequency content (first lobe at around 80 - 100 MHz depending on the rise and fall times), allows comfortably selecting the cuvette as applicator, even if the matching conditions of the structure need to be evaluated. Conversely, for shorter pulse duration (i.e., 3 ns and 1 ns), the complication of a broad-band matching, up to GHz region, becomes necessary otherwise the cuvette will cause a significant distortion of the trapezoidal signal. The use of a standard cuvette is also advantageous in the case of nanometer liposomes exposure late to the necessity to detect a fluorescent release. Indeed, due to their small dimensions, liposomes visibility under a microscope cannot be possible. In this case the fluorescent measurement is done with a spectrofluorimeter reader able to detect fluorescent molecule concentrations. This technique requires a minimum volume of solution,easily collected from the electroporation cuvette [Chen et al., 2006, McNamara and Rosenzweig, 1998].

In this chapter, a methodology for the exposure of liposomes with dimension in the nanometer scale (in particular 200 and 400 nm liposomes) is proposed in terms of design of the exposure system combined with theoretical evaluation of the electric field threshold needed to porate the liposomes with preliminary experimental data on a 250 nm liposome distribution. As a first step, an integrated approach is proposed to deal with experimental and modeling aspects, with the fundamental role of understanding and interpreting biological results. Once the specifications needed by the presented application were clarified, with particular care to the connection with the generator, the cuvette holder and the transition to the coaxial connector have been designed. A complete frequency characterization of the final structure, both with numerical modeling and measurements, has been done in order to understand the cuvette response under different experimental conditions. After the characterization of the exposure system, a microdosimetry model of the liposomes was also developed to approach the electric field needed for the poration considering the limitations imposed by the real experimental setup. As last step preliminary experiments have been settled on a 250 nm liposomes population by applying an electric field of 9 MV/m.

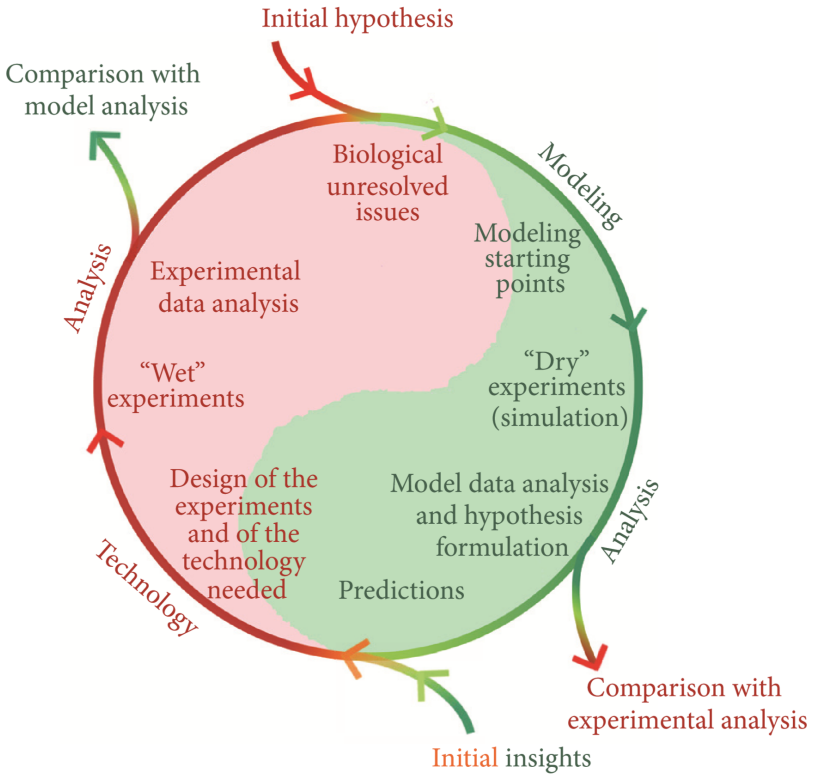

Figure 8.1: Schematic of the integrated approach necessary to understand the biological results: the cycle points out the importance of a continuous exchange between the experimental and modeling aspects.

8.2 Materials and Methods

Integrated approach for biological understanding

The researchers agree that, in biological issues resolution, the cooperation between experiments and modeling must be considered as a fundamental step [Merla et al., 2010, Apollonio et al., 2013, Denzi et al., 2015, Silve et al., 2016]. In particular, this aspect is critical and significant when one wants to investigate the interactions between the electromagnetic fields and the biological objects. In Figure 8.1 a readapted version of the Kitano cycle proposed for system biology [Kitano, 2002a,b] has been reported and applied to our issue. The basic concept is the possibility of beginning the cycle at differ-

ent points of the experimental and model parts. Wherever there is an output from the cycle,an improvement in our biological knowledge is attained. Two different strategies exist: "Model Driven" and "Experiment Driven". In the first one, corresponding to the green part of the cycle, the model part drives the experiments generating a prediction. In the latter,associated with the red part of the cycle, the process begins from the experimentation with useful information to build a model able to explain what observed. When the access to the cycle begins from a particular biological hypothesis or issue(red arrow in the Figure 8.1 with reported initial hypothesis) or comes from the previous step of experimental data analysis, starting points and data for the model are provided. It is possible to build a simulation (that is called the "dry" experiment) to take into account the biological aspects, and this can be done at different levels of complexity (atomistic level and from the cell (micro level) to the tissue and organs levels(macro level)) [Apollonio et al., 2013, Marracino et al., 2016, Denzi et al., 2015, Casciola and Tarek, 2016]. The simulation results can be used to formulate hypothesis about the biological issues or to simulate the behavior of a particular device that then can be used for the experiments. At this point it is possible to get out from the cycle and compare the modeling results with the experimental data analysis or alternatively keep cycling to use the prediction to set up a "wet" experiment. To setup a "wet" experiment,a technological step is needed starting from modeling results. Next, the analysis of the "wet" experimental results is provided, and a direct comparison is possible with modeling outcomes getting out from the cycle. Alternatively, this analysis can be reused as a starting point for a new or upgraded model in a continuous exchange of information and knowledge.

Towards "Wet" experiments for electroporation on liposomes

Starting point

The starting points for electroporation applications regard the feature of the pulse and the target of the stimulation.

The study of liposomes poration can be the first step for the use of this kind of nano-carriers in drug delivery applications driven by nano-electroporation. In the previous chapter (see Chapter 7), it has been numerically demonstrated the possibility to porate liposomes of dimension up to 400 nm with a 10 ns electric pulse [Denzi et al., 2017]. Starting from these results, here an ideal 10 ns pulse (Fig. 8.2a) has been considered in the simulations as a good model of the one that our high voltage 50 Ω pulse generator

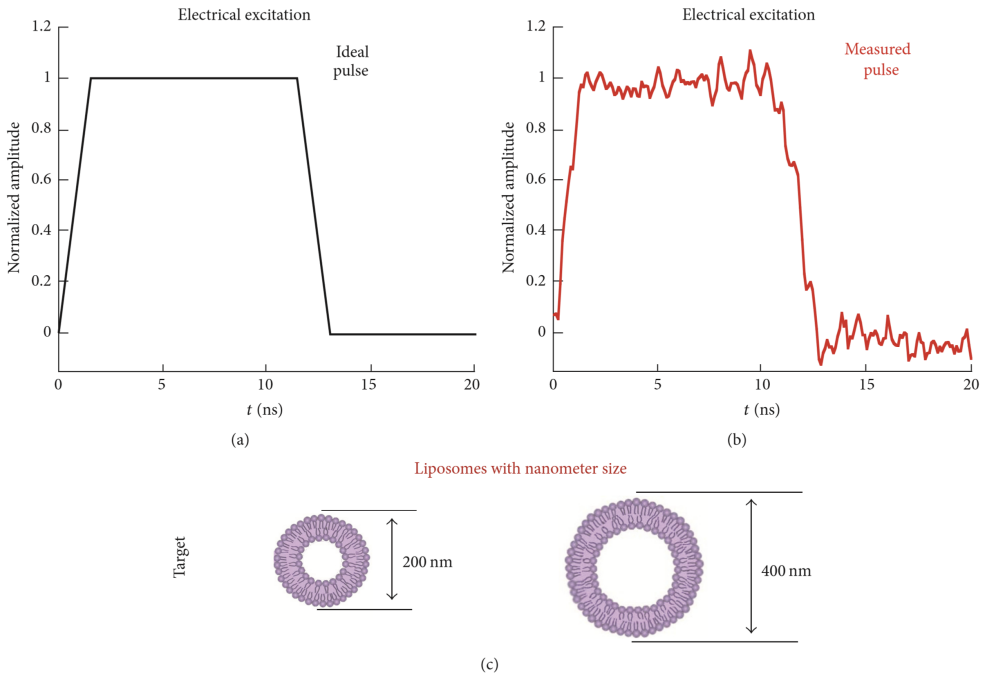

Figure 8.2: Electrical stimulus(ideal and measured pulses)and target for nanoelectroporation of liposomes.

(High Voltage Pulse Generator FPG 10-1NM10) is able to produce (i.e., Fig. 8.2b, example of a measured pulse). The target is represented by liposomes of 200 and 400 nm of diameter (see Fig. 8.2(c)). The selected stimulus and target drove the choice for the design of the experiments and of the experimental device (following the cycle in Fig. 8.1). In case of the 10 ns pulse, the spectral content (Fig. 8.2) is mainly contained in the first lobe (from 80 to 100 MHz) and hence a standard cuvette for electroporation can be selected as applicator without causing significant distortion on the pulse shape [Silve et al., 2012, Kohler et al., 2012, Kenaan et al., 2011]. The necessity to reach high electric field values for the poration of such small liposomes has led to the choice of a cuvette with 1 mm gap distance between the electrodes (1002561E, BioGenerica, ITA) and a particular attention has been taken regarding the connection of this cuvette to our 50 Ω pulse generator (High Voltage Pulse Generator FPG 10-1NM10).

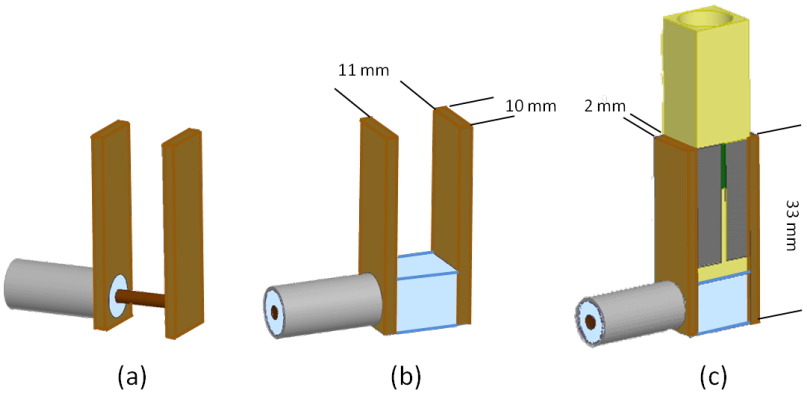

Figure 8.3: Modeling of the cuvette connection to the 50 Ω generator.

Design of the Applicator

Now, the design of the structure for the connection with the 50 Ω generator has been reported. In particular, the final proposed structure is shown in Fig. 8.3.

The idea is not to connect directly the coaxial cable to the cuvette [Kenaan et al., 2011] but to use the coaxial cable as a lateral feed of the cuvette holder.
The device consists of two brass electrodes with an area of 33 x 10 mm^2 and a thickness of 2 mm (Fig. 8.3). The gap between the electrodes is 11 mm and permits the perfect insertion of the electroporation cuvette between them. The central pin of the coaxial cable is connected with one of the two parallel electrodes (Fig. 8.3a) and the other is connected to the external sock (Fig. 8.3b). To mechanically stabilize the structure but also to avoid a central pin without any protection, a box of Teflon is placed at the bottom of the structure (Fig. 8.3b). In Fig. 8.3c the complete structure with the cuvette placed between the electrodes has been reported. The cuvette is a standard one (1002561E, BioGenerica, ITA), with dimension of active electrodes of 10 x 8 mm^2 and gap between them of 1 mm. In the first simulations the cuvette is filled with a solution with a conductivity of 0.25 S/m calculated, in order to obtain an impedance of 50 Ω, following the formulation in [Kenaan et al., 2011] for lower frequency in which the resistive behavior is predominant, $Z_{cuvette} = d/(A\sigma_{ext})$.

Furthermore, the characterization of the applicator response, for different conductivity values of the solution filling the cuvette, has been carried out in order to under-

stand the effect of this parameter on the structure performances. In particular different conductivity values have been considered: 0.25, 0.55 and 1.6 S/m. It is worth to notice that the impedance of the cuvette depends on external conductivity values (σ_{ext}) and hence the matching with the 50 Ω generator. The change of conductivity determines, at lower frequencies, a variation of the impedance from 50 Ω to around 23 and 8 Ω for 0.25, 0.55 and 1.6 S/m respectively. As a first step the cuvette is considered fully filled to guarantee the maximum exposure volume and to avoid sparks in air with higher input voltage.
To evaluate the performance both in frequency and time domains, the complete structure has been numerically simulated with finite element software ANSYS HFSS 2015. A wave port, applied to feed the coaxial cable, is used as input in the frequency domain, conversely a lumped port with the pulse as excitation is applied in the time domain.

Realization and characterization of the applicator

After the design and characterization of the structure by numerical simulations, the fabrication process has been performed following the specifications obtained from the model results.
The electrodes are made in brass; the one connected with the pin of the coaxial cable has been perforated to allow the insertion of the pin and an easy weld. The second one has a hole of larger dimension for the insertion of the dielectric. The connection with the external sock is made wrapping a cylinder of brass previously weld to the second electrode in proximity of the hole (Fig. 8.4a). The central pin has been passed through a box of Teflon to be covered. This step has been made also to obtain a stronger mechanical stability during the application of the pulse. In Fig. 8.4b the complete structure with the cuvette is reported. The cuvette can be perfectly inserted between the two electrodes and can lean on the Teflon box. In order to guarantee even more mechanical stability and a good contact between the holder and the cuvette electrodes, a further Teflon cover has been designed (Fig. 8.4c). The cover allows to insert the cuvette and the coaxial cable.
Because the cuvette is disposable, the use of a structure as the one here proposed can be very useful instead of a direct connection of the coaxial cable with the electrodes of the cuvette to be renewed at any cuvette usage [Kenaan et al., 2011]. In order to

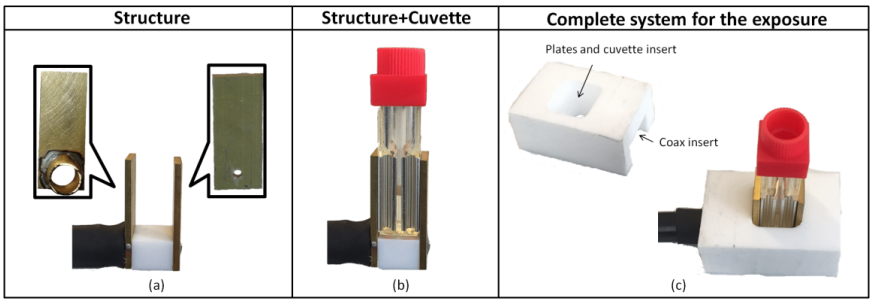

Figure 8.4: Realized Structure

characterize the structure, measurements in the frequency domain have been carried out with an Agilent Techonologies PNA Network Analyzer E8363C (10 MHz - 40 GHz) with the cuvette filled with solutions at different conductivity values (0.25, 0.55, 1.6 S/m) hence it is possible to obtain the efficiency of the structure under different experimental conditions. The conductivity values of the solutions were confirmed with measurement with a Precision LCR Meter E4980A from Agilent.

Microdosimetry model of nanoelectroporation of liposomes

Due to the possible different experimental conditions selectable in the use of liposomes (e.g. dimensions, inner conductivity and external conductivity), the microdosymetry analysis carried out on a single liposome (see Ch. 7) have been riconsidered here in order to understand the voltage needed at the generator for liposomes nano-poration. The 2D numerical simulations have been carried out using the software Comsol Multiphysics v. 5.0. as explained in the subsection 7.2. All the electrical and geometrical parameters of the model presented in the Chapter 7 are reported in Table 8.1.

Moreover, since the designed applicator is for liposomes exposure and in order to have a more realistic model of the solution that experimentally can be exposed to nsPEFs, after the efficiency evaluation and the chosen inner and outer liposome conductivity values, two simulations have been carried out considering a randomly distributed liposome population of 200 and 400 nm of diameter (see Fig. 8.5). As for the simulations on the single liposome (see Sec. 7.2), the 2D models consist of a rectangular box with dimensions of 70 μm x 100 μm representing the extracellular medium, in which 30

liposomes of 200 and 400 nm of diameter and membrane thickness of 5 nm, have been randomly placed in an area of 5 x 5 μm^2 (see Fig. 8.5). The electric field has been applied with two electrodes on the box boundaries; in particular on the upper and the lower edges the excitation of 12 ns pulse and the ground are respectively modeled. The other boundaries are electrically insulated.

The electric and geometrical parameters remain the same reported in Table 8.1 except from the external and inner liposomes conductivity values ranging from 0.25 to 1.6 S/m.

"Wet" experimental setup

By following the proposed cycle in Figure 8.1 preliminary "wet" experimental data have been carried out in collaboration with the the laboratory of Prof. Stefania Petralito, from the Pharmaceutical Chemistry and Technology (PCT) Department of "Sapienza", University of Rome.
The exposure cuvette is reported in Figure 8.6. The liposomes solution has been prepared with the thin-lipid hydration method as explained in the Section 5.2.1 exception for the magneto-nanoparticles step. The lipid used for the liposomes film is the EGG PC. Initially the aim was to create a 400 nm liposomes in order to have more chance to reach the poration with our 10 kb V pulse generator, but not a uniform population was obtained, so with the extrusion step a uniform liposome population of 250 nm of diameter has been obtained as confirmed by the DLS (dynamic light scattering, see Section 5.2.1) measurements (see Fig. 8.7). The inner and the outer liposomes conductivity values of 0.33 and 1.6 S/m respectively, have been obtained by using a PBS (phosphate buffer solution) buffer adjusted with the NaCl to reach the desired conductivity values. The osmotic pressure have been adjusted in order to avoid any

Electrical and Geometrical parameters			
	ϵ_r	σ **(S/m)**	**d(μm)**
External medium	$67^{a,b}$	$0.05 - 1.6$	$100 - 70$
Liposome membrane	$11.7^{a,b}$	$1.1x10^{-7\ (a,b)}$	$0.005^{a,b}$
Inner liposome	$67^{a,b}$	$0.05 - 1.6$	$0.2/0.4^{a}$

Table 8.1: Electric and geometrical parameters. [(a)] [Denzi et al., 2017], [(b)] [Merla et al., 2012]

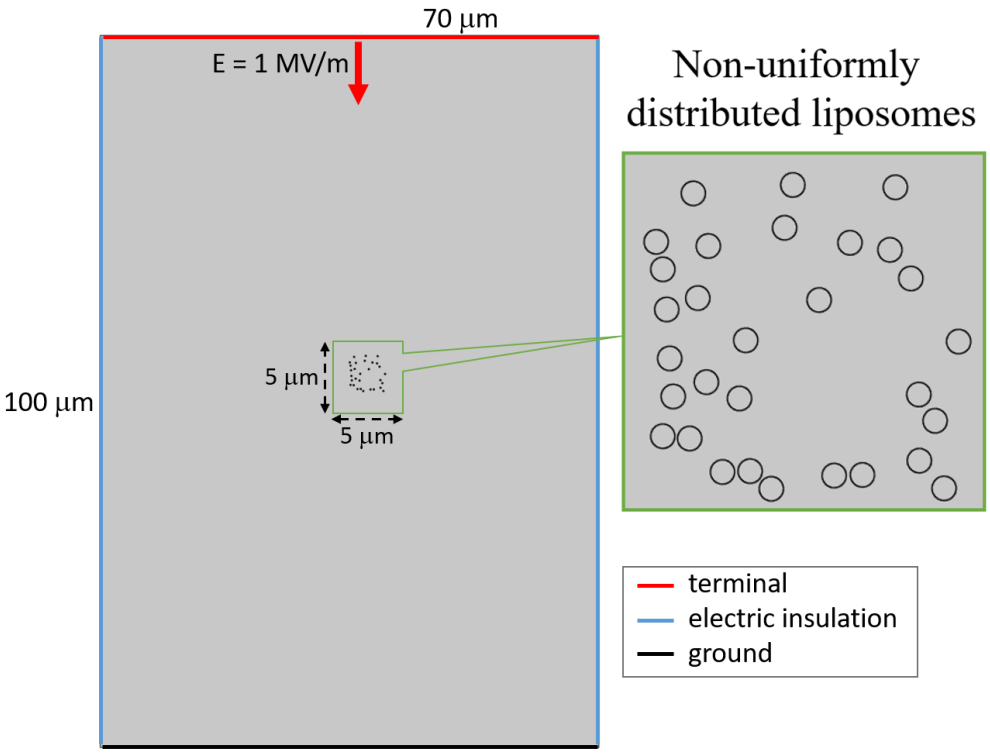

Figure 8.5: Non uniformly distributed liposome population model. The electric stimulus has been applied to the upper electrode and the ground to the lower electrode. Both sides are electrically insulated.

disruption of the vesicles due to the different inner and outer conductivity values.
An electric field of 9 MV/m have been applied to the liposomes solution using an FPG 10-1SM10 generator (FID Technology, Burbach, Germany) with 56 pulses at the frequency of 1 Hz. The signal has been monitored with a Rohde & Schwarz RTO2014 oscilloscope. In order to monitor a possible thermal increase during the 10 nsPEF exposure a Luxtron 3100 fiber optic probe have been used but no thermal increases have been detected. Moreover, the CF (5-(6)carboxyfluorescein) dye has been used as probe of the porated liposome membrane and the fluorescence before and after the nsPEF exposure have been measured as explained in the section 5.2.1.

Figure 8.6: 1 mm gap exposure cuvette used for the experiments.

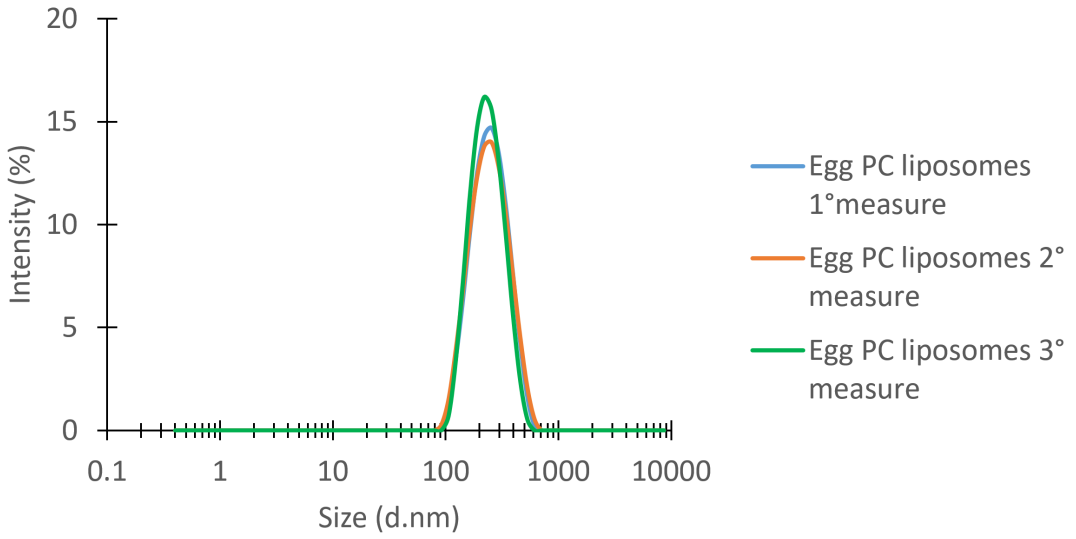

Figure 8.7: DLS (dynamics light scattering measurements) of the 250 nm of the EGG PC liposomes solution. Three different measurements with a peak at 250 nm.

8.3 Results and Discussions

Applicator frequency performances

As a first step in the analysis of the impedance behavior of the applicator, the real and the imaginary part have been numerically evaluated. The results are reported in Fig. 8.8 for the holder with the cuvette placed and filled with a solution 0.25 S/m of conductivity. As expected, at the lower frequency the resistive behavior is predominant, leaving for a capacitive one at the highest frequencies. It is worth to notice how this kind of coaxial connection reduces inductive parasitic effects; avoiding resonances within the range of the frequencies of interest (see resonance at around 350 MHz in [Kenaan et al., 2011]).
In the same frequency range the S_{11} has also been evaluated; the results are shown in Fig. 8.8 (black solid line). From both the impedance and the S_{11} parameter, it is possible to see an acceptable frequency behavior up to 100 MHz (hence up to the first lobe of 10 ns pulsed electric field). The S_{11} value is $\leq$ - 5 dB up to this frequency value. At frequencies higher than 100 MHz the mismatching of the impedance cuvette is more evident and this limits the use of this kind of applicator only for pulses with duration $\geq$ 10 ns. The results achieved are comparable with the ones reported in [Kohler et al., 2012, Kenaan et al., 2011] for a cuvette with 4 mm gap distance.

Frequency characterization for different solution conductivities

Starting from the results obtained in the Chapter 7, in which the importance of the external conductivity on the efficiency in liposomes nano-electroporation has been reported, a characterization of the applicator behavior varying the conductivity of the solution placed inside the cuvette has been carried out. Simulations were run with different solution conductivities and compared with measurements in frequency domain of the holder with the cuvette placed and filled with solutions at the same conductivity as the one simulated (Fig. 8.9). The measurements and the simulations are in perfect agreement for all the considered solutions. As expected, the performances of the applicator strongly depend on the solution parameters, with best behavior for the less conductivity value (the best value according to the formula reported in [Kenaan et al., 2011]). Increasing the conductivity, the mismatch of the applicator increases, in particular for 0.55 S/m, with an S_{11} value always higher than -10 dB and for 1.6

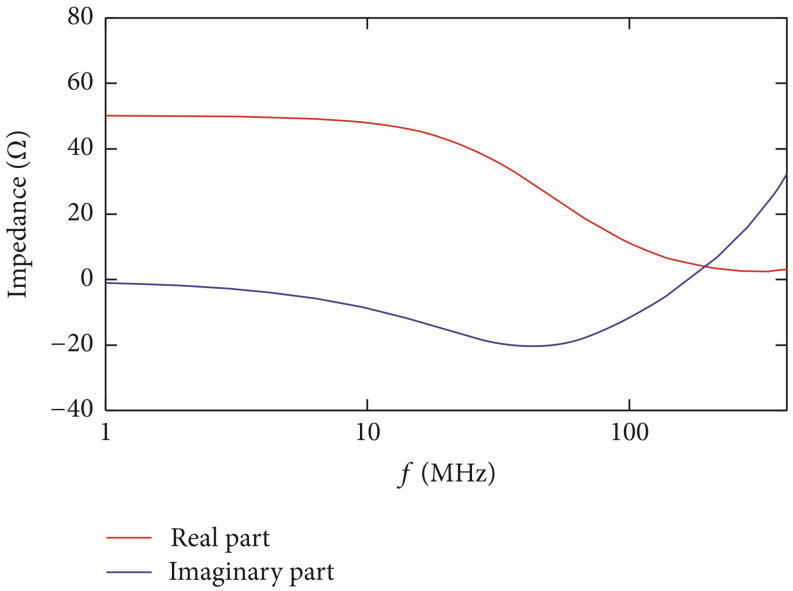

Figure 8.8: Impedance in terms of real and imaginary part of the holder with the cuvette placed and filled with a solution 0.25 S/m of conductivity.

S/m with values even higher than -5 dB. In this last case, the behavior of the structure is very close to a short connection and hence with a high negative reflection when a connection with a 50 Ω generator is made.
In order to better understand how this parameter affects the pulse transmission inside the cuvette, in the next paragraph the analysis of the cuvette response in time domain has been numerically performed.

Time domain characterization for different solution conductivities

The 10 ns pulse has been applied to the coaxial cable of the structure (Fig. 8.3c). The cuvette has been filled with solutions at different conductivities and the transmitted signal has been evaluated in the center of the cuvette gap. In Fig. 8.10 the results of transmitted electric field pulse for the different conductivity values are reported. As expected from the frequency results, for the conductivity of 0.25 S/m the amplitude of the transmitted pulse is 1000 V/m for 1 V input pulse. This is the maximum achievable value of electric field for 1 V applied to the 1 mm gap. The efficacy in transmission (η)

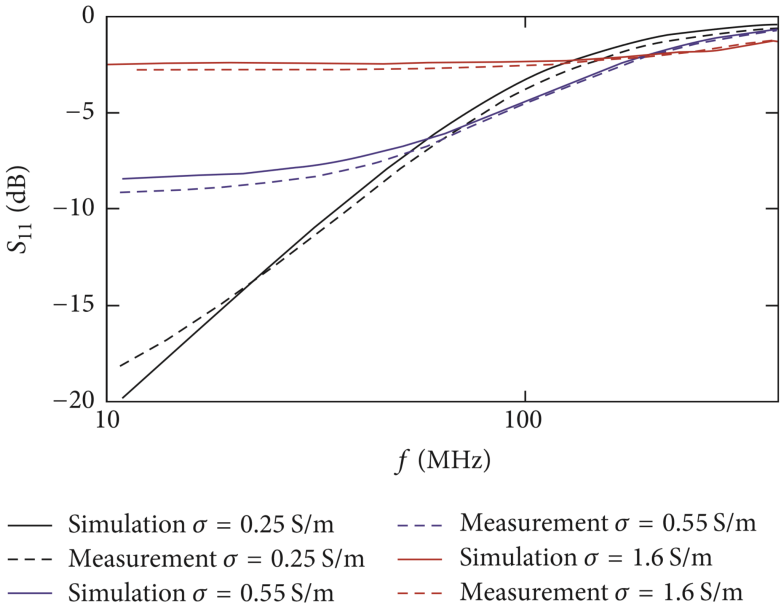

Figure 8.9: Measured (dashed lines) and simulated (solid lines) S_{11} parameters of the holder with the cuvette placed and filled with solution σ = 0.25 S/m (black line), 0.55 S/m (blue line) and 1.6 S/m (red line).

is defined as the ratio between the electric field obtained in the gap, in kV/m, and the applied voltage at the generator, in V. In case of 0.25 S/m of conductivity, η is equal to 1. The rise and fall times of the transmitted pulse, as predictable by the S_{11} trend, appear distorted with a value around double ($\approx$ 3 ns) respect to the one imposed on the generator (1.5 ns). Increasing the conductivity value, the efficacy of the structure decreases assuming values of 0.62 and 0.27 for 0.55 and 1.6 S/m respectively.
Once completely characterized the behavior of our applicator, a microdosimetry model of the liposomes is needed to derive all the necessary parameters to drive a final experiment of liposome solution exposed to a 10 ns pulse. In particular microdosimetry should provide values of liposome poration for different experimental conditions, as vesicles dimensions or inner and outer conductivity, and with regards to the efficacy of the real structure that will be used for the experiments. Hence, the results of the model have to be combined with the information about the efficiency of the real applicator here developed.

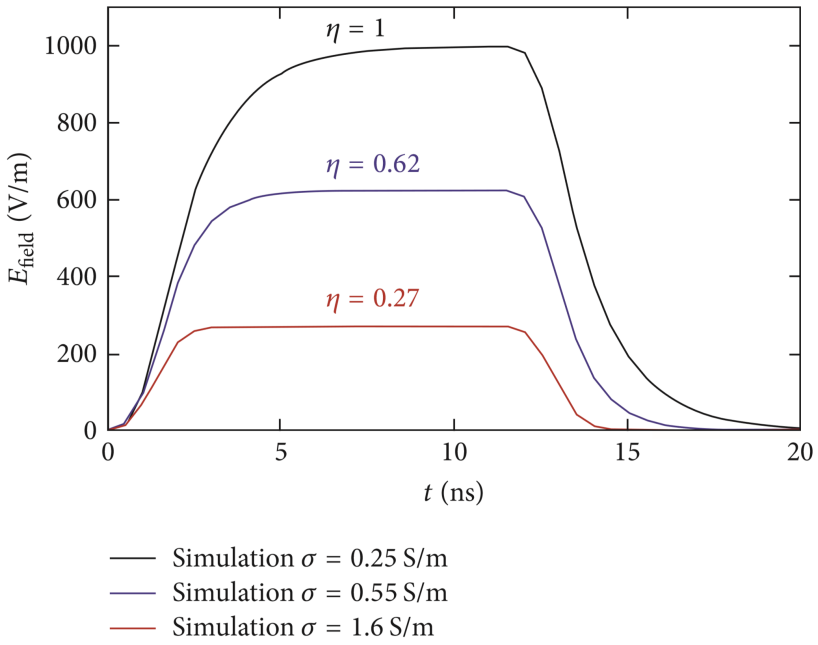

Figure 8.10: Electric field amplitude in the center of the cuvette gap. The efficiency value of the structure, η, defined as the ratio between the electric field obtained in the gap, in kV/m, and the applied voltage at the generator, in V, at different conductivity values is also reported.

Combining generator experimental results with microdosimetry on liposome

The microdosimetry model of the single liposome presented in the Chapter 7 has been used to evaluate the electric field threshold value necessary to obtain the membrane liposome poration combined with the efficacy of the generator. In particular, 1 V has been considered as the threshold value for the electroporating transmembrane potential [Joshi and Schoenbach, 2010, Breton and Mir, 2012] as already done in the previous chapter (see Ch. 7) and the field threshold has been evaluated for different conductivities of the inner liposomes medium (σ_{INT}) and of the external medium (σ_{EXT}) ranging from 0.05 S/m to 1.6 S/m. In Fig. 8.11 a 2D map of the electric field value necessary for liposomes electroporation with a diameter of 200 nm and 400 nm is shown. The maps appear perfectly symmetric at the changes of external or internal conductivities. The lower inner and outer conductivity values causes the highest intensities of the electric

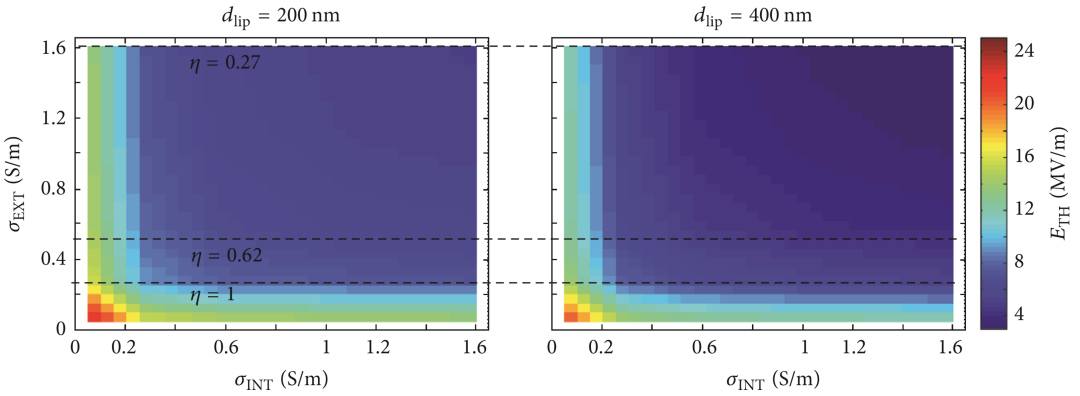

Figure 8.11: Electric field threshold for 200 nm and 400 nm liposomes poration changing the internal and external liposome conductivity.

field necessary for the liposomes poration, and the larger is the liposome dimension the lower is this value. If one considers only microdosimetry evaluation, the best conditions to obtain the liposome electroporation are those achieved with the highest inner and outer conductivity values.

Considering the designed applicator, this information has been combined with its efficacy at each external conductivity. Indeed the efficacy of the structure is higher for the 0.25 S/m conductivity and lower for the 1.6 S/m one. The value of the efficacy is also reported on the Fig. 8.11 in order to point out that the maximum efficacy is in the range in which the microdosimetry model predicts the most inconvenient conditions.

Input voltage vs generator efficacy

To weight the results of the microdosimetry model with the real experimental setup characteristics, we have taken into account not only the efficacy of the designed structure but also the capability of our generator in terms of the maximum output voltage able to generate. For the High Voltage Pulse Generator FPG 10-1NM10 we are able to provide a pulse with amplitude in the range of 2-10 kV, fixing our maximum capability to obtain 10 MV/m in 1 mm gap distance applying the highest intensity available.

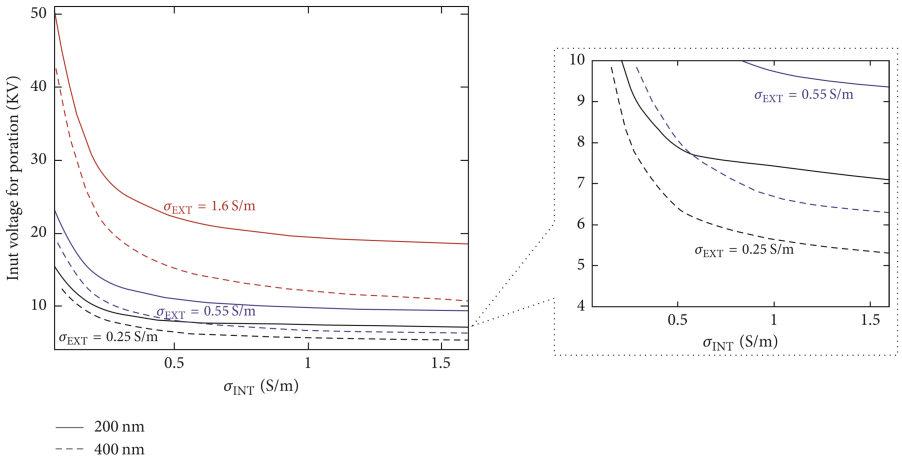

Figure 8.12: Input Voltage needed at the generator weighted with the effective efficacy of the structure.

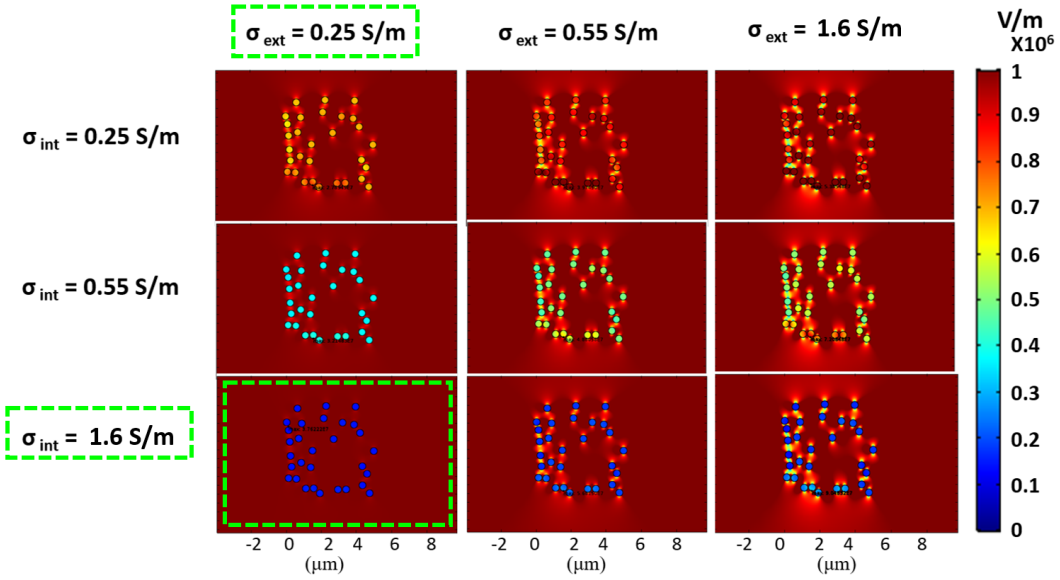

Figure 8.13: Electric field map distribution of 200 nm liposomes randomly distributed.

In Fig. 8.12 the results in terms of voltage necessary at the generator in order to obtain the poration of liposomes are reported. The results are reported for liposomes

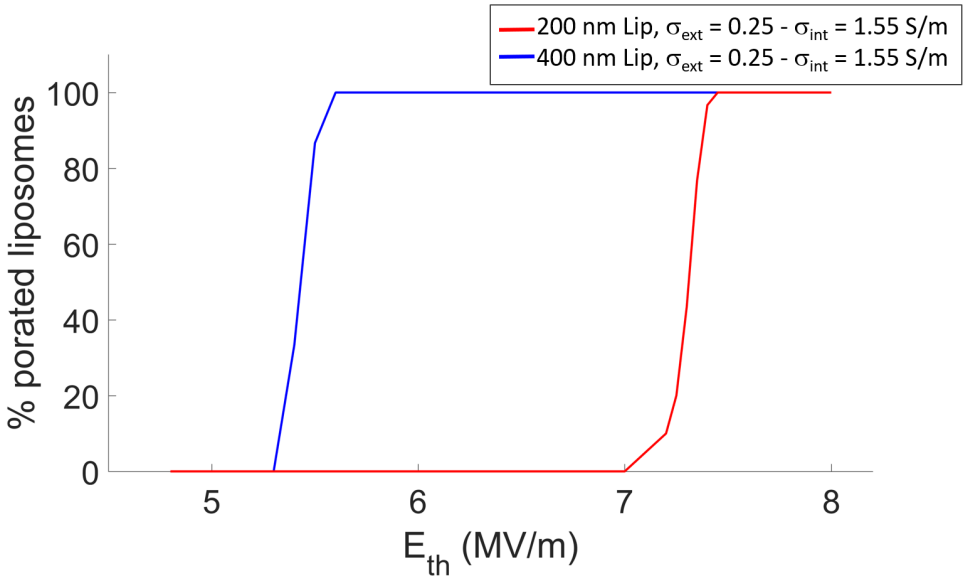

Figure 8.14: Electric field needed to porate the 200 (red) and the 400 (blue) nm liposomes population.

with dimension of 200 nm (solid line) or 400 nm (dashed line) and for all the external conductivity values tested in the structure. The voltage results are weighted with the efficacy of the structure ($\eta = 1$, 0.62 and 0.27((kV/m)/V)) at the different conductivity values in order to understand the real amplitude needed during the experiments (Fig. 8.12).

non-uniformly distributed liposomes population

Since the designed applicator is for liposomes exposure and in order to have a more realistic model of the solution that experimentally can be exposed to nsPEF, after the efficiency evaluation and the chosen inner and outer liposome conductivity values (σ_{INT} = 1.6 S/m and σ_{EXT} = 0.25 S/m), two simulations have been carried out considering a randomly distributed liposome population of 200 and 400 nm of diameter with inner and external conductivities ranging from 0.25 to 1.6 S/m. In the Fig. 8.13 the 2D map of the electric field distribution outside the liposomes population is reported for the 200 nm liposomes. It is possible to notice how with a lower external conductivity (0.25 S/m) and an higher internal conductivity (1.6 S/m), the highest electric field is experienced outside liposomes membrane.

In Fig. 8.14 the electric field needed to porate liposomes in function of their dimension

is reported. The electric field needed to porate the liposomes has been calculated considering a threshold of 1 V of the transmembrane potential as mentioned in the Section 7.3 [Smith et al., 2006]. From Figure 8.14 it can be noticed how the liposomes poration starts with a E field intensity of 5.4 and 7 MV/m respectively for the 400 and 200 nm liposomes. An intensity higher than 7.5 MV/m is required for the 100 % of 200 nm porated liposomes. Furthermore, the gap between the threshold for starting liposomes poration and the 100 % of porated liposomes, for both population, is minimum ($\backsim$ 0.3 MV/m) when the medium conductivity is lower than the inner liposomes one [Della Valle et al., 2017].

Preliminary experimental data on a 250 nm liposomes population

Keep following the cycle reported in Figure 8.1, after the model and the technological part, a preliminary "wet" experiment has been settled.
In Figure 8.15 the results of the CF fluorescent release are shown for the first day (Day 0, 1 sample) and for the second day (Day 1, 2 samples). On the first day (Day 0) as it can be noticed from the Figure 8.15, the exposed and the shame sample released the 44 and the 22 % of CF respectively. Since, the first day the nsPEF exposure and the CF release measurements have been done in two different places, both samples have experienced an high temperature of almost 35 °C due to the hand transportation between the two different departments. This could explain the high release from the shame sample. After that, the second exposure day (Day 1) it was possible to transport all the experimental equipment to the PCT department in order to perform the nsPEF exposure and the CF release measurements in the same place. Indeed, a release of 15 % for the exposed sample and of the 2 % for the shame has been reached.
These preliminary experimental data suggest the possibility to porate liposomes of 250 nm of diameter with an E field of 9 MV/m, which is higher than the predicted one ($\sim$ 7 MV/m) but it is important to keep in mind that the electric field calculation to porate the liposome membrane is an optimistic prediction, because the evaluation is done on one point of the liposome membrane, where the highest transmembrane potential is experienced.

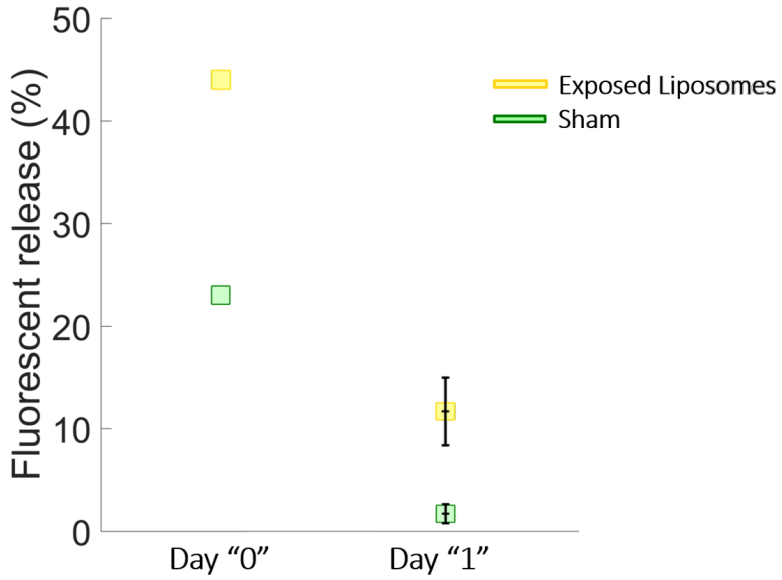

Figure 8.15: Preliminary "Wet" Experimental results on the 250 nm liposomes at the Day 0 (1 sample) and Day 1 (2 samples).

8.4 Conclusions

In this chapter, the design and characterization of an exposure system for liposomes drug delivery experiments, using a 10 nsPEF, has been carried out and preliminary experimental data have been reported. This project has been carried out with the integrated approach proposed in Fig. 8.1, with a readjustment of the cycle proposed by Kitano [Kitano, 2002a,b] for systems biology taking into account both theoretical, technological and experimental issues.

Design of the exposure system

In the design of the structure the first step was to consider the features of the excitation and of the target. Since the excitation is a 10 ns pulsed electric field and the target are liposomes with 200 or 400 nm diameter the use of a standard electroporation cuvette with 1 mm gap has been considered advantageous [Denzi et al., 2017]. The design of an appropriate cuvette holder structure proceeded, taking particular attention to the connection of the 1 mm gap electroporation cuvette to a 50 Ω high voltage pulse generator. Further analysis demonstrated the capability of the proposed structure to

deliver a 10 ns pulse without a significant signal distortion in particular for media with a 0.25 S/m of conductivity value. This structure is suitable for numerous experimental exposures, due to the indirect connection with the cuvette. Furthermore, the device guarantees a very strong mechanical stability and a good contact with the electrodes of the cuvette thanks to the Teflon box presence under it and as cover.

Characterization of the exposure system

The structure has been completely characterized in time and frequency domain to understand its capability and performances in different experimental conditions. In particular, the analysis has been performed for different conductivity values of the solution inside the cuvette both with numerical models and measurements. A perfect agreement has been found between them. The higher is the solution conductivity, the lower is the efficacy of the structure and hence the lower is the amplitude of the transmitted pulse to the cuvette.

Microdosimetric models

In order to analyze the impact of the real performances of the device on the liposomes electroporation, a microdosimetry model of liposomes with 200 or 400 nm dimension has been reported. The simulations have been carried out considering different inner and outer liposome conductivities and the results have been combined with technological outcomes. Combining microdosimetry and technological information permits to predict that the optimal condition for a 400 nm liposome is with 0.25 S/m and 1.6 S/m for external and internal liposome conductivities respectively, differently from the indications that one would follow on the basis of the microdosimetry alone (highest internal and external conductivity values). This discrepancy is due to the higher efficiency of the structure for the conductivity of 0.25 S/m. Moreover, since the exposure system has been designed for the exposure of a liposomes population, microdosimetric simulations have been carried out considering a non uniformly distributed liposomes population of 200 and also of 400 nm, with conductivity values ranging from 0.25 S/m to 1.6 S/m for external and internal liposome conductivities. By these simulations, a gap of 0.3 MV/m has been appreciated (with 0.25 S/m and 1.6 S/m for external and internal liposome conductivities respectively) between the starting of liposomes poration and when then 100 % of liposomes is porated for both simulations. An electric field of 7 MV/m is needed to porate the 200 nm liposomes, while 5 MV/m are sufficient to porate the 400 nm liposomes.

Finally, the " wet " experiment has been carried out with preliminary data of the exposure of 250 nm liposomes by applying an electric field of 9 MV/m with 56 E pulses at 1 Hz of frequency. A conductivity of 0.33 and 1.6 S/m has been used for the external and

inner liposomes. A release of 15 % of CF has been detected for the exposed samples, while the 2 % has been reached from the sham sample.

These results suggest a good agreement between the predicted possible liposomes poration from the microdosimetric models using an E field $\sim$ 7 MV/m and the one used experimentally of 9 MV/m. It is good to keep in mind that the numerical prediction in terms of electric field needed for the poration is optimistic since is done on one point on the transmembrane membrane. Moreover when prepared there is not only the lipid but also the presence of chloroform and of the dye fluorescent that could slightly change poration conditions. In fact if during the experiments, a change of some parameters becomes necessary, e.g. different volumes of solution (keeping particular attention to avoid sparks in air) or a different value of inner or outer conductivities, a characterization with new simulations and measurements has to be performed in order to understand the real transmitted signal to maximize the chance to reach the liposomes poration.

Part V

Direct EMF effects investigation on proteins structure by molecular dynamics simulations

As mentioned in the introduction (see part I), the technological progress has increased the use of magnetic fields as external stimulus for many therapies as the treatment of inflammatory diseases [Varani et al., 2002, 2017], neurologic disorders [Di Lazzaro et al., 2013] and for drug delivery research [Spera et al., 2015]. For some of these diseases it has been demonstrated how the application of pulsed magnetic fields (PEMFs) can induce anti-inflammatory effects on cells trough the interaction with protein receptors as the adenosine A_{2A} [Varani et al., 2002, 2017], an important regulator of neurotransmissions signals released from a variety of cells in response to the metabolic stress.

Starting from the experiments of Varani et al. [Varani et al., 2002, 2008], in the first chapter of this part (see Ch. 9) a study about the interaction mechanism of the magnetic B field action on the adenosine A_{2A} receptor will be presented, through the molecular dynamics simulations (MD) approach. The project has born in collaboration with the Igea institution of the Dr. Ruggero Cadossi with the aim to possibly identify the interaction mechanism between a magnetic field and the adenosine A_{2A} receptor.

We performed our simulations with the Gromacs package, usually used to simulate the action of an external electric field acting on a molecular target. Here, the integration of the Newton's motion equation is presented by introducing the Lorentz force for the magnetic field action. Firstly, the implementation and validation of the B field into the Gromacs package [Van Der Spoel et al., 2005] are reported. Latter, preliminary results are presented for MD simulations of a buffer solution (DMEM concentration) and the adenosine A_{2A} immersed in the buffer solution exposed to 1 T of magnetic field.

Because of the capability of nsPEFs to interact with intracellular organelles (see Sec. 2.3) in the second chapter of this part the possible effects of cytosolic enzyme exposed to high intense electric fields of ultra short duration have been investigated. A theoretical study based on molecular dynamics simulations, using Gromacs, is proposed choosing an important enzyme involved in the cellular antioxidant defense mechanism: the superoxide dismutase (SOD,Cu-Zn or SOD1). In the Chapter 10, the effects of the 100 nanosecond pulsed electric fields, with intensities ranging from 10^8 to $7x10^8$ V/m, on a single SOD1 enzyme are presented to study both the effects on the structure or the electrostatic effects on the active site, thanks to the dipolar response analysis and the (2D) electric field distribution around the active site. This project has born in collaboration with the laboratory of Prof. Olga Pakhomova from the Old dominion University, Norfolk, Virginia.

Chapter 9

Magnetic molecular dynamics simulations with Velocity Verlet algorithm on the Adenosine A_{2A} receptor

9.1 Introduction

Several studies have shown how the use of low frequency magnetic pulses (PEMFs) may have biological effects on different cells functions. It has been reported that PEMF application on bone structures can stimulate osteoblast growth and modulate bone metabolism [Chalidis et al., 2011]. Indeed, several studies have shown that the use of PEMFs increases the anti-inflammatory effect of different types of cells such as neutrophils granulocytes, chondrocytes and osteoblasts, with significant reduction in some of the most significant inflammatory cytokines [Varani et al., 2002, Vincenzi et al., 2013]. Vincenzi at al. [Vincenzi et al., 2013] reported an increased anti-inflammatory effect of A_{2A} and A_3 adenosine receptors in human T/C-28a2 chondrocytes and in hFOB 1.19 osteoblasts next the application of a PEMF exposure ranging from 1.5 up to 2.5 mT of magnetic field intensity. In addition, Fini et al. [Fini et al., 2005] presented a complete review of ant inflammatory PEMFs effects on articular cartilage and Kaszuba-Zwoinska et al. [Kaszuba-Zwoińska et al., 2008] showed how PEMFs of 5 mT of intensity were able to decrease IFN-gamma proinflammatory and increased IL-10

anti-inflammatory cytokine production on human peripheral blood mononuclear cells (PBMC) from Crohn's disease patients (CD).

One aspect that researchers are focusing on is the interaction between PEMFs and membrane receptors, such as adenosine (Ars), belonging to the G protein-coupled protein receptor family (GPCR).

GPCRs protein

GPCRs are proteins that perceive molecules outside the cell and transmit the signal inside by activating the cell response. The GPCR arranges itself into a tertiary structure with 7 TM (transmembrane) α-helices forming a cavity within the plasma membrane with a N terminal that serves as ligand-binding domain. When an agonist or antagonist tries to bind to the receptor then the internal cavity begins to reorganize. The agonist produces an activation of the receptor by generating the maximum cellular response, while the antagonist makes no cell physiological response. It is estimated that GPCRs are the target for about 50 % of the drugs present on the market, mainly due to their involvement in reporting pathways for many diseases such as mental, metabolic or cardiovascular disorders [Trzaskowski et al., 2012].

A_{2A} receptor

The adenosine is a GPCR protein, regulator of neurotransmission signals and it is used for drug targeting in many inflammation statuses as cancer, ischemia or neuronal disorders [Fuxe et al., 2007, Jorg et al., 2014]. It is released by a variety of cells in response to metabolic stress [Varani et al., 2002] and interacts with four GPCRs (A_1, A_{2A}, A_{2B} and A_3). A_{2A} stimulates the activity of adenylated cyclase enzyme and cAMP accumulation (cyclic adenosine monophosphate) [Varani et al., 2002]. The importance of the A_{2A} adenosine study lies in its response when different types of cells are exposed to PEMFs action. It has been experimentally proven [Varani et al., 2002, 2008] that the A_{2A} receptor, under exposure to a magnetic field of about 3 mT for a duration of 2 hours, increases its response by providing a more effective anti-inflammatory effect on neutrophilis cells. Moreover, an increased enzyme activity of adenylate cyclase and a reduction of radical superoxide anion has been reported.

The aim of the project presented in this chapter, has been to perform molecular dynamics simulations (MD) to understand if it would be possible to directly interact with proteins or enzymes using pulsed magnetic field stimulation.

B field interaction mechanisms

From several decades, by the time of the first studies of Pilla and Chiabrera [Pilla et al., 1997] the mechanism that undergoes the B field action on living objects is not fully elucidated. Several models have been advanced to explain the possible mechanisms; almost all have been essentially based on classical or quantistic description

of an ion in a binding site, and have studied the problem through the precession of ion thermal motion in magnetic fields [Muehsam and Pilla, 2009]. The basic premise of such models is that the effect of the magnetic field can energetically overcome the perturbing influences of thermal noise, moreover in almost all, a rigorous interaction between the ion and its binding site is lacking due to the inability to describe the target at molecular level.

Lately, Binhi and Prato [Binhi and Prato, 2017] presented a review about the possible action of "hypomagnetic fields" (HMF, μT range) on biological effects by proposing different mechanisms. They compared experiments and theories related to the exposure to an hypomagnetic field, in order to possibly find a relation between the magnetic field characteristics and a biological effect. No measured correlations of the HMF effects with its magnitude and inhomogeneity and type or duration has been found. Moreover, they also suggest that magnetoreception is not only associated with the magnetoreceptors in migrating animals and magnetotactic bacteria but others mechanisms could explain a magnetic field action. Among the different action proposed mechanisms [Binhi and Prato, 2017], a molecular gyroscope mechanism is presented by hypothesizing the rotation of residues with distributed electric charges that generates a magnetic moment that interacts with an external B field applied. Another proposed mechanism from Babaei et al. [Babaei et al., 2017] is a diamagnetic anisotropy in membrane proteins with higher percentage of amino acids and aromatics residues which could explain their rotation and response to an external magnetic field application.

Molecular dynamics simulations

Anyhow, the issue related to the inability to describe the target (e.g. ions, proteins, water molecules, etc.) at molecular level, seems an unavoidable requirement to produce affordable results, therefore simulations based on Molecular Dynamics (MD) to study molecules behavior, under different physical conditions of magnetic or electric fields, seem to become a strategic challenge. Molecular dynamics simulations are a useful tool for understanding the interaction between atomic molecular structures. MD simulations are usually used to analyze protein structures, membrane patches or ionic solutions subjected to the action of external agents such as thermal or electric increments [Marracino et al., 2013b, 2016].

The introduction of an external electromagnetic field into a MD simulation requires a time-dependent forcing function in Newton's second law equation, to describe the forces exerted on the charge sites by the field. For the constituent electrical and magnetic fields E and B, the forces acting on each charge site are incorporated, through Lorentz

force, as follows:

$$m_i \ddot{\mathbf{r}}_i = f_i + q_i \mathbf{E}(t) + q_i \mathbf{v}_i \times \mathbf{B}(t) \tag{9.1}$$

where q_i is the charge and f_i is the force on the site i. The electric and magnetic fields are taken to be uniform and plane-polarized. Actually, several works have considered only the electric field component in the Lorentz force [Casciola et al., 2014, Marracino et al., 2013b, Apollonio et al., 2008, English and Waldron, 2015]. The motivation was that the magnetic field, being normal to the velocity of the particle, "does not work", hence it cannot heat the charged particles, giving them energy. It follows that the magnitude of the velocity of a charged particle is not affected by the presence of a magnetic field. However, the magnitudes of the velocity components perpendicular to B can vary, as can be shown for the cyclotron motion.

Before our implementation, few works have been carried out with a magnetic fields implemented into molecular dynamics simulations (not gromacs package) [Chang and Weng, 2006, 2008, Murad, 2006, Moosavi and Gholizadeh, 2014]. In Chang et al. [Chang and Weng, 2008], MD simulations have been done considering high magnetic fields from 1 to 10 T by analyzing diffusivity values of water and ions (Na^+ and Cl^-), with a time of simulations of 150 ps. No statistics significant results have been highlighted (below 10 %). Moreover also in a work of Mura [Murad, 2006] a magnetic fields with intensity of $3x10^6$ T has been applied across of a membrane, no significant differences were appreciated with the respect to the resting condition by the analysis of ions radial distribution functions. However data reported seem not to be highly reproduced nor extremely solid from a statistical point of view.

In this project, for the first time, we implemented into the Gromacs package [Van Der Spoel et al., 2005], one of the most used tools for MD simulations, a static homogeneous magnetic field. The core of the numerical solution solved by Gromacs has been modified to take into account the magnetic force acting on a charged particle and the results have been compared with the analytic expected behavior for the very simple case of an ion in vacuum and then also with water molecules. Next, simulations of a NaCl buffer solution (DMEM concentration [Varani et al., 2002]) without and with the adenosine A_{2A} receptor have been performed applying a magnetic field of 1 T.

9.2 Materials and Methods

Update of velocities and positions with the Velocity Verlet algorithm into Gromacs package

The difficulty in implementing the B field lies in changing the velocities and positions to introduce the term of the Larmor frequency and thus generate a magnetic field. Spreiter and Wlaker [Spreiter and Walter, 1999], identified three different ways to introduce the B field in MD simulations by adding the term of the Larmor frequency Ω = (q x B)/m in the update of velocities and position through the Verlet Algorithm. They basically proposed three different ways:

- Inverse algorithm for weak B field with a limit about $\Omega\ \Delta T \ll 2\pi$, which means to find a good comprise between the intensity of the B field and the duration of the simulations
- Velocity transformation for strong B field
- Taylor expansion for strong B field

Since for the simulations a time step sufficiently small has been used (0.1 and 1 fs), the inversion algorithm has been adopted to solve the equations of positions and velocities, in which the strength of the magnetic field is dependent on the value of the time step. Moreover, since Gromacs is not a software designed for the application of a magnetic field, the first part of the work has been to fully control atom velocities and positions update by the Verlet integration and understand how to introduce the magnetic field component. Velocity Verlet [Swope et al., 1982] integration is a numerical method used to integrate Newton's equations of motion. In particular the Gromacs code it has been implemented through the update at each time step of particle positions **r** and velocities **v** (eq. 9.2 and eq. 9.3):

$$r(t + \Delta t) = r(t) + \Delta t\mathbf{v} + \frac{\Delta t^2}{2m}\mathbf{F}(t) \tag{9.2}$$

$$v(t + \Delta t) = v(t) + \frac{\Delta}{2m}\left[\mathbf{F}(t) + \mathbf{F}(t + \Delta t)\right] \tag{9.3}$$

where $F = m\text{x}a$ is the force applied, m the mass of the particles and Δt the time step used to perform the simulations. We applied the magnetic field in the z direction

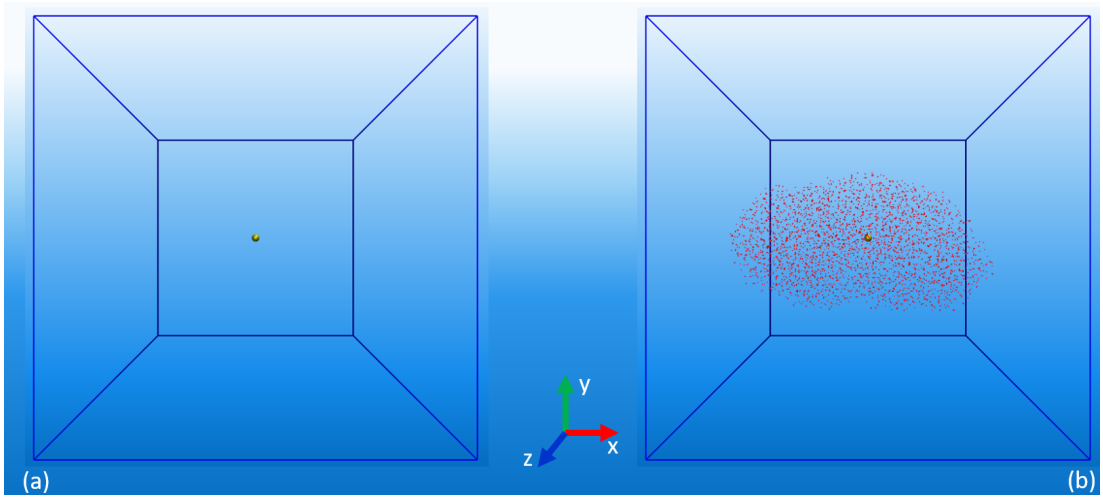

Figure 9.1: Molecular dynamics model of the Na^+ ion in vacuum **(a)** and with water molecules **(b)** in a box of 30 x 30 x 30 nm^3 and 10 x 10 x 10 nm^3 respectively.

introducing the Lorentz force along the x and y axis for both positions and velocities equations (eq. 9.4 and eq. 9.5):

$$r(t+\Delta t) = r(t) + \Delta t \mathbf{v} + \frac{\Delta t^2}{2m}\left[\mathbf{F}(t) - \Omega e_z \times v(t)\right] \tag{9.4}$$

$$v(t+\Delta t) = v(t) + \frac{\Delta}{2m}\left[\mathbf{F}(t) - \Omega e_z \times v(t) + \mathbf{F}(t+\Delta t) - \Omega e_z \times v(t+\Delta t)\right] \tag{9.5}$$

where e_z = (0, 0, 1) is the unit vector in the z direction and the Larmor frequency Ω = (q x B)/m , where B is the magnetic field intensity.

Validation of the Magnetic field implementation

To validate our implementation, MD simulations have been performed considering an Na^+ ion in vacuum and in presence of water molecules in order to verify the ion cyclotron motion.

Na^+ Ion in vacuum

MD simulations have been carried out considering a charged particle Na^+ in vacuum, to verify the cyclotron motion of the ion when an external magnetic field is applied. We used an NVT (number of particles, volume and temperature constants) ensemble at a temperature of 300 K using the Nose-Hoover thermostat in a box of 30 x 30 x 30 nm^3 of dimension (see Fig. 9.1a). Due to the limit of the algorithm related to the time step ($\Omega\ \Delta T \ll 2\pi$) and the magnetic field intensity, a magnetic field B = 10^5 T has been applied, for the ion in vacuum, in order to be able to see the particle motion in the picosecond time scale with a time step Δt = 0.1 fs, for a 35 ps of simulation. The

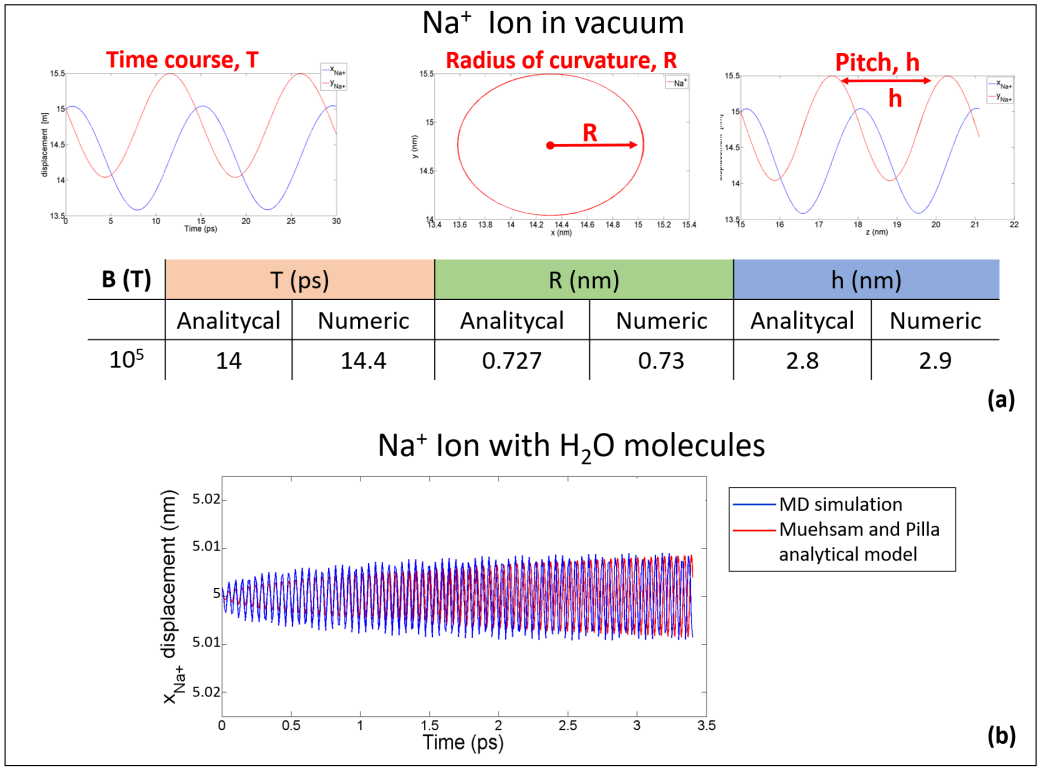

Figure 9.2: **(a)** Period (T), radius of curvature (R) and the pitch (h) of the Na^+ displacement in the x and y direction; a table is also reported for the matching between numerical and analytical results; **(b)** x displacement of the Na^+ ion obtained with MD simulation and the analytical result from the Muehsam and Pilla thermal model.

initial velocity of the particle has been settled to v = 0.37 nm/ps with an angle Θ = 1° with the respect to the magnetic field application.

The displacement (T), the radius of curvature (R) and the pitch (h) of the Na^+ ion are reported (see Fig. 9.2) due to the magnetic field application of 10^5 T. In order to verify these numerical results, an analytical model has been settled implementing the equations 9.4 and 9.5 to reproduce the Na^+ particle motion under a B field of 10^5 T of intensity. It is possible to notice in Fig. 9.2a how the analytical and numerical model match perfectly. The charged particle exhibits a sinusoidal motion in the x and y direction during the MD simulation as predicted by the analytical formula $T = 2\pi m/qB$, where q and m are the charge and mass for the Na^+ ion respectively.

Na^+ ion in water

As next step the ion cyclotron motion of the Na^+ ion in presence of water molecules has also been verified, with a density of 100 kg/m^3 (Fig. 9.1b) in a box of 10 x 10 x 10

nm^3, the box dimension is smaller because of computational cost. The initial velocity of the particle, also in this case, has been settled to v = 0.37 nm/ps. The low water density has been required in order to see the motion in ps time, due to thermal noise generated by the water molecules collisions. Moreover, because of the presence of H_2O molecules the magnitude of the B field has been increased to $3x10^7$ T for a time of 3.5 ps, also to overcome the thermal collisions and possibly appreciate the ion cyclotron motion. In Fig. 9.2b the Na^+ displacement, in the x direction, is reported. A field of $3x10^7$ T has been applied with an integration step of 0.02 fs for a time of 3.5 ps. It is possible to appreciate how there is a perfect matching between the numerical and the analytic results based on the Muehsam and Pilla thermal model [Muehsam and Pilla, 2009].

MD simulations parameters

Buffer solution Concerning the simulations of the NaCl buffer solutions (DMEM concentration [Varani et al., 2002]) we worked with an NVT (number of particles, volume and temperature constants) ensemble at a temperature of 300 K using the Nose-Hoover thermostat in a box of 12 x 12 x 12 nm^3 of dimension and with an integration step of 1 fs (Fig. 9.3a). The gromos45 force field has been used simulating 114 Na^+ and Cl^- ions (DMEM concentration, 110mM [Varani et al., 2002]) and 57577 H_20 molecules.

A_{2A} receptor For the adenosine A_{2A} molecular model, the 3PWH PDB structure has been chosen but in the unbound configuration in order to firstly analyze the protein behavior with no ligand binded (see Fig. 9.3). The adenosine A_{2A} molecule was immersed in the NaCl buffer solution and because of its positive charge (+6e) 6 more Cl^- ions were added to the simulations box to neutralize the system.

Numerical Observables

Self diffusion coefficient

Studying the transport properties of liquid water or free molecules (e.g.ions) is an important topic, both in fundamental science and in its applications. The mobility of water molecules is indicated by the value of the self-diffusion coefficient, which depends on the environment parameters as temperature, pressure or the structure [Levitt et al., 1997]. The value of the self-diffusion coefficients have been obtained through the com-

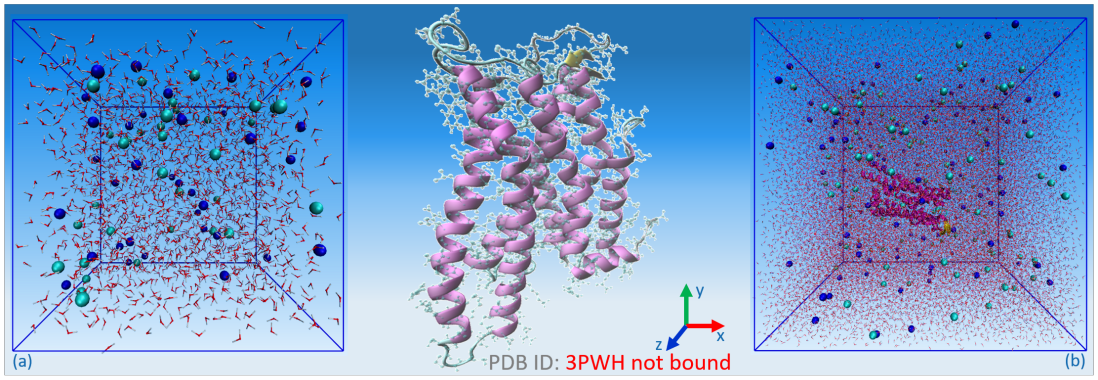

Figure 9.3: **(a)** Molecular dynamics model of the Buffer solutions with 114 Na^+ and Cl^- ions and 57577 H_20 molecules. **(b)** the adenosine A_{2A} receptor (7 transmembrane protein) immersed in the buffer solution. The dimension of the box is 12 x 12 x 12 nm^3.

mand line of the Gromacs software, *gmx_msd* command, following the Einstein relation based on the mean-square displacement function.

RMSD

In order to asses the atoms positions during the MD simulation, the rmsd has been computed. The RMSD (root-mean-square deviation) of atomic positions provides a quantitative measure of the protein structural variations, comparing the magnetic field exposure and the equilibrium state. The goal has been the understanding of possible changes in shape and size of the protein under the influence of the B field.

Secondary Structures

To evaluate possible structural changes induced by the external signals considered, the number of α-helix secondary structures has been calculated through the command line of the GROMACS package using the *do_dssp* command. The Adenosine is mainly an α-helix secondary structure with 7 transmembrane α-helix which arrange themselves depending on the lingand bonded to the N terminus. It is a regulator of neurotransmission next to a metabolic stress [Varani et al., 2002]. The calculation has been made in terms of PDF (probability density function) with 0 and 1 T of B field application.

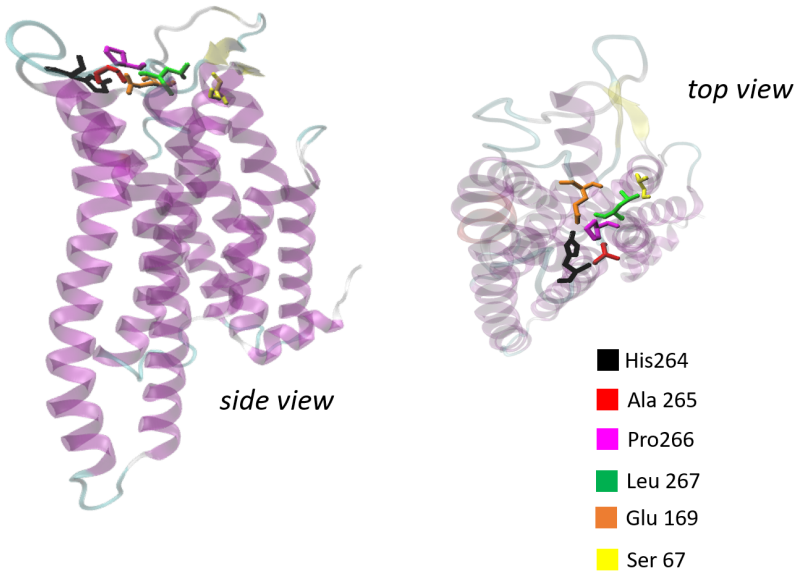

Figure 9.4: Side and top view of the adenosine receptor, highlighting the residues involved in the ligand binding process (black for histidine264, red for alanine265, purple for the proline266, green for the leucine267, orange for the glutammate169 and yellow for the serine67).

Dipole Moment

Proteins, due to their secondary structure conformation (α-helices, β-sheets, turns, coils, etc.) possess an electric dipole moment. For this reason the dipole moment of chosen residues, has also been analysed, involved in the hydrogen bond during the ligand binding (see Fig. 9.4), that could orient themselves when an external force is applied as a magnetic field.

Ramachandran plot

An extremely useful method for studying protein conformation is the Ramachandran plot [Ramachandran et al., 1963]. Ramachandran plot is a way to visualize energetically allowed regions for backbone dihedral angles ψ against ϕ of amino acid residues in protein structure (Fig. 9.5a) [Richardson, 1981]. The ω angle at the peptide bond is normally 180°, since the partial-double-bond character keeps the peptide planar (see Fig. 9.5b). Basically depending on the stability and on the value of the torsion angles is possible to distinguish different regions. As is possible to see in Fig. 9.5c, three different

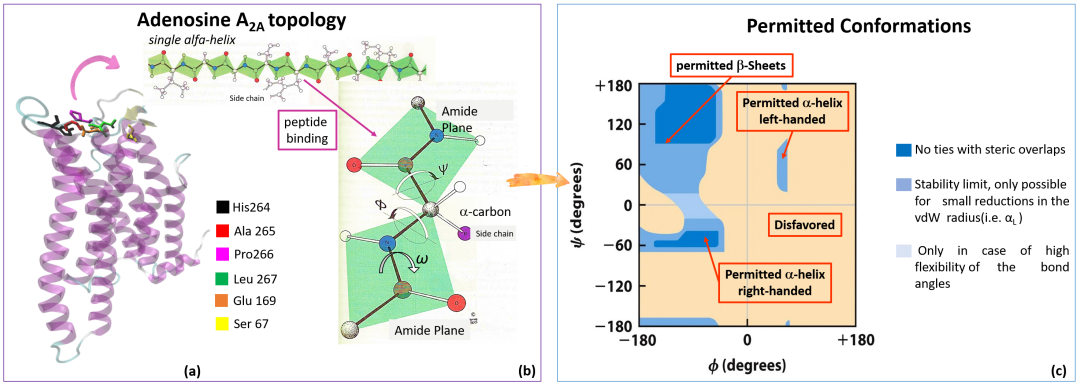

Figure 9.5: **(a)** Topology of the adenosine A_{2A} receptor with 7 TM α-helix with the 6 chosen residues; **(b)** the peptide binding concept for each peptide of the chain with the two torsion angles ψ and ϕ; **(c)** concept of the possible conformations for each residues by distinguishing three different energetic region depending on the stability of the rotation (from stable with the deep blue to the unstable rotation on light blue) and four different allowed conformations depending on the value of the torsion: β-Sheet, α-helix right handed and left handed and the a disfavored region.

stability regions can exist. The deep blue zone means that the rotation is really stable, the blue indicates a limit stability on the rotation that could led the peptide to be in different conformations and the light blue zone which means there is an high flexibility of the peptide structures. Based on that, it is possible to assign, depending on the value of the rotation, four different conformations: β-Sheet, α-helix right-handed and left-handed and a disfavored region, which indicates some angle distortions preferred under compulsions imposed by local constraints suggesting that unfavorable local interactions may be offset by other compensating factors [Jia et al., 1993, Stites et al., 1994]. As for the dipole moment, the ramachandran plot, have been computed for the six residues involved in the hydrogen bond during the ligand binding process, both with zero and 1 T of magnetic field.

9.3 Results

Buffer solution: DMEM concentration

Once, validated the implementation of the magnetic field B in the Gromacs software (see Sec. 9.2), the complexity of the target has been increased addressing first a box containing a NaCl buffer solution with DMEM concentration [Varani et al., 2002], which means 114 Na^+ and Cl^- ions hydrated with 57577 water molecules. To analyses the

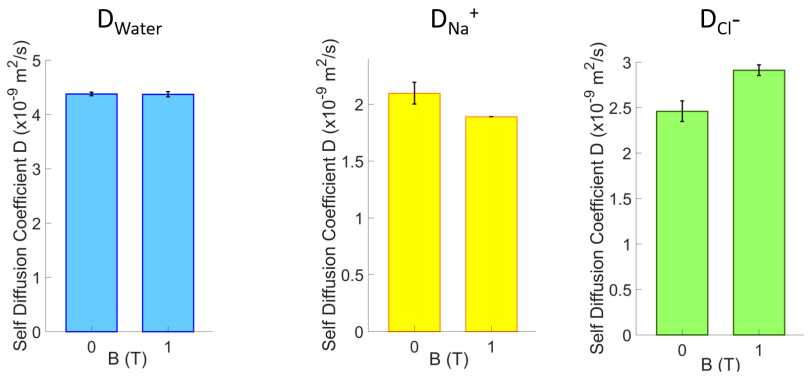

Figure 9.6: Self diffusion coefficient D, for water (blue), Na^+ (yellow) and Cl^- (green) particles.

mobility of water and ions molecules the self diffusion coefficient D in zero and with 1 T of B field, has been computed. From Fig. 9.6 can be observed the results at the last nanosecond of the simulations (t = 20 ns). For water molecules no changes occurred (see Fig. 9.6, blue label). Regarding the charge particles, in the no field conditions the diffusivity values of the Cl^- and the Na^+ ions are perfectly according to the theoretical values predicted by in a theoretic work of Salih et al. [Salih and Matthai, 2017] using NAMD, were a value of 2.2 and 1.6 is identified for the Cl^- and Na^+ diffusivity values. Here with no B field applied a value of 2.5 and 1.5 is reached for the Cl^- and Na^+ ions respectively. When the B field acts on charged particles, a decrease of 10 % is appreciated for the Na^+ ions and an increase of 18 % is reported for the Cl^- particles diffusivity (Fig. 9.6). This result suggest an interaction between the applied B field and the free charged molecules.

Adenosine A_{2A} in the buffer solution

Afterwards the adenosine A_{2A} receptor has been included in the buffer solution, adding six more Cl^- ions to neutralize the environment, and MD simulations have been done with 0 and 1 T of B field.

The first result is shown in Fig. 9.7 where the diffusivity D value is reported for the water, the ions and the protein target. For the water also in this case no changes occurred. Then we focused the attention on the protein diffusivity due to the importance of understanding the characteristics of protein self diffusion in solution, where no change of intramolecular structure as well as aggregation occurs is of great importance. With the no field application the diffusivity value is $\sim 2\text{x}10^{-9}$ m^2/s which is in accordance to the diffusivity values measured experimentally for other protein structures

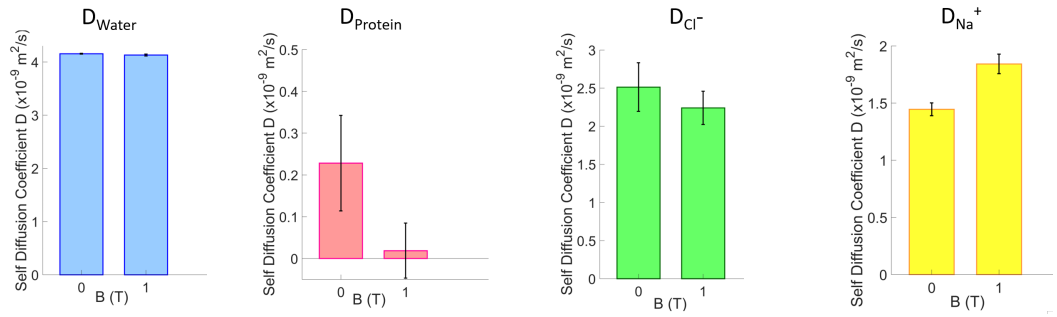

Figure 9.7: Self diffusion coefficient D, for water (blue), protein (pink), Na^+ (yellow) and Cl^- (green) particles.

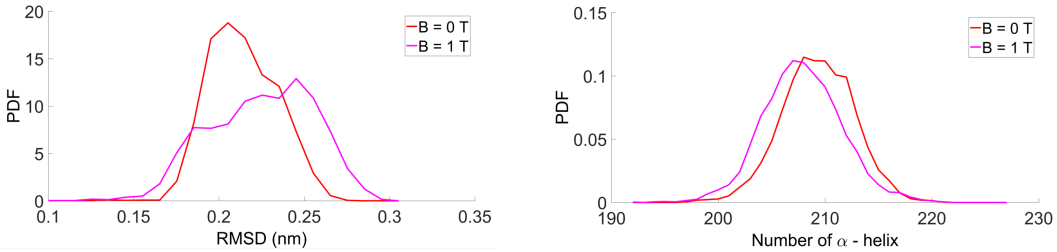

Figure 9.8: Root mean square deviation (RMSD) and α-helix secondary structures in zero field and 1 T of B field application

(myoglobin, lysozime) in a work of Nesmelova et al. [Nesmelova et al., 2002]. When the B field is applied the protein was subjected to a decrease of 80 % in its mobility. This is possible due to the action of the B field not only on charged protein residues but also on charged free particles as the ions present in the solution. Indeed, an increase of 28 % and decrease of 12 % has been detected for the Na^+ and Cl^- ions respectively. The opposite trend of the D values for the ions with the respect to the previous results (see Fig. 9.2), it may be coming from the presence of the positive charged protein and the interaction with the B field application.
In order to ensure that no structural changes where obtained due to the B field exposure the Root mean square deviation (RMSD) and the α-helix secondary structures (Fig. 9.8) have been studied. No significant differences were appreciated for both observable, meaning no protein disruption occurred next to the B field application.

Now the attention will be focused, not on the whole protein structure, but on the

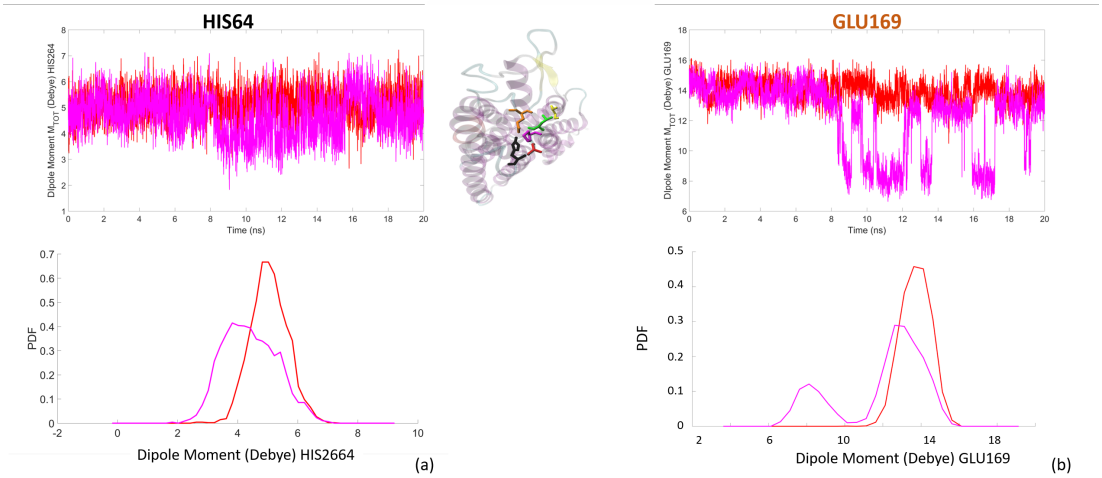

Figure 9.9: Dipole moment for the HIS264 and GLU169 residues (a and b), in time (upper panel) domain and with a PDF (lower panel) distribution calculated in the time range 8 - 20 ns.

charged residues involved in the hydrogend bond during the ligand binding process (Fig. 9.4) [Lebon et al., 2015].

To possibly detect interaction mechanisms of the B field with chosen residues of the A_{2A}, firstly the dipole moment has been computed (Fig. 9.9) of residues. In Fig. 9.9 the main results are reported for the residues histidine264 (Fig. 9.9a) and glutamate169 (Fig. 9.9b) both in time domain and with a PDF distribution. Almost, from the half of the simulation the residues seem to reorient due to the B field application, specially for the glutamate residue. This effect is confirmed looking to the PDF of dipole moment calculated between the 8^{th} and 20^{th} ns of the simulation. The significant effect of the glutamate residue could be due to its high charge of +1e that could respond to the B field application. No effects were appreciated for the other residues of the ligand binding site.

As last observable, taking a look to the A_{2A} topology, the ramachandran plot have been analysed. Ramachandran plot, as previous mentioned, (see sec. 9.2) represents the energetic regions and possible conformations permitted to peptides. In Fig. 9.10, it can be noticed how in zero field condition the residue, during the simulation (spots represent the rotation values from 0 to 20 ns) are mostly in the stability region assuming a configuration between the β-Sheet and the α-helix right-handed conformation. An exception is highlighted for the leucine residue (green spots in Fig. 9.10) founded in

the disfavored region, that as mentioned in sec. 9.2, could be due to particular state as folding state or it can indicates a different secondary structures (e.g. coil or turn).
When a B field of 1 T is applied, all the residues are subjected to rotations towards different conformation with the respect to the no field application (Fig. 9.10 right side). Almost all the residues go to the α-helix right-handed conformation exception for the serine going towards a β-Sheet structures. No changes were detected for the glutamate residue. These results in terms of residues rotations suggest a B field effects in terms of charge re-distribution on the receptor surface.

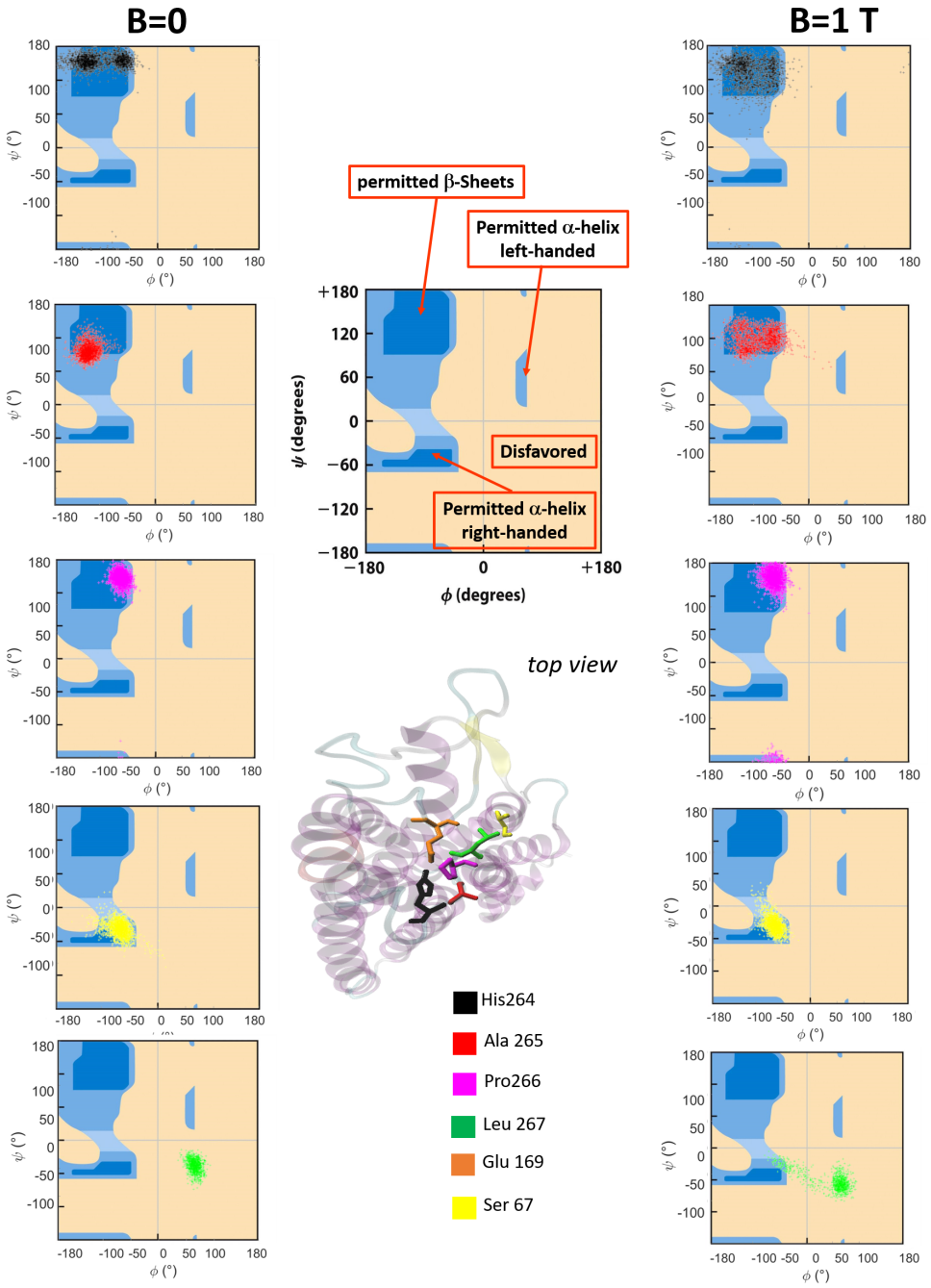

Figure 9.10: Ramachandran plot for the HIS264, ALA265, PRO266, LEU267, GLU169, SER67 in zero field (left side) and under the exposure of 1 T (right panel).

9.4 Conclusions

More often researchers are focusing their attention on the B field interactions on living objects [Varani et al., 2002, Di Lazzaro et al., 2013, Varani et al., 2017]. Recently, from Varani et al. [Varani et al., 2002, 2008, 2017] experimental studies have presented regarding the enhancing of the anti-inflammatory effects of the adenosine A_{2A} on cells next the application of a magnetic field with intensity between 0.5 and 3 mT [Varani et al., 2002].

In this chapter, the analysis of the interaction mechanism between the adenosine A_{2A} receptor and a magnetic field application has been presented.

The implementation in the Gromacs software of a static external magnetic field, for the first time, has been carried out by introducing the Lorentz force with the Larmor frequency component into the Velocity Verlet algorithm. In the update of velocities and positions the term of the Larmor frequency has been introduced to insert a magnetic field applied in the z direction. To validate the code, preliminary simulations of a charged particle, Na^+ ion, in vacuum and with water molecules have been done. A perfect matching has been obtained between the Na^+ displacement from the numerical MD simulations and the analytic models as reported in the results section 9.3. These results confirmed the expected behavior of the magnetic field acting on the single particle, giving a first validation of the method implemented.

After testing the implemented code, we performed MD simulations considering a NaCl buffer solution (DMEM concentration [Varani et al., 2002]) exposed to 1 T of magnetic field. From the diffusivity (D) analysis, no changes for water molecules occurred and a variation of 10 % and 18 % for the Na^+ (decrease) and the Cl^- ions (increase) was observed. This effects can be explained as result of the interaction of the B field with free charged particles.

Simulations of the Adenosine A_{2A} receptor in the buffer NaCl solution, highlighted a decrease of the protein diffusivity D, by the 80 %; no changes occurred for the water diffusivity and an increase of 28 % and a decrease of the 12 % was reveled for the Na^+ and the Cl^- ions. The opposite behavior for the ions diffusivity in presence of the protein can be due both to the presence of the charged adenosine A_{2A} (+6e) and to the interaction with the magnetic field which could explain the immobility of the protein with the respect the zero field application (see Fig. 9.7).

From the RMSD and the α-helix secondary structures study no changes were detected,

ensuring no protein disruption due to the B field application.

In order to analyse the ligand binding site of the adenosine A_{2A}, the Dipole moment and the ramachandran plot have been computed for six residues involved in the hydrogen bond during the ligand binding process (HIS264, ALA265, PRO266, LEU267, GLU169 and SER67, Fig. 9.4). By the dipole moment analysis a reorientation of some binding residues (GLU169 and HIS264) has occurred next the application of 1 T of B field.

To study the energetic regions allowed to single residues we calculated the Ramachandran plot, by detecting changing in bond residues torsion angles ψ and ϕ when a B field of 1 T is applied for the ligand-binding residues (HIS264, ALA265, PRO266, SER67, LEU267). A trend towards the α-helix right-handed conformation has been detected when the B field is applied (see Fig. 9.10) for almost all the residues, exception for the serine67 going towards β-Sheet structures. No changes were observed for the glutamate residue. These residues rotations suggest that our data seem to be in line with the molecular gyroscope mechanism and diamagnetic anisotropy mechanism proposed by Binhi and Prato [Binhi and Prato, 2017] and by Babaei [Babaei et al., 2017] respectively.

As whole these data advise a direct interaction between the B field applied and the charged residues of the protein surface.

Chapter 10

Molecular modeling of the metallo-enzyme superoxide dismutase exposed to nanosecond pulsed electric signals

10.1 Introduction

In the previous chapter (see Ch. 9), a molecular dynamics simulation study has been presented to explore the interaction between a magnetic field and a protein structure. Anyhow, recently many researchers have also focused the interest on intracellular enzyme modifications induced by the application of nanosecond pulsed electric fields, observing enzymatic activity loss in proteins, supported also with theoretical predictions from molecular dynamics simulations, focusing on significant variations in protein secondary structures. Here a protein has been chosen, the SOD1 enzyme, due to its important biochemical activity as an antioxydant molecule and also due to the peculiar characteristics of its active site, having an electrostatic environment particularly responsive.

The superoxide is generated by many life processes, which include aerobic metabolism, oxidative phosphorylation and photosynthesis, in addition to the respiratory burst in the immune response of stimulated macrophages and neutrophils [Fridovich, 1986]. Superoxide − dependent formation of hydroxide radicals are important in oxygen tox-

icity [Halliwell, 1982, Carlioz and Touati, 1986], if unchecked, reactive oxygen species (ROS) including the superoxide radical can result in inflammation and inflict cell injury that includes DNA damage [Imlay et al., 1988, Imlay and Linn, 1988] being implicated in many human pathologies, including ischemic reperfusion injury, cardiovascular disease, cancer, aging and neurodegenerative disease [Perry et al., 2007, Halliwell, 1992]. The enzyme superoxide dismutase (SOD) takes part to the cellular antioxidant defence mechanism, repairing cells from damages caused by the toxic reactive oxygen species (ROS) including the superoxide radical O_2^- [McCord and Fridovich, 1969, Fridovich, 1998]. SODs are enzymes that disproportionate superoxide anion radicals at some of the fastest enzyme rates known. They essentially act as a master key, controlling cellular ROS levels, with a potential use as therapeutic agents in oxidative stress-related diseases [Kawakami et al., 2009, Peixoto et al., 2009, Abdallah et al., 2009]. Specifically, the Cu-Zn,SOD (or SOD1) [Getzoff et al., 1983] is a homodimeric metalloenzyme containing a couple of copper (Cu) and zinc (Zn) metal ions that dismutate the superoxide radical O_2^-. To prevent the accumulation of the O_2^- radical, in the first step of the dismutation reaction, the O_2^- is oxidized by Cu^{2+} to molecular oxygen(O_2) and subsequently a second superoxide anion is reduced by Cu^+ to produce hydrogen peroxide (H_2O_2).

Recent studies experimentally investigated the role of the SOD1 in ALS, finding an alteration of the glutamate release from the enzyme in the mice spinal cord [Bonifacino et al., 2016], while other ones found expression of the SOD1 in patients affected by neuronal disorders [Beqollari et al., 2016, Ayers et al., 2016]. Moreover, it has been found [Cleveland and Rothstein, 2001, Wood et al., 2003] that the accumulation of the O_2^- radical, resulting in oxidative stress, is implicated in neurodegenerative diseases as is the ALS (Amyotrophic lateral sclerosis) [Kaur et al., 2016] or in the Parkinson disorder causing neuronal apoptosis [In et al., 2016].

Because the mechanism of the SOD1 enzymatic reaction has not been fully elucidated, molecular dynamics simulations (MD), providing protein conformational changes at the atomistic level, have been used as tool for the understanding of the protein stability both in physiological conditions and under external stimuli [Falconi et al., 2001, Schmidlin et al., 2013, Ding et al., 2012]. Falconi et al. [Falconi et al., 2001] analysed the differences between the wild-type and mutant a single site mutant Val29Gly-SOD1 both experimentally with spectroscopy and with MD simulations, highlighting a more accessible active site and dynamic copper accessibility for the mutant SOD1. In another

study [Schmidlin et al., 2013] MD simulations have been used to analyse the thermal SOD1 denaturation at a temperature of 498 K in 200 ps by confirming the experimental evidences. To this regard, different researchers have explored the possibility to destabilize the SOD1 protein by the application of an external stimulus as thermal or a pH variation [Schmidlin et al., 2013, Dolashka et al., 2011, Auclair et al., 2010], indeed Auclair et al [Auclair et al., 2010] founded that at melting temperature in a range between 25 °C and 45 °C, a more stable protein structure is obtained, by cross-link the two SOD1 monomers with cysteine and in this way preventing the aggregation also responsible of neuronal diseases.

However not only a pH variation or a thermal stimulus have been applied in the past to destabilize molecular enzymes as SOD1 but also external electric fields. The development of tools to map intracellular electric fields is beginning to suggest that a significant fraction of cytosolic proteins are, like the majority of membrane proteins, exposed to strong electric fields [Koo Lee et al., 2009]. In addition, there is evidence for an increasingly use of electric fields to manipulate proteins in bio-nanotechnology applications. For example, nanosecond pulsed electric fields (nsPEF) with intensities up to $2x10^7$ V/m able to permeabilize the plasma membrane due to a large population of small pores (i.e. nanopores), have been shown to directly interact with internal cell organelles [Breton and Mir, 2012, Denzi et al., 2013], or internal proteins [Beebe, 2015, Azan et al., 2017b, Carr et al., 2017]. Given the master key role in controlling cellular ROS levels of SOD1 enzymes and given their sensitivity to destabilization due to external physical agents, it is particularly interesting to elucidate the mechanism of action of intense electric fields acting on SOD1.

Therefore, the goal here is also to observe SOD1 response to electric fields, studying whether this enzyme results sensitive to the application of a 100 nsPEF with different intensities (in line with literature from 10^8 to $7x10^8$ V/m) and different shapes with a first aim to verify a possible transition to an unfolding state. In addition, we studied the pattern of the electrostatic distribution at the reaction site of the enzyme, as a marker of a facilitated or impeded reaction.

The hypothesis is the possibility to create a sort of electric environment which could enhance the interaction between the superoxide anion O_2^- and the Cu^{2+} of the SOD1 active site. In fact, the structural biology of the SOD1 enzyme reveal important features as hydrogen-bonding and metal-binding motifs making possible a mechanism known as 'electrostatic guidance' [Perry et al., 2010], that promotes the catalysis with

time scales faster than O_2^- diffusion rate. Such mechanism, firstly proposed by Getzoff and colleagues in 1983 [Getzoff et al., 1983], hypothesizes that the arrangement of electrostatic charges in the active site of SOD1 promotes productive enzyme-substrate interaction through the substrate guidance and charge complementary. More recently such electrostatic interaction has been experimentally measured for another human enzyme, showing that the organization of charged and polar groups in the folded state of proteins produces large electric fields, and that the magnitude and direction of such fields may have a substantial effect on the rate of reaction [Suydam et al., 2006]. In line with this, electric fields are being considered able to modulate enzyme catalysis: recent experiments utilizing the vibrational Stark effect made possible to measure the electric field experienced by a substrate molecule when bound inside its enzyme's active site. These experiments have provided compelling evidence supporting a major electrostatic contribution to the enzymatic catalysis [Fried and Boxer, 2017].
Moreover, very recently it has been proven that an electric field stimulation combined with X-ray crystallography of protein crystal can reveal protein mechanics using electric field strength in the order of 10^8 V/m.
For these reasons, we numerically evaluated maps of the electrostatic field distribution at the active site of the SOD1 when a 100 nsPEF of 10^8 V/m of intensity is applied looking for a modulation of the electrostatic environment of the enzyme active site. Such interaction can be considered as a first step of a cascade of events culminating in an overall cell response.

10.2 Materials and Methods

Protein Structure

To perform MD simulations we used the structure of a crystallized mutant SOD,Cu-Zn (PDB code: 1SPD23) with the biochemical activity considered equivalent to the wild-type one [Amadei et al., 2007, 2006]. The structure is a dimer with the active site present in both monomers. Moreover, in the absence of the O_2^--SOD,Cu-Zn complex, we considered the structure as reported in [D'Alessandro et al., 2004], where for the purpose of modeling of the enzyme core, an available structure of bovine SOD,Cu-Zn complexed with an azido group (PDB code: 1SXZ) has been equilibrated and minimized replacing the azido group with O_2^- [Amadei et al., 2007, 2006].

The enzyme superoxide dismutase (SOD) has the main role to defend the enzyme in the body's response to the toxicity of metabolic by-products of oxygen. To do this it eliminates the superoxide anion radical O_2^- by transforming it in hydrogen peroxide H_2O_2 after a bond with two H^+ ions. The SOD,Cu-Zn enzyme accomplished this role through its active site (Fig. 10.9b) formed by the Zn^{2+} ion, the Cu^{2+} and the superoxide anion O_2^- with which takes place in the enzymatic reaction plus three histidines coordinated by the copper ion. The environment in which the SOD1 enzyme was immersed consists of a rectangular box (10 x 11 x 9 nm^3) containing inside 32292 single point charge (SPC) water molecules with 9 Na^+ counterions, for a total of 99659 atoms (Fig. 10.1a). Resulting system density was 1000 kg/m^3.

Molecular dynamics simulations

Molecular dynamics simulations were performed with Gromacs 4.6.5 package [Hess et al., 2008], employing the GROMOS96 (ff43a1) force field [van Gunsteren et al., 1996]. All complexes were energy relaxed with 1000 step of steepest descent energy minimization. MD simulations were performed using the LINCS algorithm [Hess et al., 1997] to constrain bond lengths and periodic boundary conditions were applied in all directions. Long range electrostatic forces were treated using the Fast Particle-Mesh Ewald method (PME) [Essmann et al., 1995]. Van der Waals forces and Coulomb potential were treated using a cut-off of 0.9 nm and the simulation time step was set to 2 fs. An initial velocity obtained according to a Maxwell distribution at 300 K was given to all the atoms. All simulations were run in NVT environment employing V-rescale as temperature coupling algorithm, with reference temperature set at 300 K. The trajectories were propagated up to 150 and 200 ns in a NVT (number of particles, volume and temperature are constants) ensemble using an integration step of 2 fs for exposure and no exposure condition respectively, fixing the SOD1 center of mass, preventing translations but with no constraints on its related rotation. For the no field exposure, also four different simulations were carried out (50 ns of duration) in order to have significant statistic data.
Possible effects due to the intensity and the specificity of an applied nsPEF have been evaluated by the application of monopolar and bipolar electric pulses with rise and fall time of 2 ns. We performed the implementation of the analytic form of the trapezoidal monopolar and bipolar signals inside MD simulations by modifying the source code

sim_util.c in the GROMACS package [Van Der Spoel et al., 2005]. The E field intensity for both signals was settled from 10^8 to 7x10^8 V/m, acting in the simulation box as explained in [Marracino et al., 2013b].
Besides, the application of the electric field takes place in continuity at the last frame of the unexposed simulation, thus allowing a direct evaluation of the protein response due to the switch on of the external electric field application.

Molecular dynamics observables

Secondary Structure analysis

To evaluate possible structural changes induced by the external signals considered, we calculated the number of secondary structures through the command line of the GROMACS package using the do_dssp command. The SOD1 is mainly a β-Sheet structure, which constitute a fundamental form of bio-molecular recognition (like DNA base pairing) and are involved protein-protein interactions, and peptide and protein aggregation [Nowick, 2008].
The calculation has been made in terms of mean value of β-Sheet and Coil number during the on phase of both monopolar and bipolar pulses, with the respect to the equilibrium condition (no E field applied). P-value statistics calculations have been carried out using the student t test.

RMSD, Radius of Gyration and Solvent Accessible area

To quantify the protein atoms positions during the MD simulation we computed the rmsd. The RMSD (root-mean-square deviation) of atomic positions provides a quantitative measure of the protein structural variations, comparing the electric field exposure and the equilibrium state. Moreover, in order to quantify the distribution of the atoms in the space relative to their center of mass, we computed the radius of gyration, which provides an understanding of the changes in shape and size of the protein under the influence of an external stress. To analyse the interaction of the SOD1 protein with the environment in which is immersed, we calculated the solvent accessible area (SASA), that estimates the solvent accessible surface to the protein structure, to interact with solvents or with other molecules of similar size. It provides the hydrophobic and hydrophilic area available for the protein. All these observable have been calculated with

the GROMACS command line.

Dipole Moment Spectrogram

Usually proteins, due to their secondary structure conformation (α-helices, β-sheets, turns, coils, etc.) possess an electric dipole moment and when an external electric field is applied, the protein orients itself in the direction of the field application. Firstly, we analyzed the dipole moment of the protein in time domain both under the monopolar and bipolar pulse.
Moreover, the analysis has also been conducted in the frequency domain. The spectrogram is a time-frequency representation, able to describe the spectral content of a signal, obtained as the square modulus of the short time Fourier transform algorithm. This algorithm implying the windowing of the temporal signal under analysis and the fast Fourier transform of each time sequence. Here, temporal sequences 4.0 x 10^{-11} s long filtered through a Hamming pass-band filter [Hamming, 1989], with 50 % overlap between adjacent segments has been chosen. We obtained a frequency resolution of 0.25 GHz and a time resolution of 6 ns. The electric field was applied in the y-axis (Fig. 10.1a). The analysis of the frequency spectral content of the dipole moment of protein and water molecules have been performed. This outcome has been evaluated both considering the application of an electric field of 10^8 V/m and a temperature increase of 35 degrees (335 K, SOD1 melting temperature [Ding et al., 2012]) to compare the different molecules response.

Electrostatic distribution at the active site

With the aim to study the charge distribution of protein molecules around the active site, the electric field maps have been performed, along two main directions of the active site Cu-O_2, comparing the equilibrium condition and the one perturbed with an electrical external stimulus. As electrical stimulus, the effects of a monopolar and bipolar 100 nsPEF with intensity of $E_y = 10^8$ V/m, have been investigated.
The local electric field (Eq. 10.1) has been computed, due to the contribution of all charges related to all molecules (protein, water and Na ions) in two different planes of 4.7 x 4.7 nm^2 of dimension (centered in the Cu position), in the Cu-O_2 (x') direction and the one (y') perpendicular to x' (see π' plane in Fig. 10.9c) and the other plane (see π" plane in Fig. 10.9c) is in the Cu-O_2 (x') direction and the other one, y", is the

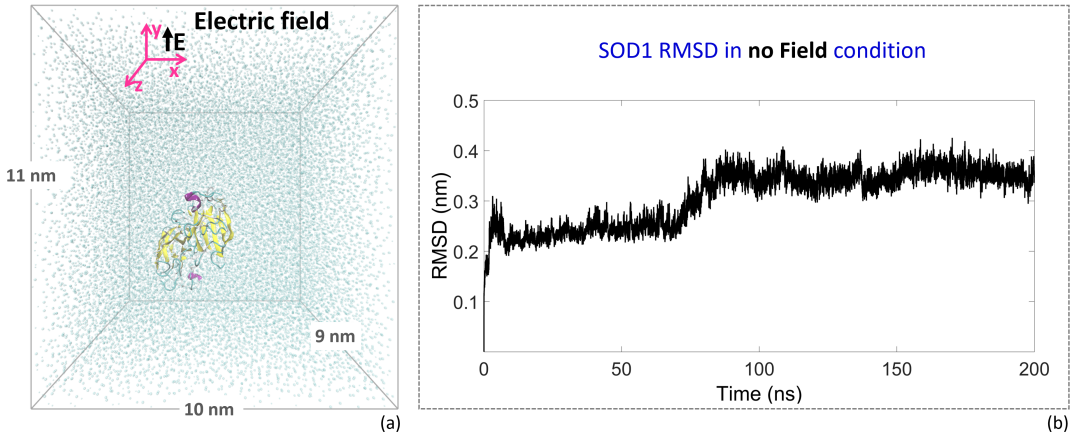

Figure 10.1: (**a**) SOD,Cu-Zn molecular model showing the simulation box (10 x 11 x 9 nm^3) containing 32292 water molecules, the SOD1 model and 9 Na^+ counterions. The SOD,Cu-Zn model is formed by two monomers, each one containing a reaction centre. The electric field is applied in the y direction. (**b**) The RMSD of the SOD1 enzyme during the equilibration (t = 200 ns).

one perpendicular to y'. The discretization step of the map has been $\Delta = 0.05$ nm (see Fig. 10.9c).

$$E_{ri} = \sum_n \frac{q_n}{4\pi\epsilon_0 |\,(r_n - r_i)\,|^{\,3}} (r_n - r_i) \tag{10.1}$$

The effects of the presence of charged residues (i.e. glutamic acids, Fig. 10.9c purple color) surroundings the SOD1 active site (Fig. 10.9c) have been evaluated to study a possible electrostatic guidance of the O_2^- ion to interact with the copper Cu^{2+} mediated by the external electric field application. Finally, to validate our electric field maps and to quantify the difference between the equilibrium and exposed condition we calculated the SMAPE (Eq. 10.2) (Symmetric mean absolute percentage error) as follows:

$$SMAPE = \frac{200\%}{n} \sum_{t=1}^{n} \frac{|\mathrm{F}_t - A_t|}{|\mathrm{F}_t| - |\mathrm{A}_t|} \tag{10.2}$$

where F_t and A_t are the mean value of the Electric field for the zero field condition and the exposed one, respectively; n is the number of points used for the maps construction.

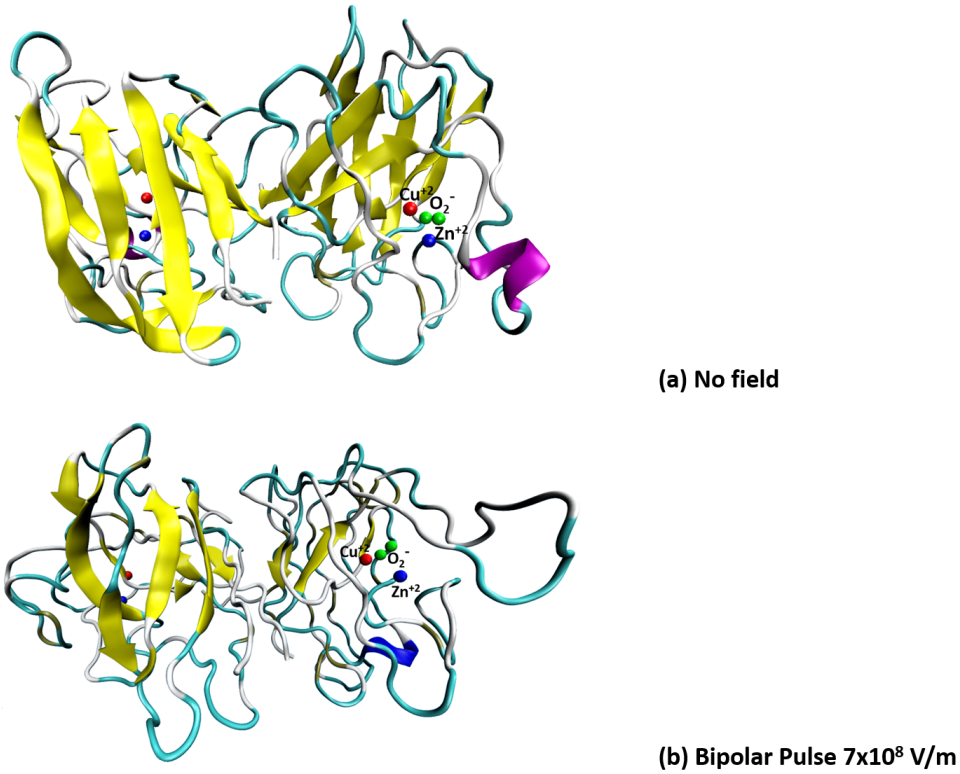

Figure 10.2: (**a**) SOD1 molecular structure in equilibrium condition (no field applied). Each of the two dimers hosts the reaction center defined by Cu and Zn atoms. In yellow β-Sheet structures are shown, coil in white, turn in chain and α-helix in pink. The active site is reported (Cu^{2+} in red, Zn^{2+} in blue and O_2^- in green). (**b**) The $7x10^8$ V/m 100 Bipolar pulse induces a remarkable loss of β-Sheets at the end of the pulse excitation suggesting an SOD starting unfolding state. The others secondary structures show a similar behavior.

10.3 Results and discussion

Equilibration of the system

The present work includes a total of 1500 ns all-atom, explicit-solvent MD simulations for the complete SOD1 enzyme. During equilibration in the water box (Fig. 10.1a), the root-mean-square deviations (RMSDs) of the structure is leveled off at a value <

0.5 nm (Fig. 10.1b), indicating that equilibrium had been reached. The equilibrated system representing the "No Field" condition, considered as a control of the protein at the equilibrium state, had a time length of 200 ns. Moreover, in order to give a statistical analysis, 4 further equilibrated systems have been simulated in "No field" condition with a duration of 50 ns each.

Conformational effects

A comparative analysis is carried out between the physiological condition of the SOD1 enzyme and the ones exposed to the external electric field to define a threshold for the intensity of the field able to interact and manipulate the SOD1 enzyme.
A first indisputable result is related to the effect of a pulse with intensity of $7x10^8$ V/m, the highest one considered for this work. The structural changes, that the protein undergoes, are visibly marked and can be appreciated in Fig. 10.2 showing the SOD1 secondary structures at the end of the "No field" simulation (t=200 ns) and at the end of the "Bipolar $7x10^8$ V/m" simulation (t = 106 ns). A visible loss of the β-Sheet (yellow) is detectable with a loss of α-helix (pink), accompanied by a simultaneous increase of the coil complex (white). This result suggests a protein unfolding state and hence a induced indirect effect on SOD1 enzyme activity.
To have a more detailed picture of enzyme unfolding, β-Sheet secondary structures are evaluated over time (see Fig. 10.3). Looking at the dynamic behavior it is possible to observe that for both the Monopolar and the Bipolar pulses there is a marked decrease in the β-Sheet structure during the time course of the signal applied. The final unfolding state seems to be related to the kind of signal applied. In particular, the Bipolar pulse during the reverse polarity of the signal (from 100 to 150 ns) is able to induce even a higher effect on secondary structures of the SOD1 if compared to the Monopolar one (Fig. 10.3a and 10.3b).
Such rearrangements are shown to be irreversible in 50 ns after the application of the pulse, hence predicting an unfolded state. In fact, a recovery of the physiological structure of the enzyme is not achieved as can be seen from 50 ns OFF of the Bipolar pulse (Fig. 10.3b, pink curve) where no recovery occurs for the β-Sheet, suggesting a protein change that is not reversible after the removal of the external E field. Similar trend is shown for the Monopolar pulse even if less marked (Fig. 10.3a, red curve).

The probability density function (PDF) of the β-Sheet structures during the OFF state computed for the two signals (Monopolar and Bipolar), evidences a difference of 60% for the Bipolar with respect to the No field state (Fig. 10.3c, purple line) while a 30% is reached when a Monopolar pulse is applied (Fig. 10.3c, red line).
Looking for a threshold in the electric field amplitude able to structurally modify the SOD1 enzyme, the average values of Coil and β-Sheet secondary structures have been evaluated for decreasing intensities of the field applied ($7x10^8$, $5x10^8$, $2x10^8$, and 10^8 V/m) comparing the "No field" condition with the Monopolar and the Bipolar pulses (Fig. 10.4).

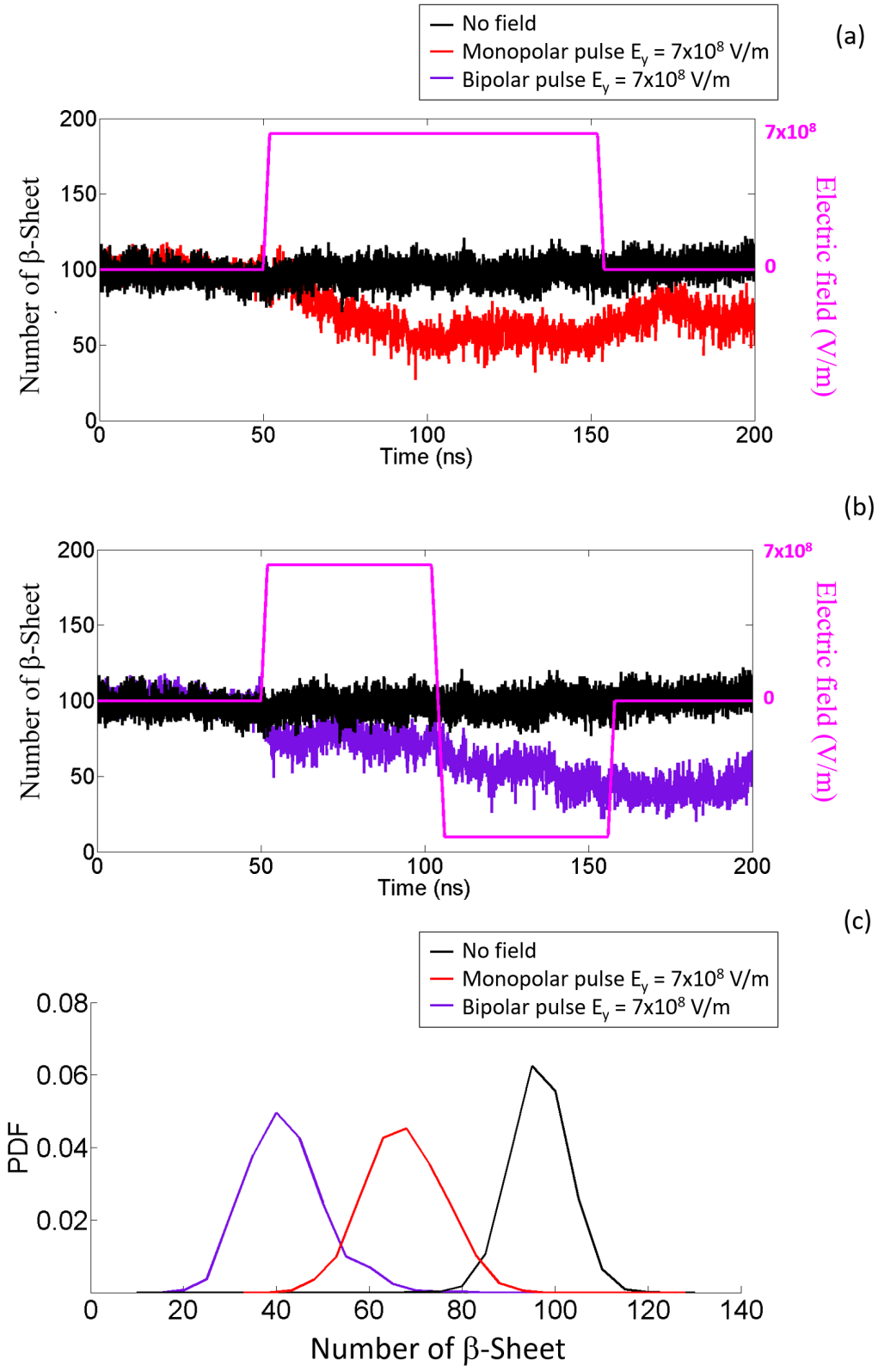

Figure 10.3: (**a,b**) SOD1 secondary structures recovery. (**a**) β-Sheet trend in time domain in no exposure condition (black line) and under a monopolar (red line, **a**) and bipolar (violet line, **b**) electric pulse with intensity of 7x10^8 V/m. (**c**) The β-Sheet probability density function is reported during the off state of 50 ns after the monopolar and bipolar pulse application. The distribution highlights the not reversible condition for the β-Sheet structures specially under the bipolar pulse exposure.

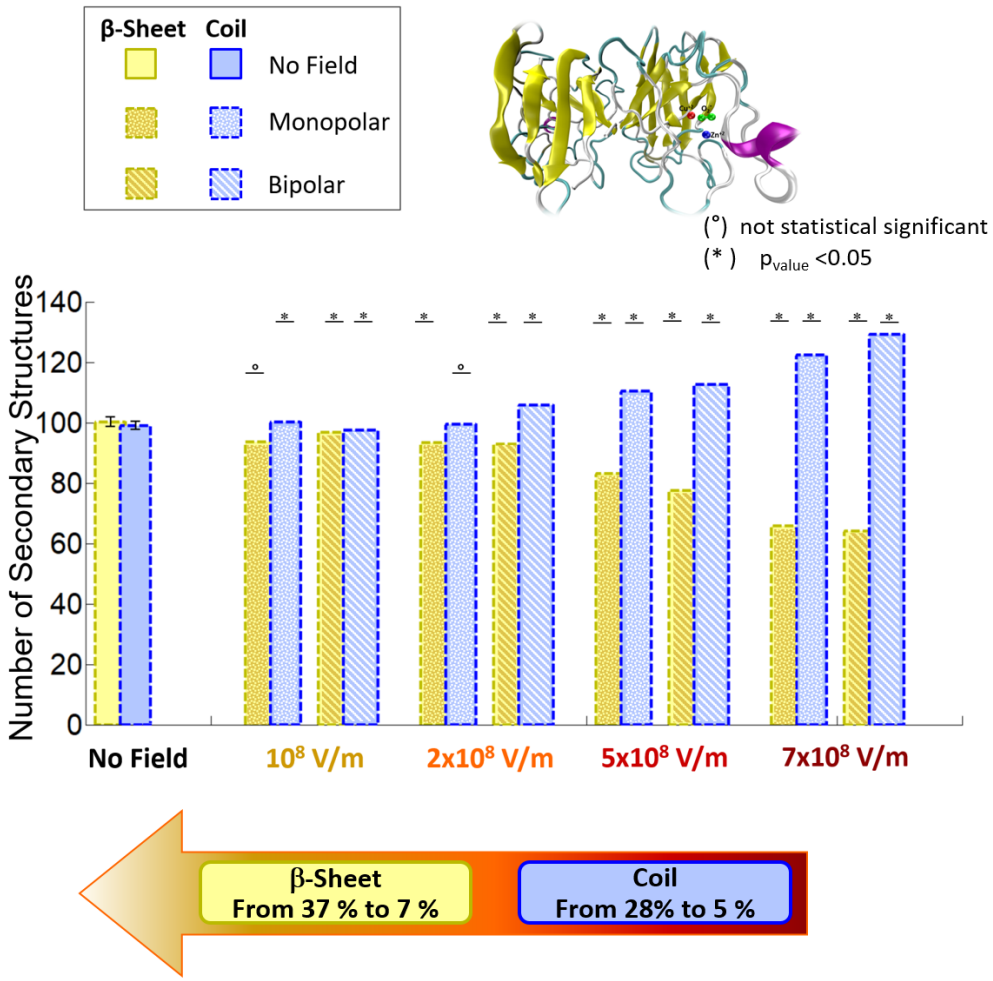

Figure 10.4: SOD1 secondary structures analysis. Coil and β-Sheet secondary structures mean values. The results are presented in no exposure condition and under monopolar and bipolar 100 nsPEF with intensity from 108 to 7x10^8 V/m. The asterisk ($*$) indicates p value smaller than 0.05 ($p<0.05$) which means a variation statistically significant, and the circle ($^\circ$) indicates no statistical significance. The statistical analysis has been performed with the Student t test. Bars on graph indicate the standard error.

We obtain at maximum (for the intensity of 7x10^8 V/m) a loss of β-Sheet up to 37% and an increase of the coil secondary complexes up to 28% while decreasing the intensity we have been able to identify three different structural states:

1. SOD1 unfolded state under the application a pulse of 7x10^8 V/m and not re-

versible in 50 ns following the switch off of the field;

2. initial SOD1 unfolding (variation of about 23 % in secondary structures) with intensity of 5x10^8 V/m of intensity, partially reversible in 50 ns after the electric pulse removal;

3. slightly reversible changes (< 5%) related to the application of field intensities equal to 10^8 and 2x10^8 V/m.

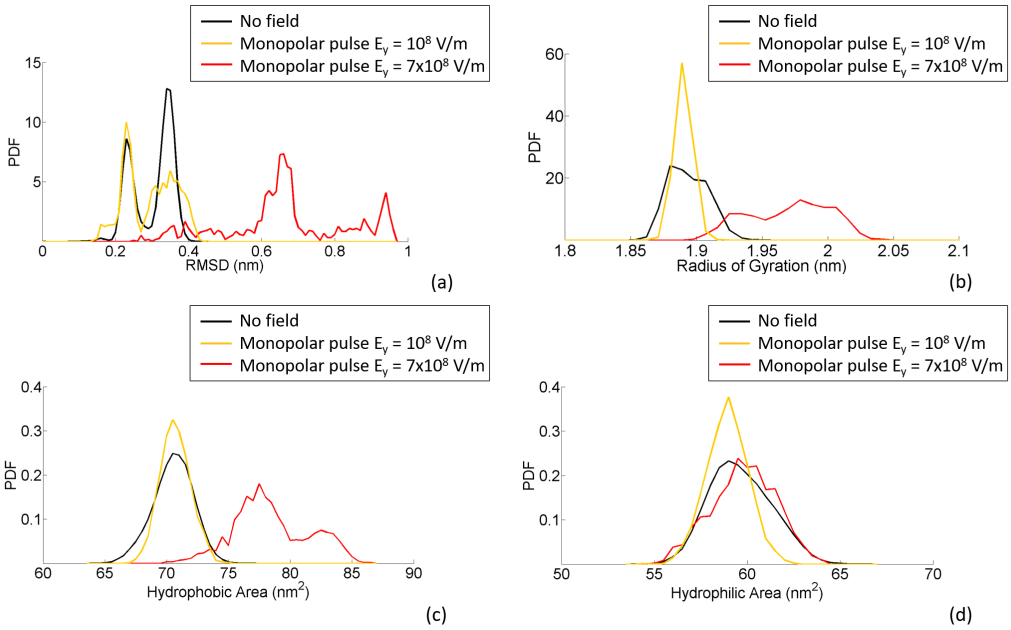

Figure 10.5: RMSD, radius of gyration and SASA analysis for the SOD1 protein. In the panel above four different main protein observables are presented: the probability density function (PDF) of RMSD (**a**); the PDF of the Radius of gyration (**b**); the PDF of the Hydrophobic (**c**) and Hydrophilic area (**d**) available for the protein structure in equilibrium condition (black line) and under an external monopolar pulse of 10^8 (yellow line) and 7x10^8 V/m (red line).

By applying the p-value statistics calculations, almost all the variations, compared with the equilibrium state, result to be statistically significant suggesting that the starting threshold for SOD1 conformational marked changes is about the electric field intensities of 5x10^8, while the intensity of 7x10^8 V/m is causing definitive protein structural rearrangements. Only in the case of 10^8 and 2x10^8 V/m the variation either

for the coil structures or for β-Sheet ones resulted to be not statistical significant. For this reason, Monopolar and Bipolar pulses of 10^8 V/m in amplitude, not able to determine any conformational change on the enzyme, have been chosen to check if they could be able to interact somehow with the protein.

Therefore, a first comparison in terms the RMSD (root-mean-square deviation), the radius of gyration and the solvent accessible surface area (SASA hydrophobic area and hydrophilic area) have been reported in Fig. 10.5 comparing the lowest (10^8 V/m) and the highest (7x10^8 V/m) values of the Monopolar pulse. In Fig. 10.5a the probability density function (PDF) of the RMSD is presented, showing for the "No-field" situation, a bimodal distribution with peaks of 0.2 and 0.3 nm, indicating that the system is fully equilibrated as also reported in Fig. 10.1a. The PDF profile for the case of 10^8 V/m is quite similar, indicating that the structure remains in the same condition of the equilibrium state, while for the highest intensity of 7x10^8 V/m the PDF is broader with range of variability between 0.2 nm and values higher than 0.9 nm. This increment is due to the partial loss of the secondary structures and denotes a protein elongation and an unfolding of the structure.

The previous results have been also confirmed by the radius of gyration (Fig. 10.5b), which quantifies the distribution of the atoms in the space relative to their center of mass, providing an insight of the protein changes in terms of shape and size under the influence of external stresses. Under the influence of a Monopolar pulse of 10^8 V/m of intensity, the SOD1 does not show significant variations with respect to the reference condition, while the loss of secondary structures already detected in Fig. 10.2 for an intensity of 7x10^8 V/m is the one responsible of the higher and wide distributed value of the radius of gyration. Finally, the total solvent accessible area has been calculated: results have been reported in Figs. 10.5c and 10.5d, split as the PDF of hydrophobic and hydrophilic area accessible for the protein, respectively. No noticeable changes have been observed for the intensity of 10^8 V/m in both cases, confirming that the lowest intensity considered in this work is not able to induce relevant changes in any of the parameter usually observed in MD of proteins. For the higher E field intensity of 7x10^8 V/m it has been observed an increase of surface hydrophobicity (Fig. 10.5c) of about 10% suggesting a decrease in protein - solvent molecules interaction, which could suggest a protein denaturation as reported in [Xiang et al., 2011]. Conversely, for the accessible hydrophilic area no changes were observed when an external electric field is applied, indicating that, differently from the hydrophobic regions which become more

exposed to water when the electric filed is applied, conversely the overall surface already exposed to water is not affected by the field (see Fig. 10.5d). Similar results have been obtained for the Bipolar pulse (see Fig. 10.6) for all the classical MD observable.

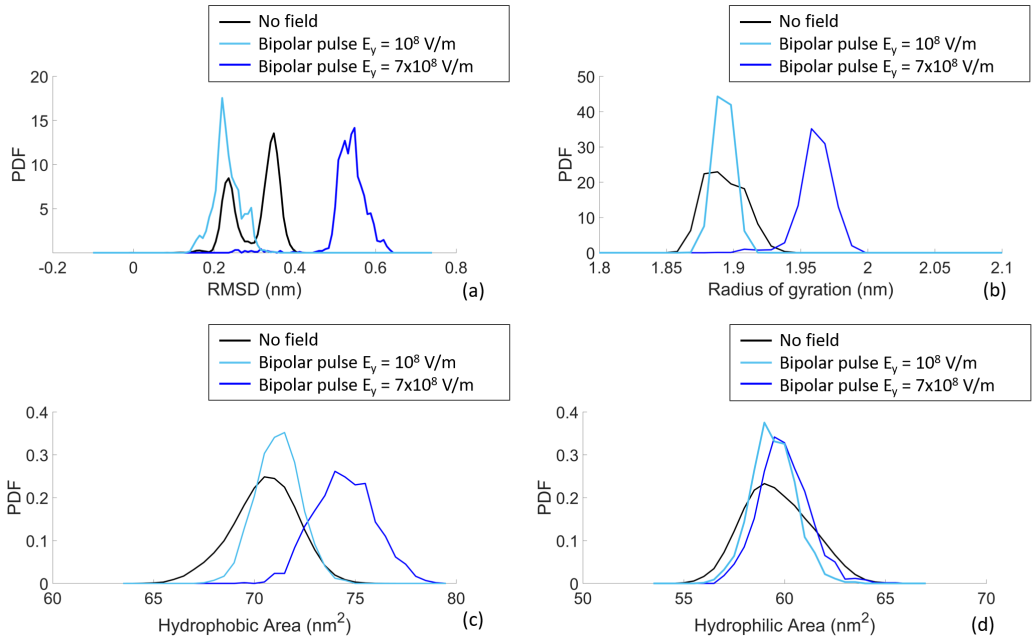

Figure 10.6: RMSD, radius of gyration and SASA analysis for the SOD1 protein. In the panel above four different main protein observables are presented: the probability density function (PDF) of RMSD (**a**); the PDF of the Radius of gyration (**b**); the PDF of the Hydrophobic (**c**) and Hydrophilic area (**d**) available for the protein structure in equilibrium condition (black line) and under an external bipolar pulse of 10^8 (light blue line) and $7x10^8$ V/m (blue line).

Electrostatic coupling

Despite that the lowest intensity of 10^8 V/m is not able to induce changes in the structure of the protein, there is still a not negligible coupling with the protein electrostatics, due to the dipolar mechanism, either mediated by the solvating water or directly with the enzyme. In fact, under the influence of an external electric field the protein residues as well as water molecules are subject to a reorientation quantified by the dipole moment.

We compared the physiological behavior of the enzyme (No-field case) with Monopolar and Bipolar pulses application of 10^8 V/m intensities, calculating both the protein and

the solvation-water 'dipole moment' alignment.

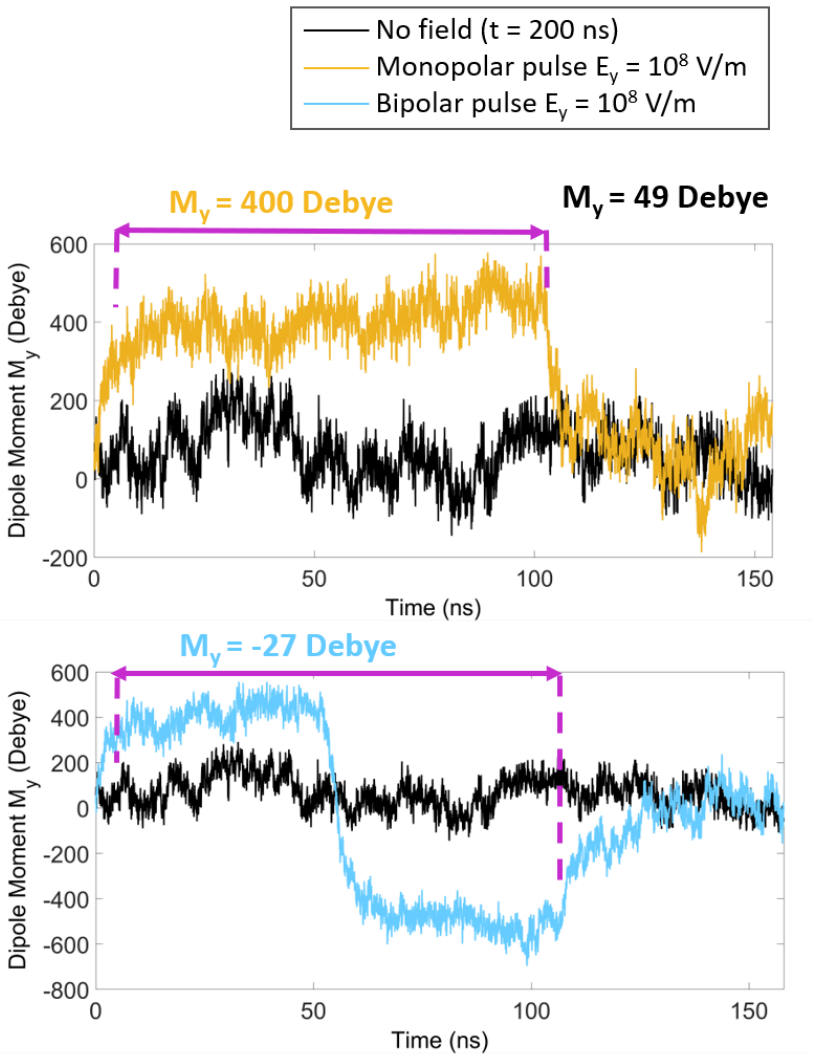

Figure 10.7: Time domain trend of the protein dipole moment in no field (black line) and when a monopolar (yellow line) and a bipolar (light blue line) pulse of 10^8 V/m is applied.

In Fig. 10.7 such coupling is reported as first in terms of time domain trend of the y component of the protein dipole moment. It is possible to notice how the protein, despite its dimension is able to follow the external field application, by suggesting a

reorientation of the protein (containing charged residues) depending to the external field applied.

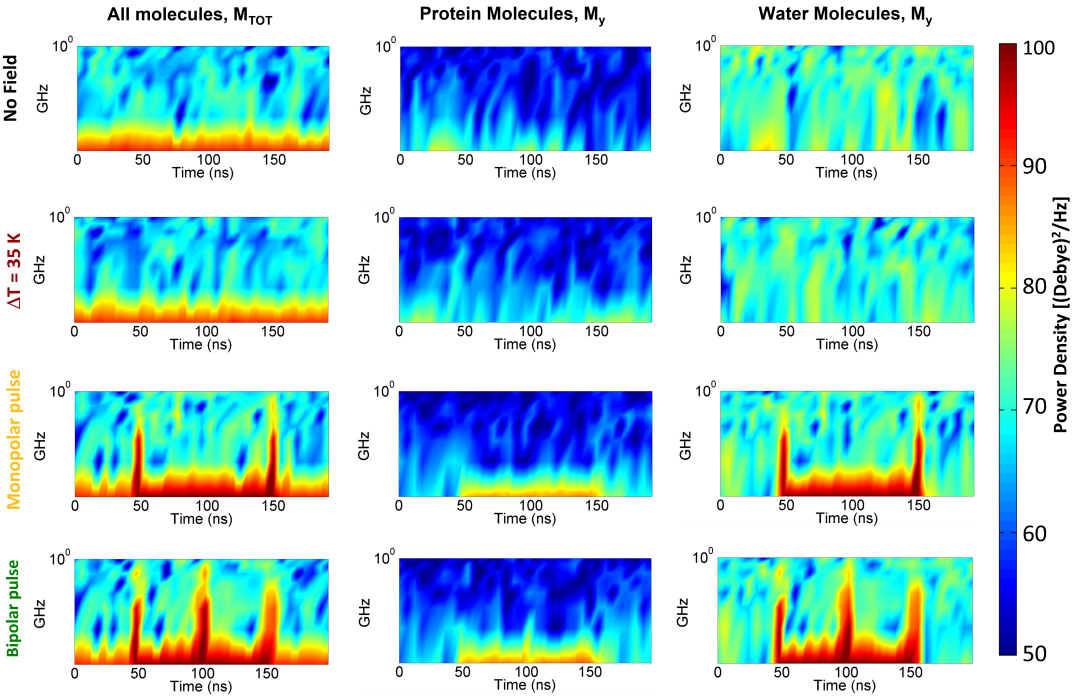

Figure 10.8: Frequency spectral content of all molecules (first column), the SOD1 and water dipole moment (second and third column respectively). Frequency spectral content of the dipole moment y-component of Cu,ZnSOD1 and water reported in no field condition (black label, first raw), with an increment of 35 K (second raw) and exposed to a 100 ns, 10^8 V/m of intensity for the Monopolar pulse (yellow label, third raw) and Bipolar one (green label, forth raw).

Successively, in Fig. 10.8 the dipolar coupling is also evaluated by means of the spectrogram of the total absolute value (M_{TOT}) and the y-component of the dipole moment.

Since a spectrogram is a visual representation of the spectrum of frequencies of a signal as it varies with time, it is built from a sequence of spectra stacking them together in time and by compressing the amplitude axis into a 'color map'. The final graph, as represented in Fig 10.8, has time along the horizontal axis, frequency along the vertical one, and the amplitude of the y-component dipole moment at any given time and frequency shown as color level. In the following spectrograms, the frequency dynamics

up to 1 GHz is compatible with the time scales of the dipole moment reorientation due to the external field applied, while the time axis is related to the signal used.
In No-field condition, as it is possible to appreciate looking at Fig. 10.8 (1st raw, 3rd column), the frequency content of water dipole alignment reaches 1 GHz for the whole observation time, while a lower frequency of about 700 MHz or less is observed for the protein (Fig. 10.8, 1st raw, 2nd column). This reflects the fact that the dynamics of water dipole moment alignment is more rapid than the one of the protein, as expected. When Monopolar or Bipolar pulses of 10^8 V/m are applied, water molecules are highly reoriented by the external E field with a frequency content always up to 1 GHz but perfectly following signal polarity changes; hence in the case of Monopolar pulse (Fig. 10.8, 3rd raw), after a first time length of 50 ns where the signal is still OFF, the rise and fall times of the signal are clearly visible in the increase of the frequency spectral content of the water dipole moment at the beginning and at the end of the signal course, while for the Bipolar one (Fig. 10.8, 4th raw) the reverse of the signal polarity is clearly observable in the increase of the spectral content also at the middle of the signal course (t=100 ns). When considering the behavior of the protein dipole moment, a similar trend is observed although with a marked decrease in the intensity of the dipole alignment, essentially due to the higher dimensions of the target. Therefore, SOD1 needs more time to reorient, but still is able to follow the external polarization (Fig. 10.8, 2nd column, 3rd and 4th raw), thanks to the electric coupling between the electric field and the protein. As last observation, by increasing the temperature of 35 K (experimental melting SOD1 temperature [Ding et al., 2012] ,Fig. 10.8, 2nd raw) no differences where appreciated with respect to the no field condition.
Such coupling of the protein electrostatic environment with 10^8 V/m Monopolar and Bipolar pulses may in principle have an effect on the SOD1 enzymatic activity. In fact, it is by now assessed that the SOD1 physiological pattern of electrostatic potential, where a positive potential region emanates from the active site and the repulsive negative potential barrier surrounds the protein, seems designed to provide a large cross-sectional area for O_2^- productive collisions [Klapper et al., 1986], hence giving an electrostatically guidance to the superoxide.
For this reason, to fully exploit the potentialities of the external electric field to affect the electrostatic guidance of the O_2^- towards the Cu^{2+}, the local electric field distribution on the active site of one of the two dimers (Fig. 10.9 a and b) has been investigated, due to the overall enzyme and water surrounding the enzyme. 2D maps have been com-

puted selecting a plane centered in the Cu^{2+} atom and with the first direction along the Cu-O_2 distance (x', Fig. 10.9c) and with the second one perpendicular to it (y', Fig. 10.9c) for the π' plane. The second plane (π" plane), is centered in the Cu^{2+} atom and with the first direction along the Cu-O_2 distance (x', Fig. 10.9c) and with the second one perpendicular to y' (y", Fig. 10.9c). Both planes have been densely meshed and at the nodes of each grid the electric field due to the overall charges from the protein and from water molecules has been calculated.

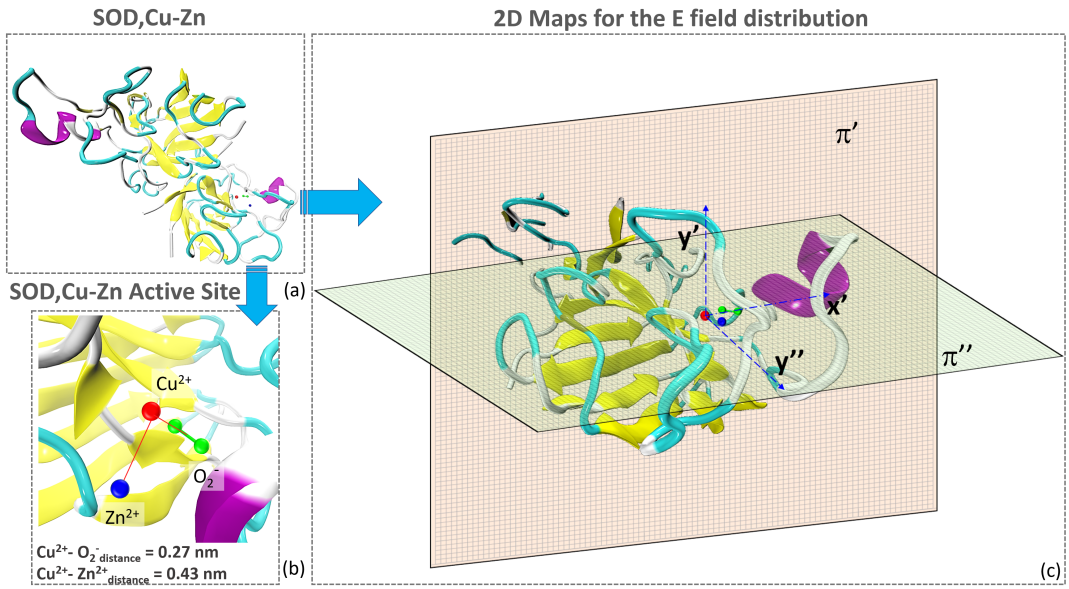

Figure 10.9: SOD,Cu-Zn dimer and active site (2D) grid for the local E field distribution calculation. (**a**) Molecular model of the SOD1 dimer viaβ-sheet ribbon representation. (**b**) Active site of one of the two dimers centered in the copper ion.(**c**) Two planes of 4.7 x 4.7 nm^2 with x'-axis oriented on (Cu^{2+}-O_2^-) direction and y'-axis normal to it for the π' plane and along the x'-axis oriented on (Cu^{2+}- O_2^-) direction and the y" normal to y'.

Results for the (2D) maps of the local electric field distribution are reported in Fig. 10.11 for the π' plane and in Fig. 10.12 for the π" plane, for which the front view is reported in Fig. 10.10 to better understand the atoms position. In No-field condition (Fig. 10.11a and Fig. 10.12a) the local electrostatic field distribution appears almost circular around the center quite elongate to be higher along the y' and y" direction respectively for both planes, due to the presence of the surroundings charged residues (Fig. 10.9c, i.e. the coils (white) and turn (chain) secondary structures along the y'

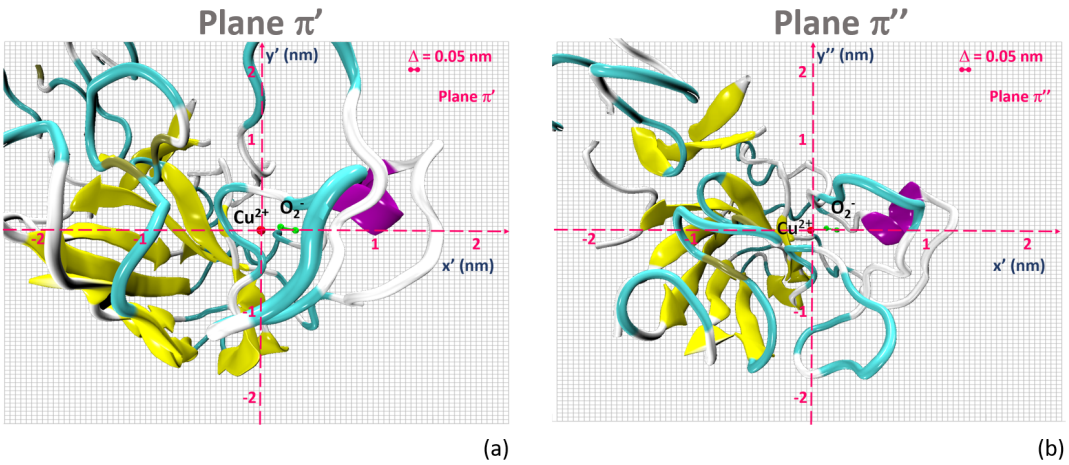

Figure 10.10: 2D Representation of the π' and π" planes in the frontal view to better comprehend the active site postion.

directions and the glutamate residue (GLU133), purple color, along x').

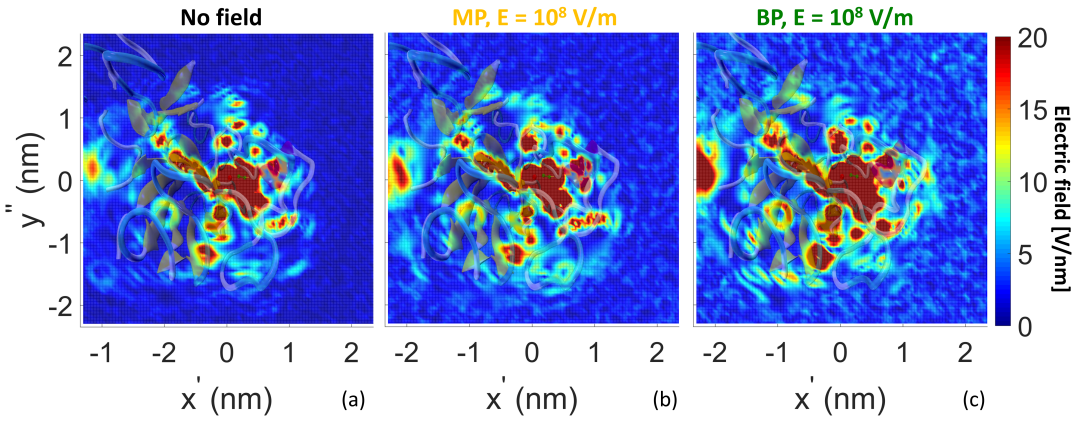

Figure 10.12: (2D) maps of the local electrostatic field around the active site on the π" plane. (**a**) No-field condition. (**b**) Monopolar (10^8(V/m), 100 ns). (**c**) Bipolar (10^8(V/m), $t_{ON-negative}$ = 50 ns). The local electrostatic field is given in units of 10^9(V/m)

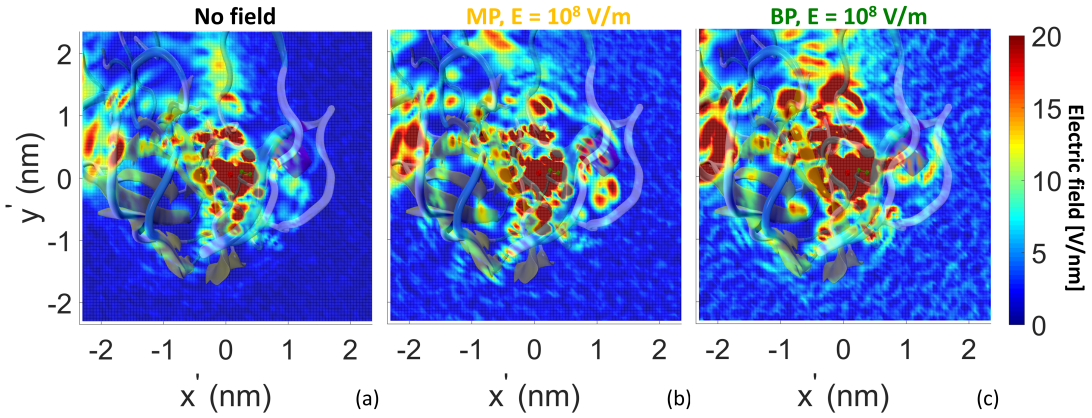

Figure 10.11: (2D) maps of the local electrostatic field around the active site on the π' plane. (**a**) No-field condition. (**b**) Monopolar (10^8(V/m), 100 ns). (**c**) Bipolar (10^8(V/m), $t_{ON-negative}$ = 50 ns). The local electrostatic field is given in units of 10^9(V/m)

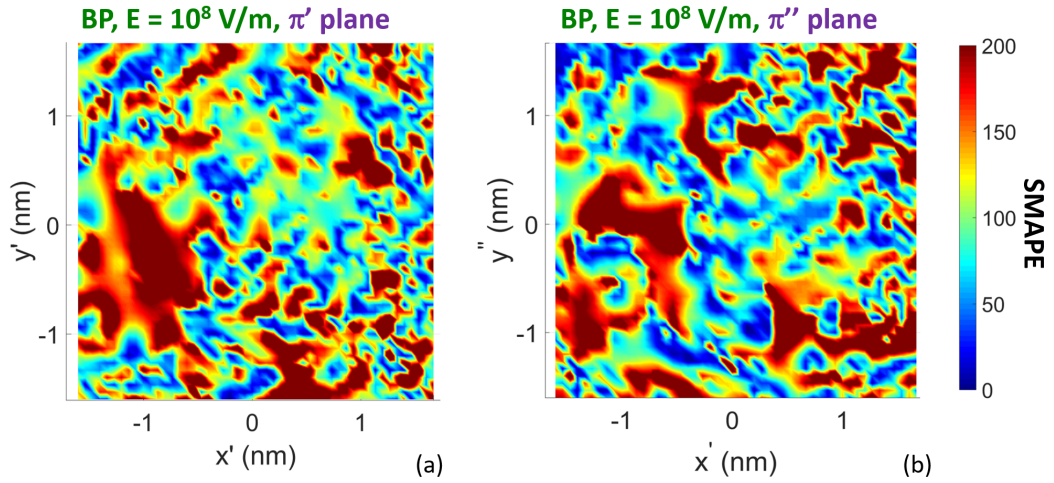

Figure 10.13: Distribution of SMAPE. (**a**) Bipolar pulse for the π' plane (10^8 V/m, $t_{ON\text{-}negative}$ = 50 ns). (**b**) Bipolar pulse (10^8 V/m, $t_{ON\text{-}negative}$ = 50 ns) for the π'' plane.

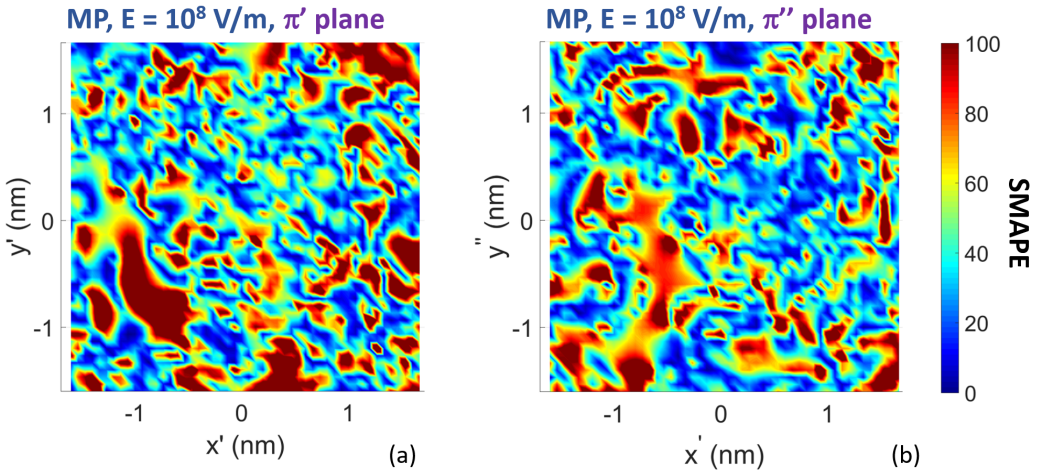

Figure 10.14: Distribution of SMAPE. (**a**) Monopolar pulse for the π' plane (10^8 V/m, 100 ns). (**b**) Monopolar pulse(10^8 V/m, 100 ns) for the π" plane.

By looking at the results for the π' plane, when the field is applied (Fig. 10.11c and 10.11d), the environment surrounding the CuO_2^- is subject to a general increase of the amplitudes of the local electrostatic field, particularly in the direction of the glutamate residue (GLU133, purple color), which has a strong electric negative charge and in the direction of the two turns along y'. Moreover, also for the π" plane, when the electric field is applied (see Fig. 10.12b and c) there is a more higher electric field more concentrated at the active site. Moreover, in the case of the Bipolar pulse, the whole area surrounding the reaction center becomes site of a higher local electrostatic field suggesting possible rotation of the protein residues due to the external field action (see Fig. 10.11 and 10.12) in both planes.

In order to quantify these effects, we computed the SMAPE [Armstrong, 1985](Symmetric Mean Absolute Percentage Error), comparing the exposure and the not exposure condition for both planes. Fig 10.13 and Fig. 10.12 report the distribution of the SMAPE for each of the pixels of the (2D) map of Fig. 10.11 in a region more focused on the active site (2.5 x 2.5 nm^2 of dimension) for the Bipolar and the Monopolar pulse respectively, in both planes. The maps show that both the application of Bipolar and Monopolar pulses induces a substantial variation of the local electrostatic field pattern with an average SMAPE value of 59% and 58 % for the Monopolar pulse in the π' and π" planes respectively (Fig. 10.14) and a value of 72% and 148 % for the Bipolar (see

Fig. 10.13) in the π' and π" planes, calculated considering the full map.
Therefore, the intensity of 10^8 V/m is a threshold intensity able to affect the electrostatic environment of the enzyme active site. Such electrostatic variation, modulating the guidance of the superoxide radical O_2^- towards the active site of the SOD1 enzyme, may as a final step influence the SOD1 enzymatic activity. This, without irreversible modifications or impact on protein functions, as derived from the dipole moment analysis, showing a protein that can reorient itself following the external field applied at the threshold intensity of 10^8 V/m.

10.4 Conclusions

It is something already known that intense electric fields are needed to act on biomolecular processes inside cells. Voltages corresponding to $\backsim$ 100 mV across a cell membrane (about 0.125 MV cm^{-1}), consistent with biological relevance, can influence conformational transitions in proteins such as ion channels [Tao et al., 2010] and G-protein-coupled receptors [Ben-Chaim et al., 2006]. In mitochondria, where the negative interior dipole potential is used as the energy source to produce ATP, the electric field across the inner membrane is as high as $3x10^7$ V/m [Hu and Webb, 2011] which corresponds to 120 mV for a membrane that is 4 nm in thickness.
Moreover, it is well known that the majority of membrane proteins are exposed to strong electric fields that range in strength from 10^4 to 10^7 V/m [Tyner et al., 2007] and that the ability of electric fields to modulate the structure of integral membrane proteins is a central dogma in voltage gating [Jensen et al., 2012].
However, few studies can be found for external field effects on water-soluble proteins [Ojeda-May and Garcia, 2010, Solomentsev et al., 2010]; in fact, at the atomistic level, protein responses and changes due to imposed electric fields can only be observed by computer simulations. To this regard, apart from few studies that have an experimental validation, the majority of the investigations are realized on the basis of molecular simulations. In particular, the effects of external electric field on the stability of protein conformations [Lugli et al., 2010, Astrakas et al., 2011, Ojeda-May and Garcia, 2010, Toschi et al., 2008, Yang, 2013, Wang et al., 2014] as well as on the stability of β-sheet structures, dependence of the field on the polarization of water molecules, mean force on the charged atom in a water cluster, and interaction forces between two charged or neutral atoms in a water cluster, have been explored using MD simulations [Yang,

2013, 2014]. Pulsed electric fields of 3.5 x 10^6 V/m induced structural changes in the secondary structure of lysozyme that are not equivalent to those caused by thermal stress [Zhao et al., 2007], illustrating that the electromechanical properties of proteins have a different physical origin at the atomistic level to their thermodynamic stability. Lysozyme and synapse associated protein are the few examples of water-soluble proteins that have been reported to undergo conformational changes in response to external electric fields [Bekard and Dunstan, 2014, Freedman et al., 2013]. These induced field effects are poorly understood but are attributed to rotational and translational movement of dipolar residues (or domains) in response to external electric fields. Almost all the papers reporting effects on the coupling of electric fields and proteins refer to quite intensities much higher than 10^8 V/m, even in the case of a recent paper giving a contribution in comprehending the complete unfolding process of a protein [Avena et al., 2015, Amadei and Marracino, 2015, Zanetti-Polzi et al., 2013, Marracino et al., 2015, 2017, 2016, Reale et al., 2013].

With the research project presented in this chapter, the effects of Monopolar and Bipolar nsPEFs acting on the SOD,Cu-Zn enzyme have been explored, by using MD simulations, in order to define a threshold for the intensity of the field able to interact and manipulate the SOD1 enzyme.

For the first time, a Monopolar and Bipolar electric pulse have been implemented in the Gromacs environment. By the analysis of the Coil and β-Sheet secondary structures, we identified three different electric field thresholds: (i) with E field intensities from 10^8 and 2x10^8 V/m slightly reversible changes (5 %) were appreciated; (ii) when a E field of 5x10^8 V/m is applied, variations around the 23 % are reported partially reversible in 50 ns after the electric pulse removal; (iii) SOD1 unfolding when the protein is exposed to an electric pulse of 7x10^8 V/m of strength with a loss of β-sheet and an increase of Coil, not reversible in 50 ns after the application of both monopolar and bipolar E pulses.

The protein structural rearrangements have been also quantified through the computation of the RMSD, the radius of gyration and the solvent accessible area. These results confirm that the SOD1 unfolds with an increment of all these parameters (meaning loss of secondary structures) when the external electric field increases to 7x10^8 V/m.

To explore the SOD1 molecules polarization under a weak external E field, we studied the spectrogram of the protein and water molecules dipole moment. We compared the reference not exposed with a thermal increase of 35 degrees (see Fig. 10.8) and with the

application of a monopolar and bipolar electric pulse of 10^8 V/m of strength. Under the external electric stimulus, the SOD1 protein, despite its size, results to follow the external signal applied in its shape, showing a high dipole moment with the respect to the not exposed condition. This result suggests an electric coupling between the external E field applied and the SOD1 protein. Conversely, the reference "No field" and the one with the thermal increase show a very behavior, confirming no water and protein molecules reorientation under a thermal external stimulus.

Due to the electric coupling between the protein dipole moment and the E field applied and based on previous studies [Getzoff et al., 1992] regarding the electrostatic recognition, we investigated a possible electrostatic guidance of the O_2^- ion towards the Cu^{2+} by analysing the electric forces acting on the SOD,Cu-Zn active site next the application of monopolar and bipolar electric pulses of 10^8 V/m. We carried out this study in terms of 2D maps of the electric field distribution on two planes passing through the Cu-O_2. By the investigation of the electric field maps, a larger electric field distribution has been obtained when an external field was applied with the respect with the not exposed reference in both planes (π' and π", see Fig. 10.11 and Fig. 10.12 respectively). To quantify the difference between the different exposure states we calculated the SMAPE obtaining a value of 59 and 72 % of the monopolar and bipolar pulse respectively for the π' plane and of 58 and 148 % for the π" plane, suggesting a significant difference with the respect to the No field condition with a possible facilitated reaction between the copper and oxygen ion.

With this numerical study it is possible to conclude that with the application of a weak electric field (10^8 V/m) is feasible to have protein molecules reorientation and an electrostatic guidance at the active site, which could enhance the enzymatic activity of the protein, by responding to the external field applied without causing structural irreversible changes. While, when intensities starting from 5x10^8 V/m are applied structural changes occurred. This numerical study can be considered as starting point for possible prediction of future experiments on the superoxide dismutase protein.

Part VI

Summary and Conclusions

Chapter 11

Summary and Conclusions

In this Ph.D. thesis, collocated in the nanomedicine panorama, the feasibility of liposomal drug delivery systems mediated by electromagnetic fields (EMFs) has been studied both by the theoretic and experimental point of view. In parallel EMFs interaction with molecular structures (e.g. protein) has been studied and well explored in order to theoretically prove the possibility to directly interact by means of EMF with proteins and/or enzymes.

As introduced with the scheme reported in the introduction (see Ch. 1, Fig. 1.2), the nanomedicine is a science that combines the medicine with the nano-technological progress. Among its different fields application (Fig. 1.2), in this thesis the attention has been focused on the therapeutic area. Generally, nanotherapeutics improve and optimize the action of a drug agents, by increasing their accumulation at pathological sites and their therapeutic efficacy [Lammers et al., 2008a, Davis et al., 2008, Ganju et al., 2017]. Particularly, stimuli-response release of a drug loaded into a nanocarrier (1-1000 nm of dimension), in a precise time and location is one of the most aimed results of the drug delivery research.

More in detail, in this research the aim has been twofold, from one side the feasibility of drug delivery systems mediated by liposomes as nanocarriers under the action of an external magnetic or electric fields has been explored. On the other side the possible interactions mechanism of electromagnetics fields with protein structures have been investigated due to their importance in cell processes and to their potential to monitor specific physiological events [Giuliano et al., 1995, Zhang et al., 2002, Provenzano et al., 2009, Niesner and Hauser, 2011].

The first step has been to give an overview of the drug delivery systems mediated by liposomes and the different activation agents, by exploring the possibility to activate them with an endogenous or external stimulus [Ganta et al., 2008, Karanth and Murthy, 2007, Pradhan et al., 2010, Preiss and Bothun, 2011] (see Sec. 2.2). The goal with this technique is to introduce into the body a nano-carriers capable to load, carry and release the drug in the place where it must act, avoiding any damage to the surrounding healthy tissue. Since the use of liposomes for drug delivery started shortly after their invention by Bangham and coworkers in 1965 [Bangham et al., 1965, Lindner and Hossann, 2010], in the section 2.2 the liposomes properties and their first use in the medical research has been reported. Moreover, among the external stimulus that can be used to activate the cargo release from these vesicles, the magnetic and the electric fields have been considered. In the Section 2.4 a survey of the existing research on low intensity magnetic fields activating liposomes release has been given. Indeed, some studies suggested that magnetic fields of low intensities are a good trigger to control the release of the drugs without causing a thermal increase to the surrounding healthy tissues [Nappini et al., 2010, Spera et al., 2014]. Nevertheless, recently the use of PEMFs for the treatment of inflammation status has become of frequent use, especially in the neurodegenerative diseases and in the bone healing.

MLs drug delivery systems

Starting from that, in the Chapter 5 experimental data concerning magnetoliposomes (MLs) exposed to a low intensity alternate (AMF) or pulsed magnetic fields (PEMFs) have been reported. The aim has been to test the potential of a magnetoliposomal drug delivery system to release a fluorescent dye (5(6)- carboxyfluorescein, CF in our study), loaded into the liposomes core, by the application of magnetic fields with intensities lower than 100 μT. To perform this study, firstly after the MLs preparation, the results obtained from Spera et al. [Spera et al., 2015] were reproduced, to asses the capability of AMF (alternate magnetic field) of low magnetic field intensity (70 μT) to trigger the CF fluorescent release from high-Tm MLs prepared with the HSPC lipid. From our experiments a triggered release was reached with a 58 % of CF release after 12 hours of exposure by switching ON (3h) and OFF (21h) the magnetic field.

Once, assessed the MLs release next to the AMF application, experiments were carried out exposing MLs to PEMFs with a magnetic field intensity of 100 μT by using the I-One medical device. The CF release was around the 26 % after switching ON and

OFF the magnetic field for a total of 9 hours of exposures (ON = 3h and OFF = 21h). By the PEMFs application it was not possible to trigger the CF release, indeed the 17 % was released in the first 3h and a release of 7 and 2 % was reached in the following PEMFs exposures. To study this effect, by the TEM (transmission electron microscopy) images analysis, it has been possible to see how after the 6 hours of ON - OFF exposures (3h + 3h) the magnetic nanoparticles escaped from the liposomes core explaining the 7 % of release, possible due to the different characteristic of the magnetic field application with the respect to the AMF experiments as explained in the result section (see Sec. 5.3).
Anyhow, it is important to highlight how with these experimental data a proof of concept of a magnetoliposomes drug release has been given by the application low intensity magnetic fields (AMF and PEMFs) due to the mechanical liposomes stimulation and not to the thermal exposure.

Next to the experimental data, with the aim to have a magnetic exposure system able to trigger the CF release (as shown for the AMF exposure, see Sec. 5.3) but with an higher magnetic field intensity (mT range), the design a powerful magnetic exposure system for magnetic field intensities higher than 100 μT has been reported in the Chapter 6. The designed system is a multipurpose exposure setup able to be used both for experimental applications as MLs poration for drug delivery and for in-vitro magnetic neuronal cells stimulation. The aim has been a dose-dependent analysis for both applications to verify the generation of a magnetic field intensity in the order of mT at frequencies up to 20 kHz. Firstly an analytic study has been performed to identify the geometric and electrical parameters of a pair of Helmholtz coils to fulfill the project requirements. A dimension of 15 cm of the two coils and a current of 0.6 A with 200 wires have been identified. Next, a numerical simulations using the software Sim4Life, was done to validate the geometric and electrical parameters and to analyze the magnetic field intensity, obtaining a B field of 1.4 mT with an homogeneity of 95 % between the coils, where is supposed to be placed an exposure sample. Next to this evaluation, two different simulations have been performed, one considering a cuvette filled with a conductivity solution of 0.049 S/m (experimentally measured) for MLs drug delivery purpose at a frequency of 20 kHz and another one with a chamber placed at the center of the coils filled with artificial cerebrospinal fluid solution for in vitro applications, at a frequency of 3 kHz (typical TMS frequency [Di Lazzaro et al., 2013]).

In both cases, by the analysis of 2D map of the electric and current density inside the solution no relevant values were obtained, (E $<$ 1 V/m and a J in the order of mA/m^2) excluding any possible thermal effect acting on the solution during the magnetic field exposure.
Next to the numerical study, a circuital study has been carried out to match the 100 Ω of load impedance of the amplifier already present in our experimental setup. In order to have the maximum current feeding the coils system, a capacity is needed to be placed in series to our coils when an sinusoidal signal is applied with values ranging from 1 to 400 nF for frequencies from 1 up to 20 kHz. Moreover, in order to match our system when a pulsed signal is applied of 1.3 ms of duration, a resistor of 50 Ω is needed in series to the coils instead of the capacity to have the maximum transferred current.
The results obtained suggest that the designed exposure setup could give the possibility to have negligible thermal increase in two of the principal therapeutic applications of low intensity magnetic fields in the IF frequency range, with the possibility to reach intensity in the order of mT without compromising the sample due to secondary effects.

Drug delivery mediated by nsPEF

Since the goal with this Ph.D. is to explore not only a magnetic but also an electric field application as external trigger for drug delivery purpose, the possibility to use electric pulses of short duration (ns) and high intensities (MV/m) as external trigger has been evaluated due to the existing applications of nsPEF in different medical areas, as electrochemotherapy [Miklavčič et al., 2012, Cadossi et al., 2014], electrofusion [Rems et al., 2013, Teissie and Rols, 1986], gene electrotransfer [Mir et al., 1999, Calvet et al., 2014] and food processing [Saulis, 2010] (see Sec. 2.3).
In the Chapter 7 a theoretical study has been presented for testing the feasibility of a simultaneous cell and liposomes electroporation. The concept is based on the broad spectra content of a 12 ns electric pulse for which the Schwan′s equation of the TMP becomes a second−order model [Postow and Polk, 1996, Kotnik and Miklavcic, 2000, Merla et al., 2012] in which the dimension effect, between the liposome (nanometer range) and the cell (micrometer range), is not as crucial as at the low frequency range (see Fig. 7.2). This has been elaborated with the analysis of the influence on the TMP in time domain due to the geometrical and electric parameters, which can be controlled in an experimental setup. As first step, simulations have been carried out considering one liposome alone of different dimensions (100, 200 and 400 nm of diameter) exposed

to a 12 nsPEF and the best choice has been a liposome with a diameter of 200 nm as it results in a good compromise between the E field intensity required for the membrane poration and the absence of recognition by the immune system. Based on these results, with the same geometric (d_{lip} = 200 nm) and electrical parameters ($\sigma_{ext} = \sigma_{int}$ = 1.5 S/m), we carried out an analysis of a complex system with one cell and a 28 liposomes distribution. Giving an excitation with a 12 nsPEF, it has been demonstrated that it is possible to permeabilize the liposomes and the cell with comparable E field intensity and it has been proved that when the 80 % of liposomes is porated, the cell membrane is porated for the 10 % of its area; in this way, the cell viability is not compromised, and the liposomes and cell poration can occur with the same E field intensity.

To explore experimentally this possibility in the Chapter 8 the design, realization and characterization of a 10nsPEF exposure setup for liposomes, has been reported and preliminary experiments on 250 nm liposomes poration have been presented.
Since the excitation is a 10 ns pulsed electric field and the target are liposomes with 200 or 400 nm diameter the use of a standard electroporation cuvette with 1 mm gap has been considered advantageous [Denzi et al., 2017]. The design of an appropriate cuvette holder structure proceeded, taking particular attention to the connection of the 1 mm gap electroporation cuvette to a 50 Ω high voltage pulse generator. The structure has been completely characterized in frequency domain to understand its capability and performances in different experimental conditions. Indeed, the study demonstrated the capability of the proposed structure to deliver a 10 ns pulse without a significant signal distortion in particular for media with a 0.25 S/m of conductivity value. In particular, the higher is the solution conductivity, the lower is the efficacy of the structure and hence the lower is the amplitude of the transmitted pulse to the cuvette. Moreover, by combining microdosimetry (regarding 200 and 400 nm liposomes) and technological information permits to predict that the optimal condition for a 400 nm liposome is with 0.25 S/m and 1.6 S/m, in order to guarantee the higher efficiency of the structure (0.25 S/m) and the lowest electric field needed to porate the liposomes (at 1.6 S/m). Indeed from simulations of non uniformly distributed liposomes, an electric field of 7 MV/m has been identified to porate the 200 nm liposomes, while 5 MV/m are sufficient to porate the 400 nm liposomes with a gap of 0.3 MV/m between the starting of liposomes poration and when then 100 % of liposomes is porated for both simulations. Finally, preliminary experimental data of the exposure of 250 nm liposomes by applying an

electric field of 9 MV/m with 56 E pulses at 1 Hz of frequency, have been reported. A conductivity of 0.33 and 1.6 S/m has been used for the external and inner liposomes. A release of 15 % of CF has been detected for the exposed samples, while the 2 % has been reached from the sham sample.
From the modeling analysis we can conclude that a proof of concept has been given of the potentiality of nsPEF to activate a liposome release and to possible porate the cell with comparable E field intensities to the one of liposomes. Moreover from the technological and experimental aspects we demonstrate the poration of liposomes of 250 nm of diameter opening the way for a possible drug delivery system controlled by the electropulsation.

In the Medical research besides new nanotechnologies for the diseases treatment, another major challenge is the accurate measurement of cells signals in order to possibly prevent the upcoming of inflammations or serious illnesses as cancers or cardiac disorders. For this reasons, researchers started to perform methods to measure protein biomarkers, cells, and pathogen agents in biological samples [Cheng et al., 2006, Wulfkuhle et al., 2003].
Due to the importance of proteins in the signaling from the cells and due to the medical applications mediated by electromagnetic fields, in the chapter 9 and 10 molecular dynamics (MD) simulations are reported regarding the exposure of proteins under the electromagnetic fields action.

MD simulations on adenosine A_{2A} receptor

In detail, in the chapter 9, MD simulations have been reported for the action of a magnetic field of 1 T of intensity on the receptor adenosine A_{2A}. The Adenosine A_{2A} is an important receptor involved in the transmission of the signals from the neuronal cells in response to a metabolic stress. From the experiments carried out from Varani et al. [Varani et al., 2008], an increase of the receptor activity has been highlighted under the action of a magnetic field of 3 mT for exposures time up two hours. Since, experimental evidences, the aim has been to study the interaction between the magnetic field and adenosine A_{2A}. The Gromacs package has been used to perform MD simulations and for the first time a magnetic field has been implemented by the modification of the update of atom positions and velocities following the Verlet algorithm (see Sec. 9.2). Firstly, the validation of the B field implementation with simulations of a sodium ion in vacuum and with water molecules has been done. Latter, MD simulations considering a NaCl buffer solution (DMEM concentration [Varani et al., 2002]) have been

performed exposed to 1 T of magnetic field and a variation of 10 % and 18 % for the Na^+ (decrease) and the Cl^- ions (increase) was observed. This effects can be explained as result of the interaction of the B field with free charged particles.
After that, the simulations of the Adenosine A_{2A} receptor in the buffer NaCl solution, highlighted a decrease of the protein diffusivity D, by the 80 % and no structural changes occurred by the analysis of the RMSD and the α-helix secondary structures (the adenosine A_{2A} is an α-helix protein), ensuring no protein disruption due to the B field application.
In order to analyse the ligand binding site of the adenosine A_{2A}, the dipole moment and the ramachandran plot have been computed for six residues involved in the hydrogen bond during the ligand binding process (HIS264, ALA265, PRO266, LEU267, GLU169 and SER67, Fig. 9.4). By the dipole moment analysis a reorientation of some binding residues (GLU169 and HIS264) has occurred next the application of 1 T of B field. By the study of the energetic regions allowed to single residues (the Ramachandran plot), a trend towards the α-helix right-handed conformation has been detected when the B field is applied (see Fig. 9.10) for almost all the residues, exception for the serine67 going towards β-Sheet structures.
For the first time with this work a magnetic field has been implemented into the gromacs package giving the possibility to study the interactions between a magnetic field and a molecular target. Moreover, the residues rotations suggest that our data seem to be in line with the molecular gyroscope mechanism and diamagnetic anisotropy mechanism proposed by Binhi and Prato [Binhi and Prato, 2017] and by Babaei [Babaei et al., 2017] respectively, were the rotations of the charged residues seems to be the response of the proteins residues to the external magnetic field applied.

SOD,Cu-Zn exposed to 100 nsPEFs

Since, the aim with this thesis has been to investigate the interaction mechanism between molecular structures and electromagnetic fields, in the last chapter (see Ch. 10), MD simulations have been reported regarding the enzyme SOD,Cu-Zn exposed to monopolar and bipolar electric pulses of 100 ns of duration and intensities from 10^8 to $7x10^8$ V/m. The superoxide dismutase is an important enzyme involved in the body response to the oxidative stress produced by the toxic oxygen products (e.g. free radicals). With this numerical study, for the first time, a Monopolar and Bipolar electric pulses have been implemented in the Gromacs environment. Thanks to the analysis of secondary structures and the classical MD observable (RMSD, radius of gyration and

the hydrophilic and hydrophobic area), three different threshold have been identified in order to detect structural rearrangements. With an electric field of 10^8 V/m no structural changes occurred, while when intensities starting from 5x10^8 V/m are applied structural changes were observed and with 7x10^8 V/m the SOD1 is in an unfolding state not reversible in 50 ns after the signal application.
On the other side looking to the electrostatic environment, with the application of a weak electric field (10^8 V/m) is possible to have protein molecules reorientation and an electrostatic guidance at the active site as highlighted by the dipole moment and the electric field maps on the SOD,Cu-Zn active site, which could enhance the enzymatic activity of the protein, by responding to the external field applied without causing structural irreversible changes. Indeed by performing two electric field maps, in two different planes at the SOD1 active site, an overall effects of 59 and 72 % has been obtained for the monopolar and bipolar pulses respectively, in terms of symmetric mean absolute percentage error (SMAPE) with the respect to the no field application. This numerical study can be considered as the basis to investigate the interaction of nsPEFs electric fields with enzyme molecules also in terms of electrostatic effects and not only in terms of protein conformational changes.

As whole, this Ph.D. thesis wants to be a multidisciplinary and multiscale approach for the investigation of both low intensity magnetic fields and nanosecond electric pulses interactions with nanosystems target. The goal has been to explore the use of electromagnetic fields as remote activators of lipid-nanosystems used as drug carriers for the treatment and the prevention of inflammations status and disease thanks to a modeling, technological and experimental standpoint. A proof of concept, has been given theoretically and experimentally of the feasibility of liposomal drug delivery systems mediated by electric or magnetic fields. An analysis with experimental data have been done for both studies. As latter, because the proteins represent the major pathway of the signals transmission to the cells and they could prevent the upcoming of inflammations, thanks to molecular dynamics simulations the interaction between the magnetic field on the adenosine A_{2A} and of the nsPEFs on the SOD,Cu-Zn protein, have been explored. With both numerical studies the interaction between the electromagnetic fields and the protein have been explored and demonstrated, highlighting in both cases the response of the protein to the external stimulus without corrupting the protein structures and with a dipolar response from charged residues on proteins surface.

Part VII

Publications

International Journal

- **2017** "Exploring the Applicability of Nanoporation for Remote Control in Smart Drug Delivery Systems", Agnese Denzi, **Elena della Valle**, Francesca Apollonio, Marie Breton, Lluis Mir, Micaela Liberti, *The Journal of Membrane Biology*, 2017, 250.1: 31-40.

- **2017** "Technological and Theoretical Aspects for Testing Electroporation on Liposomes", Agnese Denzi, **Elena della Valle**, Gianluca Esposito, Lluis Mir, Francesca Apollonio, Micaela Liberti, *BioMed Research International*, 10 pages, 2017.

- **2017** "Nanosecond pulsed electric signals can affect electrostatic environment of the SOD1 below the threshold of conformational effects: a molecular simulation study", **Elena della Valle**, Paolo Marracino, Olga Pakhomova, Micaela Liberti, Francesca Apollonio, *In Submission to Plos One.*

- **2017** "Nanosecond Pulsed E fields action on Cu/Zn superoxide dismutase: theoretical and experimental results", **Elena della Valle**, Paolo Marracino, Micaela Liberti, Olga Pakhomova, Francesca Apollonio, *In Preparation for Bioelectrochemistry Journal.*

- **2017** "Can pulsed electromagnetic fields trigger on-demand drug release from high-Tm magnetoliposomes?", Martina Nardoni,**Elena della Valle**, Francesca Apollonio, Micaela Liberti, Stefania Setti, Ruggero Cadossi, M. Antonietta Casadei, Patrizia Paolicelli, Stefania Petralito *Submitted as short communication to Journal of Materials Chemistry B.*

Conferences

- **2014** "Pulsed E fields acting on metallo-enzymes: theoretical and experimental results", **Elena della Valle**, Olga Pakhomova, Paolo Marracino, Shu Xiao, Andrei Pakhomov, Micaela Liberti, Francesca Apollonio, *BioEM2014 conference, June 08 - 13, 2014*,Cape Town, South Africa.

- **2014** "PEF-induced structural and functional modifications of metalloenzyme SOD1 by MD simulation and in experiments", **Elena della Valle**, Olga Pakho-

mova, Paolo Marracino, Shu Xiao, Andrei Pakhomov, Micaela Liberti, Francesca Apollonio, *Gordon Research Conference on Bioelectrochemistry, July 06 - 11, 2014*, University of New England, Biddeford, ME, USA.

- **2016** "Diversity of monopolar and bipolar nanosecond pulsed electric signals action on the metallo-enzyme superoxide dismutase (SOD): a modelling approach", **Elena della Valle**, Olga Pakhomova, Paolo Marracino, Micaela Liberti, Francesca Apollonio, *BioEM2016 conference, June 05 - 10, 2016*, Ghent, Belgium.

- **2016** "Drug delivery mediated by magnetic fields: first experiments and design of a magnetic exposure system", **Elena della Valle**, Martina Molinaro, Stefania Petralito, Patrizia Paolicelli, Martina Nardoni, Maria Antonietta Casadei, Maria Cristina Annesini, Caterina Merla, Rosanna Pinto, Micaela Liberti, Francesca Apollonio, *BioEM2016 conference, June 05 - 10, 2016*, Ghent, Belgium.

- **2016** "Exploring the Applicability of Nano-poration for Remote Control in Smart Drug Delivery Systems", Agnese Denzi, **Elena della Valle**, Francesca Apollonio, Marie Breton, Lluis Mir, Micaela Liberti, *Icemb, Interaction between EMF and Biosystems, July 4-6, 2016*, Milan, Italy.

- **2017** "Numerical estimation of a 10 nanosecond pulse effects on non-uniformly distributed liposomes", **Elena della Valle**, Agnese Denzi,Lluis Mir, Francesca Apollonio, Micaela Liberti, *Second World Congress on Electroporation and pulsed electric fields in biology, medicine, food and environmental technologies, September 24-28, 2017*, Norfolk, Virginia.

- **2017** "Molecular modelling of the metallo-enzyme superoxide dismutase exposed to nanosecond pulsed electric signals", **Elena della Valle**, Paolo Marracino, Olga Pakhomova, Micaela Liberti, Francesca Apollonio, *Second World Congress on Electroporation and pulsed electric fields in biology, medicine, food and environmental technologies, September 24-28, 2017*, Norfolk, Virginia.

- **2017** "Diversity of Monopolar and Bipolar Nanosecond Pulsed Electric Signals on the Metallo-Enzyme Superoxide Dismutase (SOD), a Modelling Approach", **Elena della Valle**, Olga Pakhomova, Paolo Marracino, Micaela Liberti, Francesca Apollonio, *In: Antennas and Propagation (EUCAP), 2017 11th European Conference on. IEEE*, 2017. p. 1366-1368.

- **2017** "Numerical estimation of a 10 nanosecond pulse effects on non-uniformly distributed liposomes", **Elena della Valle**, Agnese Denzi, Francesca Apollonio, Lluis M. Mir, Micaela Liberti", *In Synthesis, Modeling, Analysis and Simulation Methods and Applications to Circuit Design (SMACD), 2017 14th International Conference on (pp. 1-3), IEEE.*

- **2017** "Magnetic molecular dynamics simulations with Velocity Verlet algorithm", **Elena della Valle**, Paolo Marracino, Stefano Setti, Ruggiero Cadossi, Micaela Liberti, Francesca Apollonio,*In: 2nd URSI GASS Conference, Montreal,19 - 20 August, IEEE, In press.*

- **2017** "Versatile exposure system for laboratory experiments finalized to therapeutic applications in the IF range", **Elena della Valle**, Francesca Camera, Alessandra Paffi A, Stefania Petralito, Vincenzo Roncac, Burattini C, GIorgio Aicardi, Micaela Liberti, Francesca Apollonio, *In: 32nd URSI GASS Conference, Montreal,19 - 20 August, IEEE, In press.*

Bibliography

Dalaal M Abdallah, Hanan S El-Abhar, and Dalia H Abdel-Aziz. Tempol, a membrane-permeable radical scavenger, attenuates gastric mucosal damage induced by ischemia/reperfusion: a key role for superoxide anion. *European journal of pharmacology*, 603 (1):93–97, 2009. [Cited on page 170]

Zahraa S Al-Ahmady, WafaT Al-Jamal, Jeroen V Bossche, Tam T Bui, Alex F Drake, A James Mason, and Kostas Kostarelos. Lipid–peptide vesicle nanoscale hybrids for triggered drug release by mild hyperthermia in vitro and in vivo. *ACS nano*, 6(10):9335–9346, 2012. [Cited on pages 23, 24]

Mai Alhajlan, Moayad Alhariri, and Abdelwahab Omri. Efficacy and safety of liposomal clarithromycin and its effect on pseudomonas aeruginosa virulence factors. *Antimicrobial agents and chemotherapy*, 57(6):2694–2704, 2013. [Cited on page 21]

Theresa M Allen and Pieter R Cullis. Liposomal drug delivery systems: from concept to clinical applications. *Advanced drug delivery reviews*, 65(1):36–48, 2013. [Cited on pages 18, 27]

A Amadei and P Marracino. Theoretical–computational modelling of the electric field effects on protein unfolding thermodynamics. *RSC Advances*, 5(117):96551–96561, 2015. [Cited on page 193]

A. Amadei, M. D'Abramo, I. Daidone, M. D'Alessandro, A. Di Nola, and M. Aschi. Statistical mechanical modelling of chemical reactions in complex systems: the kinetics of the haem carbon monoxide binding-unbinding reaction in myoglobin. *Theor. Chem. Acc.*, 117:637–647, 2007. [Cited on pages 45, 172]

Andrea Amadei, Maira D'Alessandro, Maurizio Paci, Alfredo Di Nola, and Massimiliano Aschi. On the effect of a point mutation on the reactivity of cuzn superoxide dismutase: a theoretical study. *The Journal of Physical Chemistry B*, 110(14):7538–7544, 2006. [Cited on page 172]

Hans C Andersen. Rattle: A velocity version of the shake algorithm for molecular dynamics calculations. *Journal of Computational Physics*, 52(1):24–34, 1983. [Cited on page 48]

Francesca Apollonio, Micaela Liberti, Andrea Amadei, Massimiliano Aschi, Monica Pellegrino, Maira D'Alessandro, Marco D'Abramo, Alfredo Di Nola, and Guglielmo d'Inzeo. Mixed

quantum-classical methods for molecular simulations of biochemical reactions with microwave fields: The case study of myoglobin. *IEEE Transactions on Microwave Theory and Techniques*, 56(11):2511–2519, 2008. [Cited on page 154]

Francesca Apollonio, Micaela Liberti, Alessandra Paffi, Caterina Merla, Paolo Marracino, Agnese Denzi, Carmela Marino, and Guglielmo d'Inzeo. Feasibility for microwaves energy to affect biological systems via nonthermal mechanisms: a systematic approach. *IEEE Transactions on Microwave Theory and Techniques*, 61(5):2031–2045, 2013. [Cited on pages 43, 54, 127, 128]

DW Armitage, HH LeVeen, and R Pethig. Radiofrequency-induced hyperthermia: computer simulation of specific absorption rate distributions using realistic anatomical models. *Physics in medicine and biology*, 28(1):31, 1983. [Cited on page 57]

J Scott Armstrong. Forecasting methods for conflict situations. 1985. [Cited on page 191]

Delia Arnaud-Cormos, Philippe Leveque, Yu-Hsuan Wu, Jason M Sanders, Martin A Gundersen, and TP Vernier. Microchamber setup characterization for nanosecond pulsed electric field exposure. *IEEE Transactions on Biomedical Engineering*, 58(6):1656–1662, 2011. [Cited on page 125]

Loukas Astrakas, Christos Gousias, and Margaret Tzaphlidou. Electric field effects on chignolin conformation. *Journal of Applied Physics*, 109(9):094702, 2011. [Cited on page 192]

Jared R Auclair, Kristin J Boggio, Gregory A Petsko, Dagmar Ringe, and Jeffrey N Agar. Strategies for stabilizing superoxide dismutase (sod1), the protein destabilized in the most common form of familial amyotrophic lateral sclerosis. *Proceedings of the National Academy of Sciences*, 107(50):21394–21399, 2010. [Cited on page 171]

Massimiliano Avena, Paolo Marracino, Micaela Liberti, Francesca Apollonio, and Niall J English. Communication: Influence of nanosecond-pulsed electric fields on water and its subsequent relaxation: Dipolar effects and debunking memory, 2015. [Cited on page 193]

Jacob I Ayers, Susan E Fromholt, Veronica M ONeal, Jeffrey H Diamond, and David R Borchelt. Prion-like propagation of mutant sod1 misfolding and motor neuron disease spread along neuroanatomical pathways. *Acta neuropathologica*, 131(1):103–114, 2016. [Cited on page 170]

Antoine Azan, Valérie Untereiner, Lucie Descamps, Caterina Merla, Cyril Gobinet, Marie Breton, Olivier Piot, and Lluis M Mir. Comprehensive characterization of the interaction between pulsed electric fields and live cells by confocal raman microspectroscopy. *Analytical Chemistry*, 2017a. [Cited on page 11]

Antoine Azan, Valérie Untereiner, Cyril Gobinet, Ganesh D Sockalingum, Marie Breton, Olivier Piot, and Lluis M Mir. Demonstration of the protein involvement in cell electropermeabilization using confocal raman microspectroscopy. *Scientific reports*, 7:40448, 2017b. [Cited on pages 11, 171]

MA Mohd Azmi, Z Tehrani, RP Lewis, K-AD Walker, DR Jones, DR Daniels, SH Doak, and OJ Guy. Highly sensitive covalently functionalised integrated silicon nanowire biosensor

devices for detection of cancer risk biomarker. *Biosensors and Bioelectronics*, 52:216–224, 2014. [Cited on page 5]

Mahnoush Babaei, Isaac C Jones, Kaushik Dayal, and Meagan S Mauter. Computing the diamagnetic susceptibility and diamagnetic anisotropy of membrane proteins from structural subunits. *Journal of Chemical Theory and Computation*, 2017. [Cited on pages 153, 168, 203]

Prasanta Kumar Banerjee and Roy Butterfield. *Boundary element methods in engineering science*, volume 17. McGraw-Hill London, 1981. [Cited on page 57]

AD Bangham, Malcolm M Standish, and JC Watkins. Diffusion of univalent ions across the lamellae of swollen phospholipids. *Journal of molecular biology*, 13(1):238–IN27, 1965. [Cited on pages 21, 198]

Stephen J Beebe. Considering effects of nanosecond pulsed electric fields on proteins. *Bioelectrochemistry*, 103:52–59, 2015. [Cited on pages 11, 35, 37, 171]

Stephen J Beebe, Paula M Fox, Laura J Rec, E LAUREN K WILLIS, and Karl H Schoenbach. Nanosecond, high-intensity pulsed electric fields induce apoptosis in human cells. *The FASEB journal*, 17(11):1493–1495, 2003a. [Cited on page 27]

Stephen J Beebe, Jody White, Peter F Blackmore, Yuping Deng, Kenneth Somers, and Karl H Schoenbach. Diverse effects of nanosecond pulsed electric fields on cells and tissues. *DNA and cell biology*, 22(12):785–796, 2003b. [Cited on pages 26, 109]

Stephen J Beebe, Yeong-Jer Chen, Nova M Sain, Karl H Schoenbach, and Shu Xiao. Transient features in nanosecond pulsed electric fields differentially modulate mitochondria and viability. *PLoS One*, 7(12):e51349, 2012. [Cited on page 37]

Innocent Bekard and Dave E Dunstan. Electric field induced changes in protein conformation. *Soft Matter*, 10(3):431–437, 2014. [Cited on page 193]

Yair Ben-Chaim, Chanda Baron, Nathan Dascal, Francisco Bezanilla, Itzchak Parnas, and Hanna Parnas. Movement of'gating charge'is coupled to ligand binding in a g-protein-coupled receptor. *Nature*, 444(7115):106, 2006. [Cited on page 192]

Donald Beqollari, Christin F Romberg, Gabriella Dobrowolny, Martina Martini, Andrew A Voss, Antonio Musarò, and Roger A Bannister. Progressive impairment of ca v 1.1 function in the skeletal muscle of mice expressing a mutant type 1 cu/zn superoxide dismutase (g93a) linked to amyotrophic lateral sclerosis. *Skeletal muscle*, 6(1):24, 2016. [Cited on page 170]

Vladimir N Binhi and Frank S Prato. Biological effects of the hypomagnetic field: An analytical review of experiments and theories. *PloS one*, 12(6):e0179340, 2017. [Cited on pages 153, 168, 203]

Tiziana Bonifacino, Laura Musazzi, Marco Milanese, Mara Seguini, Antonella Marte, Elena Gallia, Luca Cattaneo, Franco Onofri, Maurizio Popoli, and Giambattista Bonanno. Altered mechanisms underlying the abnormal glutamate release in amyotrophic lateral sclerosis at a pre-symptomatic stage of the disease. *Neurobiology of disease*, 95:122–133, 2016. [Cited on page 170]

Marie Breton and Lluis M Mir. Microsecond and nanosecond electric pulses in cancer treatments. *Bioelectromagnetics*, 33(2):106–123, 2012. [Cited on pages 10, 26, 109, 110, 139, 171]

Marie Breton, Mooud Amirkavei, and Lluis M Mir. Optimization of the electroformation of giant unilamellar vesicles (guvs) with unsaturated phospholipids. *The Journal of membrane biology*, 248(5):827–835, 2015. [Cited on page 110]

Akin Budi, F Sue Legge, Herbert Treutlein, and Irene Yarovsky. Electric field effects on insulin chain-b conformation. *The Journal of Physical Chemistry B*, 109(47):22641–22648, 2005. [Cited on page 38]

Ruggero Cadossi. The role of physical forces in the management of bone and cartilage diseases and bone consolidation. *Aging clinical and experimental research*, 23(2 Suppl):49–51, 2011. [Cited on page 35]

Ruggero Cadossi, Mattia Ronchetti, and Matteo Cadossi. Locally enhanced chemotherapy by electroporation: clinical experiences and perspective of use of electrochemotherapy. *Future Oncology*, 10(5):877–890, 2014. [Cited on pages 9, 109, 200]

Melis Çağdaş, Ali Demir Sezer, and Seyda Bucak. Liposomes as potential drug carrier systems for drug delivery. In *Application of Nanotechnology in Drug Delivery*. InTech, 2014. [Cited on page 20]

Christophe Y Calvet, Jessie Thalmensi, Christelle Liard, Elodie Pliquet, Thomas Bestetti, Thierry Huet, Pierre Langlade-Demoyen, Lluis M Mir, et al. Optimization of a gene electrotransfer procedure for efficient intradermal immunization with an htert-based dna vaccine in mice. *Molecular Therapy-Methods & Clinical Development*, 1:14045, 2014. [Cited on pages 9, 109, 200]

Enrica Capelli, Filippo Torrisi, Letizia Venturini, Maria Granato, Lorenzo Fassina, Giuseppe Francesco Damiano Lupo, and Giovanni Ricevuti. Low-frequency pulsed electromagnetic field is able to modulate mirnas in an experimental cell model of alzheimers disease. *Journal of Healthcare Engineering*, 2017, 2017. [Cited on pages 11, 35]

Antoine Carlioz and Danide Touati. Isolation of superoxide dismutase mutants in escherichia coli: is superoxide dismutase necessary for aerobic life ? *The EMBO journal*, 5(3):623, 1986. [Cited on page 170]

Lynn Carr, Sylvia M Bardet, Ryan C Burke, Delia Arnaud-Cormos, Philippe Lévêque, and Rodney P Oconnor. Calcium-independent disruption of microtubule dynamics by nanosecond pulsed electric fields in u87 human glioblastoma cells. *Scientific reports*, 7, 2017. [Cited on pages 11, 171]

M Casciola, D Bonhenry, M Liberti, F Apollonio, and M Tarek. A molecular dynamic study of cholesterol rich lipid membranes: comparison of electroporation protocols. *Bioelectrochemistry*, 100:11–17, 2014. [Cited on pages 10, 154]

Maura Casciola and Mounir Tarek. A molecular insight into the electro-transfer of small molecules through electropores driven by electric fields. *Biochimica et Biophysica Acta (BBA)-Biomembranes*, 1858(10):2278–2289, 2016. [Cited on page 128]

B Chalidis, N Sachinis, A Assiotis, G Maccauro, and Filippo Graziani. Stimulation of bone formation and fracture healing with pulsed electromagnetic fields: biologic responses and clinical implications. *International journal of immunopathology and pharmacology*, 24(1_suppl2): 17–20, 2011. [Cited on pages 35, 151]

Kai-Tai Chang and Cheng-I Weng. The effect of an external magnetic field on the structure of liquid water using molecular dynamics simulation. *Journal of Applied physics*, 100(4): 043917, 2006. [Cited on page 154]

Kai-Tai Chang and Cheng-I Weng. An investigation into the structure of aqueous nacl electrolyte solutions under magnetic fields. *Computational Materials Science*, 43(4):1048–1055, 2008. [Cited on page 154]

Chien-Sheng Chen, Jie Yao, and Richard A Durst. Liposome encapsulation of fluorescent nanoparticles: Quantum dots and silica nanoparticles. *Journal of Nanoparticle Research*, 8 (6):1033–1038, 2006. [Cited on page 126]

Huabing Chen, Hongda Zhu, Jingnan Zheng, Dongsheng Mou, Jiangling Wan, Junyong Zhang, Tielin Shi, Yingjun Zhao, Huibi Xu, and Xiangliang Yang. Iontophoresis-driven penetration of nanovesicles through microneedle-induced skin microchannels for enhancing transdermal delivery of insulin. *Journal of Controlled Release*, 139(1):63–72, 2009. [Cited on page 26]

Dengfeng Cheng, Xiao Li, Guoxin Zhang, and Hongcheng Shi. Morphological effect of oscillating magnetic nanoparticles in killing tumor cells. *Nanoscale research letters*, 9(1):195, 2014. [Cited on pages 9, 30, 65]

Mark Ming-Cheng Cheng, Giovanni Cuda, Yuri L Bunimovich, Marco Gaspari, James R Heath, Haley D Hill, Chad A Mirkin, A Jasper Nijdam, Rosa Terracciano, Thomas Thundat, et al. Nanotechnologies for biomolecular detection and medical diagnostics. *Current opinion in chemical biology*, 10(1):11–19, 2006. [Cited on pages 33, 202]

Amedeo Chiribiri, Sebastian Kelle, Stephan Götze, Charalampos Kriatselis, Thomas Thouet, Tarinee Tangcharoen, Ingo Paetsch, Bernhard Schnackenburg, Eckart Fleck, and Eike Nagel. Visualization of the cardiac venous system using cardiac magnetic resonance. *The American journal of cardiology*, 101(3):407–412, 2008. [Cited on page 4]

Louise Chopinet and Marie-Pierre Rols. Nanosecond electric pulses: A mini-review of the present state of the art. *Bioelectrochemistry*, 103:2–6, 2015. [Cited on pages 26, 27]

Don W Cleveland and Jeffrey D Rothstein. From charcot to lou gehrig: deciphering selective motor neuron death in als. *Nature reviews. Neuroscience*, 2(11):806, 2001. [Cited on page 170]

Wendy D Cornell, Piotr Cieplak, Christopher I Bayly, Ian R Gould, Kenneth M Merz, David M Ferguson, David C Spellmeyer, Thomas Fox, James W Caldwell, and Peter A Kollman. A second generation force field for the simulation of proteins, nucleic acids, and organic

molecules j. am. chem. soc. 1995, 117, 5179- 5197. *Journal of the American Chemical Society*, 118(9):2309–2309, 1996. [Cited on page 50]

E Corthout, A Barker, and A Cowey. Transcranial magnetic stimulation. *Experimental brain research*, 141(1):128–132, 2001. [Cited on page 90]

Gale L Craviso, Paroma Chatterjee, Gabriel Maalouf, Alex Cerjanic, Jihwan Yoon, Indira Chatterjee, and P Thomas Vernier. Nanosecond electric pulse-induced increase in intracellular calcium in adrenal chromaffin cells triggers calcium-dependent catecholamine release. *IEEE Transactions on Dielectrics and Electrical Insulation*, 16(5), 2009. [Cited on page 9]

Rocco P Croce, Assunta De Vita, Vincenzo Pierro, and Innocenzo M Pinto. A thermal model for pulsed em field exposure effects in cells at nonthermal levels. *IEEE Transactions on Plasma Science*, 38(2):149–155, 2010. [Cited on page 55]

Sara Crocetti, Christian Beyer, Grit Schade, Marcel Egli, Jürg Fröhlich, and Alfredo Franco-Obregón. Low intensity and frequency pulsed electromagnetic fields selectively impair breast cancer cell viability. *PLoS One*, 8(9):e72944, 2013. [Cited on page 35]

M. D'Alessandro, M. Aschi, M. Paci, A. Di Nola, and A. Amadei. Theoretical modeling of enzyme reactions chemistry: the electron transfer of the reduction mechanism in cuzn superoxide dismutase. *J. Phys. Chem.*, 108:16255–16260, 2004. [Cited on pages 45, 172]

Claire Dalmay, Julien Villemejane, Vanessa Joubert, Olivier Français, Lluis M Mir, and Bruno Le Pioufle. Design and realization of a microfluidic device devoted to the application of ultra-short pulses of electrical field to living cells. *Sensors and Actuators B: Chemical*, 160 (1):1573–1580, 2011a. [Cited on page 125]

Claire Dalmay, Julien Villemejane, Vanessa Joubert, Aude Silve, Delia Arnaud-Cormos, Olivier Français, Lluis M Mir, Philippe Lévêque, and Bruno Le Pioufle. A microfluidic biochip for the nanoporation of living cells. *Biosensors and Bioelectronics*, 26(12):4649–4655, 2011b. [Cited on page 125]

Fabienne Danhier, Olivier Feron, and Véronique Préat. To exploit the tumor microenvironment: passive and active tumor targeting of nanocarriers for anti-cancer drug delivery. *Journal of Controlled Release*, 148(2):135–146, 2010. [Cited on page 7]

Mark E Davis, Dong M Shin, et al. Nanoparticle therapeutics: an emerging treatment modality for cancer. *Nature reviews. Drug discovery*, 7(9):771, 2008. [Cited on pages 6, 197]

Marie-Amelie De Menorval, Franck M Andre, Aude Silve, Claire Dalmay, Olivier Français, Bruno Le Pioufle, and Lluis M Mir. Electric pulses: a flexible tool to manipulate cytosolic calcium concentrations and generate spontaneous-like calcium oscillations in mesenchymal stem cells. *Scientific reports*, 6, 2016. [Cited on page 125]

Elena Della Valle, Francesca Apollonio, Micaela Liberti, Agnese Denzi, and Lluis M Mir. Numerical estimation of a 10 nanosecond pulse effects on non-uniformly distributed liposomes. In *Synthesis, Modeling, Analysis and Simulation Methods and Applications to Circuit Design (SMACD), 2017 14th International Conference on*, pages 1–3. IEEE, 2017. [Cited on page 143]

Pascal Demange, Valérie Réat, Stefan Weinandy, Remy Ospital, Louise Chopinet-Mayeux, Pauline Henri, Alain Milon, and Justin Teissié. Targeted macromolecules delivery by large lipidic nanovesicles electrofusion with mammalian cells. *Journal of Biomaterials and Nanobiotechnology*, 2:527, 2011. [Cited on page 111]

Agnese Denzi, Caterina Merla, Paola Camilleri, Alessandra Paffi, Guglielmo dInzeo, Francesca Apollonio, and Micaela Liberti. Microdosimetric study for nanosecond pulsed electric fields on a cell circuit model with nucleus. *The Journal of membrane biology*, 246(10):761–767, 2013. [Cited on pages 26, 55, 109, 118, 171]

Agnese Denzi, Caterina Merla, Cristiano Palego, Alessandra Paffi, Yaqing Ning, Caroline R Multari, Xuanhong Cheng, Francesca Apollonio, James CM Hwang, and Micaela Liberti. Assessment of cytoplasm conductivity by nanosecond pulsed electric fields. *IEEE Transactions on Biomedical Engineering*, 62(6):1595–1603, 2015. [Cited on pages xix, 114, 125, 127, 128]

Agnese Denzi, Elena della Valle, Francesca Apollonio, Marie Breton, Lluis M Mir, and Micaela Liberti. Exploring the applicability of nano-poration for remote control in smart drug delivery systems. *The Journal of membrane biology*, 250(1):31–40, 2017. [Cited on pages xix, 25, 128, 133, 144, 201]

Pranali P Deshpande, Swati Biswas, and Vladimir P Torchilin. Current trends in the use of liposomes for tumor targeting. *Nanomedicine*, 8(9):1509–1528, 2013. [Cited on page 22]

Pascal Detampel, Dominik Witzigmann, Stephan Krähenbühl, and Jörg Huwyler. Hepatocyte targeting using pegylated asialofetuin-conjugated liposomes. *Journal of drug targeting*, 22 (3):232–241, 2014. [Cited on page 19]

Vincenzo Di Lazzaro, Fioravante Capone, Francesca Apollonio, Pier Andrea Borea, Ruggero Cadossi, Lorenzo Fassina, Claudio Grassi, Micaela Liberti, Alessandra Paffi, Marta Parazzini, et al. A consensus panel review of central nervous system effects of the exposure to low-intensity extremely low-frequency magnetic fields. *Brain stimulation*, 6(4):469–476, 2013. [Cited on pages 9, 35, 90, 93, 98, 103, 104, 149, 167, 199]

Awa Dicko, Lawrence D Mayer, and Paul G Tardi. Use of nanoscale delivery systems to maintain synergistic drug ratios in vivo. *Expert opinion on drug delivery*, 7(12):1329–1341, 2010. [Cited on page 22]

Feng Ding, Yoshiaki Furukawa, Nobuyuki Nukina, and Nikolay V Dokholyan. Local unfolding of cu, zn superoxide dismutase monomer determines the morphology of fibrillar aggregates. *Journal of molecular biology*, 421(4):548–560, 2012. [Cited on pages 170, 175, 187]

Pavlina Dolashka, Vesela Moshtanska, Aleksander Dolashki, Lyudmila Velkova, Gita Subba Rao, Maria Angelova, Christian Betzel, Wolfgang Voelter, and Boris Atanasov. Structural analysis and molecular modelling of the cu/zn-sod from fungal strain humicola lutea 103. *Spectrochimica Acta Part A: Molecular and Biomolecular Spectroscopy*, 83(1):67–73, 2011. [Cited on page 171]

Ruth Duncan and Rogerio Gaspar. Nanomedicine (s) under the microscope. *Molecular pharmaceutics*, 8(6):2101–2141, 2011. [Cited on page 5]

Premkumar Ellappan and Raji Sundararajan. A simulation study of the electrical model of a biological cell. *Journal of Electrostatics*, 63(3):297–307, 2005. [Cited on page 55]

Niall J English and Conor J Waldron. Perspectives on external electric fields in molecular simulation: progress, prospects and challenges. *Physical Chemistry Chemical Physics*, 17 (19):12407–12440, 2015. [Cited on page 154]

W Scott Enochs, Griffith Harsh, Fred Hochberg, and Ralph Weissleder. Improved delineation of human brain tumors on mr images using a long-circulating, superparamagnetic iron oxide agent. *Journal of Magnetic Resonance Imaging*, 9(2):228–232, 1999. [Cited on page 7]

Axel T Esser, Kyle C Smith, TR Gowrishankar, Zlatko Vasilkoski, and James C Weaver. Mechanisms for the intracellular manipulation of organelles by conventional electroporation. *Biophysical journal*, 98(11):2506–2514, 2010. [Cited on page 37]

Ulrich Essmann, Lalith Perera, Max L Berkowitz, Tom Darden, Hsing Lee, and Lee G Pedersen. A smooth particle mesh ewald method. *The Journal of chemical physics*, 103(19):8577–8593, 1995. [Cited on page 173]

M Falconi, ME Stroppolo, P Cioni, G Strambini, A Sergi, M Ferrario, and A Desideri. Dynamics-function correlation in cu, zn superoxide dismutase: a spectroscopic and molecular dynamics simulation study. *Biophysical journal*, 80(6):2556–2567, 2001. [Cited on page 170]

M Fini, G Giavaresi, A Carpi, A Nicolini, S Setti, and d R Giardino. Effects of pulsed electromagnetic fields on articular hyaline cartilage: review of experimental and clinical studies. *Biomedicine & Pharmacotherapy*, 59(7):388–394, 2005. [Cited on page 151]

Christian Fink, Fabian Kiessling, Michael Bock, Matthias Philipp Lichy, Bernd Misselwitz, Peter Peschke, Norbert E Fusenig, Rainer Grobholz, and Stefan Delorme. High-resolution three-dimensional mr angiography of rodent tumors: Morphologic characterization of intratumoral vasculature. *Journal of Magnetic Resonance Imaging*, 18(1):59–65, 2003. [Cited on page 4]

Emanuel Fleige, Mohiuddin A Quadir, and Rainer Haag. Stimuli-responsive polymeric nanocarriers for the controlled transport of active compounds: concepts and applications. *Advanced drug delivery reviews*, 64(9):866–884, 2012. [Cited on page 22]

Kevin J Freedman, S Raza Haq, Joshua B Edel, Per Jemth, and Min Jun Kim. Single molecule unfolding and stretching of protein domains inside a solid-state nanopore by electric field. *Scientific reports*, 3, 2013. [Cited on page 193]

Irwin Fridovich. Superoxide dismutases. *Adv Enzymol Relat Areas Mol Biol*, 58(6):61–97, 1986. [Cited on page 169]

Irwin Fridovich. The trail to superoxide dismutase. *Protein Science*, 7(12):2688–2690, 1998. [Cited on page 170]

Stephen D Fried and Steven G Boxer. Electric fields and enzyme catalysis. *Annual Review of Biochemistry*, 2017. [Cited on page 172]

Kjell Fuxe, Daniel Marcellino, Susanna Genedani, and Luigi Agnati. Adenosine a2a receptors, dopamine d2 receptors and their interactions in parkinson's disease. *Movement Disorders*, 22(14):1990–2017, 2007. [Cited on page 152]

Aditya Ganju, Sheema Khan, Bilal B Hafeez, Stephen W Behrman, Murali M Yallapu, Subhash C Chauhan, and Meena Jaggi. mirna nanotherapeutics for cancer. *Drug discovery today*, 22(2):424–432, 2017. [Cited on pages 6, 197]

Srinivas Ganta, Harikrishna Devalapally, Aliasgar Shahiwala, and Mansoor Amiji. A review of stimuli-responsive nanocarriers for drug and gene delivery. *Journal of controlled release*, 126 (3):187–204, 2008. [Cited on pages 17, 22, 198]

Guang Hui Gao, Min Jung Park, Yi Li, Geun Ho Im, Jae-Hoon Kim, Hun Nyun Kim, Jae Won Lee, Pyoung Jeon, Oh Young Bang, Jung Hee Lee, et al. The use of ph-sensitive positively charged polymeric micelles for protein delivery. *Biomaterials*, 33(35):9157–9164, 2012. [Cited on page 22]

Jun Ge, Evgenios Neofytou, Thomas J Cahill III, Ramin E Beygui, and Richard N Zare. Drug release from electric-field-responsive nanoparticles. *ACS nano*, 6(1):227–233, 2011. [Cited on page 25]

Elizabeth D Getzoff, John A Tainer, Paul K Weiner, Peter A Kollman, Jane S Richardson, and David C Richardson. Electrostatic recognition between superoxide and copper, zinc superoxide dismutase. *Nature*, 306(5940):287–290, 1983. [Cited on pages 170, 172]

Elizabeth D Getzoff, Diane E Cabelli, Cindy L Fisher, Hans E Parge, Maria Silvia Viezzoli, Lucia Banci, and Robert A Hallewell. Faster superoxide dismutase mutants designed by enhancing electrostatic guidance. *Nature*, 358(6384):347–351, 1992. [Cited on page 194]

Kenneth A Giuliano, Penny L Post, Klaus M Hahn, and D Lansing Taylor. Fluorescent protein biosensors: measurement of molecular dynamics in living cells. *Annual review of biophysics and biomolecular structure*, 24(1):405–434, 1995. [Cited on pages 33, 34, 197]

Alberto Gobbi, Georgios Karnatzikos, and Sanyam Chaurasia. Pulsed electromagnetic fields for the treatment of symptomatic patellofemoral cartilage lesions of the knee. In *The Patellofemoral Joint*, pages 261–266. Springer, 2014. [Cited on page 66]

Jesus E Gonzalez and Roger Y Tsien. Voltage sensing by fluorescence resonance energy transfer in single cells. *Biophysical journal*, 69(4):1272–1280, 1995. [Cited on page 34]

Thiruvallur R Gowrishankar, Kyle C Smith, and James C Weaver. Transport-based biophysical system models of cells for quantitatively describing responses to electric fields. *Proceedings of the IEEE*, 101(2):505–517, 2013. [Cited on page 54]

Pablo Guardia, Riccardo Di Corato, Lenaic Lartigue, Claire Wilhelm, Ana Espinosa, Mar Garcia-Hernandez, Florence Gazeau, Liberato Manna, and Teresa Pellegrino. Water-soluble iron oxide nanocubes with high values of specific absorption rate for cancer cell hyperthermia treatment. *ACS nano*, 6(4):3080–3091, 2012. [Cited on pages 30, 65]

Barry Halliwell. Superoxide and superoxide-dependent formation of hydroxyl radicals are important in oxygen toxicity. *Trends in Biochemical Sciences*, 7(8):270–272, 1982. [Cited on page 170]

Barry Halliwell. Reactive oxygen species and the central nervous system. *Journal of neurochemistry*, 59(5):1609–1623, 1992. [Cited on page 170]

Richard Wesley Hamming. *Digital filters*. Courier Corporation, 1989. [Cited on page 175]

Mukesh G Harisinghani, Jelle Barentsz, Peter F Hahn, Willem M Deserno, Shahin Tabatabaei, Christine Hulsbergen van de Kaa, Jean de la Rosette, and Ralph Weissleder. Noninvasive detection of clinically occult lymph-node metastases in prostate cancer. *New England Journal of Medicine*, 348(25):2491–2499, 2003. [Cited on page 4]

Roger F Harrington and Jan L Harrington. *Field computation by moment methods*. Oxford University Press, 1996. [Cited on page 56]

Chris M Hempel, Pierre Vincent, Stephen R Adams, Roger Y Tsien, and Allen I Selverston. Spatio-temporal dynamics of cyclic amp signals in an intact neural circuit. *Nature*, 384(6605): 166, 1996. [Cited on page 34]

Berk Hess, Henk Bekker, Herman JC Berendsen, Johannes GEM Fraaije, et al. Lincs: a linear constraint solver for molecular simulations. *Journal of computational chemistry*, 18(12): 1463–1472, 1997. [Cited on pages 48, 173]

Berk Hess, Carsten Kutzner, David Van Der Spoel, and Erik Lindahl. Gromacs 4: algorithms for highly efficient, load-balanced, and scalable molecular simulation. *Journal of chemical theory and computation*, 4(3):435–447, 2008. [Cited on pages 50, 173]

Todd Hoare, Brian P Timko, Jesus Santamaria, Gerardo F Goya, Silvia Irusta, Samantha Lau, Cristina F Stefanescu, Debora Lin, Robert Langer, and Daniel S Kohane. Magnetically triggered nanocomposite membranes: a versatile platform for triggered drug release. *Nano letters*, 11(3):1395–1400, 2011. [Cited on page 31]

MJ Hope, MB Bally, G Webb, and PR Cullis. Production of large unilamellar vesicles by a rapid extrusion procedure. characterization of size distribution, trapped volume and ability to maintain a membrane potential. *Biochimica et Biophysica Acta (BBA)-Biomembranes*, 812(1):55–65, 1985. [Cited on page 20]

Q Hu and RP Joshi. Transmembrane voltage analyses in spheroidal cells in response to an intense ultrashort electrical pulse. *Physical Review E*, 79(1):011901, 2009. [Cited on pages 55, 113]

Q Hu, S Viswanadham, RP Joshi, Karl H Schoenbach, Stephen J Beebe, and PF Blackmore. Simulations of transient membrane behavior in cells subjected to a high-intensity ultrashort electric pulse. *Physical Review E*, 71(3):031914, 2005. [Cited on pages 54, 55]

Wenhui Hu and Lauren J Webb. Direct measurement of the membrane dipole field in bicelles using vibrational stark effect spectroscopy. *The Journal of Physical Chemistry Letters*, 2(15): 1925–1930, 2011. [Cited on page 192]

Bennett L Ibey, Caleb C Roth, Andrei G Pakhomov, Joshua A Bernhard, Gerald J Wilmink, and Olga N Pakhomova. Dose-dependent thresholds of 10-ns electric pulse induced plasma membrane disruption and cytotoxicity in multiple cell lines. *PLoS One*, 6(1):e15642, 2011. [Cited on pages 10, 121]

Djaudat Idiyatullin, Curt Corum, Michael Garwood, Donald Nixdorf, and Gregor Adriany. System and method for multi-roi mri imaging using an rf loop coil, January 10 2017. US Patent 9,541,615. [Cited on page 9]

Ji S Im, Byong Ch Bai, and Young-Seak Lee. The effect of carbon nanotubes on drug delivery in an electro-sensitive transdermal drug delivery system. *Biomaterials*, 31(6):1414–1419, 2010. [Cited on page 25]

Anna Imhof, Philippe Brunner, Nicolas Marincek, Matthias Briel, Christian Schindler, Helmut Rasch, Helmut R Mäcke, Christoph Rochlitz, Jan Müller-Brand, and Martin A Walter. Response, survival, and long-term toxicity after therapy with the radiolabeled somatostatin analogue [90y-dota]-toc in metastasized neuroendocrine cancers. *Journal of clinical oncology*, 29(17):2416–2423, 2011. [Cited on page 6]

James A Imlay and Stuart Linn. Dna damage and oxygen radical toxicity. *Science(Washington)*, 240(4857):1302–1309, 1988. [Cited on page 170]

James A Imlay, Sherman M Chin, and Stuart Linn. Toxic dna damage by hydrogen peroxide through the fenton reaction in vivo and in vitro. *Science*, 240(4852):640, 1988. [Cited on page 170]

Sua In, Chang-Won Hong, Boyoung Choi, Bong-Geum Jang, and Min-Ju Kim. Inhibition of mitochondrial clearance and cu/zn-sod activity enhance 6-hydroxydopamine-induced neuronal apoptosis. *Molecular neurobiology*, 53(1):777–791, 2016. [Cited on page 170]

Kevin Ita. Transdermal iontophoretic drug delivery: advances and challenges. *Journal of drug targeting*, 24(5):386–391, 2016. [Cited on page 26]

Tenderwealth Clement Jackson, Bernard Opatimidi Patani, and Daniel Effiong Ekpa. Nanotechnology in diagnosis: A review. *Advances in Nanoparticles*, 6(03):93, 2017. [Cited on page 5]

Rakesh K Jain and Triantafyllos Stylianopoulos. Delivering nanomedicine to solid tumors. *Nature reviews Clinical oncology*, 7(11):653–664, 2010. [Cited on page 19]

Morten Ø Jensen, Vishwanath Jogini, David W Borhani, Abba E Leffler, Ron O Dror, and David E Shaw. Mechanism of voltage gating in potassium channels. *Science*, 336(6078): 229–233, 2012. [Cited on page 192]

Zongchao Jia, Margaret Vandonselaar, J Wilson Quail, and Louis TJ Delbaere. Active-centre torsion-angle strain revealed in 1.6 å-resolution structure of histidine-containing phosphocarrier protein. *Nature*, 361(6407):94–97, 1993. [Cited on page 161]

Jian-Ming Jin. *The finite element method in electromagnetics*. John Wiley & Sons, 2015. [Cited on page 57]

Mayank V Jog, Robert X Smith, Kay Jann, Walter Dunn, Belen Lafon, Dennis Truong, Allan Wu, Lucas Parra, Marom Bikson, and Danny JJ Wang. In-vivo imaging of magnetic fields induced by transcranial direct current stimulation (tdcs) in human brain using mri. *Scientific reports*, 6, 2016. [Cited on page 9]

M Jorg, PJ Scammells, and B Capuano. The dopamine d2 and adenosine a2a receptors: past, present and future trends for the treatment of parkinson's disease. *Current medicinal chemistry*, 21(27):3188–3210, 2014. [Cited on page 152]

William L Jorgensen, David S Maxwell, and Julian Tirado-Rives. Development and testing of the opls all-atom force field on conformational energetics and properties of organic liquids. *J. Am. Chem. Soc*, 118(45):11225–11236, 1996. [Cited on page 50]

Ravi P Joshi and KH Schoenbach. Bioelectric effects of intense ultrashort pulses. *Critical Reviews in Biomedical Engineering*, 38(3), 2010. [Cited on pages 9, 10, 109, 139]

Ravindra P Joshi, Ashutosh Mishra, and Karl H Schoenbach. Model assessment of cell membrane breakdown in clusters and tissues under high-intensity electric pulsing. *IEEE Transactions on Plasma Science*, 36(4):1680–1688, 2008. [Cited on page 55]

RP Joshi and KH Schoenbach. Electroporation dynamics in biological cells subjected to ultrafast electrical pulses: a numerical simulation study. *Physical review E*, 62(1):1025, 2000. [Cited on page 55]

H Karanth and RSR Murthy. ph-sensitive liposomes-principle and application in cancer therapy. *Journal of pharmacy and pharmacology*, 59(4):469–483, 2007. [Cited on pages 17, 198]

J Kaszuba-Zwoińska, I Ciećko-Michalska, D Madroszkiewicz, T Mach, Z Słodowska-Hajduk, E Rokita, W Zaraska, and P Thor. Magnetic field anti-inflammatory effects in crohn's disease depends upon viability and cytokine profile of the immune competent cells. *Journal of physiology and pharmacology: an official journal of the Polish Physiological Society*, 59 (1):177–187, 2008. [Cited on page 151]

Simran J Kaur, Stephanie R McKeown, and Shazia Rashid. Mutant sod1 mediated pathogenesis of amyotrophic lateral sclerosis. *Gene*, 577(2):109–118, 2016. [Cited on page 170]

Toshifumi Kawakami, Shinji Urakami, Hiroshi Hirata, Yuichiro Tanaka, Koichi Nakajima, Hideki Enokida, Hiroaki Shiina, Tatsuya Ogishima, Takashi Tokizane, Ken Kawamoto, et al. Superoxide dismutase analog (tempol: 4-hydroxy-2, 2, 6, 6-tetramethylpiperidine 1-oxyl) treatment restores erectile function in diabetes-induced impotence. *International journal of impotence research*, 21(6):348, 2009. [Cited on page 170]

Mohamad Kenaan, Saad El Amari, Aude Silve, Caterina Merla, Lluis M Mir, Vincent Couderc, Delia Arnaud-Cormos, and Philippe Leveque. Characterization of a 50-ω exposure setup for high-voltage nanosecond pulsed electric field bioexperiments. *IEEE Transactions on Biomedical Engineering*, 58(1):207–214, 2011. [Cited on pages 126, 129, 130, 131, 136]

Azadeh Kheirolomoom, Lisa M Mahakian, Chun-Yen Lai, Heather A Lindfors, Jai Woong Seo, Eric E Paoli, Katherine D Watson, Eric M Haynam, Elizabeth S Ingham, Li Xing, et al.

Copper- doxorubicin as a nanoparticle cargo retains efficacy with minimal toxicity. *Molecular pharmaceutics*, 7(6):1948–1958, 2010. [Cited on pages 23, 24]

Akihiko Kikuchi and Teruo Okano. Pulsatile drug release control using hydrogels. *Advanced drug delivery reviews*, 54(1):53–77, 2002. [Cited on page 23]

Hoon Kim, Sang-Mi Jeong, and Ji-Woong Park. Electrical switching between vesicles and micelles via redox-responsive self-assembly of amphiphilic rod- coils. *Journal of the American Chemical Society*, 133(14):5206–5209, 2011. [Cited on page 25]

Jeong Ah Kim and Won Gu Lee. Role of weakly polarized nanoparticles in electroporation. *Nanoscale*, 3(4):1526–1532, 2011. [Cited on page 28]

Hiroaki Kitano. Computational systems biology. *Nature*, 420(6912):206, 2002a. [Cited on pages 127, 144]

Hiroaki Kitano. Systems biology: a brief overview. *Science*, 295(5560):1662–1664, 2002b. [Cited on pages 127, 144]

Isaac Klapper, Ray Hagstrom, Richard Fine, Kim Sharp, and Barry Honig. Focusing of electric fields in the active site of cu-zn superoxide dismutase: Effects of ionic strength and amino-acid modification. *Proteins: Structure, Function, and Bioinformatics*, 1(1):47–59, 1986. [Cited on page 187]

Gouze N KM Weltring, Martin, and F Gramatica Pereira, I Baanante. Strategic research and innovation agenda for nanomedicine 2016 2030. *ETP Nanomedicine*, 2016. [Cited on page 3]

Tomowo KOBAYASHI, Shigeru TSUKAGOSHI, and Yoshio SAKURAI. Enhancement of the cancer chemotherapeutic effect of cytosine arabinoside entrapped in liposomes on mouse leukemia l-1210. *GANN Japanese Journal of Cancer Research*, 66(6):719–720, 1975. [Cited on page 21]

Sophie Kohler, P Jarrige, Nicolas Ticaud, RP O'connor, L Duvillaret, G Gaborit, Delia Arnaud-Cormos, and Philippe Lévêque. Simultaneous high intensity ultrashort pulsed electric field and temperature measurements using a unique electro-optic probe. *IEEE Microwave and Wireless Components Letters*, 22(3):153–155, 2012. [Cited on pages 125, 129, 136]

Sophie Kohler, Zachary A Levine, Miguel Á García-Fernández, Ming-Chak Ho, P Thomas Vernier, Philippe Leveque, and Delia Arnaud-Cormos. Electrical analysis of cell membrane poration by an intense nanosecond pulsed electric field using an atomistic-to-continuum method. *IEEE Transactions on Microwave Theory and Techniques*, 63(6):2032–2040, 2015. [Cited on page 59]

Ahn Na Koo, Hong Jae Lee, Sung Eun Kim, Jeong Ho Chang, Chiyoung Park, Chulhee Kim, Jae Hyung Park, and Sang Cheon Lee. Disulfide-cross-linked peg-poly (amino acid) s copolymer micelles for glutathione-mediated intracellular drug delivery. *Chemical Communications*, (48):6570–6572, 2008. [Cited on pages 17, 22]

Yong-Eun Koo Lee, Ron Smith, and Raoul Kopelman. Nanoparticle pebble sensors in live cells and in vivo. *Annual review of analytical chemistry*, 2:57–76, 2009. [Cited on page 171]

Tadej Kotnik and Damijan Miklavcic. Theoretical evaluation of the distributed power dissipation in biological cells exposed to electric fields. *Bioelectromagnetics*, 21(5):385–394, 2000. [Cited on pages 111, 116, 123, 200]

Tadej Kotnik and Damijan Miklavčič. Theoretical evaluation of voltage inducement on internal membranes of biological cells exposed to electric fields. *Biophysical journal*, 90(2):480–491, 2006. [Cited on page 110]

Tadej Kotnik, Feda Bobanović, and Damijian Miklavcic. Sensitivity of transmembrane voltage induced by applied electric fieldsa theoretical analysis. *Bioelectrochemistry and bioenergetics*, 43(2):285–291, 1997. [Cited on page 115]

Tadej Kotnik, Damijan Miklavčič, and Tomaž Slivnik. Time course of transmembrane voltage induced by time-varying electric fieldsa method for theoretical analysis and its application. *Bioelectrochemistry and bioenergetics*, 45(1):3–16, 1998. [Cited on page 116]

Tadej Kotnik, Gorazd Pucihar, and Damijan Miklavčič. Induced transmembrane voltage and its correlation with electroporation-mediated molecular transport. *The Journal of membrane biology*, 236(1):3–13, 2010. [Cited on pages 54, 55, 109]

Wanda Krassowska and Petar D Filev. Modeling electroporation in a single cell. *Biophysical journal*, 92(2):404–417, 2007. [Cited on page 54]

Priyanka R Kulkarni, Jaydeep D Yadav, Kumar A Vaidya, et al. Liposomes: a novel drug delivery system. *Int J Curr Pharm Res*, 3(2):10–18, 2011. [Cited on page 20]

TGGM Lammers, WE Hennink, and G Storm. Tumour-targeted nanomedicines: principles and practice. *British journal of cancer*, 99(3):392, 2008a. [Cited on pages 6, 197]

TGGM Lammers, V Subr, P Peschke, R Kühnlein, WE Hennink, K Ulbrich, F Kiessling, M Heilmann, J Debus, PE Huber, et al. Image-guided and passively tumour-targeted polymeric nanomedicines for radiochemotherapy. *British journal of cancer*, 99(6):900, 2008b. [Cited on page 6]

Twan Lammers, Fabian Kiessling, Wim E Hennink, and Gert Storm. Drug targeting to tumors: principles, pitfalls and (pre-) clinical progress. *Journal of controlled release*, 161(2):175–187, 2012. [Cited on page 18]

Guillaume Lebon, Patricia C Edwards, Andrew GW Leslie, and Christopher G Tate. Molecular determinants of cgs21680 binding to the human adenosine a2a receptor. *Molecular pharmacology*, 87(6):907–915, 2015. [Cited on page 164]

Jung S Lee, Tom Groothuis, Claudia Cusan, Daniel Mink, and Jan Feijen. Lysosomally cleavable peptide-containing polymersomes modified with anti-egfr antibody for systemic cancer chemotherapy. *Biomaterials*, 32(34):9144–9153, 2011. [Cited on page 22]

Soo Hyeon Lee, Seung Ho Choi, Sun Hwa Kim, and Tae Gwan Park. Thermally sensitive cationic polymer nanocapsules for specific cytosolic delivery and efficient gene silencing of sirna: swelling induced physical disruption of endosome by cold shock. *Journal of Controlled Release*, 125(1):25–32, 2008. [Cited on page 24]

Yan Lee and Kazunori Kataoka. Delivery of nucleic acid drugs. In *Nucleic Acid Drugs*, pages 95–134. Springer, 2011. [Cited on page 20]

Joel A Lefferts, Paul Jannetto, and Gregory J Tsongalis. Evaluation of the nanosphere verigene® system and the verigene® f5/f2/mthfr nucleic acid tests. *Experimental and molecular pathology*, 87(2):105–108, 2009. [Cited on page 4]

Michael Levitt, Miriam Hirshberg, Ruth Sharon, Keith E Laidig, and Valerie Daggett. Calibration and testing of a water model for simulation of the molecular dynamics of proteins and nucleic acids in solution. *The Journal of Physical Chemistry B*, 101(25):5051–5061, 1997. [Cited on page 158]

Yingqiu Li, Zhengxing Chen, and Haizhen Mo. Effects of pulsed electric fields on physicochemical properties of soybean protein isolates. *LWT-Food Science and Technology*, 40(7): 1167–1175, 2007. [Cited on page 37]

Yuanpei Li, Kai Xiao, Juntao Luo, Wenwu Xiao, Joyce S Lee, Abby M Gonik, Jason Kato, Tiffany A Dong, and Kit S Lam. Well-defined, reversible disulfide cross-linked micelles for on-demand paclitaxel delivery. *Biomaterials*, 32(27):6633–6645, 2011. [Cited on pages 17, 22]

Hsin-Yi Lin and Yu-Jen Lin. In vitro effects of low frequency electromagnetic fields on osteoblast proliferation and maturation in an inflammatory environment. *Bioelectromagnetics*, 32(7): 552–560, 2011. [Cited on page 35]

Lars H Lindner and Martin Hossann. Factors affecting drug release from liposomes. *Current opinion in drug discovery & development*, 13(1):111–123, 2010. [Cited on pages 21, 198]

Kun-Ho Liu, Ting-Yu Liu, San-Yuan Chen, and Dean-Mo Liu. Drug release behavior of chitosan–montmorillonite nanocomposite hydrogels following electrostimulation. *Acta Biomaterialia*, 4(4):1038–1045, 2008. [Cited on pages 23, 25]

Yue Lu, Wujin Sun, and Zhen Gu. Stimuli-responsive nanomaterials for therapeutic protein delivery. *Journal of controlled release*, 194:1–19, 2014. [Cited on page 23]

Francesca Lugli, Francesca Toschi, Fabio Biscarini, and Francesco Zerbetto. Electric field effects on short fibrils of aβ amyloid peptides. *Journal of chemical theory and computation*, 6(11): 3516–3526, 2010. [Cited on page 192]

Alex D MacKerell Jr, Donald Bashford, MLDR Bellott, Roland Leslie Dunbrack Jr, Jeffrey D Evanseck, Martin J Field, Stefan Fischer, Jiali Gao, H Guo, Sookhee Ha, et al. All-atom empirical potential for molecular modeling and dynamics studies of proteins. *The journal of physical chemistry B*, 102(18):3586–3616, 1998. [Cited on page 50]

M Malekigorji, ADM Curtis, and C Hoskins. The use of iron oxide nanoparticles for pancreatic cancer therapy. *J. Nanomed. Res*, 1:1, 2014. [Cited on page 22]

K Malinovskaja-Gomez, S Espuelas, MJ Garrido, J Hirvonen, and T Laaksonen. Comparison of liposomal drug formulations for transdermal iontophoretic drug delivery. *European Journal of Pharmaceutical Sciences*, 2017. [Cited on page 26]

Erik G Marklund, Tomas Ekeberg, Mathieu Moog, Justin LP Benesch, and Carl Caleman. Controlling protein orientation in vacuum using electric fields. *The Journal of Physical Chemistry Letters*, 8(18):4540–4544, 2017. [Cited on page 11]

P Marracino, A Paffi, R Reale, M Liberti, G d'Inzeo, and F Apollonio. Technology of high-intensity electric-field pulses: a way to control protein unfolding. *J Phys Chem Biophys*, 3 (117):2161–0398, 2013a. [Cited on page 38]

P Marracino, F Castellani, PT Vernier, M Liberti, and F Apollonio. Geometrical characterization of an electropore from water positional fluctuations. *The Journal of membrane biology*, 250(1):11–19, 2017. [Cited on page 193]

Paolo Marracino, Francesca Apollonio, Micaela Liberti, Guglielmo dInzeo, and Andrea Amadei. Effect of high exogenous electric pulses on protein conformation: myoglobin as a case study. *The Journal of Physical Chemistry B*, 117(8):2273–2279, 2013b. [Cited on pages 38, 54, 153, 154, 174]

Paolo Marracino, Micaela Liberti, Guglielmo d'Inzeo, and Francesca Apollonio. Water response to intense electric fields: A molecular dynamics study. *Bioelectromagnetics*, 36(5):377–385, 2015. [Cited on page 193]

Paolo Marracino, Micaela Liberti, Erika Trapani, Christian J Burnham, Massimiliano Avena, José-Antonio Garate, Francesca Apollonio, and Niall J English. Human aquaporin 4 gating dynamics under perpendicularly-oriented electric-field impulses: A molecular dynamics study. *International journal of molecular sciences*, 17(7):1133, 2016. [Cited on pages 128, 153, 193]

Jeffrey D McBride, Luis Rodriguez-Menocal, and Evangelos V Badiavas. Extracellular vesicles as biomarkers and therapeutics in dermatology: a focus on exosomes. *Journal of Investigative Dermatology*, 2, 2017. [Cited on page 6]

Joe M McCord and Irwin Fridovich. Superoxide dismutase an enzymic function for erythrocuprein (hemocuprein). *Journal of Biological chemistry*, 244(22):6049–6055, 1969. [Cited on page 170]

Kerry P McNamara and Zeev Rosenzweig. Dye-encapsulating liposomes as fluorescence-based oxygen nanosensors. *Analytical Chemistry*, 70(22):4853–4859, 1998. [Cited on page 126]

Caterina Merla, Saad El Amari, Mohamad Kenaan, Micaela Liberti, Francesca Apollonio, Delia Arnaud-Cormos, Vincent Couderc, and Philippe Leveque. A 10-ω high-voltage nanosecond pulse generator. *IEEE transactions on microwave theory and techniques*, 58(12):4079–4085, 2010. [Cited on pages 125, 126, 127]

Caterina Merla, Alessandra Paffi, Francesca Apollonio, Philippe Leveque, Guglielmo dInzeo, and Micaela Liberti. Microdosimetry for nanosecond pulsed electric field applications: a parametric study for a single cell. *IEEE Transactions on Biomedical Engineering*, 58(5): 1294–1302, 2011. [Cited on pages 55, 110]

Caterina Merla, Agnese Denzi, Alessandra Paffi, Maura Casciola, Guglielmo dInzeo, Francesca Apollonio, and Micaela Liberti. Novel passive element circuits for microdosimetry of nanosecond pulsed electric fields. *IEEE Transactions on Biomedical Engineering*, 59(8):2302–2311, 2012. [Cited on pages xix, 55, 111, 114, 118, 123, 133, 200]

D Miklavčič, G Serša, E Brecelj, J Gehl, D Soden, Giuseppe Bianchi, P Ruggieri, Carlo Riccardo Rossi, LG Campana, and Tomaz Jarm. Electrochemotherapy: technological advancements for efficient electroporation-based treatment of internal tumors. *Medical & biological engineering & computing*, 50(12):1213–1225, 2012. [Cited on pages 9, 109, 200]

Lluis M Mir, Michel F Bureau, Julie Gehl, Ravi Rangara, Didier Rouy, Jean-Michel Caillaud, Pia Delaere, Didier Branellec, Bertrand Schwartz, and Daniel Scherman. High-efficiency gene transfer into skeletal muscle mediated by electric pulses. *Proceedings of the National Academy of Sciences*, 96(8):4262–4267, 1999. [Cited on pages 9, 109, 200]

Agha Zeeshan Mirza and Farhan Ahmed Siddiqui. Nanomedicine and drug delivery: a mini review. *International Nano Letters*, 4(1):94, 2014. [Cited on page 18]

Panagiotis Mitsopoulos and Zacharias E Suntres. Protective effects of liposomal n-acetylcysteine against paraquat-induced cytotoxicity and gene expression. *Journal of toxicology*, 2011, 2011. [Cited on page 110]

Shuichi Miyamoto and Peter A Kollman. Settle: an analytical version of the shake and rattle algorithm for rigid water models. *Journal of computational chemistry*, 13(8):952–962, 1992. [Cited on page 48]

Kanjiro Miyata, R James Christie, and Kazunori Kataoka. Polymeric micelles for nano-scale drug delivery. *Reactive and Functional Polymers*, 71(3):227–234, 2011. [Cited on pages 110, 111, 120]

Fatemeh Moosavi and Mostafa Gholizadeh. Magnetic effects on the solvent properties investigated by molecular dynamics simulation. *Journal of Magnetism and Magnetic Materials*, 354:239–247, 2014. [Cited on page 154]

David J Muehsam and Arthur A Pilla. A lorentz model for weak magnetic field bioeffects: part ithermal noise is an essential component of ac/dc effects on bound ion trajectory. *Bioelectromagnetics*, 30(6):462–475, 2009. [Cited on pages 153, 158]

Simona Mura, Julien Nicolas, and Patrick Couvreur. Stimuli-responsive nanocarriers for drug delivery. *Nature materials*, 12(11):991, 2013. [Cited on pages 6, 23]

S Murad. The role of magnetic fields on the membrane-based separation of aqueous electrolyte solutions. *Chemical physics letters*, 417(4):465–470, 2006. [Cited on page 154]

BS Murty, P Shankar, Baldev Raj, BB Rath, and James Murday. Unique properties of nanomaterials. In *Textbook of Nanoscience and Nanotechnology*, pages 29–65. Springer, 2013. [Cited on page 1]

Tina Batista Napotnik, Yu-Hsuan Wu, Martin A Gundersen, Damijan Miklavčič, and P Thomas Vernier. Nanosecond electric pulses cause mitochondrial membrane permeabilization in jurkat cells. *Bioelectromagnetics*, 33(3):257–264, 2012. [Cited on pages 26, 27]

Tina Batista Napotnik, Matej Reberšek, P Thomas Vernier, Barbara Mali, and Damijan Miklavčič. Effects of high voltage nanosecond electric pulses on eukaryotic cells (in vitro): a systematic review. *Bioelectrochemistry*, 110:1–12, 2016. [Cited on page 27]

Silvia Nappini, Francesca Baldelli Bombelli, Massimo Bonini, Bengt Nordèn, and Piero Baglioni. Magnetoliposomes for controlled drug release in the presence of low-frequency magnetic field. *Soft Matter*, 6(1):154–162, 2010. [Cited on pages 9, 30, 31, 32, 65, 90, 198]

Boris A Nasseri, Kohei Ogawa, and Joseph P Vacanti. Tissue engineering: an evolving 21st-century science to provide biologic replacement for reconstruction and transplantation. *Surgery*, 130(5):781–784, 2001. [Cited on page 6]

Radford M Neal. *Bayesian learning for neural networks*, volume 118. Springer Science & Business Media, 2012. [Cited on page 10]

Irina V Nesmelova, Vladimir D Skirda, and Vladimir D Fedotov. Generalized concentration dependence of globular protein self-diffusion coefficients in aqueous solutions. *Biopolymers*, 63(2):132–140, 2002. [Cited on page 163]

Eberhard Neumann and Kurt Rosenheck. Permeability changes induced by electric impulses in vesicular membranes. *Journal of Membrane Biology*, 10(1):279–290, 1972. [Cited on page 10]

Mariana I Neves, Marissa E Wechsler, Manuela E Gomes, Rui L Reis, Pedro L Granja, and Nicholas A Peppas. Molecularly imprinted intelligent scaffolds for tissue engineering applications. *Tissue Engineering Part B: Reviews*, 23(1):27–43, 2017. [Cited on page 6]

Raluca A Niesner and Anja E Hauser. Recent advances in dynamic intravital multi-photon microscopy. *Cytometry Part A*, 79(10):789–798, 2011. [Cited on pages 33, 197]

James S Nowick. Exploring β-sheet structure and interactions with chemical model systems. *Accounts of chemical research*, 41(10):1319–1330, 2008. [Cited on page 174]

Richard Nuccitelli, Uwe Pliquett, Xinhua Chen, Wentia Ford, R James Swanson, Stephen J Beebe, Juergen F Kolb, and Karl H Schoenbach. Nanosecond pulsed electric fields cause melanomas to self-destruct. *Biochemical and biophysical research communications*, 343(2): 351–360, 2006. [Cited on page 10]

Richard Nuccitelli, Kaying Lui, Mark Kreis, Brian Athos, and Pamela Nuccitelli. Nanosecond pulsed electric field stimulation of reactive oxygen species in human pancreatic cancer cells is ca 2+-dependent. *Biochemical and biophysical research communications*, 435(4):580–585, 2013. [Cited on page 10]

Satish K Nune, Padmaja Gunda, Praveen K Thallapally, Ying-Ying Lin, M Laird Forrest, and Cory J Berkland. Nanoparticles for biomedical imaging. *Expert opinion on drug delivery*, 6 (11):1175–1194, 2009. [Cited on pages 1, 29, 89]

Yu-Kyoung Oh and Tae Gwan Park. sirna delivery systems for cancer treatment. *Advanced drug delivery reviews*, 61(10):850–862, 2009. [Cited on page 21]

Pedro Ojeda-May and Martin E Garcia. Electric field-driven disruption of a native β-sheet protein conformation and generation of a helix-structure. *Biophysical journal*, 99(2):595–599, 2010. [Cited on page 192]

Chris Oostenbrink, Alessandra Villa, Alan E Mark, and Wilfred F Van Gunsteren. A biomolecular force field based on the free enthalpy of hydration and solvation: the gromos force-field parameter sets 53a5 and 53a6. *Journal of computational chemistry*, 25(13):1656–1676, 2004. [Cited on page 50]

Alessandra Paffi, Francesca Camera, Filippo Carducci, Gianluigi Rubino, Paolo Tampieri, Micaela Liberti, and Francesca Apollonio. A computational model for real-time calculation of electric field due to transcranial magnetic stimulation in clinics. *International Journal of Antennas and Propagation*, 2015, 2015. [Cited on page 90]

Andrei G Pakhomov, Amy Phinney, John Ashmore, K Walker, Juergen F Kolb, Susumu Kono, Karl H Schoenbach, and Michael R Murphy. Characterization of the cytotoxic effect of high-intensity, 10-ns duration electrical pulses. *IEEE Transactions on Plasma Science*, 32 (4):1579–1586, 2004. [Cited on page 125]

Andrei G Pakhomov, Damijan Miklavcic, and Marko S Markov. *Advanced electroporation techniques in biology and medicine*. CRC Press, 2010. [Cited on page 111]

Andrei G Pakhomov, Shu Xiao, Olga N Pakhomova, Iurii Semenov, Marjorie A Kuipers, and Bennett L Ibey. Disassembly of actin structures by nanosecond pulsed electric field is a downstream effect of cell swelling. *Bioelectrochemistry*, 100:88–95, 2014. [Cited on page 37]

Olga N Pakhomova, Betsy Gregory, Iurii Semenov, and Andrei G Pakhomov. Calcium-mediated pore expansion and cell death following nanoelectroporation. *Biochimica et Biophysica Acta (BBA)-Biomembranes*, 1838(10):2547–2554, 2014. [Cited on page 10]

Tamar Pashut, Dafna Magidov, Hana Ben-Porat, Shuki Wolfus, Alex Friedman, Eli Perel, Michal Lavidor, Izhar Bar-Gad, Yosef Yeshurun, and Alon Korngreen. Patch-clamp recordings of rat neurons from acute brain slices of the somatosensory cortex during magnetic stimulation. *Frontiers in cellular neuroscience*, 8, 2014. [Cited on page 90]

von H Pauly and HP Schwan. Über die impedanz einer suspension von kugelförmigen teilchen mit einer schale. *Zeitschrift für Naturforschung B*, 14(2):125–131, 1959. [Cited on page 54]

Elisa BMI Peixoto, Bruno S Pessoa, Subrata K Biswas, and Jose B Lopes De Faria. Antioxidant sod mimetic prevents nadph oxidase-induced oxidative stress and renal damage in the early stage of experimental diabetes and hypertension. *American journal of nephrology*, 29(4): 309–318, 2009. [Cited on page 170]

Steven D Perrault, Carl Walkey, Travis Jennings, Hans C Fischer, and Warren CW Chan. Mediating tumor targeting efficiency of nanoparticles through design. *Nano letters*, 9(5): 1909–1915, 2009. [Cited on page 4]

Yvonne Perrie, Peter M Frederik, and Gregory Gregoriadis. Liposome-mediated dna vaccination: the effect of vesicle composition. *Vaccine*, 19(23-24):3301–3310, 2001. [Cited on pages 28, 110]

J Jefferson P Perry, Li Fan, and John A Tainer. Developing master keys to brain pathology, cancer and aging from the structural biology of proteins controlling reactive oxygen species and dna repair. *Neuroscience*, 145(4):1280–1299, 2007. [Cited on page 170]

JJP Perry, DS Shin, ED Getzoff, and JA Tainer. The structural biochemistry of the superoxide dismutases. *Biochimica et Biophysica Acta (BBA)-Proteins and Proteomics*, 1804(2):245–262, 2010. [Cited on page 171]

Stefania Petralito, Romina Spera, Adriana Memoli, Guglielmo D'Inzeo, Micaela Liberti, and Francesca Apollonio. Preparation and characterization of lipid vesicles entrapping iron oxide nanoparticles. *Asia-Pacific Journal of Chemical Engineering*, 7(S3), 2012. [Cited on page 20]

AA Pilla, DJ Muehsam, and MS Markov. A dynamical systems/larmor precession model for weak magnetic field bioeffects: Ion binding and orientation of bound water molecules. *Bioelectrochemistry and bioenergetics*, 43(2):239–249, 1997. [Cited on page 152]

Marina Pinheiro, Marlene Lúcio, José LFC Lima, and Salette Reis. Liposomes as drug delivery systems for the treatment of tb. *Nanomedicine*, 6(8):1413–1428, 2011. [Cited on page 21]

Vincent Plassat, Claire Wilhelm, Véronique Marsaud, Christine Ménager, Florence Gazeau, Jack-Michel Renoir, and Sylviane Lesieur. Anti-estrogen-loaded superparamagnetic liposomes for intracellular magnetic targeting and treatment of breast cancer tumors. *Advanced Functional Materials*, 21(1):83–92, 2011. [Cited on pages 23, 24, 30, 31]

Letterio S Politi, Marco Bacigaluppi, Elena Brambilla, Marcello Cadioli, Andrea Falini, Giancarlo Comi, Giuseppe Scotti, Gianvito Martino, and Stefano Pluchino. Magnetic resonance-based tracking and quantification of intravenously injected neural stem cell accumulation in the brains of mice with experimental multiple sclerosis. *Stem Cells*, 25(10):2583–2592, 2007. [Cited on page 4]

Thomas Portet, Chloé Mauroy, Vincent Démery, Thibault Houles, Jean-Michel Escoffre, David S Dean, and Marie-Pierre Rols. Destabilizing giant vesicles with electric fields: an overview of current applications. *The Journal of membrane biology*, 245(9):555–564, 2012. [Cited on page 110]

Geertruida A Posthuma-Trumpie, Jakob Korf, and Aart van Amerongen. Lateral flow (immuno) assay: its strengths, weaknesses, opportunities and threats. a literature survey. *Analytical and bioanalytical chemistry*, 393(2):569–582, 2009. [Cited on page 4]

Elliot Postow and Charles Polk. *Handbook of biological effects of electromagnetic fields*. Boca Raton: CRC Press, 1996. [Cited on pages 111, 114, 116, 123, 200]

Uma Prabhakar, Hiroshi Maeda, Rakesh K Jain, Eva M Sevick-Muraca, William Zamboni, Omid C Farokhzad, Simon T Barry, Alberto Gabizon, Piotr Grodzinski, and David C Blakey. Challenges and key considerations of the enhanced permeability and retention effect for nanomedicine drug delivery in oncology, 2013. [Cited on page 19]

Pallab Pradhan, Jyotsnendu Giri, Finn Rieken, Christian Koch, Olga Mykhaylyk, Markus Döblinger, Rinti Banerjee, Dhirendra Bahadur, and Christian Plank. Targeted temperature sensitive magnetic liposomes for thermo-chemotherapy. *Journal of Controlled Release*, 142 (1):108–121, 2010. [Cited on pages 18, 30, 65, 198]

Matthew R Preiss and Geoffrey D Bothun. Stimuli-responsive liposome-nanoparticle assemblies. *Expert opinion on drug delivery*, 8(8):1025–1040, 2011. [Cited on pages 18, 30, 65, 198]

Paolo P Provenzano, Kevin W Eliceiri, and Patricia J Keely. Multiphoton microscopy and fluorescence lifetime imaging microscopy (flim) to monitor metastasis and the tumor microenvironment. *Clinical & experimental metastasis*, 26(4):357–370, 2009. [Cited on pages 33, 197]

G Pucihar, T Kotnik, B Valič, and D Miklavčič. Numerical determination of transmembrane voltage induced on irregularly shaped cells. *Annals of biomedical engineering*, 34(4):642, 2006. [Cited on page 55]

Gorazd Pucihar, Damijan Miklavcic, and Tadej Kotnik. A time-dependent numerical model of transmembrane voltage inducement and electroporation of irregularly shaped cells. *IEEE Transactions on Biomedical Engineering*, 56(5):1491–1501, 2009. [Cited on page 55]

MIHAI Radu, M Ionescu, N Irimescu, K Iliescu, R Pologea-Moraru, and E Kovacs. Orientation behavior of retinal photoreceptors in alternating electric fields. *Biophysical journal*, 89(5): 3548–3554, 2005. [Cited on page 113]

Nahla Rahoui, Bo Jiang, Nadia Taloub, and Yu Dong Huang. Spatio-temporal control strategy of drug delivery systems based nano structures. *Journal of Controlled Release*, 2017. [Cited on pages 6, 8]

Gopalasamudram Narayana Ramachandran et al. Aspects of protein structure. In *International Symposium on Protein Structure and Crystallography (1963: Madras, India)*. Academic Press, 1963. [Cited on page 160]

Corinne Ramos, David Bonato, Mathias Winterhalter, Toon Stegmann, and Justin Teissié. Spontaneous lipid vesicle fusion with electropermeabilized cells. *FEBS letters*, 518(1-3):135–138, 2002. [Cited on page 111]

GC Ramos, D Fernandes, CT Charao, DG Souza, MM Teixeira, and J Assreuy. Apoptotic mimicry: phosphatidylserine liposomes reduce inflammation through activation of peroxisome proliferator-activated receptors (ppars) in vivo. *British journal of pharmacology*, 151 (6):844–850, 2007. [Cited on page 66]

Natalya Rapoport, Kweon-Ho Nam, Roohi Gupta, Zhongao Gao, Praveena Mohan, Allison Payne, Nick Todd, Xin Liu, Taeho Kim, Jill Shea, et al. Ultrasound-mediated tumor imaging and nanotherapy using drug loaded, block copolymer stabilized perfluorocarbon nanoemulsions. *Journal of Controlled Release*, 153(1):4–15, 2011. [Cited on page 24]

Riccardo Reale, Niall J English, José-Antonio Garate, Paolo Marracino, Micaela Liberti, and Francesca Apollonio. Human aquaporin 4 gating dynamics under and after nanosecond-scale

static and alternating electric-field impulses: A molecular dynamics study of field effects and relaxation. *The Journal of chemical physics*, 139(20):11B616_1, 2013. [Cited on page 193]

Peter Reimer and Thomas Balzer. Ferucarbotran (resovist): a new clinically approved res-specific contrast agent for contrast-enhanced mri of the liver: properties, clinical development, and applications. *European radiology*, 13(6):1266–1276, 2003. [Cited on page 4]

Lea Rems, Marko Ušaj, Maša Kandušer, Matej Reberšek, Damijan Miklavčič, and Gorazd Pucihar. Cell electrofusion using nanosecond electric pulses. *Scientific reports*, 3, 2013. [Cited on pages 109, 200]

Lea Retelj, Gorazd Pucihar, and Damijan Miklavčič. Electroporation of intracellular liposomes using nanosecond electric pulsesa theoretical study. *IEEE Transactions on Biomedical Engineering*, 60(9):2624–2635, 2013. [Cited on page 110]

Jane S Richardson. The anatomy and taxonomy of protein structure. *Advances in protein chemistry*, 34:167–339, 1981. [Cited on page 160]

Alexandra Rodzinski, Rakesh Guduru, Emmanuel Stimphil, Tiffanie Stewart, Ping Liang, Carolyn Runowicz, and Sakhrat Khizroev. Targeted, controlled anticancer drug delivery and release with magnetoelectric nanoparticles, 2016. [Cited on pages 9, 29, 89]

Christine Rohde, Austin Chiang, Omotinuwe Adipoju, Diana Casper, and Arthur A Pilla. Effects of pulsed electromagnetic fields on interleukin-1β and postoperative pain: A double-blind, placebo-controlled, pilot study in breast reduction patients. *Plastic and reconstructive surgery*, 125(6):1620–1629, 2010. [Cited on page 35]

Christina L Ross. The use of magnetic field for the reduction of inflammation: a review of the history and therapeutic results. *Alternative therapies in health and medicine*, 19(2):47, 2013. [Cited on pages 9, 29, 89]

Jean-Paul Ryckaert, Giovanni Ciccotti, and Herman JC Berendsen. Numerical integration of the cartesian equations of motion of a system with constraints: molecular dynamics of n-alkanes. *Journal of Computational Physics*, 23(3):327–341, 1977. [Cited on page 48]

Go Saito, Joel A Swanson, and Kyung-Dall Lee. Drug delivery strategy utilizing conjugation via reversible disulfide linkages: role and site of cellular reducing activities. *Advanced drug delivery reviews*, 55(2):199–215, 2003. [Cited on page 22]

Rangeen Salih and CC Matthai. Computer simulations of the diffusion of na+ and cl- ions across popc lipid bilayer membranes. *The Journal of Chemical Physics*, 146(10):105101, 2017. [Cited on page 162]

Gintautas Saulis. Electroporation of cell membranes: the fundamental effects of pulsed electric fields in food processing. *Food Engineering Reviews*, 2(2):52–73, 2010. [Cited on pages 9, 109, 200]

Shaka S Scarlett, Jody A White, Peter F Blackmore, Karl H Schoenbach, and Juergen F Kolb. Regulation of intracellular calcium concentration by nanosecond pulsed electric fields. *Biochimica et Biophysica Acta (BBA)-Biomembranes*, 1788(5):1168–1175, 2009. [Cited on pages 26, 109]

Tamar Schlick, Eric Barth, and Margaret Mandziuk. Biomolecular dynamics at long timesteps: Bridging the timescale gap between simulation and experimentation. *Annual review of biophysics and biomolecular structure*, 26(1):181–222, 1997. [Cited on page 48]

Tom Schmidlin, Ken Ploeger, Amanda L Jonsson, and Valerie Daggett. Early steps in thermal unfolding of superoxide dismutase 1 are similar to the conformational changes associated with the als-associated a4v mutation. *Protein Engineering, Design & Selection*, 26(8):503–513, 2013. [Cited on pages 170, 171]

Karl H Schoenbach, Stephen J Beebe, and E Stephen Buescher. Intracellular effect of ultrashort electrical pulses. *Bioelectromagnetics*, 22(6):440–448, 2001. [Cited on pages 10, 37]

Karl H Schoenbach, Ravindra P Joshi, Juergen F Kolb, Nianyong Chen, Michael Stacey, Peter F Blackmore, E Stephen Buescher, and Stephen J Beebe. Ultrashort electrical pulses open a new gateway into biological cells. *Proceedings of the IEEE*, 92(7):1122–1137, 2004. [Cited on page 55]

Karl H Schoenbach, Stephen J Hargrave, Ravindra P Joshi, Juergen F Kolb, Richard Nuccitelli, Christopher Osgood, Andrei Pakhomov, Michael Stacey, R James Swanson, Jody A White, et al. Bioelectric effects of intense nanosecond pulses. *IEEE Transactions on Dielectrics and Electrical Insulation*, 14(5), 2007. [Cited on pages 10, 55]

Avi Schroeder, Reuma Honen, Keren Turjeman, Alberto Gabizon, Joseph Kost, and Yechezkel Barenholz. Ultrasound triggered release of cisplatin from liposomes in murine tumors. *Journal of controlled release*, 137(1):63–68, 2009. [Cited on pages 23, 24]

R Seigneuric, L Markey, D SA Nuyten, C Dubernet, C TA Evelo, E Finot, and C Garrido. From nanotechnology to nanomedicine: applications to cancer research. *Current Molecular Medicine*, 10(7):640–652, 2010. [Cited on pages 19, 110]

Iurii Semenov, Shu Xiao, and Andrei G Pakhomov. Primary pathways of intracellular ca 2+ mobilization by nanosecond pulsed electric field. *Biochimica et Biophysica Acta (BBA)-Biomembranes*, 1828(3):981–989, 2013. [Cited on page 37]

Nina Senutovitch, Lawrence Vernetti, Robert Boltz, Richard DeBiasio, Albert Gough, and D Lansing Taylor. Fluorescent protein biosensors applied to microphysiological systems. *Experimental Biology and Medicine*, 240(6):795–808, 2015. [Cited on page 33]

Stefania Setti, Vincenzo Di Lazzaro, Fiore Capone, and Alessia Ongaro3 Ruggero Cadossi. A new approach to treating acute ischemic stroke in human brain: Pulsed electromagnetic fields. 2017. [Cited on page 66]

Donglu Shi. Integrated multifunctional nanosystems for medical diagnosis and treatment. *Advanced Functional Materials*, 19(21):3356–3373, 2009. [Cited on pages 1, 29, 89]

Yunhua Shi, Mark J Acerson, Kevin L Shuford, and Bryan F Shaw. Voltage-induced misfolding of zinc-replete als mutant superoxide dismutase-1. *ACS chemical neuroscience*, 6(10):1696–1707, 2015. [Cited on page 37]

A Silve, A Guimerà Brunet, B Al-Sakere, A Ivorra, and LM Mir. Comparison of the effects of the repetition rate between microsecond and nanosecond pulses: Electropermeabilization-induced electro-desensitization? *Biochimica et Biophysica Acta (BBA)-General Subjects*, 1840(7):2139–2151, 2014. [Cited on page 10]

Aude Silve, Isabelle Leray, and Lluis M Mir. Demonstration of cell membrane permeabilization to medium-sized molecules caused by a single 10ns electric pulse. *Bioelectrochemistry*, 87: 260–264, 2012. [Cited on pages 125, 126, 129]

Aude Silve, Isabelle Leray, Michael Leguèbe, Clair Poignard, and Lluis M Mir. Cell membrane permeabilization by 12-ns electric pulses: Not a purely dielectric, but a charge-dependent phenomenon. *Bioelectrochemistry*, 106:369–378, 2015. [Cited on pages xix, 111, 114]

Aude Silve, Isabelle Leray, Clair Poignard, and Lluis M Mir. Impact of external medium conductivity on cell membrane electropermeabilization by microsecond and nanosecond electric pulses. *Scientific reports*, 6:19957, 2016. [Cited on pages 125, 127]

Ashutosh Singh, Valérie Orsat, and Vijaya Raghavan. Soybean hydrophobic protein response to external electric field: a molecular modeling approach. *Biomolecules*, 3(1):168–179, 2013. [Cited on page 38]

Kyle C Smith, TR Gowrishankar, Axel T Esser, Donald A Stewart, and James C Weaver. The spatially distributed dynamic transmembrane voltage of cells and organelles due to 10 ns pulses: meshed transport networks. *IEEE transactions on Plasma Science*, 34(4):1394–1404, 2006. [Cited on pages 119, 143]

Gleb Y Solomentsev, Niall J English, and Damian A Mooney. Hydrogen bond perturbation in hen egg white lysozyme by external electromagnetic fields: A nonequilibrium molecular dynamics study. *The Journal of chemical physics*, 133(23):12B607, 2010. [Cited on page 192]

C Song, X Wang, Y Wang, H Yu, Y Cui, and T Ma. Advances in the use of multifunctional mesoporous silica nanoparticles and related nanomaterials as carriers for the cancer treatment. *Current drug metabolism*, 2017. [Cited on page 7]

Laura Soriano-Romaní, Marta Vicario-de-la Torre, Mario Crespo-Moral, Antonio López-García, Rocío Herrero-Vanrell, Irene T Molina-Martínez, and Yolanda Diebold. Novel anti-inflammatory liposomal formulation for the pre-ocular tear film: In vitro and ex vivo functionality studies in corneal epithelial cells. *Experimental eye research*, 154:79–87, 2017. [Cited on page 66]

Romina Spera, Stefania Petralito, Micaela Liberti, Caterina Merla, Guglielmo d'Inzeo, Rosanna Pinto, and Francesca Apollonio. Controlled release from magnetoliposomes aqueous suspensions exposed to a low intensity magnetic field. *Bioelectromagnetics*, 35(4):309–312, 2014. [Cited on pages 9, 30, 31, 32, 65, 198]

Romina Spera, Francesca Apollonio, Micaela Liberti, Alessandra Paffi, Caterina Merla, Rosanna Pinto, and Stefania Petralito. Controllable release from high-transition temperature magnetoliposomes by low-level magnetic stimulation. *Colloids and Surfaces B: Biointerfaces*, 131:136–140, 2015. [Cited on pages 9, 63, 66, 67, 80, 81, 83, 85, 87, 90, 92, 149, 198]

Q Spreiter and M Walter. Classical molecular dynamics simulation with the velocity verlet algorithm at strong external magnetic fields. *Journal of Computational Physics*, 152(1): 102–119, 1999. [Cited on page 155]

Sarah A Stanley, Jennifer E Gagner, Shadi Damanpour, Mitsukuni Yoshida, Jonathan S Dordick, and Jeffrey M Friedman. Radio-wave heating of iron oxide nanoparticles can regulate plasma glucose in mice. *Science*, 336(6081):604–608, 2012. [Cited on page 32]

Wesley E Stites, Alan K Meeker, and David Shortle. Evidence for strained interactions between side-chains and the polypeptide backbone. *Journal of molecular biology*, 235(1):27–32, 1994. [Cited on page 161]

Clare A Stokes, Randip Kaur, Michael R Edwards, Madhav Mondhe, Darren Robinson, Elizabeth C Prestwich, Robert D Hume, Chloe A Marshall, Yvonne Perrie, Valerie Bridget O'Donnell, et al. Human rhinovirus-induced inflammatory responses are inhibited by phosphatidylserine containing liposomes. *Mucosal immunology*, 9(5):1303, 2016. [Cited on page 66]

Martien A Cohen Stuart, Wilhelm TS Huck, Jan Genzer, Marcus Müller, Christopher Ober, Manfred Stamm, Gleb B Sukhorukov, Igal Szleifer, Vladimir V Tsukruk, Marek Urban, et al. Emerging applications of stimuli-responsive polymer materials. *Nature materials*, 9(2):101, 2010. [Cited on pages 19, 110]

Ian T Suydam, Christopher D Snow, Vijay S Pande, and Steven G Boxer. Electric fields at the active site of an enzyme: Direct comparison of experiment with theory. *Science*, 313(5784): 200–204, 2006. [Cited on page 172]

William C Swope, Hans C Andersen, Peter H Berens, and Kent R Wilson. A computer simulation method for the calculation of equilibrium constants for the formation of physical clusters of molecules: Application to small water clusters. *The Journal of Chemical Physics*, 76(1): 637–649, 1982. [Cited on page 155]

Tatsuaki Tagami, Warren D Foltz, Mark J Ernsting, Carol M Lee, Ian F Tannock, Jonathan P May, and Shyh-Dar Li. Mri monitoring of intratumoral drug delivery and prediction of the therapeutic effect with a multifunctional thermosensitive liposome. *Biomaterials*, 32(27): 6570–6578, 2011. [Cited on pages 23, 24]

Sayuri Takahashi, Takumi Shiraishi, Nancy Miles, Bruce J Trock, Prakash Kulkarni, and Robert H Getzenberg. Nanowire analysis of cancer-testis antigens as biomarkers of aggressive prostate cancer. *Urology*, 85(3):704–e1, 2015. [Cited on page 5]

Xiao Tao, Alice Lee, Walrati Limapichat, Dennis A Dougherty, and Roderick MacKinnon. A gating charge transfer center in voltage sensors. *Science*, 328(5974):67–73, 2010. [Cited on page 192]

Mounir Tarek. Membrane electroporation: a molecular dynamics simulation. *Biophysical journal*, 88(6):4045–4053, 2005. [Cited on pages 10, 54]

J Teissie and MP Rols. Fusion of mammalian cells in culture is obtained by creating the contact between cells after their electropermeabilization. *Biochemical and biophysical research communications*, 140(1):258–266, 1986. [Cited on pages 109, 200]

Ephrem Tekle, Hammou Oubrahim, Sergey M Dzekunov, Juergen F Kolb, Karl H Schoenbach, and PB Chock. Selective field effects on intracellular vacuoles and vesicle membranes with nanosecond electric pulses. *Biophysical journal*, 89(1):274–284, 2005. [Cited on pages 27, 119]

D Peter Tieleman. The molecular basis of electroporation. *BMC biochemistry*, 5(1):10, 2004. [Cited on page 10]

Gleb P Tolstykh, Hope T Beier, Caleb C Roth, Gary L Thompson, Jason A Payne, Marjorie A Kuipers, and Bennett L Ibey. Activation of intracellular phosphoinositide signaling after a single 600 nanosecond electric pulse. *Bioelectrochemistry*, 94:23–29, 2013. [Cited on page 10]

Francesca Toschi, Francesca Lugli, Fabio Biscarini, and Francesco Zerbetto. Effects of electric field stress on a β-amyloid peptide. *The Journal of Physical Chemistry B*, 113(1):369–376, 2008. [Cited on page 192]

B Trzaskowski, D Latek, S Yuan, U Ghoshdastider, A Debinski, and S Filipek. Action of molecular switches in gpcrs-theoretical and experimental studies. *Current medicinal chemistry*, 19 (8):1090–1109, 2012. [Cited on page 152]

Katherine M Tyner, Raoul Kopelman, and Martin A Philbert. nanosized voltmeter enables cellular-wide electric field mapping. *Biophysical journal*, 93(4):1163–1174, 2007. [Cited on page 192]

Sepideh Zununi Vahed, Roya Salehi, Soodabeh Davaran, and Simin Sharifi. Liposome-based drug co-delivery systems in cancer cells. *Materials Science and Engineering: C*, 71:1327–1341, 2017. [Cited on page 7]

Roy van der Meel, Laurens JC Vehmeijer, Robbert J Kok, Gert Storm, and Ethlinn VB van Gaal. Ligand-targeted particulate nanomedicines undergoing clinical evaluation: current status. *Advanced drug delivery reviews*, 65(10):1284–1298, 2013. [Cited on page 19]

David Van Der Spoel, Erik Lindahl, Berk Hess, Gerrit Groenhof, Alan E Mark, and Herman JC Berendsen. Gromacs: fast, flexible, and free. *Journal of computational chemistry*, 26(16): 1701–1718, 2005. [Cited on pages 149, 154, 174]

Wilfred F van Gunsteren, Salomon R Billeter, Alice A Eising, Philippe H Hünenberger, PKHC Krüger, Alan E Mark, Walter RP Scott, and Ilario G Tironi. Biomolecular simulation: the {GROMOS96} manual and user guide. 1996. [Cited on page 173]

Ann Van Loey, B Verachtert, and Marc Hendrickx. Effects of high electric field pulses on enzymes. *Trends in Food Science & Technology*, 12(3):94–102, 2001. [Cited on page 37]

K Varani, M De Mattei, F Vincenzi, S Gessi, S Merighi, A Pellati, A Ongaro, A Caruso, R Cadossi, and PA Borea. Characterization of adenosine receptors in bovine chondrocytes

and fibroblast-like synoviocytes exposed to low frequency low energy pulsed electromagnetic fields. *Osteoarthritis and cartilage*, 16(3):292–304, 2008. [Cited on pages 9, 11, 35, 36, 149, 152, 167, 202]

Katia Varani, Stefania Gessi, Stefania Merighi, Valeria Iannotta, Elena Cattabriga, Susanna Spisani, Ruggero Cadossi, and Pier Andrea Borea. Effect of low frequency electromagnetic fields on a2a adenosine receptors in human neutrophils. *British journal of pharmacology*, 136 (1):57–66, 2002. [Cited on pages 11, 35, 36, 149, 151, 152, 154, 158, 159, 161, 167, 202]

Katia Varani, Fabrizio Vincenzi, Annalisa Ravani, Silvia Pasquini, Stefania Merighi, Stefania Gessi, Stefania Setti, Matteo Cadossi, Pier Andrea Borea, and Ruggero Cadossi. Adenosine receptors as a biological pathway for the anti-inflammatory and beneficial effects of low frequency low energy pulsed electromagnetic fields. *Mediators of inflammation*, 2017, 2017. [Cited on pages 9, 36, 66, 149, 167]

Loup Verlet. Computer" experiments" on classical fluids. i. thermodynamical properties of lennard-jones molecules. *Physical review*, 159(1):98, 1967. [Cited on page 48]

P Thomas Vernier, Aimin Li, Laura Marcu, Cheryl M Craft, and Martin A Gundersen. Ultrashort pulsed electric fields induce membrane phospholipid translocation and caspase activation: differential sensitivities of jurkat t lymphoblasts and rat glioma c6 cells. *IEEE Transactions on Dielectrics and Electrical Insulation*, 10(5):795–809, 2003a. [Cited on page 26]

P Thomas Vernier, Yinghua Sun, Laura Marcu, Sarah Salemi, Cheryl M Craft, and Martin A Gundersen. Calcium bursts induced by nanosecond electric pulses. *Biochemical and biophysical research communications*, 310(2):286–295, 2003b. [Cited on pages 27, 37]

P Thomas Vernier, Yinghua Sun, Laura Marcu, Cheryl M Craft, and Martin A Gundersen. Nanosecond pulsed electric fields perturb membrane phospholipids in t lymphoblasts. *FEBS letters*, 572(1-3):103–108, 2004. [Cited on page 27]

P Thomas Vernier, Yinghua Sun, and Martin A Gundersen. Nanoelectropulse-driven membrane perturbation and small molecule permeabilization. *BMC cell biology*, 7(1):37, 2006. [Cited on page 9]

F Veronesi, P Torricelli, G Giavaresi, M Sartori, F Cavani, S Setti, M Cadossi, A Ongaro, and M Fini. In vivo effect of two different pulsed electromagnetic field frequencies on osteoarthritis. *Journal of Orthopaedic Research*, 32(5):677–685, 2014. [Cited on page 66]

Fabrizio Vincenzi, Martina Targa, Carmen Corciulo, Stefania Gessi, Stefania Merighi, Stefania Setti, Ruggero Cadossi, Mary B Goldring, Pier Andrea Borea, and Katia Varani. Pulsed electromagnetic fields increased the anti-inflammatory effect of a2a and a3 adenosine receptors in human t/c-28a2 chondrocytes and hfob 1.19 osteoblasts. *PLoS One*, 8(5):e65561, 2013. [Cited on page 151]

Susanne Wagner, JÖrg Schnorr, Herbert Pilgrimm, Bernd Hamm, and Matthias Taupitz. Monomer-coated very small superparamagnetic iron oxide particles as contrast medium for magnetic resonance imaging: preclinical in vivo characterization. *Investigative radiology*, 37 (4):167–177, 2002. [Cited on page 4]

Jian Wang, Shouxian She, and Sijiong Zhang. An improved helmholtz coil and analysis of its magnetic field homogeneity. *Review of scientific instruments*, 73(5):2175–2179, 2002. [Cited on pages 91, 94]

Shengnian Wang, Xulang Zhang, Bo Yu, Robert J Lee, and L James Lee. Targeted nanoparticles enhanced flow electroporation of antisense oligonucleotides in leukemia cells. *Biosensors and Bioelectronics*, 26(2):778–783, 2010. [Cited on page 28]

Xianwei Wang, Yongxiu Li, Xiao He, Shude Chen, and John ZH Zhang. Effect of strong electric field on the conformational integrity of insulin. *The Journal of Physical Chemistry A*, 118 (39):8942–8952, 2014. [Cited on pages 38, 192]

Douglas S Watson, Aaron N Endsley, and Leaf Huang. Design considerations for liposomal vaccines: influence of formulation parameters on antibody and cell-mediated immune responses to liposome associated antigens. *Vaccine*, 30(13):2256–2272, 2012. [Cited on pages 28, 110]

James C Weaver, Kyle C Smith, Axel T Esser, Reuben S Son, and TR Gowrishankar. A brief overview of electroporation pulse strength–duration space: a region where additional intracellular effects are expected. *Bioelectrochemistry*, 87:236–243, 2012. [Cited on pages 10, 26]

Brittany J Wetzel, G Nindl, DN Vesper, JA Swez, AC Jasti, and MT Johnson. Electromagnetic field effects: changes in protein phosphorylation in the jurkat e6. 1 cell line. *Biomedical sciences instrumentation*, 37:203–208, 2001. [Cited on page 35]

Andreas Wicki, Dominik Witzigmann, Vimalkumar Balasubramanian, and Jörg Huwyler. Nanomedicine in cancer therapy: challenges, opportunities, and clinical applications. *Journal of controlled release*, 200:138–157, 2015. [Cited on page 1]

JD Wood, TP Beaujeux, and PJ Shaw. Protein aggregation in motor neurone disorders. *Neuropathology and applied neurobiology*, 29(6):529–545, 2003. [Cited on page 170]

Julia D Wulfkuhle, Lance A Liotta, and Emanuel F Petricoin. Proteomic applications for the early detection of cancer. *Nature reviews. Cancer*, 3(4):267, 2003. [Cited on pages 33, 202]

Younan Xia, Yujie Xiong, Byungkwon Lim, and Sara E Skrabalak. Shape-controlled synthesis of metal nanocrystals: Simple chemistry meets complex physics ? *Angewandte Chemie International Edition*, 48(1):60–103, 2009. [Cited on page 1]

BY Xiang, MO Ngadi, BK Simpson, and MV Simpson. Pulsed electric field induced structural modification of soy protein isolate as studied by fluorescence spectroscopy. *Journal of Food Processing and Preservation*, 35(5):563–570, 2011. [Cited on page 183]

Tian-Xiang Xiang and Bradley D Anderson. Liposomal drug transport: a molecular perspective from molecular dynamics simulations in lipid bilayers. *Advanced drug delivery reviews*, 58 (12):1357–1378, 2006. [Cited on pages 19, 110]

Ting Xu, John Forsayeth, and Katherine Ferrara. Nanocarriers for cancer treatment, November 11 2016. US Patent App. 15/349,946. [Cited on page 7]

Hung-Wei Yang, Mu-Yi Hua, Hao-Li Liu, Chiung-Yin Huang, Rung-Ywan Tsai, Yu-Jen Lu, Ju-Yu Chen, Hsiang-Jun Tang, Han-Yi Hsien, Yu-Sun Chang, et al. Self-protecting core-shell magnetic nanoparticles for targeted, traceable, long half-life delivery of bcnu to gliomas. *Biomaterials*, 32(27):6523–6532, 2011. [Cited on page 30]

Pei-Kun Yang. Dependence of interaction free energy between solutes on an external electrostatic field. *International journal of molecular sciences*, 14(7):14408–14425, 2013. [Cited on page 192]

Pei-Kun Yang. Effect of external electrostatic field on the stability of β sheet structures. *Biopolymers*, 101(8):861–870, 2014. [Cited on page 193]

Ruijin Yang, Si-Quan Li, and Q Howard Zhang. Effects of pulsed electric fields on the activity and structure of pepsin. *Journal of Agricultural and Food Chemistry*, 52(24):7400–7406, 2004. [Cited on page 37]

Chenguo Yao, Xiaoqian Hu, Yan Mi, Chengxiang Li, and Caixin Sun. Window effect of pulsed electric field on biological cells. *IEEE Transactions on dielectrics and electrical insulation*, 16(5), 2009. [Cited on page 55]

Mohd Iqbal Yatoo, Archana Saxena, Mohd Hussain Malik, MK Kumar, and Umesh Dimri. Nanotechnology based drug delivery at cellular level: a review. *J Anim Sci Adv*, 4(2):705–709, 2014. [Cited on page 18]

Milton B Yatvin, John N Weinstein, Warren H Dennis, and Robert Blumenthal. Design of liposomes for enhanced local release of drugs by hyperthermia. *Science*, 202(4374):1290–1293, 1978. [Cited on page 30]

Kane Yee. Numerical solution of initial boundary value problems involving maxwell's equations in isotropic media. *IEEE Transactions on antennas and propagation*, 14(3):302–307, 1966. [Cited on page 56]

Laura Zanetti-Polzi, Paolo Marracino, Massimiliano Aschi, Isabella Daidone, Antonella Fontana, Francesca Apollonio, Micaela Liberti, Guglielmo DInzeo, and Andrea Amadei. Modeling triplet flavin-indole electron transfer and interradical dipolar interaction: a perturbative approach. *Theoretical Chemistry Accounts*, 132(11):1393, 2013. [Cited on page 193]

Jin Zhang, Robert E Campbell, Alice Y Ting, and Roger Y Tsien. Creating new fluorescent probes for cell biology. *Nature reviews. Molecular cell biology*, 3(12):906, 2002. [Cited on pages 33, 197]

Ruobing Zhang, Lun Cheng, Liming Wang, and Zhicheng Guan. Inactivation effects of pef on horseradish peroxidase (hrp) and pectinesterase (pe). *IEEE Transactions on Plasma Science*, 34(6):2630–2636, 2006. [Cited on page 37]

Wei Zhao, Ruijin Yang, Rongrong Lu, Yali Tang, and Wenbin Zhang. Investigation of the mechanisms of pulsed electric fields on inactivation of enzyme: lysozyme. *Journal of agricultural and food chemistry*, 55(24):9850–9858, 2007. [Cited on pages 37, 193]

Lin Zhu and Vladimir P Torchilin. Stimulus-responsive nanopreparations for tumor targeting. *Integrative Biology*, 5(1):96–107, 2013. [Cited on page 22]

Barbara Zorec, Sid Becker, Matej Reberšek, Damijan Miklavčič, and Nataša Pavšelj. Skin electroporation for transdermal drug delivery: the influence of the order of different square wave electric pulses. *International journal of pharmaceutics*, 457(1):214–223, 2013. [Cited on page 10]